Characterization of the microbial methane oxidation for landfill studies by stable isotope analysis

Dissertation

zur Erlangung des akademischen Grades eines

Doktors der Naturwissenschaften

– Dr. rer. nat. –

vorgelegt von

Sven Marcel Schulte

geboren in Mülheim an der Ruhr

Fakultät für Chemie
der
Universität Duisburg-Essen

2016

Die vorliegende Arbeit wurde im Zeitraum von September 2011 bis November 2016 im Arbeitskreis von Prof. Dr. Schmidt am Institut für Instrumentelle Analytische Chemie der Universität Duisburg-Essen durchgeführt.

Tag der Disputation: 23.2.2017

Gutachter:	Prof. Dr. Torsten C. Schmidt
	Prof. Dr. Martin Denecke
Vorsitzender:	Jun.-Prof. Dr. André Gröschel

Summary

Next to water, carbon dioxide (CO_2) and methane (CH_4) are the most important greenhouse gases with regard to their radiative forcing effect. While the amount of CH_4 in the atmosphere is by two orders of magnitude lower than that of CO_2 its global warming potential is up to 28 times greater than that of CO_2. The waste and wastewater sector contribute an important share to the total anthropogenic emissions of methane. In this particular case, landfills play an important role because worldwide the major amount of waste is deposited at landfill sites. Emissions of CH_4 at landfill sites arise due to the production of landfill gas mainly from fermentation by obligate anaerobic microorganisms. It can be collected for energy production which allows an economic use and the mitigation of CH_4 emissions to the atmosphere at the same time. Yet, both amount and concentration of CH_4 released from the waste body decrease throughout time. As a consequence, for older landfills, the utilization of landfill gas for economic purposes is no longer possible. However, the German legislation demands the treatment of the landfill gas to reduce CH_4 emissions to the atmosphere. An extension or alternative to active gas extraction and treatment are landfill cover layers that serve as methane oxidation layers. On the one hand their advantage is that they represent passive systems and in contrast to active systems need no additional machinery and little maintenance. On the other hand a general problem with these systems is the assessment of the performance of methane oxidation by an appropriate method. One suitable technique for that purpose is stable isotope analysis (SIA). It relies on the preferential consumption of the lighter $^{12}CH_4$ over the heavier $^{13}CH_4$ by methanotrophic bacteria within the cover layer which can be described by the isotopic enrichment factor ε. This preference results in an isotopic fractionation between the CH_4 produced in the anaerobic zone of the waste body and the partially consumed CH_4 emitted at the landfill's surface. Apart from the isotopic composition of the anaerobic and emitted CH_4 ε is the crucial parameter for the estimation of the performance of the cover layer in terms of biodegradation. In this work the focus was on the determination of this parameter at different temperatures and for different methanotrophs (type I and II) by using gas chromatography isotope ratio mass spectrometry for SIA. The overall average ± standard deviation was $\varepsilon = -0.021 \pm 0.004$ (mixed methanotrophs in topsoil: $\varepsilon = -0.0202 \pm 0.0047$ at 22°C and $\varepsilon = -0.0231 \pm 0.0059$ at 30°C; mixed methanotrophs enrichment culture at 22°C: $\varepsilon = -0.0136 \pm 0.0036$; type I enrichment culture: $\varepsilon = -0.0242 \pm 0.0007$ at 22°C and $\varepsilon = -0.0202 \pm 0.0030$ at 30°C; type II enrichment culture: $\varepsilon = -0.0204 \pm 0.0028$ at 22°C; $\varepsilon = -0.0232 \pm 0.0020$ at 30°C). Comparison with the literature revealed similar values for ε. It was also shown that the high variability and uncertainty of ε resulted in no statistical difference for either different temperatures or for type I or II

methanotrophs. Further statistical analysis revealed that corrections suggested in literature based on a temperature dependency of ε are of minor relevance when regarding the uncertainty in ε (in the typical operational range of a cover soil of 10-40°C). Another factor influencing isotopic fractionation is diffusion. In landfills where methane transport to the surface is dominated by diffusion the estimation of biodegradation by SIA has to be corrected for the former. The isotopic fractionation by diffusion was determined for a potential landfill cover material at 22.5°C and 30°C and compared with literature values. With an average of ε_{diff} = -0.0212 ± 0.005 at 22.5°C and ε_{diff} = -0.0218 ± 0.003 at 30°C it was of the same order of magnitude as the determined isotopic fractionation by methane oxidation and thus within the range of analytical uncertainty of the theoretical value for isotopic fractionation by diffusion of ε_{diff} = -0.0191. Having determined these important parameters, the biodegradation in a new reactor setup could be investigated by SIA for the study of topsoil as a potential cover layer. Apart from SIA, different methods based on mass balancing and stoichiometry were used and compared by statistical means in terms of correlation, measurement uncertainty, and biodegradation. The results based on SIA for a closed system and for stoichiometric balancing of product (CH_4) and reactant (CO_2) correlated well with the mass balance method. However, highest biodegradation was determined by mass balancing, followed by stoichiometry, and finally SIA that resulted in the lowest estimates, in general. The investigated topsoil proved to be very suitable as a potential cover layer by removing up to 99% of methane for CH_4 loads of 35 - 65 $gm^{-2}d^{-1}$ that are typical in the aftercare phase of landfills. Finally, SIA and the stoichiometric approach were used to trace microbial activity within the reactor system and were able to validate a newly employed technique by thermographic imaging. It was shown that methane consumption and temperature increase -as a cause of high microbial activity- correlated very well. In future studies this will allow investigating the response of cover materials to additional simulated environmental changes such as fissure formation by plant root penetration and the influence of weather conditions such as desiccation or high precipitation. These exemplify events whose influences on the cover layer are not well understood, yet. All in all this work improves the understanding and comparability of techniques to evaluate methane oxidation. Based on this work, further opportunities in terms of forecasting and modelling the behavior of the methane oxidation layer are facilitated.

Zusammenfassung

Neben Wasser stellen Methan (CH_4) und Kohlenstoffdioxid (CO_2) die wichtigsten Treibhausgase dar. Während Methan einen um zwei Größenordnungen geringeren Anteil in der Atmosphäre aufweist als Kohlenstoffdioxid, hat es im Vergleich zu CO_2 ein bis zu 28 mal größeres Treibhausgaspotential. In Bezug auf anthropogene Methanemissionen nimmt der Abfallsektor eine wichtige Stelle ein. Mülldeponien sind hier von besonderem Interesse, da weltweit die Deponierung den Hauptentsorgungsweg von Müll darstellt. Durch Fermentation im anaeroben Müllkörper entsteht das sogenannte Deponiegas, welches zum größten Teil aus CH_4 und CO_2 besteht. Letzteres wird wegen seines zunächst hohen Brennwerts zur Produktion von Energie und Wärme genutzt. Auf einer Deponie nehmen jedoch sowohl der Anteil an CH_4 als auch die Menge an gebildeten Deponiegas im Laufe der Zeit ab. Eine wirtschaftliche Nutzung ist dann nicht mehr möglich. Da die Deponieverordnung aber eine Behandlung des entstandenen Gases vorschreibt, stellen passive Systeme wie die Methanoxidationsschicht eine Alternative zu aktiven Systemen zur Behandlung von sogenannten Restmengen bzw. Schwachgas dar. Sie benötigen, im Gegensatz zu aktiven Systemen, keine zusätzliche Technik und Maschinen, die oft mit einem hohen Wartungsaufwand verbunden sind. Ein Nachteil besteht jedoch darin, die Menge des oxidierten Methans zu bestimmen und somit die Leistungsfähigkeit einer Methanoxidationsschicht einzuschätzen. Hierfür kommen verschiedene Techniken zum Einsatz. Darunter zählt auch die Analytik stabiler Isotope (SIA). Sie beruht auf der Gegebenheit, dass die für die Oxidation verantwortlichen methanotrophen Bakterien das leichtere Isotop $^{12}CH_4$ gegenüber dem schwereren $^{13}CH_4$ bevorzugen. Diese Präferenz lässt sich durch den Anreicherungsfaktor ε beschreiben. Als Folge der bakteriellen Metabolisierung fraktioniert das zum Teil oxidierte CH_4 und unterscheidet sich so von dem gebildeten Methan im anaeroben Müllkörper. Dieser Unterschied ermöglicht die Abschätzung der relativen Biodegradation. Neben der Isotopensignatur des gebildeten und des teiloxidierten Methans, ist die Kenntnis des sogenannten Anreicherungsfaktors von großer Bedeutung. In der vorliegenden Arbeit wurden hierzu die Anreicherungsfaktoren bei unterschiedlichen Temperaturen und für unterschiedliche Bakterientypen (Typ I und II) mittels der Gaschromatographie mit Kopplung an die Isotopenverhältnis-Massenspektrometrie (GC-IRMS) bestimmt. Der Mittelwert ± Standardabweichung lag bei ε = -0.021 ± 0.004 (gemischte Methanotrophe in Mutterboden: ε = -0.0202 ± 0.0047 bei 22°C und ε = -0.0231 ± 0.0059 bei 30°C; gemischte Anreicherungskultur bei 22°C: ε = -0.0136 ± 0.0036; Typ I Anreicherungs-kultur: ε = -0.0242 ± 0.0007 bei 22°C und ε = -0.0202 ± 0.0030 bei 30°C; Typ II Anreicherungskultur: ε = -0.0204 ± 0.0028 bei 22°C; ε = -0.0232 ±0.0020 bei 30°C). Beim Vergleich mit der Literatur

zeigten sich ähnliche Werte, dessen Unsicherheit in Bezug auf die Standardabweichung aber generell sehr hoch ist (bis zu ~20%). Ein Unterschied von ε durch die verschiedenen Faktoren ließ sich statistisch nicht nachweisen. Weiterhin zeigte sich, dass die Standardabweichung von ε den Wert für vorgeschlagene temperaturabhängige Korrekturen umschließt. Dies bedeutet, dass für den Bereich von 10-40°C, was den regulären Aktivitätsbereich der Oxidationsschicht umfasst, eine Korrektur im Vergleich zu einem Wert mit entsprechender Standardabweichung statistisch nicht signifikant ist und somit eine untergeordnete Rolle spielt. Ein weiterer Faktor, der die Isotopenfraktionierung beeinflusst ist die Diffusion. Sie muss bei Berechnungen entsprechend berücksichtigt werden. Der Diffusionskoeffizient und die diffusionsabhängige Isotopenfraktionierung für ein potentielles Abdeckmaterial wurden bei 22.5°C und 30°C bestimmt und mit der Literatur verglichen. Mit einem Mittelwert von ε_{diff} = -0.0212 ± 0.005 bei 22.5°C und ε_{diff} = -0.0218 ± 0.003 bei 30°C lagen die Werte in derselben Größenordnung wie für die Methanoxidation, und weiterhin im Rahmen der analytischen Unsicherheit für den theoretischen Wert von ε_{diff} = -0.0191. Die so bestimmten, wichtigen Parameter konnten nun verwendet werden, um die Biodegradation eines organisch geprägten Mutterbodens als potentielles Abdeckmaterial, der in einem neuen Reaktordesign eingesetzt wurde, zu berechnen. Unterschiedliche Methoden, darunter die Bilanzierung durch Massenbilanz, ein stöchiometrischer Ansatz basierend auf CH_4 und CO_2, und SIA, wurden dabei angewandt und u.a. statistisch miteinander verglichen. Alle Methoden zeigten untereinander eine gute Korrelation. Zusätzlich ergab sich, dass die Massenbilanz die höchste Abschätzung aufwies, gefolgt vom stöchiometrischen Ansatz und SIA. Der untersuchte Mutterboden zeigte sich schließlich als geeignet für die Entfernung von bis zu 99% an CH_4 für Gasfrachten von 35 - 65 $gm^{-2}Tag^{-1}$, die in der Nachsorgephase einer Deponie üblich sind. Im letzten Kapitel kamen SIA und der stöchiometrische Ansatz zum Einsatz, um die aktive Zone der Methanoxidation im Reaktor zu lokalisieren. Die Ergebnisse wurden mit einer neu angewandten Technik, der Thermographie, verglichen. Es konnte gezeigt werden, dass der berechnete Methanumsatz mit einer entsprechenden Temperaturerhöhung einherging. Somit erweist sich die Thermographie als geeignetes Mittel, um die Aktivität der Bakterien unter verschiedenen Einflussfaktoren zu erfassen. Sie ermöglicht es weiterhin zukünftige Untersuchungen zu unterschiedlichen Umwelteinflüssen wie Austrocknung, verstärkte Regenereignisse, oder die Rissbildung durch Wurzelbildung in Abstimmung mit der SIA durchzuführen. Schließlich erweitert diese Arbeit das Verständnis für die Veränderlichkeit der bakteriellen Methanoxidationsschicht unter verschiedenen Umweltaspekten und unterstützt somit die Modellierung der Methanoxidationsschicht für eine bessere Vorhersage auf Deponien.

Table of Content

1 Introduction

1.1 Methane and carbon dioxide in the environment

Carbon dioxide (CO_2) and methane (CH_4) are the most important greenhouse gases (GHG) with regards to their absolute radiative forcing effect of $1.82 \pm 0.19\ Wm^{-2}$ and $0.48 \pm 0.05\ Wm^{-2}$ (Myhre and T. Nakajima, 2013), respectively. The difference in radiative forcing is due to different atmospheric abundances and global warming potentials (see Figure 1-1). Anthropogenic activities are the main reason for the steady increase in emissions of these GHG to the atmosphere since the beginning of the industrial age. In case of carbon dioxide the main anthropogenic sources are the burning of fossil fuels (e.g., used for energy production, cement production, construction works, and traffic) and land use change (deforestation) (Ciais et al., 2013). In the years 2002-2011 fossil fuel combustion and cement production contributed $8.3 \pm 0.7\ Pg{\cdot}a^{-1}$ ($1Pg = 10^{15}g$) and land use $0.9 \pm 0.8\ Pg{\cdot}a^{-1}$ of the total CO_2 emissions, respectively. (Ciais et al., 2013). The estimated overall budget of methane emissions was estimated to be 497-525 $Tg{\cdot}a^{-1}$ for the years 1984-2003 (Bousquet et al., 2006), and $556 \pm 56\ Tg{\cdot}a^{-1}$ in the year 2011 ($1Tg = 10^{12}g$) (Ciais et al., 2013). Of these, roughly 271 $Tg{\cdot}a^{-1}$ for the years 1984-2003, and about $331\ Tg{\cdot}a^{-1}$ for the year 2011 originated from anthropogenic activity (Bousquet et al., 2006; Ciais et al., 2013). The anthropogenic emissions of CH_4 arise from agriculture, fossil fuels, biomass burning, and from waste and wastewater (Ciais et al., 2013). Of these about 39% can be attributed to fossil fuels and biomass burning (Ciais et al., 2013) but the majority to ruminants, rice fields, and landfills and waste (Conrad, 2009). All these are due to CH_4 production by methanogenic archaea. In case of fossil fuels for energy production the methane emissions are due to leaks in natural gas recovery, coal mining, and losses during pipeline transmission (Wahlen, 1993). The waste and wastewater sector adds estimated annual methane emissions of 75 Tg CH_4 (Ciais et al., 2013) and in 2004 contributed 18% of the total anthropogenic emissions of methane (Bogner et al., 2008). In particular landfills play an important role for anthropogenic greenhouse gas emissions because not only in north America (Aelion et al., 2010) but also worldwide the major amount of waste is deposited at landfill sites (Kranert, 2010).

An example of the global atmospheric mixing ratios for CO_2 and CH_4 from 1980 to 2016 as obtained from data of the National Oceanic and Atmospheric Administration is given in Figure 1-1. The global atmospheric mixing ratio for methane has been increasing from an average of ~695 ppb before the preindustrial age (before ~1750) (Etheridge et al., 1998), to as high as ~1840 ppb (Dlugokencky, 2016) in 2016. However, the annual growth rates have shown to fluctuate. Before the 1980s the annual growth rate was around 10%, while a decade later it nearly

ceased (Lelieveld, 2006). These fluctuations have been suggested to result from decreased atmospheric CH_4 lifetimes as simulations on the atmospheric lifetime of methane resulted in a decrease by more than 8% from 1970 to 2012 (Dalsøren et al., 2016). The reduced lifetime was explained to result from increased atmospheric oxidation capacity. On the other hand, the emissions from wetlands in the tropics are a dominant factor for natural fluctuations and emissions during dry periods decrease (Lelieveld, 2006). Although for CH_4 the global mixing ratio is by two orders of magnitude lower than that of CO_2 it plays an important role as a greenhouse gas. This is because of its high global warming potential (GWP) of up to 28 (Myhre and T. Nakajima, 2013). The GWP which has been suggested to be termed "relative cumulative forcing index" instead is a measure that compares the ratio of the absolute global warming potential (AGWP) of a certain greenhouse gas with the AGWP for the reference gas CO_2 (Myhre and T. Nakajima, 2013). The AGWPs are calculated based on an emission pulse of a respective gas and the resulting radiative forcing, that is integrated over a chosen time period, generally 100 years (Myhre and T. Nakajima, 2013).

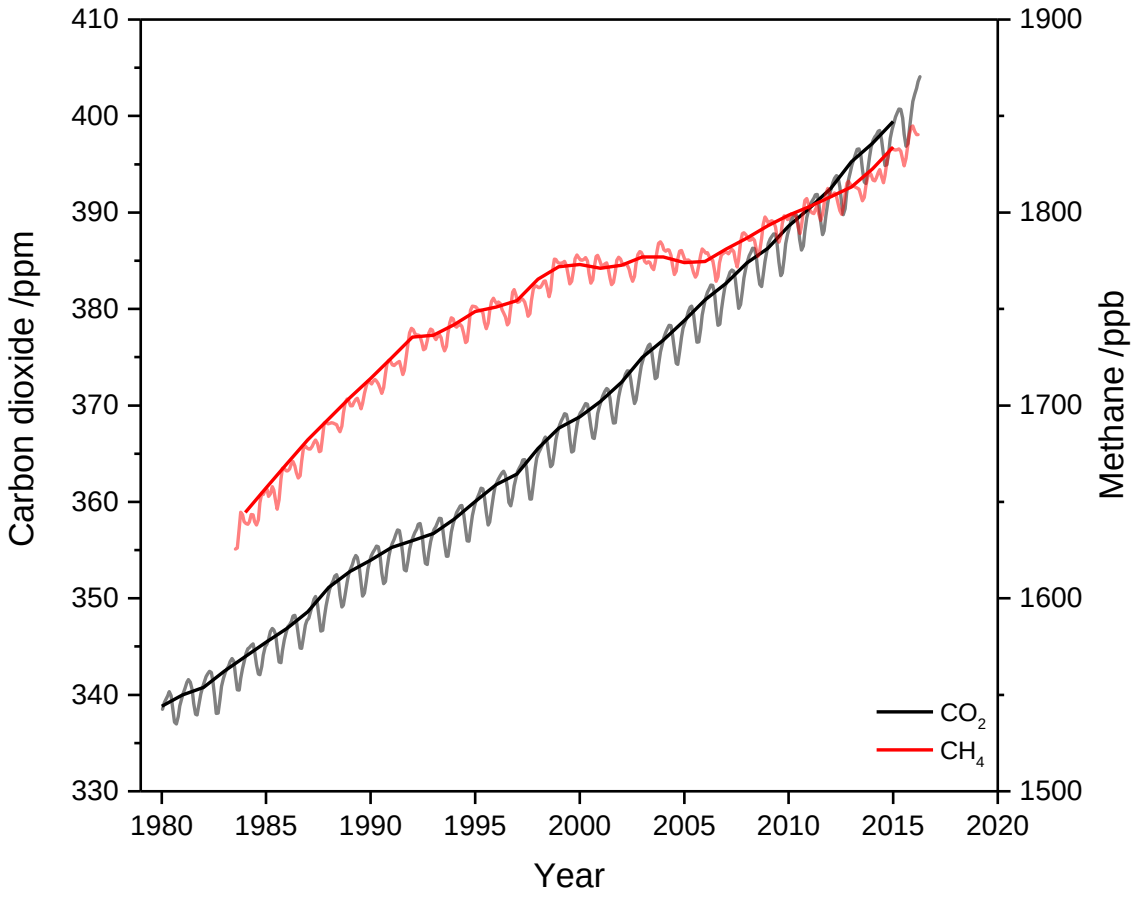

Figure 1-1 Atmospheric concentrations of CO_2 & CH_4 adapted from (Dlugokencky, 2016)
The lines are annual concentrations and shaded lines are monthly variations of CO_2 and CH_4. (www.esrl.noaa.gov/gmd/ccgg/trends_ch4/ & www.esrl.noaa.gov/gmd/ccgg/trends_co2/)

The removal of methane in the atmosphere occurs mainly by OH radicals in the troposphere and stratosphere (Dlugokencky et al., 2011) and is estimated to account for 485 $Tg \cdot CH_4 \cdot a^{-1}$ (Bousquet et al., 2006). The atmospheric lifetime of CH_4 ranges between eight and 14 years with a mean turnover time of ~10 years (Rasmussen and Khalil, 1981). Another component of atmospheric methane removal is the methane oxidation in soils (Conrad, 2009). In certain cases the mitigation of CH_4 emissions from agriculture, coal mines, and landfills can be inexpensive for short-term reductions in greenhouse gases, as it can be captured as a source of energy (Dlugokencky et al., 2011).

1.2 Landfills

The main global waste disposal at landfill sites is by waste compaction and in Germany this was also the case until 2005 (Kranert, 2010). This is primarily due to the enforcement of the landfill ordinance "Deponieverordnung" (DepV) from which on waste material had to be treated mechanically and biologically prior to deposition and thus only organically poor or biologically stabilized materials reached the landfill. On the one hand, this type of disposal has the advantage that a lot of material can be deposited. Another is the possibility of easy deposition of the waste by trucks that are able to maneuver on the landfill and thus no highly-specialized machinery is required. On the other hand, there is a high risk of fires and material settling, and large amounts of landfill gas are produced (Kranert, 2010). In Germany the importance of landfills has decreased significantly already since the 1960s, as the number of active landfills for municipal household waste has fallen from ~85.000 before the 1970s to as low as 162 in 2005 (Kranert, 2010). In North-Rhine-Westphalia the number of active landfills in 2012 was 125 of which 19 were of class II and thus suitable for municipal household waste (LANUV, 2012). Nevertheless, landfills with waste disposal by compaction are the most relevant in terms of planning and taking measures for the release from aftercare and landfill closure (Kranert, 2010). Here, the most important aspects are the control of settling events in the waste material layer as well as the control and treatment of leachate and landfill gas.

Formerly, the fate of waste deposited on landfills was regulated by a number of landfill ordinances and technical notes existing in Germany. In 2009 these were replaced by the DepV which was further updated in 2013. Based on the DepV (Deponieverordnung, 2013) landfills are classified depending on the type of deposited waste material as follows:

- Landfill class 0: landfill for inert wastes
- Landfill class I: landfill for municipal waste with low organic content
- Landfill class II: landfill for municipal waste with moderate organic content
- Landfill class III: landfill for toxic waste
- Landfill class IV: subsurface landfill in salt rock

The design and function of a landfill can vary, which also depends on the landfill class. However, every landfill requires a certain type of sealing. Its general setup has changed over the past decades and is well summarized in (Gruyters, 2013). A recent example is depicted in Figure 1-2. The deposited waste material is surrounded by a seal both at its bottom and its top. At the bottom, the seal is composed of a geological barrier which may be topped by a membrane layer and a mineral seal. Its purpose is to prevent the release of leachate into the surrounding environment and groundwater. Above this is a water drainage system followed by the actual waste. At the top, the seal is composed of a gas distribution layer, a mineral seal layer, a water drainage layer, and a recultivation layer. Irrespective of the deposited waste every landfill requires this recultivation layer with a thickness of ≥1 m. Next to the protection from frost and the penetration of the lower drainage layer by plant roots it is important for the water balance (Boley, 2012). Table 1-1 summarizes the principle prerequisites of the bottom and surface sealing system.

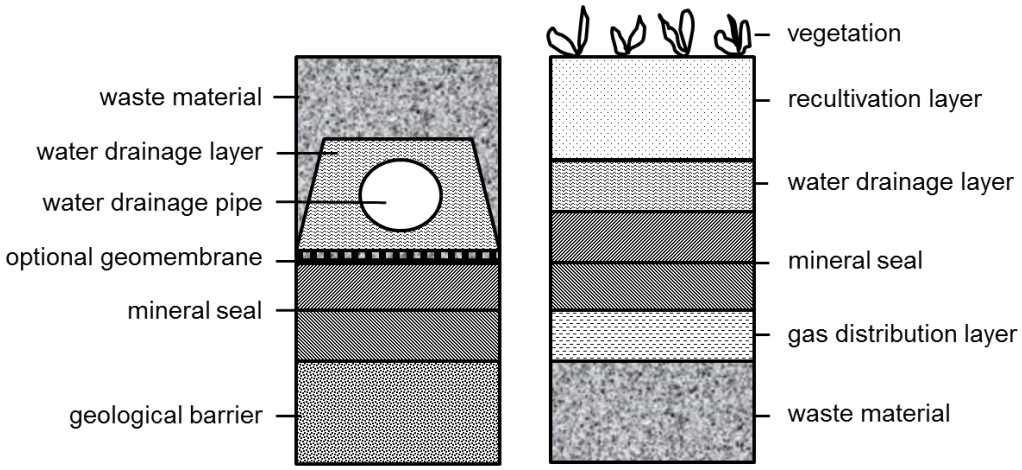

Figure 1-2 Typical landfill sealing bottom (left) and surface (right) redrawn from (Kranert, 2010)

Table 1-1 Setup of bottom and surface seal simplified from DepV (Deponieverordnung, 2013)

Seal	System component	Class 0	Class I	Class II	Class III
Bottom	Geological barrier[1]	d ≥ 1.00 m	d ≥ 1.00 m	d ≥ 1.00 m	d ≥ 5.00 m
	Primary seal	not required	required	required	required
	Secondary seal	not required	not required	required	required
	Mineral water drainage layer[2]	d ≥ 0.30 m	d ≥ 0.50 m	d ≥ 0.50 m	d ≥ 0.50 m
Top	Compensation or balancing layer	not required	possibly required	possibly required	possibly required
	Gas distribution layer	not required	not required	possibly required	possibly required
	Primary seal	not required	required	required	required
	Secondary seal	not required	not required	required	required
	Seal control system	not required	not required	not required	required
	Water drainage layer[3]	not required	required	required	required
	Recultivation- /Technical functional layer	required	required	required	required

[1]field capacity (k) ≤ $1 \cdot 10^{-7}$ ms^{-1}; [2]granulation by DIN 19667; [3]d ≥ 0.30 m, k ≥ $1 \cdot 10^{-3} ms^{-1}$, elevation > 5%

The period of regulation of a landfill is categorized into the different stages: construction, deposition phase, sealing period, and aftercare phase. The latter covers a usual period of 30 years but is not regulated formally (Boley, 2012). After temporary or final sealing and during the aftercare phase the DepV demands the measurement and control of gas emissions. In the aftercare phase the recultivation layer may also be utilized as methane oxidation layer if additional requirements considering methane oxidation and water balance are met (Deponieverordnung, 2013). The release from the aftercare phase is of economic interest for the landfill operator as the public authorities do not demand measures concerning the control and monitoring of emissions at regular intervals beyond this point. However, as described by the DepV it is bound to not very precisely defined terms: "A gas production does not occur or has ceased as much as no more active collection of gas is required, emitting residual gases are sufficiently oxidized, and toxic effects on the surrounding environment by gas migration can be excluded. A sufficient methane oxidation of the residual gases has to be demonstrated."(Deponieverordnung, 2013). For this purpose, possible techniques for the measurement of surface emissions are by a mobile flame ionization detector (FID) or by laser absorption spectroscopy. Examples of recent studies at landfill sites using either technique are given by (Foster-Wittig et al., 2015; Monster et al., 2015; Rachor et al., 2013).

In the past, more accurate criteria for the release from aftercare have been suggested (Stegmann, 2005). With respect to landfill gas emissions limits were suggested for a gas composition of 50% CH_4 and 50% CO_2. The maximum amount of extracted gas should not exceed 50-70 m^3h^{-1} and surface emissions of CH_4 not exceed 0.5-1.0 $Lm^{-2}h^{-1}$. Later on, Heyer et al. (2006) suggested that at methane emissions of ≤25 m^3h^{-1} for the total landfill and area-wise of ≤5 $m^3h^{-1}ha^{-1}$ the change from an active treatment to a passive system such as a methane oxidizing layer should be allowed with the following prerequisite. The emissions of CH_4 into the recultivation layer must not exceed 0.5 $Lm^{-2}h^{-1}$ as well as a total of 25 ppm of hydrocarbons.

As mentioned previously, the DepV demands the reduction and control of emissions such as leachate (e.g. by drainage system), odor, and greenhouse gas emissions (e.g. by gas extraction system). In case of landfill gas, relevant amounts produced in biological processes at a landfill site have to be collected and treated by state of the art technical means already during the deposition of waste material. Also, if possible the gas has to be utilized for energy production. In case of low emissions, the landfill operator has to prove that most of the methane is oxidized before emitting to the atmosphere.

Landfill gas is produced from the waste material by a series of aerobic degradation processes and to a major extent by fermentation by obligate anaerobic microorganisms (Kranert, 2010). It is composed of up to 60 vol.-% methane, and 45 vol.-% carbon dioxide (Huber-Humer et al., 2008) and is usually water saturated. But also smaller amounts of hydrogen sulfide and ammonia and trace amounts of hydrocarbons such as alkanes, aromatics, halogenated hydrocarbons and organic sulfur species are emitted from landfills (Rettenberger and Stegmann, 1996).

The process of landfill gas generation can be categorized into the following nine characteristic phases (Figure 1-3). In phases I-III microbial respiration processes produce carbon dioxide and eliminate oxygen of the residual air in the waste material. Methane begins to appear from starting anaerobic fermentation processes. The next phase (IV) is characterized by a stable production of landfill gas. During phase V, the pore space of the waste material is saturated with methane and carbon dioxide. While the concentrations of CH_4 and CO_2 rise, the overall emissions of landfill gas decrease as readily degradable waste material is almost decomposed completely. The drop in methane concentration in phase VI is due to the penetration of air into the waste body. Aerobic microbial degradation processes start. In phase VII, increased aeration increases aerobic degradation and methanotrophic activity starts which leads to a further decrease in methane concentration and increased CO_2 production. Emissions of methane nearly cease in the following

phase (VIII). Finally, in phase IX the degradable components of the waste material are virtually removed entirely.

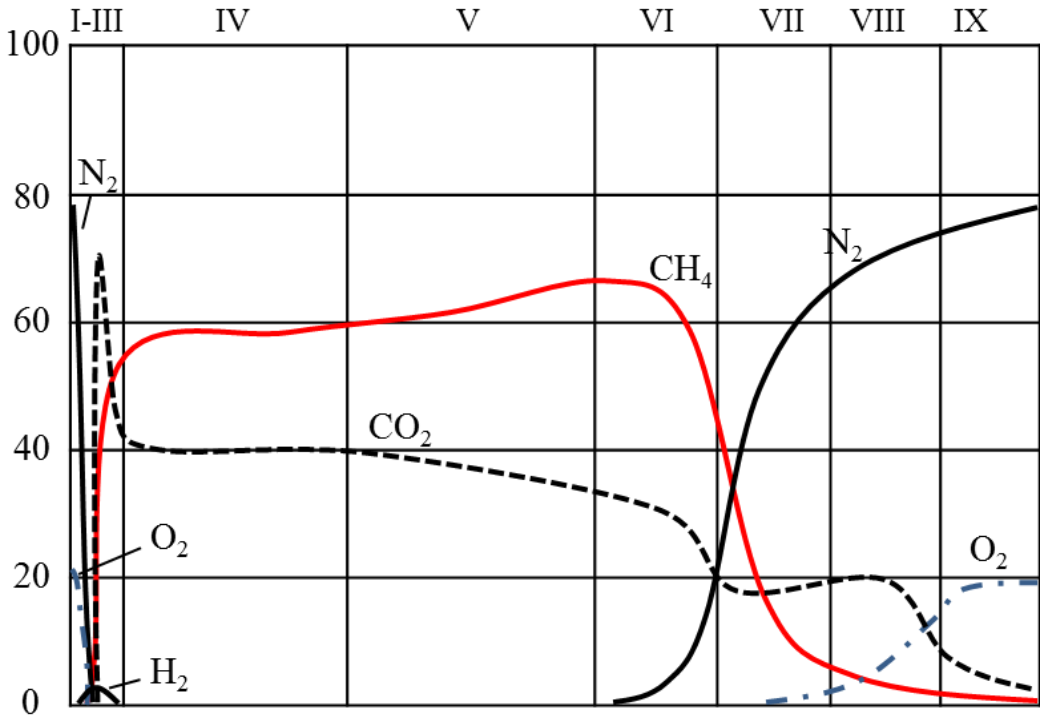

Figure 1-3 Progress of landfill gas constituents redrawn from (Rettenberger, 1996)

As the production of landfill gas in terms of total amount and concentration of CH_4 changes with a landfill's lifetime different techniques are required for proper treatment. An example of the landfill gas production of a typical landfill in Germany is given in Figure 1-4. About 50-60% of the landfill gas can be recovered by extraction (Börjesson et al., 2007; Börjesson et al., 2009). Combined heat and power units can utilize the gas for energy production. In the U.S.A, the percent oxidation of landfill methane emitted to the atmosphere is suggested to be at least 25% for landfills with gas collection systems (Chanton et al., 2011). However, at older landfills the lower emissions of landfill gas are also a cause of lower concentrations of methane. Yet, an economic use of landfill gas requires a methane content of ≥ 40% (Roth, 2015). After combined heat and power units, the next applicable technique is the high temperature gas torch. It can be modified further to operate down to a range of >25 vol.-% to >12 vol.-% methane (Kranert, 2010). Below this point, there is a set of available techniques to treat the landfill gas such as a fluidized bed plant (>5 vol.-% CH_4) and regenerative thermal oxidation (<1 vol.-% CH_4).

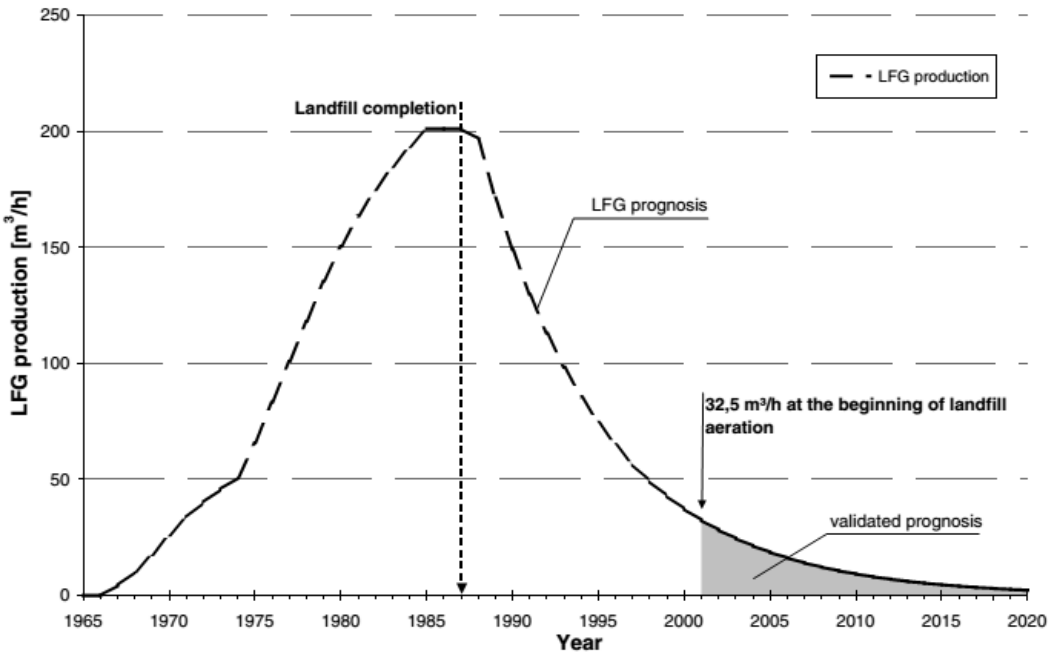

Figure 1-4 Progress of landfill gas production of a german landfill (Ritzkowski et al., 2006)
Depicted is the landfill gas (LFG) production with time for a german landfill.

To cover the total range of methane concentrations and loads, the given set of technical instrumentation is expanded by biological systems suitable for the treatment of landfill gas. These include biofilters and soil covers or biocovers as reviewed in (Huber-Humer et al., 2008; Scheutz et al., 2009). An example for the treatment of CH_4 emissions of <18 vol.-% in a biofilter is a system developed by (Haubrichs, 2007). It operates by separately regulating the air supply in different layers within the biofilter. In addition, a recently developed laboratory scale one-phase system for the treatment of CH_4 based on a liquid bacterial suspension is a promising approach for standalone systems (Gehrke et al., 2015). Advantages of this system are the separate introduction of artificial landfill gas and air which prevents the formation of explosive gas mixtures, an increase in spatial capacity by enrichment of bacteria in the liquid phase, and no risk of clogging of the filter by the formation of biofilms. Methane oxidation rates of up to 60 $gm^{-3}h^{-1}$ were achieved in this manner. Furthermore, when emissions have decreased significantly passive systems may be applied. These usually require that the landfill is finally sealed. In this case the gas can be fed locally into biofilters (by using the preinstalled gas extraction system) or evenly into the recultivation layer which then serves as a methane oxidation layer (by redirecting gas from gas wells into the cover). Recently, however, it was shown that an interim cover layer of incineration slag also functioned as a methane oxidation layer for area loadings of <0.2 $Lm^{-2}h^{-1}$ (Gruyters, 2013). In this case it was suggested to maintain the layer operational in order to allow further degradation of the lower waste material and methane oxidation instead of sealing the landfill and thus lowering oxygen supply and limiting aerobic degradation.

1.3 Methanotrophs

Methanotrophic bacteria resemble a subtype of methylotrophic bacteria that are able to utilize methane as sole carbon and energy source (Hanson and Hanson, 1996). They are found in many environments, as for example, swamps and marshes, rice paddies, lakes, hypersaline lakes and oceans, deserts, forest soils, sewage sludge, coal mine surfaces, and landfills (Bowman, 2006; Hanson and Hanson, 1996). Interestingly, certain methanotrophs (type I) undergo symbiosis with different organisms such as, deep sea mussels (Petersen and Dubilier, 2009), tube worms (Schmaljohann and Flugel, 1987), and wetland plants (Raghoebarsing et al., 2005). Methanotrophs are gram negative aerobic eubacteria (Lieberman and Rosenzweig, 2004) and belong to *Verrucomicrobia*, *Alphaproteobacteria*, and *Gammaproteobacteria* (Petersen and Dubilier, 2009; Semrau et al., 2010). The enzyme responsible for the conversion of methane into methanol is the methane monooxygenase, which consists of three subunits (Lieberman and Rosenzweig, 2004). There are two forms, a particulate (pMMO) and a soluble (sMMO). The pMMO is located in the bacterial cytoplasmic membrane and most known methanotrophs possess it (Hanson and Hanson, 1996). In contrast, the soluble form is present only in some methanotrophs and is located in the cytoplasm (Semrau et al., 2010). In methanotrophs that have both enzymes the expression of either type depends on the presence of copper. Under copper rich conditions, the pMMO is expressed and under copper limiting conditions the sMMO is expressed (Stanley et al., 1983). The resulting methanol is converted into formaldehyde by methanol dehydrogenase (MDH). Formaldehyde represents a branching point in the metabolism. Either it is assimilated or it is oxidized further to carbon dioxide. In the latter case formaldehyde is oxidized to formic acid by a formaldehyde dehydrogenase (FADH) followed by oxidation to carbon dioxide by formic acid dehydrogenase (FDH) (Ballantyne et al., 2012; Lieberman and Rosenzweig, 2004). In case of carbon assimilation, there are two main metabolic pathways. Based on these two pathways, methanotrophs are categorized into two groups, type I and type II. While type I methanotrophs mainly utilize the ribulose monophosphate pathway (RuMP), type II methanotrophs use the serine pathway. However, certain methanotrophs using the RuMP pathway also possess enzymes for the serine pathway (Hanson and Hanson, 1996). They were formerly denoted as type X and represent a subset of type I methanotrophs (Bowman, 2006). The net reaction for carbon assimilation by RuMP is:

$$3HCHO + ATP \rightarrow \text{Glyceraldehyde-3-phosphate} + ADP \quad (1.3.1)$$

And for the serine cycle:

$$2HCHO + CO_2 + 3ATP + 2NADH \rightarrow \text{2-Phosphoglycerate} + 2ADP + P_i + NAD^+ \quad (1.3.2)$$

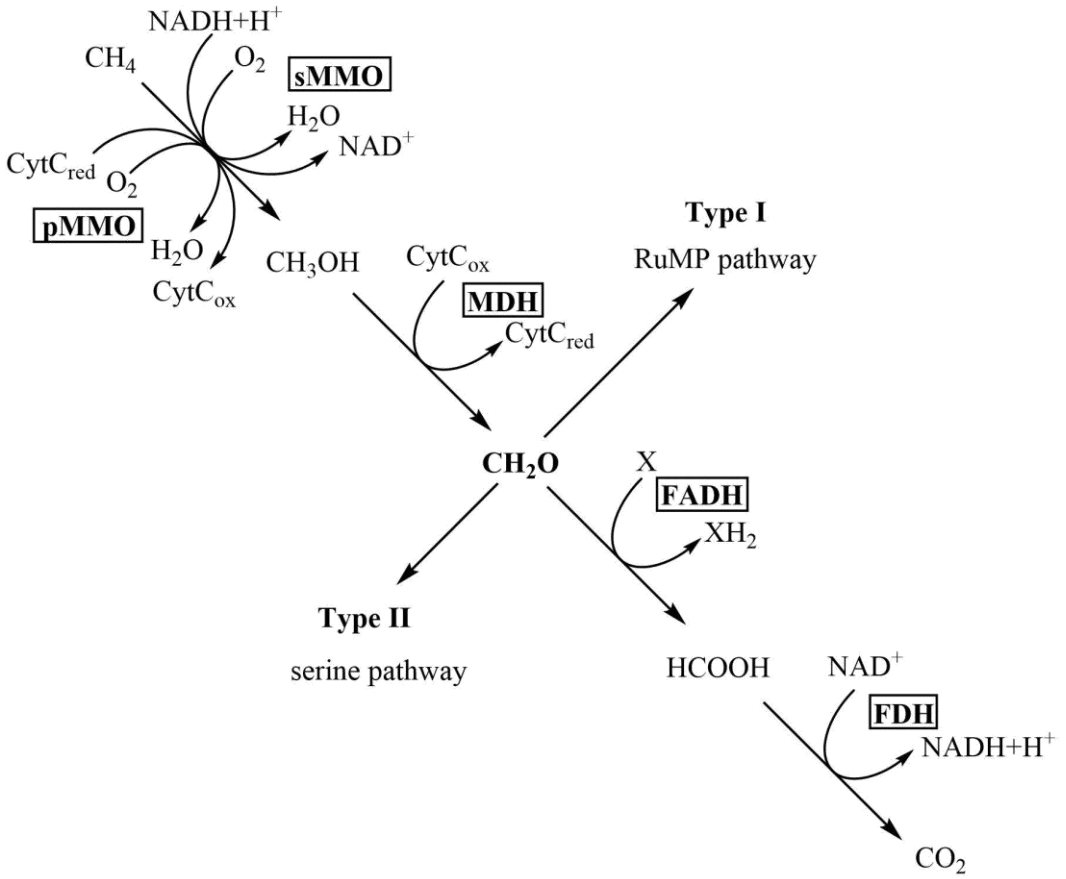

Figure 1-5 Scheme of methanotrophic metabolism redrawn from (Hanson and Hanson, 1996)

The methane assimilation is depicted along with the indicated serine and RuMP pathway. sMMO: soluble methane monooxygenase; pMMO: particulate methane monooxygenase; MDH: methanol dehydrogensase; FADH: formaldehyde dehydrogenase; FDH: formic acid dehydrogenase; RuMP: ribulose monophosphate pathway; $NADH/NAD^+$: reduced/oxidized form of nicotinamide adenine dinucleotide; $CytC_{ox}/CytC_{red}$: oxidized/reduced form of cytochrome c

As a consequence of the higher amount of required reducing agents by the serine pathway, type I methanotrophs that utilize the RuMP pathway tend to outgrow type II methanotrophs (Scheutz et al., 2009).

1.3.1 Factors influencing CH_4 oxidation

Considering their importance for the removal of methane in active and passive filter systems, the influence of several factors on the activity of methanotrophs has been investigated for bacterial cell suspensions and different cover materials. Among others, these include temperature, soil moisture content, oxygen availability/gas permeability, and soil inorganic nitrogen. In case of maximum activity of methane oxidation, the several factors are often interlinked.

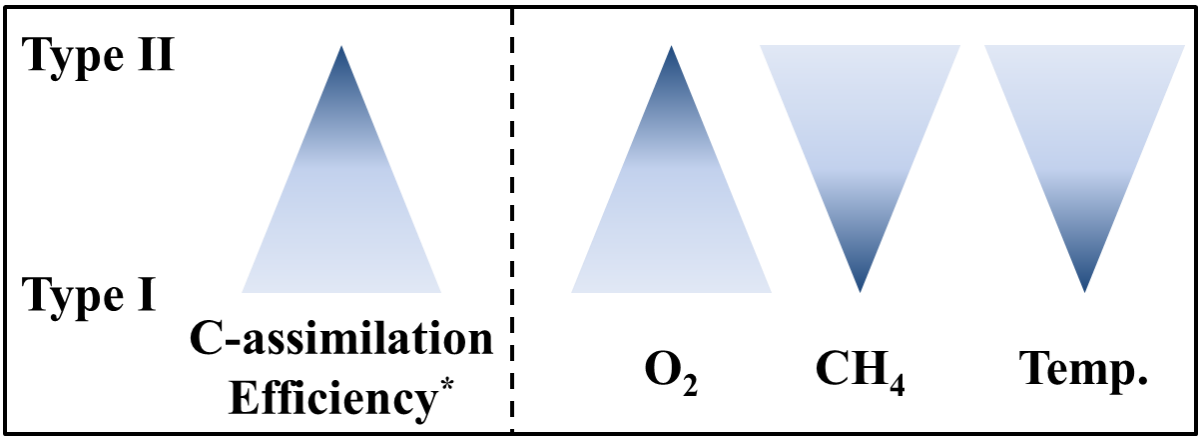

Figure 1-6 Carbon fixation and factors influencing growth and population of methanotrophs
On the left side the asterisk indicates that type I more efficiently assimilate carbon (from formaldehyde onwards) than type II (see equations (1.3.1) and (1.3.2)). Depicted on the right are conditions wich either type I or II prefers. The pyramids' bases indicate a high value and the tip a low value of the respective parameter (values not to scale).

Temperature

Although psychrophilic (growth below 15°C) and thermophilic (growth above 40°C) strains have been isolated (Semrau et al., 2010) most available methanotrophic cell cultures are mesophilic (Hanson and Hanson, 1996) and grow best at moderate pH (5-8) and at temperatures ranging from 20-35°C (Semrau et al., 2010). For example, temperature optima were determined for a fresh biofilter material at 38°C, and for a methanotrophic enrichment culture at 22°C (Gebert et al., 2003) and 35°C (Gehrke et al., 2013b). In laboratory experiments with air tight bottles containing landfill cover soil, Boeckx et al. (1996) determined highest CH_4 oxidation rates at 20°C and 15% w/w soil moisture content. In contrast to type II methanotrophs, type I methanotrophs grow better at lower temperatures and are more dominant at 10°C while type II are more dominant at 20°C, as was determined by phospholipid fatty acids analysis in a landfill cover by Börjesson et al. (2004).

Soil moisture content

The soil moisture content is very important in terms of gas permeability, NH_4^+ turnover, and water availability. Maximum activity was found at soil moisture contents of 10% w/w (Park et al., 2005), between 15.6 and 18.8% w/w (Boeckx et al., 1996), and of 18% w/w (Gebert et al., 2003). Overall, soils that retain enough water for microbial activity but also have a high share of coarse pores should be considered as potential cover layer (Scheutz et al., 2009).

Inorganic nitrogen

In soils the presence of ammonia can have an inhibitory effect on CH_4 oxidation (King and Schnell 1994 in (Boeckx et al., 1996)). However, as the decreasing effect of CH_4 oxidation by ammonia was found also to correlate with increasing soil moisture content (Boeckx et al., 1996) concluded that the turnover rate of ammonia is the driving factor rather than the actual NH_4^+ content. In contrast nitrate was found to only exhibit inhibition by osmotic effects (Scheutz et al., 2009).

Oxygen availability and gas permeability

Methanotrophs can grow over a large range of oxygen concentration (<0.5 vol.-% to 60 vol.-%) (Bowman, 2006). While type I are better adapted to low CH_4 and high O_2 concentrations type II dominate under high CH_4 and low O_2 concentrations (Scheutz et al., 2009). Yet, below 3 vol.-% (Czepiel et al., 1996), 2 vol.-% (Bender, 1992), and 1.7-2.6 vol.-% (Gebert et al., 2003) respectively, O_2 concentrations have been found to limit methane oxidation. At landfill sites, the oxygen penetration depth and thus oxygen availability is dependent on soil composition, particle size, and porosity (Scheutz et al., 2009). For example, high soil compaction decreased aeration and thus also methane oxidation was found to be strongly reduced at air-filled porosities below 10% (Gebert et al., 2011a). The authors suggested applying soils with a minimum value of 14 vol.-%. But also the production of exopolymeric substances in filter systems can lead to reduced gas permeability or clogging and thus may severely reduce methane oxidation (see (Scheutz et al., 2009) and reference therein).

1.4 Stable isotope analysis

Isotopes are elements with the same number of protons (*Z*) in their nucleus but with differing numbers of neutrons (*N*), which results in a different mass number (*A*). The mass number is described as the sum of neutrons and protons of a nuclide ($A = N + Z$). In contrast to radioactive isotopes, stable isotopes are composed of nuclides which have such long decay times that they cannot be measured (Jochmann and Schmidt, 2012).

In stable isotope analysis (SIA) it is easier to measure relative changes in isotope composition by comparison of a standard of known composition rather than to determine absolute isotopic amounts. The latter requires the calibration of a mass spectrometer with gravimetrically prepared material (Coplen, 2011). The relative changes in isotopic composition are determined by the isotopic ratio of an element as follows:

$$R\left({}^{\mathrm{h}}E / {}^{\mathrm{l}}E\right) = \frac{n\left({}^{\mathrm{h}}E\right)}{n\left({}^{\mathrm{l}}E\right)} \tag{1.4.1}$$

where the ratio *R* corresponds to the amount of the heavy isotope of a chemical element $n({}^{h}E)$ divided by the amount of the light isotope $n({}^{l}E)$. Another term is the isotope-amount fraction $x({}^{i}E)$. It differs from the isotopic ratio by the denominator which is the total number of atoms of the element in a compound $n({}^{i}E) + n({}^{j}E)$.

$$x\left({}^{i}E\right) = \frac{n\left({}^{i}E\right)}{n\left({}^{i}E\right) + n\left({}^{j}E\right)} \tag{1.4.2}$$

In this case, ${}^{i}E$ and ${}^{j}E$ are the isotopes in an element (e.g. ^{12}C and ^{13}C).

An important mass balance equation in SIA is based on this isotope-amount fraction, as exemplified for carbon below:

$$n_{\mathrm{tot}} \cdot x\left({}^{13}\mathrm{C}\right)_{\mathrm{tot}} = n_1 \cdot x\left({}^{13}\mathrm{C}\right)_1 + n_2 \cdot x\left({}^{13}\mathrm{C}\right)_2 \tag{1.4.3}$$

where n_{tot} equals the sum of substances n_1 and n_2.

At natural abundance, values for stable isotopic composition are usually reported using the delta notation (1.4.4) and they are often given in parts per thousand (‰, per mil). The delta notation is defined by the relative difference of the isotope ratio of a sample (R_{sample}) to the isotope ratio of a reference material ($R_{\mathrm{reference}}$). The Ratio corresponds to the absolute amount of the heavy isotope

divided by the absolute amount of the light isotope of the respective sample or reference. Reference materials are normalized to international measurement standards that define the delta scale. Examples of international reference materials are given in Table 1-2.

$$\delta = \frac{R_{\text{sample}}}{R_{\text{reference}}} - 1 \tag{1.4.4}$$

When using delta values, mass balancing based on equation (1.4.3) may be further simplified. An example for stable carbon isotopes is given in (1.4.5).

$$n_{\text{tot}} \cdot \delta^{13}C_{\text{tot}} = n_1 \cdot \delta^{13}C_1 - n_2 \cdot \delta^{13}C_2 \tag{1.4.5}$$

The difference between two delta values (1.4.6) is often termed "big delta". An example for carbon is given below.

$$\Delta^{13}C_{i-j} = \delta^{13}C_i - \delta^{13}C_j \tag{1.4.6}$$

Here, the subscripts *i* and *j* correspond to the delta value of compound *i* and *j*.

Table 1-2 Examples of international measurement standards adapted from (Jochmann and Schmidt, 2012)

Element	Scale	Reference material	delta value /10^3	Accepted isotopic ratio /10^6
Hydrogen	$\delta^2H_{\text{VSMOW-SLAP}}$	VSMOW (H_2O)	0	155.75 ± 0.08
		SLAP (H_2O)	-428	-
Carbon	$\delta^{13}C_{\text{VPDB}}$	VPDB (carbonate)	0	11180.2 ± 2.8
		NBS-19 (Calcite)	+1.95	-
		LSVEC (Li_2CO_3)	-46.6	-
Nitrogen	$\delta^{15}N_{\text{AIR}}$	AIR-N2 (atmospheric N_2)	0	3678.2 ± 1.5
Oxygen	$\delta^{18}O_{\text{VSMOW-SLAP}}$	VSMOW (H_2O)	0	2005.2 ± 0.45
		SLAP (H_2O)	-55.5	-
Sulfur	$\delta^{34}S_{\text{V-CDT}}$	VCDT (Ag_2S)	0	44159.9 ± 11.7

1.4.1 Isotope effects

In case of most biological, physical, and chemical processes molecules containing different stable isotopes may be fractionated, which results in different isotopic abundances (Coplen, 2011). As a consequence, the analysis of stable isotopes is an important technique, often used in environmental studies for source identification of pollutants, tracing origins of compounds, authenticity control, and calculation of biodegradation. Changes in isotopic abundances can result from mass dependent isotope effects such as an equilibrium isotope effect (*EIE*) or a kinetic isotope effect (*KIE*). An *EIE* can be described by the product of mass moments of inertia, excitation of higher-energy vibrational levels, and differences in zero point energies (E_0). The most important fundamental aspect is the difference in E_0 as its contribution dominates an isotope effect, in most cases.

The zero point energy is described as:

$$E_0 = \frac{1}{2} \cdot h \cdot \nu \tag{1.4.7}$$

where h is the Planck constant and ν the frequency of vibration. It can be explained by the harmonic oscillator as given below.

$$\nu = \frac{1}{2} \cdot \pi \sqrt{\frac{f}{\mu}} \tag{1.4.8}$$

In this case f is the force constant and μ the reduced mass.

$$\mu = \frac{m_A \cdot m_B}{m_A + m_B} \tag{1.4.9}$$

Here, m_A and m_B are the masses of the atoms with the respective isotope substitution.

If only the zero point energies are considered the *EIE* can be estimated as follows:

$$EIE = \exp\left[\frac{\Delta E_0^R - \Delta E_0^P}{f \cdot T}\right] \tag{1.4.10}$$

where c is the speed of light, ΔE_0^R the difference in zero point energies of the reactant of heavy and light isotope, and ΔE_0^P the difference in zero point energy of the product of heavy and light isotope.

A kinetic isotope effect is often associated with fast, incomplete, or unidirectional processes (Sharp, 2007). Examples are effusion, diffusion, evaporation, and chemical reaction (Jochmann and Schmidt, 2012). It is defined as the ratio of the chemical reaction rate for the light isotope (^{l}k) to the one of the heavy isotope (^{h}k):

$$KIE = \frac{^{l}k}{^{h}k} \tag{1.4.11}$$

Similar to the *EIE*, a rough estimate of the *KIE* can be described by (1.4.12) if only the zero point energies are considered and tunneling is neglected. Tunneling occurs, when molecules can react although they do not have enough energy to overcome the potential energy barrier.

$$KIE = \exp\left[\frac{h \cdot c \cdot \nu}{2 \cdot f \cdot T} \cdot \left(1 - \sqrt{\frac{^{l}\mu}{^{h}\mu}}\right)\right] \tag{1.4.12}$$

where h is the Planck constant, c is the speed of light, ν is the frequency of vibration, f is the force constant, T is temperature, and μ is the reduced mass of the respective isotope.

For molecules where the isotopes of interest are exclusively located at the reactive position (e.g., for carbon in small molecules like CH_4) the reciprocal of the *KIE* is the isotopic fractionation factor (α). It is further related to the isotopic enrichment factor (ε).

$$\alpha = (\varepsilon + 1) = \frac{^{h}k}{^{l}k} \tag{1.4.13}$$

For a closed system reaction in which the reactant is removed and does not react with the product the following relationship between the chemical rate constants can be written.

$$\frac{\partial\, ^{h/l}N}{\partial t} = -\,^{h/l}k \cdot\, ^{h/l}N \tag{1.4.14}$$

Where N is the amount of the respective isotope, t is the time, and k the kinetic rate constant. After separation of variables one obtains the following equations for the heavy and light isotope:

$$\frac{\partial\, ^{h}N}{^{h}N} = -\,^{h}k \cdot \partial t \tag{1.4.15}$$

$$\frac{\partial\, ^{l}N}{^{l}N} = -\,^{l}k \cdot \partial t \tag{1.4.16}$$

Integration of both (1.4.15) and (1.4.16) from $t = 0$ to t gives:

$$\ln\frac{1}{{}^{h}N_t} - \ln\frac{1}{{}^{h}N_0} = -kt \tag{1.4.17}$$

$$\ln\frac{1}{{}^{l}N_t} - \ln\frac{1}{{}^{l}N_0} = -kt \tag{1.4.18}$$

Rearranging and combining (1.4.17) and (1.4.18) gives:

$$\ln\left(\frac{{}^{h}N_t}{{}^{h}N_0}\right) / {}^{h}k = t = \ln\left(\frac{{}^{l}N_t}{{}^{l}N_0}\right) / {}^{l}k \tag{1.4.19}$$

$$\ln\left(\frac{{}^{h}N_t}{{}^{h}N_0}\right) = \ln\left(\frac{{}^{l}N_t}{{}^{l}N_0}\right) \cdot \frac{{}^{h}k}{{}^{l}k} \tag{1.4.20}$$

Conversion on both sides results in:

$$\frac{{}^{h}N_t}{{}^{h}N_0} = \left(\frac{{}^{l}N_t}{{}^{l}N_0}\right)^{\alpha} \tag{1.4.21}$$

Finally dividing by $\frac{{}^{l}N_t}{{}^{l}N_0}$ one obtains a correlation including the isotopic ratios:

$$\frac{R_t}{R_0} = \frac{\delta_t + 1}{\delta_0 + 1} = \left(\frac{{}^{l}N_t}{{}^{l}N_0}\right)^{(\alpha-1)} \approx f^{(\alpha-1)} \tag{1.4.22}$$

In this case f is the fraction of remaining reactant (c_t/c_0) which can be approximated for small changes in isotopic ratios by:

$$f = \left(\frac{c_t}{c_0}\right) = \frac{{}^{l}N_t + {}^{h}N_t}{{}^{l}N_0 + {}^{h}N_0} = \frac{{}^{l}N_t \cdot (1 + R_t)}{{}^{l}N_0 \cdot (1 + R_0)} \tag{1.4.23}$$

The isotopic enrichment factor can be determined by linearizing (1.4.22) which results in the following equation:

$$\ln\frac{R_t}{R_0} = \varepsilon \cdot \ln\frac{c_t}{c_0} \tag{1.4.24}$$

Another simplified version is:

$$\delta^{13}C_t = \delta^{13}C_0 + \varepsilon \cdot \ln \frac{c_t}{c_0} \tag{1.4.25}$$

Different methods for the determination of ε based on Rayleigh distillation have been compared by Scott et al. (2004). At this point it must be noted that the definition of α is not very consistent within the literature and sometimes is defined as:

$\alpha = \frac{^{h}k}{^{l}k}$ (as in this thesis) or vice versa ($\alpha = \frac{^{l}k}{^{h}k}$).

For example, Mahieu et al. (2006) compared different approaches to determine the isotopic fractionation factor $\alpha = \frac{^{l}k}{^{h}k}$ such as described in (Elsner et al., 2005; Mahieu et al., 2006; Scott et al., 2004).

In addition to (1.4.24) the isotopic enrichment factor can be derived from the accumulated product by a simplified equation based on the mass balance by delta values(1.4.5) and (1.4.25).

$$\delta_{\mathrm{P,a}} = \delta_{\mathrm{Q,0}} - 10^3 \varepsilon \frac{f \cdot \ln(f)}{1-f} \tag{1.4.26}$$

Where *P,a* and *Q,0* are the accumulated product and the initial reactant, respectively.

In case of a closed system the same correlation for the determination of α or ε can be used for the estimation of the biodegradation. By defining the term 1-*f* as fraction oxidized (f_{ox}) and after rearranging (1.4.22) one obtains:

$$f_{\mathrm{ox}} = 1 - \left(\frac{\delta_i + 1}{\delta_0 + 1} \right)^{\frac{1}{\varepsilon}} \tag{1.4.27}$$

For a reversible reaction in a closed system and an irreversible reaction in an open system at steady state the isotopic fractionation factor is related to the reactant and product as follows:

$$\alpha = \frac{\delta_{\mathrm{P}} + 1}{\delta_{\mathrm{Q}} + 1} \tag{1.4.28}$$

P and *Q* represent the product and the reactant, respectively.

An approximation of the biodegradation or fraction oxidized can be calculated by combining the simplified mass balance ((1.4.5)) and (1.4.28).

$$f_{ox} = \frac{\left(\delta_P - \delta_Q\right)}{\delta_P - \varepsilon - \delta_P \cdot \alpha} \tag{1.4.29}$$

If α is near to 1 and δ_P small, a further simplification is possible which yields:

$$f_{ox} = \frac{\left(\delta_Q - \delta_P\right)}{\varepsilon} \tag{1.4.30}$$

An example of the relationship of the delta value and the fraction of remaining reactant for a closed and an open system is given in Figure 1-7.

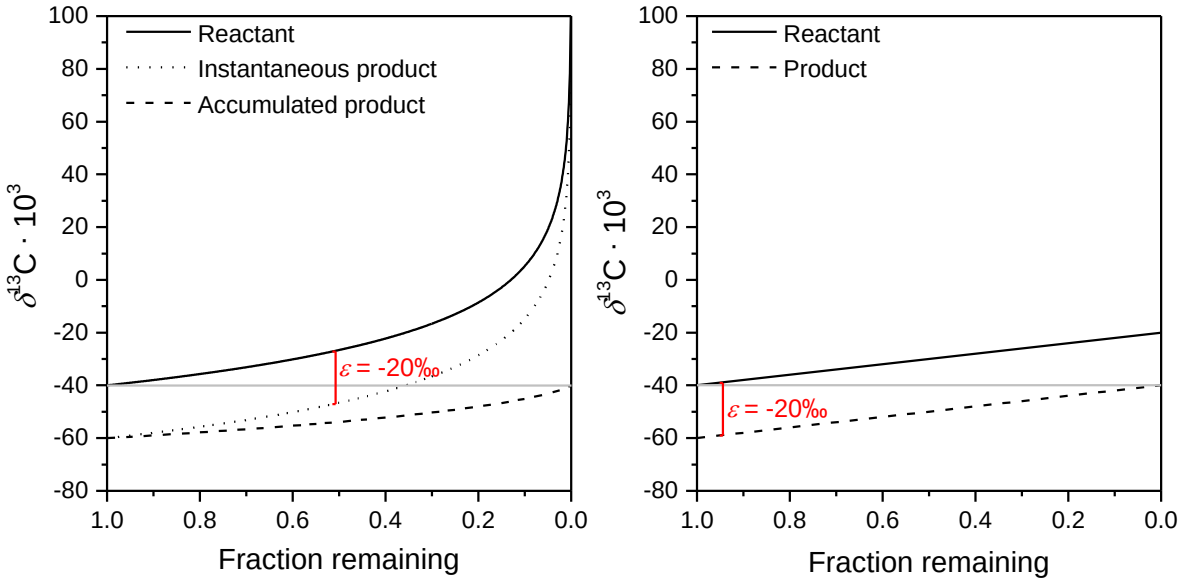

Figure 1-7 Principle of isotopic fractionation in a closed (left) and an open system (right) The course of the isotopic composition of a reactant with an initial value of $\delta^{13}C$= -40‰ is shown for an isotopic enrichment factor of ε = -20‰ along with the corresponding instantaneous and accumulated product for a closed system (left side) and the product for an open system (right side).

An important example of a *KIE* is isotopic fractionation by diffusion, which is also a mass dependent isotope effect. Fick's first law of diffusion describes the net flux density of a compound (J_c) through a unit surface area as follows.

$$J_c = -D_c \frac{dc_c}{dx} \tag{1.4.31}$$

Where dc/dx is the concentration gradient of the compound and D_c is the diffusion coefficient of the compound in m^2s^{-1}. The diffusion coefficient is directly proportional to the square root of temperature and the square root of the reciprocal of the reduced mass of the compound.

$$D_c \propto \sqrt{\frac{k_B T}{\mu}} \tag{1.4.32}$$

Where k_B is the Boltzmann constant, T the temperature in K, and μ is the reduced mass. Thus the isotopic fractionation factor α can be calculated by (1.4.33) for example for methane and carbon dioxide in air.

$$\alpha_{\text{diff}} = \frac{{}^{h}D}{{}^{l}D} = \sqrt{\frac{{}^{l}\mu}{{}^{h}\mu}} = \sqrt{\frac{{}^{h}M_A + M_B}{{}^{h}M_A \cdot M_B} \cdot \frac{{}^{l}M_A \cdot M_B}{{}^{l}M_A + M_B}} \tag{1.4.33}$$

According to the equation given above, the theoretical isotopic fractionation factor by diffusion α_{diff} for $^{13}CH_4$, and $^{13}CO_2$ in air (28.8 $gmol^{-1}$) corresponds to $\alpha_{\text{diff}}\left({}^{13}C_{{}^{13}CH_4-air}\right) = 0.9809$ and $\alpha_{\text{diff}}\left({}^{13}C_{{}^{13}CO_2-air}\right) = 0.9956$, respectively.

1.4.2 Instrumentation

Common instruments for stable isotope analysis are magnetic sector field instruments also termed isotope ratio mass spectrometer (IRMS). Prior to SIA, the compound of interest has to be transformed into a measurement gas such as CO_2 for carbon, N_2 for nitrogen, CO for oxygen, and H_2 for hydrogen. An IRMS is composed of an ion source, a mass analyzer, and a detector. In the ion source the measurement gases are transformed into positively charged molecules (e.g. CO_2^+) by electron ionization (EI). The efficiency for a molecule being ionized in this way is $\sim 10^{-3}$. An example for CO_2 is:

$$CO_2 + 1e^- \rightarrow CO_2^{+\cdot} + 2e^- \tag{1.4.34}$$

Afterwards, the ions are accelerated by a repeller and focused by electronic lenses, and are transferred to the mass analyzer. In principle, the ions are separated by their momentum but when considering the ions have the same velocity the mass analyzer separates them by their mass-to-charge ratio (m/z) in a magnetic field. Based on the Lorentz force, the ion trajectory occurs on different radii (r) by the following:

$$r = \frac{1}{B}\sqrt{\frac{2 \cdot m \cdot U}{z \cdot e}} \tag{1.4.35}$$

where B is the magnetic field, U the accelerating voltage, m the mass of the ion, z the charge of the ion, and e the elementary charge.

Depending on their radii, the ions enter a set of Faraday cups in the detector and result in a respective signal. In case of CO_2, the three m/z ratios 44, 45, and 46 are measured. The three m/z ratios correspond to an identical molecule (carbon dioxide) in which only the isotopic composition differs, also termed isotopologue.

m/z 44: $^{12}C^{16}O^{16}O^{+\cdot}$

m/z 45: $^{13}C^{16}O^{16}O^{+\cdot}$, $^{12}C^{16}O^{17}O^{+\cdot}$, $^{12}C^{17}O^{16}O^{+\cdot}$

m/z 46: $^{13}C^{17}O^{16}O^{+\cdot}$, $^{13}C^{16}O^{17}O^{+\cdot}$, $^{12}C^{18}O^{16}O^{+\cdot}$, $^{12}C^{16}O^{18}O^{+\cdot}$, $^{12}C^{17}O^{17}O^{+\cdot}$

However, it is not possible to determine the isotopic ratio for carbon or for oxygen from CO_2 directly. This is due to the different possible isotopologues of m/z 45 and m/z 46. A solution for the determination of the isotopic ratio of carbon by considering oxygen has been addressed by Santrock et al. (1985). In brief, one may consider the ratios of the different isotopes for oxygen and carbon (i.e. $^{18}R = {}^{18}O$, $^{17}R = {}^{17}O$, etc.). For this purpose, the isotopic abundances (F) of the corresponding isotopologues of CO_2 of a certain m/z are divided by the isotopic abundance of m/z=44. For example, the ratio ^{45}R is calculated as follows:

Abundance of m/z 45: $^{45}F = {}^{13}C^{16}O^{16}O^{+\cdot} + 2\left({}^{12}C^{16}O^{17}O^{+\cdot}\right)$

$$^{45}R = \frac{^{45}F}{^{44}F} = \frac{^{13}C^{16}O^{16}O^{+\cdot} + 2\left(^{12}C^{16}O^{17}O^{+\cdot}\right)}{^{12}C^{16}O^{16}O^{+\cdot}} = {}^{13}C + 2\,{}^{17}O = \underline{^{13}R + 2\,{}^{17}R}$$

The calculation of ^{18}R, ^{17}R, and ^{13}R can be achieved by a series of calculations based on the ratios ^{45}R and ^{46}R.

$$^{45}R = {}^{13}R + 2\,{}^{17}R \tag{1.4.36}$$

$$^{46}R = 2\,{}^{18}R + 2\,{}^{13}R\,{}^{17}R + {}^{17}R^2 \tag{1.4.37}$$

Substitution of ^{17}R by an equation concerning the isotopic fractionation factor of oxygen (α) (Santrock et al., 1985) gives:

$$^{17}R = {}^{18}R^{\alpha}K \tag{1.4.38}$$

with

$$K = \frac{^{18}R^{\alpha}_{\mathrm{SMOW}}}{^{17}R_{\mathrm{SMOW}}} \tag{1.4.39}$$

where K represents the relationship of ^{17}R and ^{18}R in the terrestrial oxygen pool (Santrock et al., 1985) as related to the meteoric water line. Combining (1.4.36) and (1.4.37) with the respective substitution (1.4.38) returns the following:

$$2\,^{18}R^{\alpha}K\,^{45}R - 3\,^{18}R^{2\alpha}K^{2} + 2\,^{18}R - {}^{46}R = 0 \tag{1.4.40}$$

Finally, this allows calculating ^{46}R and subsequently ^{17}R and ^{13}R but has to be solved numerically as it requires the knowledge of α and K. Along with $\alpha = 0.516$ best results of $\delta^{13}\mathrm{C}$ were determined by the relationship given by Santrock et al. (1985):

$$K = 0.04103\alpha - 0.011387 \tag{1.4.41}$$

More recently, a value of $\alpha = 0.528$ was found by Brand, Assonov, and Coplen and was stated to be more suitable for general use in $^{17}\mathrm{O}$ corrections (Brand et al., 2010).

GC-IRMS

In case of gas chromatography isotope ratio mass spectrometry (GC-IRMS) the compounds within a sample of interest are separated by a GC column and are afterwards oxidized in a combustion oven. For carbon analysis, the oven consisting of an aluminum oxide tube usually contains Pt, Ni, and Cu wires. Nickel and copper are oxidized with oxygen to NiO and CuO and serve as an oxygen reservoir for the platinum catalyzed oxidation of the compounds at around 940-960°C. Subsequently the resulting H_2O is removed by a Nafion™ membrane water trap to reduce interferences by $CO_2H^{+\cdot}$ and instrument wear-off. Finally, CO_2 is transferred to the MS by an open split. If nitrogen containing analytes are measured an optional reduction reactor can be utilized. Elemental copper (heated at ~600°C) reduces the nitrous oxides from the combustion process to N_2 and thus reduces isobaric interferences of CO_2 in the IRMS.

LC-IRMS

In liquid chromatography isotope ratio mass spectrometry (LC-IRMS) the analysis is restricted to aqueous solutions as the mobile phase, as carbon from organic solvents would severely overload

the ion source of the MS and also overlap with the signal of the compound of interest. However, the application of high temperature LC can be used. At elevated temperatures the elution strength of an aqueous eluent increases caused by the decrease of static permittivity of water(Yang et al., 1998). The oxidation of the analytes after separation by LC is performed by peroxodisulfate at 99.9°C in presence of phosphoric acid. Afterwards H_2O, CO_2 and other gases are transferred by pervaporation into a helium gas stream which is dried via a Nafion™ membrane before entering the IRMS by an open split.

1.4.3 Stable isotope analysis at landfill sites

The analysis of stable carbon isotopes in landfill studies has been applied for various purposes including the estimation of fractionation between produced CO_2 from methane oxidation and anaerobically produced CH_4 (Zyakun et al., 2010), estimation of biodegradation based on the stable isotopic signature of anaerobic and emitted methane ((Liptay et al., 1998)), and for the assessment of waste stability by analysis of landfill leachate (Mohammadzadeh et al., 2005; Wimmer et al., 2013). Figure 1-8 summarizes characteristic ranges of delta values of ^{2}H and ^{13}C for methane of different origins.

The characteristic isotopic composition of methane derived from the anaerobic zone of the waste material in landfills is usually around $\delta^{13}C$ = -50‰ to $\delta^{13}C$ = -61‰ (Chanton et al., 1999; Scheutz et al., 2009). Thus based on SIA, methane from landfill gas may be distinguished from other sources of methane. Apart from stable isotope analysis, another possibility to differentiate landfill gas methane from other sources such as thermogenic methane is the analysis of ^{14}C activity. This is because municipal waste contains ^{14}C while the amounts of ^{14}C in thermogenic CH_4 are negligible (Aelion et al., 2010).

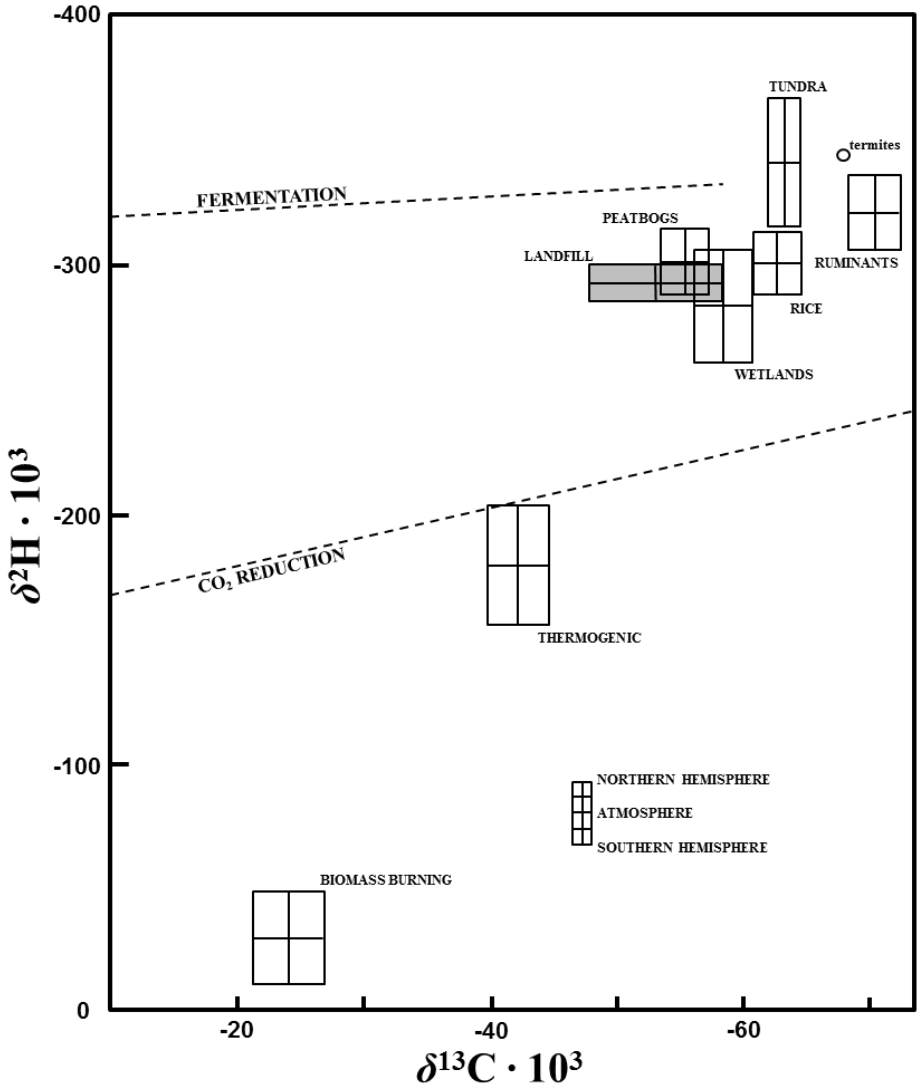

Figure 1-8 ^2H and ^{13}C dual isotope plot on CH_4 of different origins redrawn and modified from (Wahlen, 1993)

For the estimation of biodegradation the isotopic enrichment factor usually has to be known (see (1.4.27) and (1.4.30)). Different approaches for its determination have been applied both in the field and in the laboratory. In the field, *KIEs* are often estimated by a top to bottom approach (see (Scheutz et al., 2009)). One example for the top to bottom approach is the determination of both the concentration and the $\delta^{13}C$ value of methane from the anaerobic zone of the landfill body (e.g., from a gas well) and the partially oxidized CH_4 at the soil surface (e.g., by using a static chamber). The chamber technique is a technique where the topsoil is covered with a hood or chamber and the accumulating methane is measured over time (e.g., (Abichou et al., 2006)). In the lab, *KIEs* can be determined from batch incubations. Table 1-3 summarizes selected values for lab and field studies for different methane oxidizing materials and cell cultures of different environmental origin.

Table 1-3 Isotopic enrichment factors and kinetic isotope effects of methane oxidation

Experiment	°C	$10^3 \cdot (\varepsilon \pm \sigma)$	$10^3 \cdot CI(\varepsilon)$	$CI(KIE)$	n	approach	method	Reference
Pure cultures								
Methylococcus capsulatus (Cu rich)	45	-27.9 ± 1.7	-27.9 ± 4.2	1.029 ± 0.004	3	batch sacr.	$\ln(R/R_0)/\ln(C/C_0)$	(Feisthauer et al., 2011)
Methylosinus sporium (Cu rich)	30	-18.8 ± 1.4	-18.8 ± 3.5	1.019 ± 0.003	3	batch sacr.	$\ln(R/R_0)/\ln(C/C_0)$	(Feisthauer et al., 2011)
Methylocystis parvus (Cu rich)	30	-19.1 ± 1	-19.1 ± 2.5	1.019 ± 0.003	3	batch sacr.	$\ln(R/R_0)/\ln(C/C_0)$	(Feisthauer et al., 2011)
Methylomonas methanica (Cu rich)	30	-27.7 ± 2.3	-27.7 ± 5.7	1.028 ± 0.006	3	batch sacr.	$\ln(R/R_0)/\ln(C/C_0)$	(Feisthauer et al., 2011)
Methylocaldum gracile (with Cu)	30	-14.8 ± 0.9	-14.8 ± 2.2	1.015 ± 0.002	3	batch sacr.	$\ln(R/R_0)/\ln(C/C_0)$	(Feisthauer et al., 2011)
Methylococcus capsulatus (Cu free)	45	-22.9 ± 3.2	-22.9 ± 7.9	1.023 ± 0.008	3	batch sacr.	$\ln(R/R_0)/\ln(C/C_0)$	(Feisthauer et al., 2011)
Methylosinus sporium (Cu free)	30	-21.5 ± 2.7	-21.5 ± 6.7	1.022 ± 0.007	3	batch sacr.	$\ln(R/R_0)/\ln(C/C_0)$	(Feisthauer et al., 2011)
Methylomonas methanica (with Cu)	22±1	6*	-	-	-	open system	$\Delta\delta^{13}C_{\text{biomass-CO}_2}$	(Templeton et al., 2006)
Methylosinus trichosporium OB3b (with Cu)	22±1	15*	-	-	-	open system	$\Delta\delta^{13}C_{\text{biomass-CO}_2}$	(Templeton et al., 2006)
Enrichment cultures								
Shane seep	15	-26.6 ± 1.6	-26.6 ± 4.0	1.027 ± 0.004	3	batch inc.	$\ln(R/R_0)/\ln(C/C_0)$	(Kinnaman et al., 2007)
Brian seep	15	-24.9 ± 1.2	-24.9 ± 3.0	1.026 ± 0.003	3	batch inc.	$\ln(R/R_0)/\ln(C/C_0)$	(Kinnaman et al., 2007)
Drip tray ice-making machine	26	-24.6 ± 0.7	-24.6 ± 1.7	1.025 ± 0.002	3	batch inc.	$10^3 \cdot \delta^{13}C/\ln(C/C_0)$	(Coleman et al., 1981)
Drip tray ice-making	11.5	-12.8 ± 0.2	-12.8 ± 0.5	1.013 ± 0	3	batch inc.	$10^3 \cdot \delta^{13}C/\ln(C/C_0)$	(Coleman et al., 1981)

machine								
"gassy water well"	26	-23.8 ± 1.4	-23.8 ± 3.6	1.024 ± 0.004	3	batch inc.	$10^3 \cdot \delta^{13}C/\ln(C/C_0)$	(Coleman et al., 1981)
"gassy water well"	26	-15.4 ± 0.3	-15.4 ± 0.7	1.016 ± 0.001	3	batch inc.	$10^3 \cdot \delta^{13}C/\ln(C/C_0)$	(Coleman et al., 1981)
Tap water type I	21	-24.2 ± 0.7	-24.2 ± 1.7	1.025 ± 0.002	3	batch sacr.	$\ln(R/R_0)/\ln(C/C_0)$	this study
Tap water type II	21	-20.4 ± 2.8	-20.4 ± 7.0	1.021 ± 0.007	3	batch sacr.	$\ln(R/R_0)/\ln(C/C_0)$	this study
Tap water type I	30	-20.2 ± 3	-20.2 ± 7.5	1.021 ± 0.008	3	batch sacr.	$\ln(R/R_0)/\ln(C/C_0)$	this study
Tap water type II	30	-23.2 ± 2	-23.2 ± 5.0	1.024 ± 0.005	3	batch sacr.	$\ln(R/R_0)/\ln(C/C_0)$	this study
Tap water mixed methanotrophs	22	-13.6 ± 3.6	-13.6 ± 3.0	1.014 ± 0.003	8	batch inc.	$\ln(R/R_0)/\ln(C/C_0)$	this study
Mixed methanotrophs	22±1	15*	-	-	-	batch inc.	$\Delta\delta^{13}C_{\text{biomass-CO}_2}$	(Templeton et al., 2006)
Stream sediment	23±3	-	-	1.005 – 1.031‡	5	batch inc.	$\alpha_{CH_4\text{-}CO_2} = {}^{13}R_{CH_4} / {}^{13}R_{CO_2} \approx \Delta\delta^{13}C_{CH_4\text{-}CO_2}$	(Barker and Fritz, 1981)
Landfill covers/filter materials								
Clay	8	-38.6 ± 11.3	-38.6 ± 101.7	1.040 ± 0.012	2	batch inc.	$10^3 \cdot \delta^{13}C/\ln(C/C_0)$	(Chanton and Liptay, 2000)
Clay	12	-35.8 ± 2.5	-35.8 ± 22.7	1.037 ± 0.003	2	batch inc.	$10^3 \cdot \delta^{13}C/\ln(C/C_0)$	(Chanton and Liptay, 2000)
Clay	24	-34.5 ± 2.1	-34.5 ± 18.4	1.036 ± 0.002	2	batch inc.	$10^3 \cdot \delta^{13}C/\ln(C/C_0)$	(Chanton and Liptay, 2000)
Clay	35	-35.2 ± 1.5	-35.2 ± 13.1	1.036 ± 0.002	2	batch inc.	$10^3 \cdot \delta^{13}C/\ln(C/C_0)$	(Chanton and Liptay, 2000)
Mulch	8	-29.3 ± 0.6	-29.3 ± 5.7	1.030 ± 0.001	2	batch inc.	$10^3 \cdot \delta^{13}C/\ln(C/C_0)$	(Chanton and Liptay, 2000)
Mulch	12	-31.2 ± 1	-31.2 ± 9.3	1.032 ± 0.001	2	batch inc.	$10^3 \cdot \delta^{13}C/\ln(C/C_0)$	(Chanton and Liptay, 2000)

Mulch	24	-27.2 ± 0.4	-27.2 ± 3.5	1.028 ± 0	2	batch inc.	$10^3 \cdot \delta^{13}C/\ln(C/C_0)$	(Chanton and Liptay, 2000)
Mulch	35	-24.6 ± 0.9	-24.6 ± 8.3	1.025 ± 0.001	2	batch inc.	$10^3 \cdot \delta^{13}C/\ln(C/C_0)$	(Chanton and Liptay, 2000)
Biofilter sand/compost	22	-17.7 ± 0.5	-17.7 ± 0.8	1.018 ± 0.001	4	batch inc.	$\log(ppmV)/\log(10^3 \cdot \delta^{13}C + 10^3)$	(Powelson et al., 2007)
Biofilter sand/compost	22	-23.8 ± 0.6	-23.8 ± 0.9	1.024 ± 0.001	4	batch inc.	$\log(ppmV)/\log(10^3 \cdot \delta^{13}C + 10^3)$	(Powelson et al., 2007)
Topsoil + enrichment culture	22	-20.2 ± 4.6	-20.2 ± 3.7	1.021 ± 0.004	14	batch inc.	$\ln(R/R_0)/\ln(C/C_0)$	this study
Topsoil + enrichment culture	30	-23.1 ± 5.1	-23.1 ± 3.2	1.024 ± 0.003	20	batch inc.	$\ln(R/R_0)/\ln(C/C_0)$	this study
Iowa	24	-31.8 ± 2.2	-31.8 ± 20	1.033 ± 0.021	2	batch inc.	$\ln(C)/\ln(10^3 \cdot \delta^{13}C + 10^3)$	(Chanton et al., 2008a)
Outer Loop Unit 5	25	-25.8 ± 0.1	-25.8 ± 1.2	1.026 ± 0.001	2	batch inc.	$\ln(C)/\ln(10^3 \cdot \delta^{13}C + 10^3)$	(Chanton et al., 2008a)
Peoria 1	26	-23.9 ± 1.4	-23.9 ± 4.2	1.024 ± 0.004	3	batch inc.	$\ln(C)/\ln(10^3 \cdot \delta^{13}C + 10^3)$	(Chanton et al., 2008a)
Peoria 2	24	-46.3 ± 0.8	-46.3 ± 2.4	1.049 ± 0.003	3	batch inc.	$\ln(C)/\ln(10^3 \cdot \delta^{13}C + 10^3)$	(Chanton et al., 2008a)
Springhill 10-20 cm	6	-27.8 ± 8.5	-27.8 ± 76.8	1.029 ± 0.081	2	batch inc.	$\ln(C)/\ln(10^3 \cdot \delta^{13}C + 10^3)$	(Chanton et al., 2008a)
Springhill 10-20 cm	15	-28.3 ± 3.9	-28.3 ± 34.6	1.029 ± 0.037	2	batch inc.	$\ln(C)/\ln(10^3 \cdot \delta^{13}C + 10^3)$	(Chanton et al., 2008a)
Springhill 10-20 cm 1	25	-30.7 ± 0.2	-30.7 ± 2.2	1.032 ± 0.002	2	batch inc.	$\ln(C)/\ln(10^3 \cdot \delta^{13}C + 10^3)$	(Chanton et al., 2008a)
Springhill 10-20 cm 2	25	-26.4 ± 1.7	-26.4 ± 15.6	1.027 ± 0.016	2	batch inc.	$\ln(C)/\ln(10^3 \cdot \delta^{13}C + 10^3)$	(Chanton et al., 2008a)
Springhill 10-20 cm	33	-28.7 ± 3.2	-28.7 ± 29	1.03 ± 0.031	2	batch inc.	$\ln(C)/\ln(10^3 \cdot \delta^{13}C + 10^3)$	(Chanton et al., 2008a)
Springhill 10-20 cm	43	-30.2 ± 0.3	-30.2 ± 2.3	1.031 ± 0.002	2	batch inc.	$\ln(C)/\ln(10^3 \cdot \delta^{13}C + 10^3)$	(Chanton et al., 2008a)
Springhill 20-30 cm	6	-37.5 ± 3.8	-37.5 ± 33.9	1.039 ± 0.037	2	batch inc.	$\ln(C)/\ln(10^3 \cdot \delta^{13}C + 10^3)$	(Chanton et al., 2008a)

Springhill 20-30 cm	15	-29.2 ± 0.8	-29.2 ± 7.5	1.03 ± 0.008	2	batch inc.	$\ln(C)/\ln(10^3 \cdot \delta^{13}C + 10^3)$	(Chanton et al., 2008a)
Springhill 20-30 cm 1	25	-31.8 ± 1.2	-31.8 ± 10.5	1.033 ± 0.011	2	batch inc.	$\ln(C)/\ln(10^3 \cdot \delta^{13}C + 10^3)$	(Chanton et al., 2008a)
Springhill 20-30 cm 2	25	-25 ± 0.5	-25 ± 4.6	1.026 ± 0.005	2	batch inc.	$\ln(C)/\ln(10^3 \cdot \delta^{13}C + 10^3)$	(Chanton et al., 2008a)
Springhill 20-30 cm	33	-25.3 ± 1.2	-25.3 ± 10.3	1.026 ± 0.011	2	batch inc.	$\ln(C)/\ln(10^3 \cdot \delta^{13}C + 10^3)$	(Chanton et al., 2008a)
Springhill 20-30 cm	43	-27.5 ± 3.4	-27.5 ± 30.3	1.028 ± 0.032	2	batch inc.	$\ln(C)/\ln(10^3 \cdot \delta^{13}C + 10^3)$	(Chanton et al., 2008a)
Belgian landfill	n.r.			1.017 ± 0.001		batch inc.	$\ln(C/C_0)/\ln(R/R_0)$	(Mahieu et al., 2006)
Dutch landfill	n.r.			1.019 ± 0.002		batch inc.	$\ln(C/C_0)/\ln(R/R_0)$	(Mahieu et al., 2006)
Swedish landfills				1.023-1.038		static chamber	$10^3 \cdot \delta^{13}C/\ln(C/C_0)$	(Börjesson et al., 2001)
Filborna	5-20	-	-	1.018-1.021*	-	batch inc.	$10^3 \cdot \delta^{13}C/\ln(C/C_0)$	(Börjesson et al., 2007)
Heljestorp	3-20	-	-	1.034-1.023*	-	batch inc.	$10^3 \cdot \delta^{13}C/\ln(C/C_0)$	(Börjesson et al., 2007)
Högbytorp	3-20	-	-	1.023-1.019*	-	batch inc.	$10^3 \cdot \delta^{13}C/\ln(C/C_0)$	(Börjesson et al., 2007)
Sundsvall	3-20	-	-	1.034-1.022*	-	batch inc.	$10^3 \cdot \delta^{13}C/\ln(C/C_0)$	(Börjesson et al., 2007)
Hagby	3-20	-	-	1.026-1.021*	-	batch inc.	$10^3 \cdot \delta^{13}C/\ln(C/C_0)$	(Börjesson et al., 2007)
Visby	3-20	-	-	1.020-1.017*	-	batch inc.	$10^3 \cdot \delta^{13}C/\ln(C/C_0)$	(Börjesson et al., 2007)
Tundra soil								
Permafrost (polygon tundra soil) 1.5 vol.-%	4	-30.1 ± 1.9	-30.1 ± 4.7	1.031 ± 0.005	3	batch inc.	$10^3 \cdot \delta^{13}C/\ln(C/C_0)$	(Preuss et al., 2013)
Permafrost (polygon tundra soil) 1.5 vol.-%	4	-22.5 ± 1.9	-22.5 ± 4.7	1.023 ± 0.005	3	batch inc.	$10^3 \cdot \delta^{13}C/\ln(C/C_0)$	(Preuss et al., 2013)
Permafrost (polygon tundra soil) 1.5 vol.-%	4	-5 ± 1	-5 ± 2.5	1.005 ± 0.002	3	batch inc.	$10^3 \cdot \delta^{13}C/\ln(C/C_0)$	(Preuss et al., 2013)

Permafrost (polygon tundra soil) 1.5 vol.-%	4	-8.9 ± 6.9	-8.9 ± 17.1	1.009 ± 0.017	3	batch inc.	$10^3 \cdot \delta^{13}C/\ln(C/C_0)$	(Preuss et al., 2013)
Permafrost (polygon tundra soil) 1.5 vol.-%	4	-16.7 ± 1	-16.7 ± 2.4	1.017 ± 0.002	3	batch inc.	$10^3 \cdot \delta^{13}C/\ln(C/C_0)$	(Preuss et al., 2013)
Permafrost (polygon tundra soil) 1.5 vol.-%	4	-19.6 ± 1.9	-19.6 ± 4.8	1.02 ± 0.005	3	batch inc.	$10^3 \cdot \delta^{13}C/\ln(C/C_0)$	(Preuss et al., 2013)
Alaska	4	-26	-	1.027	-	flux chamber	-	(King et al., 1989)
Alaska	14	-16	-	1.016	-	flux chamber	-	(King et al., 1989)
Forest soils								
Pullman, Washington, USA	17	-17.8 ± 0.4	-17.8 ± 1	1.018 ± 0.001	3	flux chamber	$\ln(R/R_0)/\ln(C/C_0)$	(Snover and Quay, 2000)
Leigh woods, England		-13.6 ± 1	-13.6 ± 2.4	1.022 ± 0.002	3	soil probe	flux ratio; top bottom;	(Maxfield et al., 2008)
Bronydd Mawr, Wales		-13.6 ± 1.9	-13.6 ± 4.8	1.021 ± 0.005	3	soil probe	$10^3 \cdot \delta^{13}C /\ln(C/C_0)$	(Maxfield et al., 2008)
Grassland								
Seattle, Washington, USA	21	-17 ± 1	-17 ± 2.4	1.017 ± 0.002	3	flux chamber	$\ln(R/R_0)/\ln(C/C_0)$	(Snover and Quay, 2000)
Lakes								
Artificial lake/water column	15-20[+]	-13.3 ± 2.9	-13.3 ± 7.2	1.013 ± 0.007	3	top bottom (closed system)	-	(Nitzsche et al., 2009)
Lake/water column	5/20	-18.1 to -20.4	-	1.0184-1.0208	4	batch inc.	$10^3 \cdot \delta^{13}C/\ln(C/C_0)$	(Bastviken et al., 2002)
Artic lake				1.02 - 1.06	-	top bottom (open system)		(Cadieux et al., 2016)

CI: Confidence intervals were determined by error propagation from reported standard deviations and degrees of freedom unless stated otherwise or given in the reference; [*]: Isotopic fractionation between biomass and carbon dioxide, [+]: Values estimated from graphs; [‡]: Isotopic fractionation between CH_4 and CO_2; sacr. batch: sacrificial batch; batch inc.: batch incubation

2 Scope of the thesis

In this thesis, the focus was on the investigation of the bacterial methane oxidation for landfill studies by stable isotope analysis. Apart from the knowledge of the isotopic composition of anaerobic and emitted methane the isotopic enrichment factor (ε) is required for stable isotope analysis in order to estimate the biodegradation. While at landfill sites the isotopic signature of the anaerobic methane is easily determined, and usually within a narrow range, the isotopic signature of the emitted CH_4 and even more the isotopic enrichment factor is highly variable. In SIA the isotopic enrichment factor has the largest impact on the calculated biodegradation. However, the value of the isotopic enrichment factor for the bacterial methane oxidation reported in the literature is variable and has been stated to depend on several factors.

Different factors that have been reported to influence the isotopic enrichment factor (temperature, type of methanotroph, and diffusion processes) were investigated in this thesis in order to clarify their potential impact on ε as well as the consequences for the estimation of biodegradation under varying conditions. The isotopic enrichment factor of methane by diffusion along with its diffusion coefficient is determined experimentally for a potential cover layer material in chapter 3. The results are discussed and compared with the literature, and possible implications for the estimation of the bacterial methane oxidation in the field are addressed. Chapter 4 addresses the issue of variability in detail by investigating the ^{13}C isotopic enrichment factor of methane oxidation for different experimental setups and respective conditions including type of methanotrophic enrichment culture and temperature. The results are compared with observations and trends reported in the literature by statistical means. Possible considerations for field measurements are discussed.

Several approaches and techniques for the estimation of the methane oxidation of landfill cover layers have been utilized for lab and field studies. Among these, stable carbon isotope analysis of CH_4 represents one possibility. In contrast to quantitative methods, this method is generally not prone to dilution processes such as landfill gas migration or mixing with atmospheric air. In chapter 5, topsoil serves as a methane oxidation layer for a laboratory experiment, which investigates three common scenarios in the aftercare phase of a landfill. The methane oxidation capacity is evaluated and compared with different methods including mass balance, stoichiometric considerations, and stable isotope analysis. In the latter case, the essential isotopic enrichment factors determined in chapter 3 and 4 were incorporated in the calculations.

Chapter 6 includes the profiling of the concentration of CH_4 and CO_2 and their isotopic composition. Based on the CO_2/CH_4 ratio and by applying closed system calculations for stable isotopes the methanotrophic activity within a new reactor setup is located within the system and compared with results from thermographic imaging.

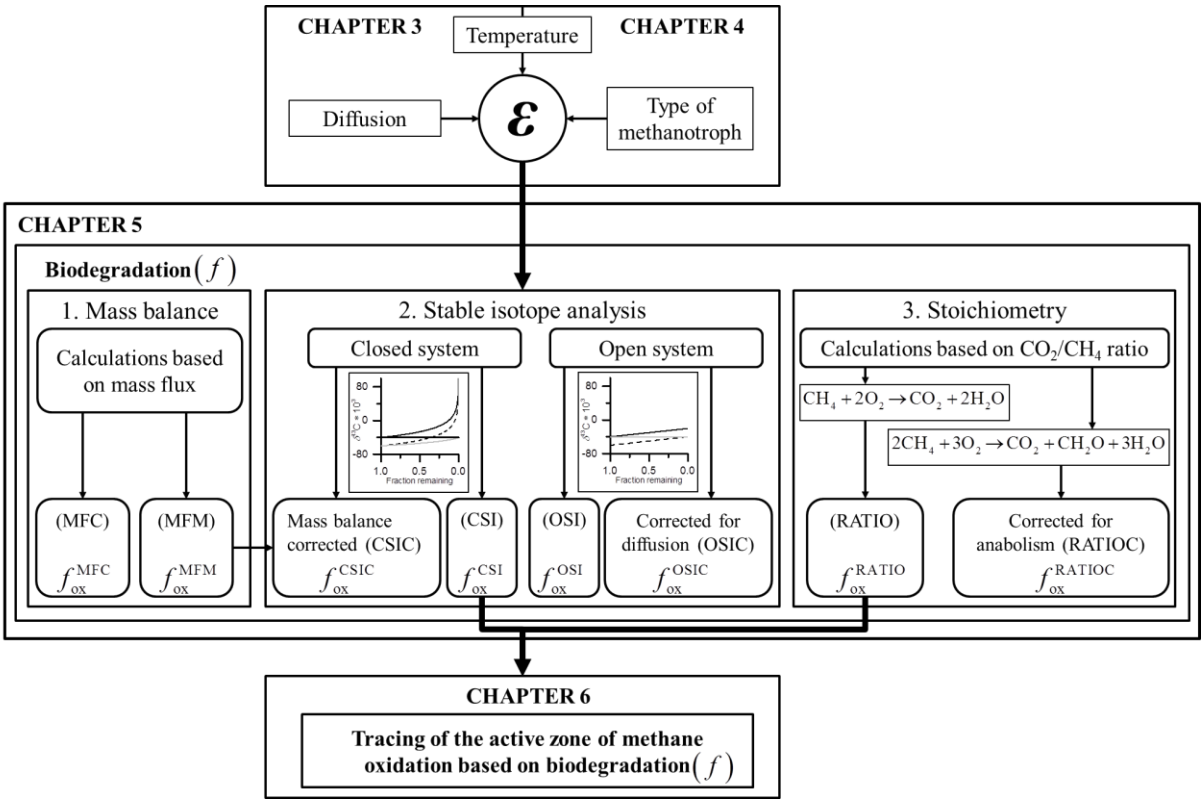

Figure 2-1 Schematic overview of the experimental topics addressed in the individual chapters

Summarized is the experimental work of chapters three to six. In chapter three the isotopic enrichment factor of diffusion was determined for a potential cover material. In chapter four, temperature and type of methanotroph were investigated with respect to their influence on the isotopic enrichment factor. These two chapters are the basis for chapters five and six, as the knowledge of the isotopic enrichment factor is essential for the calculation of the biodegradation based on stable isotopes. In chapter five, the biodegradation of methane by a potential cover material was calculated by three main approaches. Finally in chapter 6, the biological active zone of methane oxidation could be located and identified based on the results in chapter five (by stable isotopes and stoichiometry). The arrows indicate the link within or between different chapters.

3 Evaluating the isotopic fractionation by diffusion for a potential cover material

3.1 Introduction

Stable isotope analysis can be utilized for the estimation of biodegradation in the environment. Apart from biodegradation and dilution, diffusion processes can play an important role in the environmental fate of a compound. As diffusion can affect the isotopic composition of a compound, forecasting its effect is very important for adequate estimation of biodegradation by stable isotope analysis. Several studies on the fate of contaminants in the vadose zone (e.g. volatile organic compounds) have addressed different effects such as diffusion, dilution, and biodegradation by modelling approaches (Bouchard et al., 2011; Bouchard et al., 2008; Hunkeler et al., 2004; Pasteris et al., 2002; Van De Steene and Hohener, 2009). Also, the stable carbon isotopic composition of carbon dioxide in soil gas (Cerling et al., 1991) has been determined. With respect to landfill cover soils the diffusion coefficients of oxygen in different landfill cover materials have been investigated and diffusion coefficients increased exponentially with increasing air-filled porosity space (Gebert et al., 2011a). In case of methane and its fate in terms of stable carbon isotopic composition and concentration in landfill cover layers, models have been developed earlier (De Visscher and Van Cleemput, 2003; Mahieu et al., 2008). For methane, the diffusion coefficient and the kinetic isotope effect by diffusion of methane have been determined in column studies (De Visscher, 2004; Gebert et al., 2013). In the study by De Visscher the respective values determined at 25°C were $D_m = 5.56 \cdot 10^{-2}\ cm^2 s^{-1}$ and $KIE_{diff} = 1.0178 \pm 0.0009$ (De Visscher, 2004). In this case, the value of the isotopic fractionation factor by diffusion was close to the theoretical value of methane in air of $KIE_{diff} = 1.0195$. In the study by Gebert et al., the kinetic isotope effect by diffusion of methane increased with decreasing level of compaction from $KIE_{diff} = 1.008$ to 1.016 (Gebert et al., 2013). Also, diffusion coefficients for methane determined for different horizons of permafrost soil increased exponentially with an increase of air-filled pore space (Preuss et al., 2013). The kinetic isotope effect by diffusion of methane in the permafrost soil ranged from $KIE_{diff} = 1.007$ to 1.018 (Preuss et al., 2013).

The aim of this study was to determine the diffusion coefficient of methane in a potential cover material. In addition, the isotopic enrichment factor by diffusion of methane in the reactor body should be determined. Both are important parameters for reactive gas transport modeling (see (Mahieu et al., 2008)) and for the determination of the biodegradation by stable isotope analysis of methane in landfill cover soils.

3.2 Experimental setup

The experiments were performed in 20 L stainless steel batch reactors (see Figure 3-1). It was filled with 15 kg of basaltic rock and 400 g of autoclaved topsoil. This mixture had a void fraction of 60%. The reactor had eight vertical sampling ports (SP1-SP8) with 6 cm of spacing between each. The sampling ports were sealed with butyl-rubber septa. In the lower part of the reactor a gas space was created to dispense the injected methane gas homogenously before the diffusion process started. For this purpose, two metal sieve layers and a perforated metal plate were installed which separated the porous medium from the gas space. This resulted in an air-filled space of 3.0 L with a height of 8.8 cm. At the top, the batch reactor was kept open to maintain a concentration gradient. Stainless steel cannulas of 80 mm length (Sarstedt AG und Co., Nümbrecht, Germany), were inserted into the sampling ports SP1-SP4. The basalt rock/topsoil mixture was placed into the reactor in layers to allow the insertion of the sampling cannulas and the measurement of their respective height. These were at 5 cm, 9 cm, 14 cm, and 20 cm above the gas/soil boundary. An additional inlet located at the very bottom of the batch reactor was used for flushing the reactor with nitrogen after every experiment. It also served as the injection point for the methane gas. At the beginning of every run, 20 mL of methane were inserted from below and concentration profiles were measured directly by GC-FID from different sampling points SP1-SP6. The experiments with GC-FID were performed at 22.5°C. As the sensitivity of the GC-IRMS system was lower, 40 mL were injected instead during every run. The experiments with GC-IRMS were performed at 22.5°C and 30°C.

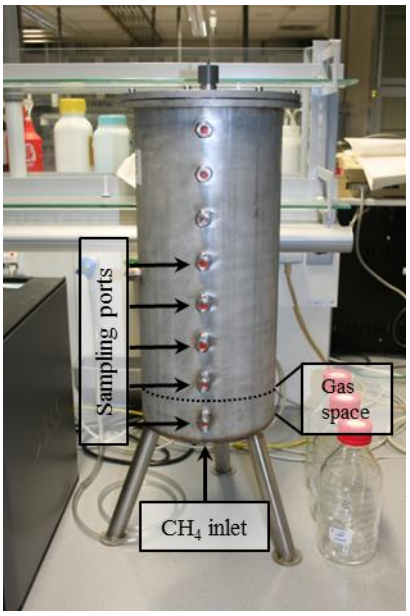

Figure 3-1 Batch reactor system for degradation and diffusion experiments
Picture of the modified reactor for the diffusion experiment. Methane was injected into the gas space in the lower part of the reactor from below. Sampling ports sealed with butyl rubber septa and with equal spacing were used for sample withdrawal by 80 mm cannulas. The respective sampling distances above the gas space were 5, 9, 14, and 20 cm. Note the lid was removed during the experiments.

3.3 Quantitative and stable isotope analysis

3.3.1 GC-FID

Concentration profiles were obtained from GC-FID measurements (Shimadzu GC-2014) using a 30-m FS-Supreme-5 column with an inner diameter of 0.25 mm and a film thickness of 0.25 µm (CS - Chromatographie Service GmbH, Langerwehe, Germany). Injector and oven temperature were 30°C. Nitrogen of 5.0 quality served as the carrier gas (Air Liquide, Düsseldorf, Germany). The column flow was 1.9 mL min^{-1} and the split ratio was 50. The detector's temperature was set to 280 °C with a sampling rate of 80 ms^{-1}.

3.3.2 GC-IRMS

Gas concentrations and stable isotope composition of CH_4 and CO_2 were determined by means of GC-IRMS. The gas samples were analyzed with a GC Trace Ultra (Thermo Fisher Scientific, Bremen, Germany) using a 30-m Qbond column with an inner diameter of 0.32 mm and a film thickness of 10 µm (Restek GmbH, Bad Homburg, Germany). The helium carrier gas flow was 1.6 mL min^{-1} and the split ratio 100. Samples were taken with a 0.5-mL gas tight syringe (Vici Precision Sampling, Baton Rouge, USA). In case of degradation experiments, the injection volumes were varied depending on methane concentration. For diffusion experiments the injection volume was 0.5 mL. Following the separation by GC and combustion with Pt/Ni/Cu at

960°C via a GC-Combustion III Interface (Thermo Fisher Scientific, Bremen, Germany) the stable carbon isotope composition of the combustion product CO_2 was measured by a MAT 253 isotope ratio mass spectrometer (Thermo Fisher Scientific, Bremen, Germany). The reported $\delta^{13}C$ values are relative to the CO_2 reference gas. The samples were measured at a minimum in triplicates.

3.4 Data acquisition and calculations

For data acquisition and processing the software Isodat 2.5 was used. Microsoft Excel 2010 and OriginPro 2015G were used for tabular calculations, statistical testing, model fits, and construction of graphics. The model fits for the diffusion experiment were based on the calculations described in (De Visscher, 2004) with:

$$C_i = C_{i,0} e^{\left(\frac{z\theta}{L} + \frac{\theta D_i}{L^2} t\right)} erfc\left(\frac{z}{2}\sqrt{\frac{\theta}{D_i t}} + \frac{\sqrt{\theta D_i t}}{L}\right) \tag{3.4.1}$$

Here, C_i is the concentration at time i, $C_{i,0}$ the initial methane concentration in the gas space, z the sampling height, L the height of the gas space below the basalt rock/topsoil mixture, θ the void fraction, t the time, and D_i the diffusion coefficient.

Similar to (Preuss et al., 2013) but with isotopic ratios instead of delta values the isotopic enrichment factors of diffusion were determined by the following equation, where R_0 and R are the ratios of initial reactant and of reactant at time t, and c_0 and c are the concentrations of the initial reactant and of the reactant at time t.

$$\ln\frac{R}{R_0} = \varepsilon \cdot \ln\frac{c}{c_0} \tag{3.4.2}$$

3.5 Results and discussion

The concentration profiles and respective diffusion coefficients of methane were determined at 22.5°C with a GC-FID prior to the experiments on the isotopic enrichment factor by diffusion by GC-IRMS. The results are given in Figure 3-2 and Table 3-1. The diffusion coefficients D_m were determined from a model fit based on equation (3.4.1). The average value ± standard deviation of the determined diffusion coefficient in this setup was $(6.17 \pm 0.46) \cdot 10^{-2}$ cm^2s^{-1}. This is in the same order of magnitude and within 1.5σ of the value of $5.54 \cdot 10^{-2} cm^2s^{-1}$ determined by De Visscher (2004).

At 0 cm and 5 cm sampling height the determined diffusion coefficients of $5.79 \cdot 10^{-2} cm^2 s^{-1}$ and $5.63 \cdot 10^{-2} cm^2 s^{-1}$ were closest to the reported value by De Visscher, but the determined values at 9, 14, and 20 cm were higher. This may be due to an increased compaction of the substrate in the lower part of the reactor which would reduce the air-filled porosity of the basalt rock/flower soil mixture.

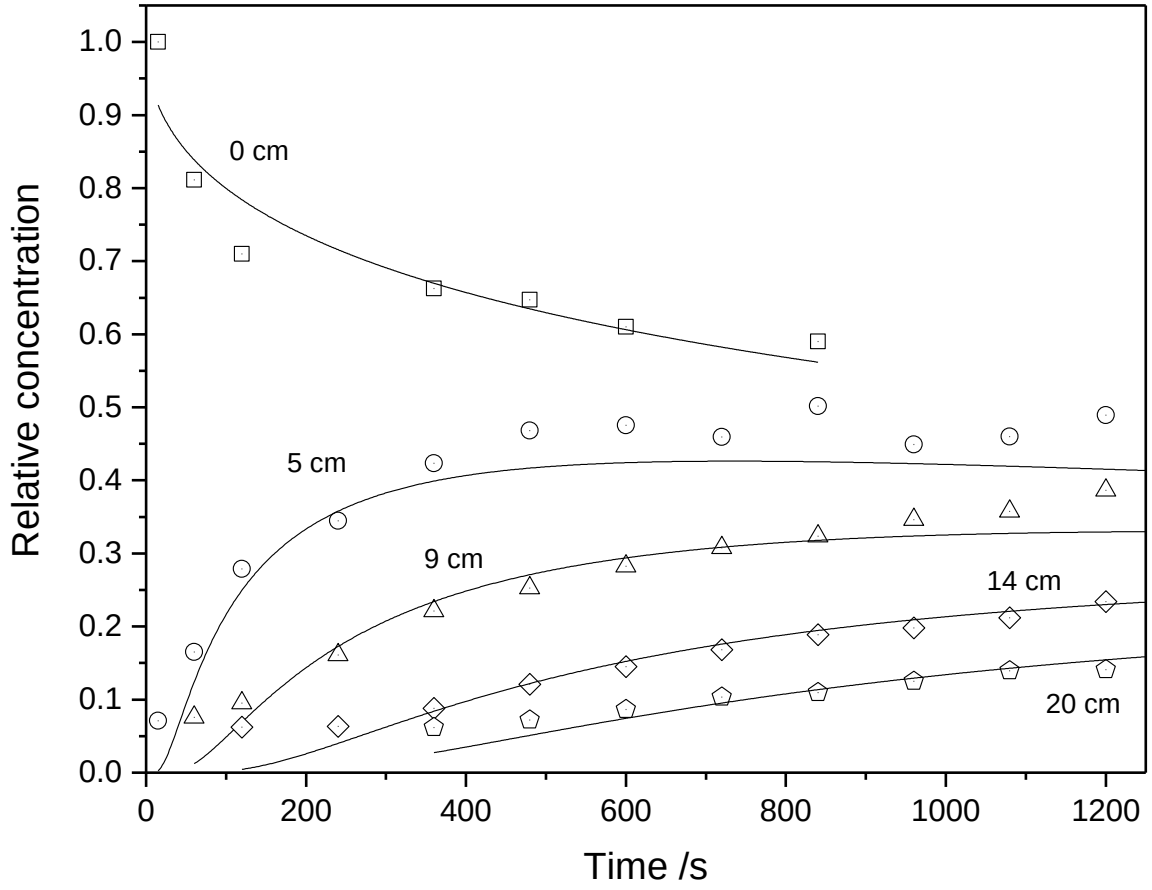

Figure 3-2 Concentration profiles of the diffusion experiment by GC-FID at 22.5°C
Depicted by different symbols are the relative methane concentration profiles for the gas space (at 0 cm) and the sampling heights above the gas space (5 - 20 cm). The black lines correspond to the fit based on (3.4.1).

Table 3-1 Diffusion coefficients of methane determined by GC-FID at 22.5°C
The diffusion coefficients determined based on the model described by De Visscher (2004) at the respective sampling heights are listed along with the corrected correlation coefficients.

z /cm	D_m /10^{-2}cm^{2}s^{-1}	$R^2_{corrected}$
0	**5.79**	**0.88**
5	**5.63**	**0.82**
9	**6.58**	**0.89**
14	**6.23**	**0.92**
20	**7.55**	**0.73**

The results of the experiments analyzed by GC-IRMS are depicted in Figure 3-3. The concentration profiles are shown along with the respective isotopic signature of methane. The average diffusion coefficient at 22.5°C was $D_{m,\,22.5°C} = 6.09 \cdot 10^{-2}$ cm^{2}s^{-1} and is thus comparable with De Visscher's results at 25°C ($D_{m,\,25°C} = 5.54 \cdot 10^{-2}$cm^{2}s^{-1} (De Visscher, 2004)). At 22.5°C the fits (red line) of the concentration profiles (blue symbols) show varying correlations with average values of $R^2_{corrected} = 0.85$ for 0 cm, $R^2_{corrected} = 0.61$ for 9 cm, and $R^2_{corrected} = 0.91$ for 14 cm. Similar to the previous experiment, the diffusion coefficients at 22.5°C for z = 0 cm and z = 9 cm are in good agreement with the reported value by De Visscher. Again, at greater distance from the methane inlet with z = 14 cm the value of $D_{m,\,22.5°C} = (7.02 \pm 0.67) \cdot 10^{-2}$ cm^{2}s^{-1} differs (by 2.2σ) somewhat from De Visscher's result.

At 30°C the average value for the diffusion coefficient was $D_{m,\,30°C} = (8.13 \pm 0.88) \cdot 10^{-2}$ cm^{2}s^{-1} and thus is larger than at 22.5°C. This is as expected from the increase in temperature and the following proportionality:

$$D \propto \sqrt{\frac{kT}{\mu}} \tag{3.4.3}$$

However, the diffusion coefficient $D_{m,\,30°C} = (8.13 \pm 0.88) \cdot 10^{-2}$ cm^{2}s^{-1} is much larger than the expected value of $D_m = 7.11 \cdot 10^{-2}$ cm^{2}s^{-1} that would result from the change in temperature from 22.5°C to 30°C (as calculated by multiplying $D_{m,\,22.5°C}$ by the factor $\sqrt{\frac{303.15\text{K}}{295.65\text{K}}} \approx 1.013$). The determined diffusion coefficients are summarized in Table 3-2.

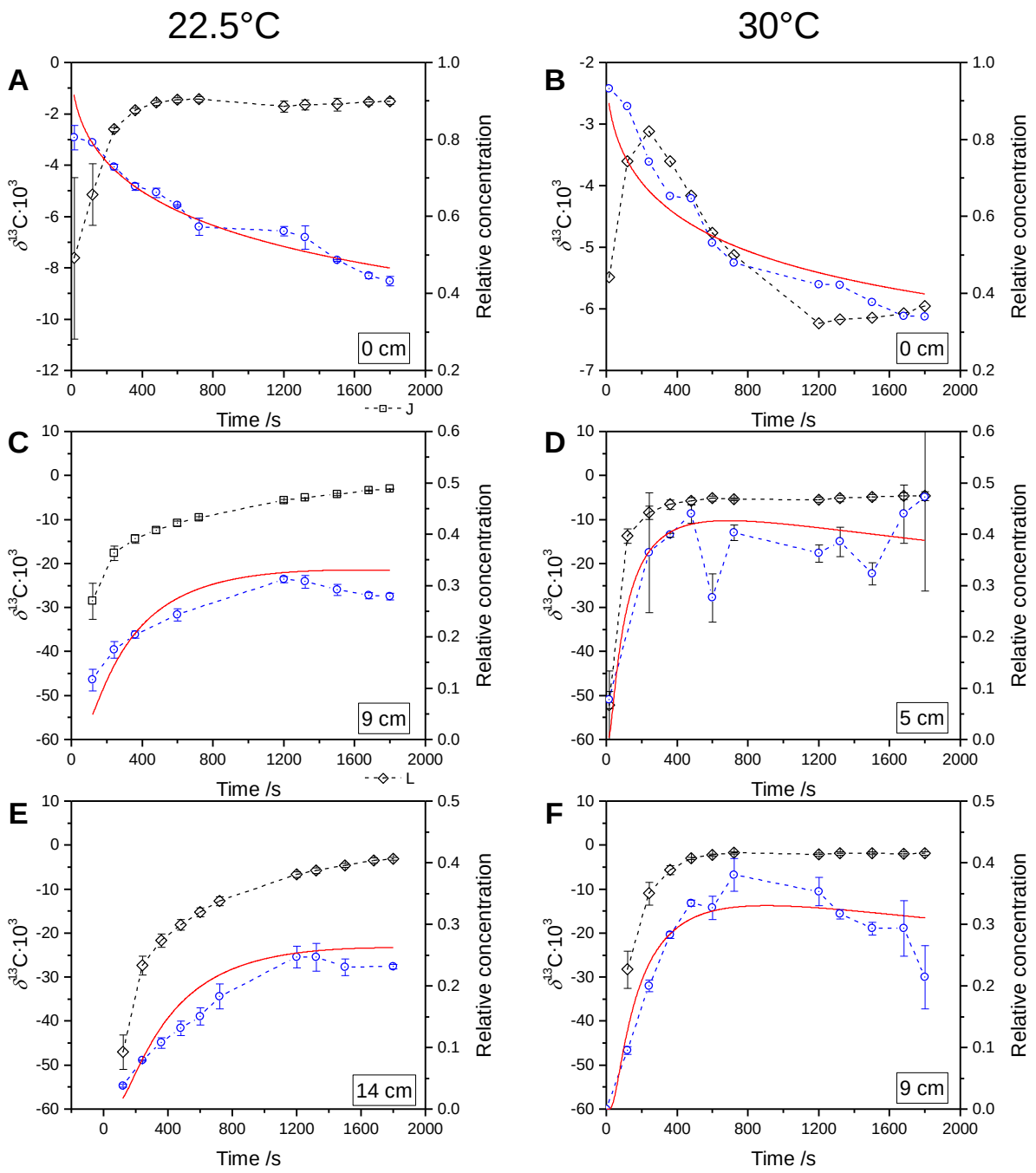

Figure 3-3 Diffusion experiment by GC-IRMS at 22.5°C and 30°C

Depicted are relative concentrations of methane (c/c_0) represented by blue symbols and stable carbon isotopic composition profiles of methane by black symbols at the indicated sampling heights above the bottom gas space for 22.5°C (left side) and 30°C (right side). Red lines correspond to the fit based on (3.4.1).

Table 3-2 Diffusion coefficients of methane determined by GC-IRMS
The mean diffusion coefficients of three individual experiments and determined based on the model described by De Visscher (2004) at the respective sampling heights are listed along with their standard deviations. Value for a single measurement is indicated with an asterisk at z = 0 at 30°C.

z /cm	22.5°C		30°C	
	D_m /10^{-2}cm^{2}s^{-1}	$R^2_{corrected}$	D_m /10^{-2}cm^{2}s^{-1}	$R^2_{corrected}$
0	**5.47 ± 0.51**	**0.85**	**7.33***	**0.90***
5	**-**	**-**	**7.57 ± 1.28**	**0.85**
9	**5.78 ± 0.79**	**0.61**	**8.96 ± 0.36**	**0.88**
14	**7.02 ± 0.67**	**0.91**	**-**	**-**

Next to the obtained diffusion coefficients, the data from GC-IRMS were used to determine the isotopic fractionation factor by diffusion of methane. In Figure 3-4 the isotopic fractionation factors were determined from the slope of the regression line. At 22.5°C the average isotopic enrichment factor of diffusion was ε_{diff} = -0.0212 ± 0.005 and at 30°C ε_{diff} = -0.0218 ± 0.003.

Although the values for 22.5°C and 30°C are higher than the theoretical value of the isotopic fractionation by diffusion of methane in air (ε_{diff} = -0.01909), the theoretical value is within the range of the mean ± standard deviation of 22.5°C and 30°C. The determined values for ε_{diff} are also comparable with the results in (De Visscher, 2004; Gebert et al., 2013; Preuss et al., 2013). On the contrary, isotopic enrichment factors for diffusion can be highly variable. For example, Preuss et al. (2013) obtained values for KIE_{diff} ranging from KIE_{diff}= 1.007 to KIE_{diff}= 1.018 at room temperature and at 20°C for an arctic wetland soil at unsaturated conditions. These *KIEs* correspond to ε_{diff} = -0.007 and ε_{diff} = -0.018, respectively.

Table 3-3 Isotopic enrichment factors determined by GC-IRMS

z /cm	ε_{diff} at 22.5°C	$R^2_{corrected}$	ε_{diff} at 30°C	$R^2_{corrected}$
0	**-0.0150**	**0.95**	**-**	**-**
5	**-**	**-**	**-0.0237**	**0.82**
9	**-0.0251**	**0.95**	**-0.0198**	**0.89**
14	**-0.0236**	**0.98**	**-**	**-**

The isotopic enrichment factor of diffusion was determined for the respective sampling heights. Values were determined from triplicate measurements.

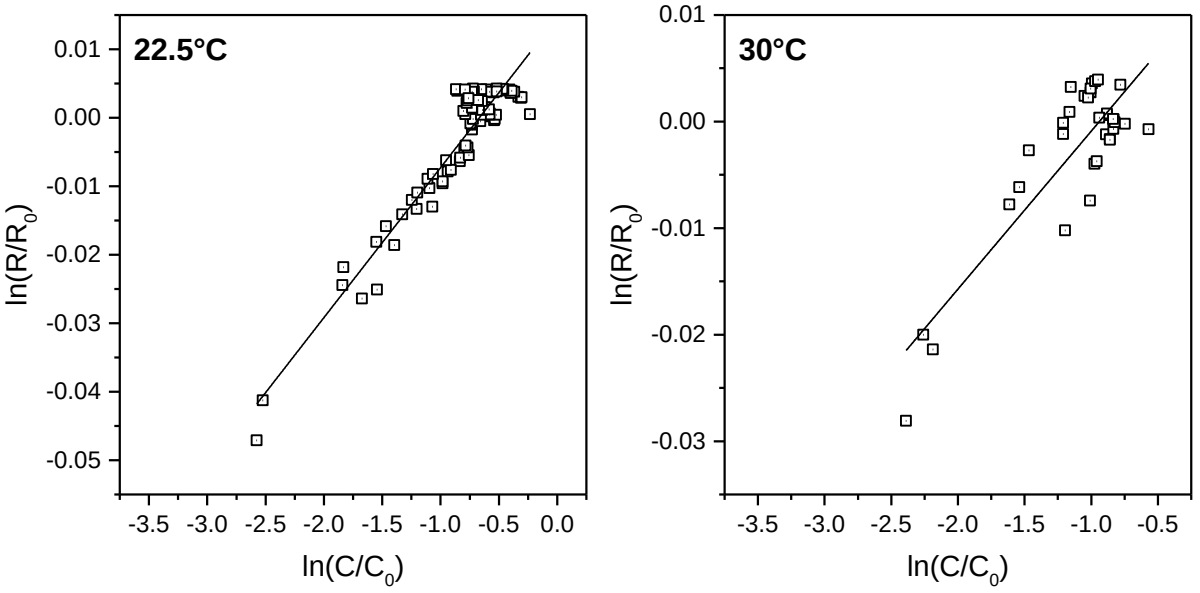

Figure 3-4 Double logarithmic plot for the determination of ε_{diff}
For 22.5°C an average value of ε_{diff} = -0.0219 was determined based on the results obtained from the sampling ports at 0, 9, and 14 cm. In case of 30°C only the first five sampling times for 5 cm and 9 cm (15-600 s) were used. The average value at 30°C was ε_{diff} = -0.0218.

3.6 Conclusion

The given reactor setup proved to be suitable for the determination of the diffusion coefficient. With an average value of $D_{m,\ 22.5°C} = (6.17 \pm 0.46) \cdot 10^{-2}$ cm^{2}s^{-1} by GC-FID, and average values of $D_{m,\ 22.5°C} = (6.09 \pm 0.8) \cdot 10^{-2}$ cm^{2}s^{-1} and $D_{m,\ 30°C} = (8.13 \pm 0.88) \cdot 10^{-2}$ cm^{2}s^{-1} by GC-IRMS these values are very well comparable with the literature value of $D_{m,\ 25°C} = 5.54 \cdot 10^{-2}$cm^{2}s^{-1} (De Visscher, 2004) as well as values given in (Preuss et al., 2013). Additionally, the theoretical value of isotopic fractionation by diffusion of CH_4 in air (ε_{diff} = -0.0191) is within the range of standard deviation of the experimentally determined values of ε_{diff} = -0.0212 ± 0.005 at 22.5°C and ε_{diff} = -0.0218 ± 0.003 at 30°C. Since the determined values are of the same order of magnitude as reported values for isotopic enrichment factors of bacterial methane oxidation (see Table 1-3) they require consideration for the estimation of the biodegradation by landfill cover soils. Yet, appointing a fixed value to ε_{diff} seems problematic. This is because the determined values for ε_{diff} as well as reported values for ε_{diff} are variable. Also, the presence or absence of diffusion processes within cover materials cannot be generalized as the physical and chemical conditions of the top layer - especially in terms of gas permeability - are influenced by many external factors (e.g., changing weather conditions, and degree of vegetation). Additionally, the presence of gas extraction systems will increase the inward flow of air which alters the gas flow through the top cover. As a consequence, including the diffusion coefficient within the

calculations will allow determining a more exact value for the biodegradation under well-known conditions. In contrast, a conservative and more secure value, in terms of estimating the maximum emissions of CH_4 from the cover to the atmosphere, will result from the calculations if diffusion is excluded for poorly characterized cover layers and unknown conditions of gas flow.

4 Isotopic enrichment factors of bacterial methane oxidation

4.1 Introduction

At landfill sites the biodegradation of methane can be estimated from stable isotope analysis. For this purpose, the isotopic signature of methane both from the anaerobic zone and from the surface of the cover layer or near the soil-gas boundary have to be determined. It also requires the knowledge of the isotopic enrichment factor of the bacterial methane oxidation (ε). The carbon isotopic enrichment factor of the bacterial methane oxidation has been determined for different environments such as forest soils (Maxfield et al., 2008), from water columns in lakes (Bastviken et al., 2002; Nitzsche et al., 2009), natural grassland (Snover and Quay, 2000), arctic wetland soils (Preuss et al., 2013), and landfill cover materials. Many factors have shown to influence the bacterial methane oxidation by changing the cover material's physical and chemical properties (Huber-Humer et al., 2008; Scheutz et al., 2009). Among others, these include temperature, soil moisture, soil gas permeability, and ammonia content (Boeckx et al., 1996; Huber-Humer et al., 2008; Scheutz et al., 2009). In case of temperature, one of the major driving factors of methane oxidation, it has been reported to also affect the isotopic enrichment factor of methane oxidation (Börjesson et al., 2007; Chanton and Liptay, 2000; Chanton et al., 2008a; Coleman et al., 1981; Powelson et al., 2007; Tyler et al., 1994). Also, the applied landfill cover materials such as mulch, compost, and several soils show different isotopic enrichment factors as summarized in (Chanton et al., 2008a). The values for the isotope enrichment factors for landfill cover soils show a high variability (see Table 1-3). In addition, the isotopic enrichment factor depends on the type of the expressed methane monooxygenase (MMO). The particulate MMO is expressed if copper is available for the bacteria while under copper limiting conditions the soluble MMO is expressed (Stanley et al., 1983). Jahnke et al. (1999) discovered that the particulate MMO shows a higher discrimination for heavy methane than the soluble MMO. In a study by Feisthauer et al. (2011), isotopic enrichment factors for ^{13}C and ^{2}H have been reported for pure bacterial strains expressing either sMMO or pMMO. Apart from temperature and type of MMO, isotopic enrichment factors have also been reported to be cell density dependent (Kampara et al., 2009; Templeton et al., 2006). However, this has been discussed controversially (Nihous, 2008; Nihous, 2010) and may as well be due to specific experimental setups (Nihous, 2010). Furthermore, in the oxidation zone of landfill covers the bacterial population may be regarded to be under steady state conditions (Chanton et al., 2008a). Thus, while the isotopic enrichment factor may be applied for the estimation of biodegradation by stable isotope analysis, it often is determined individually for each specific cover material and site. A temperature dependency of the isotopic enrichment factor of methane oxidation has been reported earlier

(Börjesson et al., 2001; Börjesson et al., 2007; Chanton and Liptay, 2000; Chanton et al., 2008a)and a correction has been suggested by (Chanton et al., 2008a) based on a literature review and own experimental data. In certain studies, the suggested temperature correction was applied (Preuss et al., 2013) for isotopic enrichment factors determined at temperatures that were different from the actual conditions on site (e.g. in the lab instead of in the field). The determination of the isotopic enrichment factor is performed by batch degradation experiments in a closed system, in general. These include the determination in one system or container (Börjesson et al., 2007; De Visscher et al., 1999; Powelson et al., 2007), or by sacrificial sampling of single batch containers such as serum flasks (Feisthauer et al., 2011).

Considering the different isotopic enrichment factors for different soils and bacterial strains, the aim of this study was to determine the isotopic fractionation factors at different initial CH_4 concentrations (a), at different temperatures for a soil with high organic carbon content amended with a mixed methanotrophic cell culture (b), and for bacterial enrichment cultures of type I and II methanotrophs (c). The possible implications of the initial CH_4 concentration, a temperature trend and a respective correction, as well as differences between types of methanotrophs on the estimation of the biodegradation should be investigated further by statistical means.

4.2 Experimental setup

4.2.1 Batch reactor experiments

The experiments were performed in 20 L stainless steel batch reactors. The reactors were filled with 15 kg of basaltic rock and 400 g of autoclaved topsoil. This mixture had a void fraction of 60%. For the degradation experiments 100 mL of a mixed methanotrophic enrichment culture was added. The gas concentrations were set by first flushing the reactors with nitrogen for 15 min to saturate the reactor's gas phase followed by the addition of oxygen (20 vol.-%) and CH_4 (8 vol.-% and 20 vol.-%) for final gas concentrations. At the top of the reactor a multilayer foil gas sampling bag served as gas reservoir. The multilayer foil gas sampling bag was composed of a 5-layer barrier of (1) 60-gauge nylon (outer layer), (2) metalized aluminum, (3) polyethylene - 0.0003", (4) aluminum foil - 0.002", and (5) polyethylene (inner layer) (Restek, Bad Homburg, Germany). Samples of 50 mL were taken from a three way stop-cock between gas bag and reactor by using a 100-mL gas tight syringe (Hamilton, Bonaduz, Switzerland) and transferred to multilayer foil gas sampling bags for later analysis. The incubation temperature was controlled by a heating sleeve which was placed around the reactor. Experiments were conducted at 30°C.

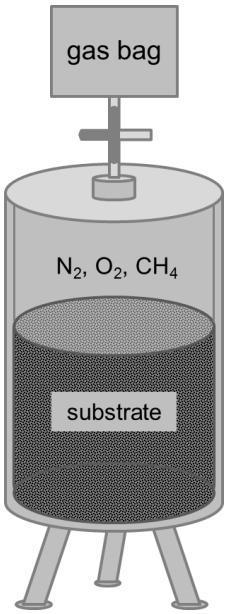

Figure 4-1 Batch reactor system for degradation experiments
Scheme of the reactor setup for the degradation experiments. Indicated is the substrate composed of a basalt rock/topsoil mixture amended with a mixed cell culture of methanotrophs. The gas bag served as a gas reservoir. Samples were taken from the three was stop-cock between gas bag and reactor.

4.2.2 Centrifuge tube experiments with topsoil

In previous experiments with stainless steel batch reactors (see also 4.2.1) CH_4 availability for the methanotrophs was limited due to diffusion processes within the reactor system. In order to increase the methane availability for the bacteria, a system was constructed in which the gas was circulated. The system for the determination of the isotopic enrichment factor by bacterial methane oxidation (ε) was constructed from different components. These included a membrane pump (Schego, Offenbach, Germany), PVC-tubing (Rehau AG und Co, Rehau, Germany), a 0.5 L multilayer gas sampling bag composed of a laminated film of 120 µm thickness of nylon, polyethylene, aluminum foil and polyethylene (GL Sciences Inc., Tokyo, Japan), two centrifuge tubes (Sarstedt AG und Co., Nümbrecht, Germany), a three way stop-cock (Sarstedt AG und Co., Nümbrecht, Germany), and luer connectors (Wolfram Droh GmbH, Mainz, Germany). The gases within the system were circulated by the membrane pump in order to prevent substrate limitation. The setup is depicted in Figure 4-2 A. The centrifuge tube was filled with 35 g of topsoil (water content: 9.7% w/w, organic dry substance: 2.2% w/w; determined from 30 g soil by standard method DIN 12880, 2001) amended with methanotrophic suspension (10 mL bacterial suspension for 500 g soil) from a filter system described by Gehrke et al. (2015), and cotton wool was placed at each end to improve gas mixing in the soil and to avoid carry-over e.g., into the membrane pump. The other tube functioned both as water trap which should avoid the

circulation of water from condensation and as a pressure reduction. In order to maintain a constant temperature, the setup was placed into a water bath in an incubator (INFORS AG, Bottmingen, Switzerland) set to 22°C (room temperature) or 30°C. 100 mL of air and 20 mL of CH_4 of 5.0 quality (Air Liquide, Düsseldorf, Germany) were injected into the setup via the three-way stopcock using a 100-mL gastight syringe (Hamilton, Bonaduz, Switzerland).

Prior to sampling, the membrane pump was switched off. Next a 0.5 mL gas tight syringe (Vici Precision Sampling, Baton Rouge, USA) was connected to the three way stop-cock. In order to allow for proper mixing of the gas, the plunger was pulled and pushed twice to minimum and maximum position (0/0.5 mL) before withdrawing the desired sample volume (0.05 - 0.5 mL). Afterwards the membrane pump was switched on again and the sample was measured by GC-IRMS. Three sets of the described system were run in parallel, and for each system methane was measured once for each sampling time point.

4.2.3 Centrifuge tube experiments with mixed methanotrophic cell cultures

A modified setup as described in 4.2.2 was used in order to perform degradation experiments with a mixed methanotrophic cell culture (Figure 4-2 B). In this case, 35 mL of cell culture were added to the centrifuge tube instead of the amended topsoil. A volume of 10 mL of air was added and CH_4 was adjusted to 7 - 8 vol.-% initial concentration with a 0.5-mL gas tight syringe. An extra setup containing the bacterial cell culture and air only served as a control for the generation of biomass. For analysis by GC-IRMS, 0.05-0.5 mL of sample was withdrawn with a gas tight syringe Vici Precision Sampling, Baton Rouge, USA). Samples were measured in triplicates. In addition to the gas samples, 200-µL samples of the liquid phase were taken from the reaction vessels at different time points and transferred into 1.5-mL screw neck glass vials with 250-µL conical glass inserts (BGB Analytik Vertrieb GmbH, Rheinfelden, Germany). These samples were stored at 4°C until further analysis by flow injection analysis (FIA) at the end of the experiment.

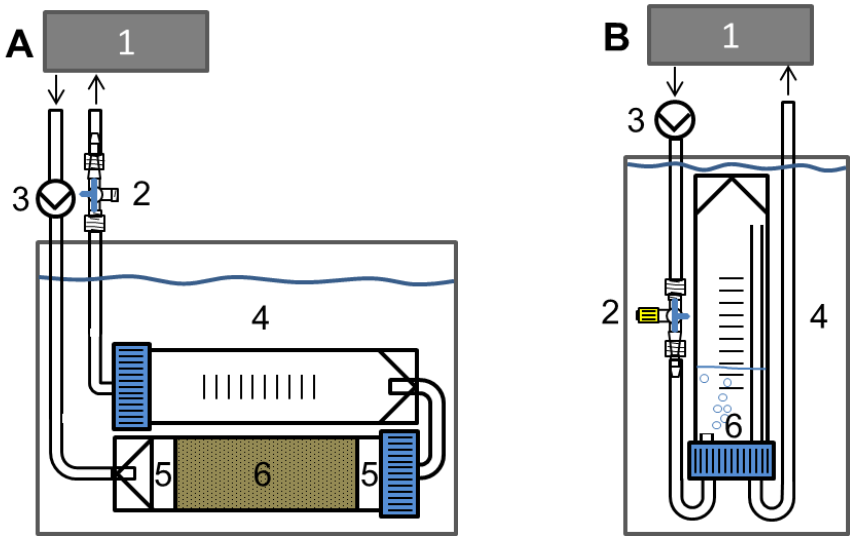

Figure 4-2 Setup of centrifuge tube experiment
The setup of the degradation experiments in centrifuge tubes with topsoil (A) and mixed methanotrophic cell culture (B) is shown schematically: (1) multilayer gas bag, (2) three-way stop cock used for sampling, (3) membrane pump, (4) water bath, (5) cotton wool, (6) topsoil amended with methanotrophic cell culture (A)/mixed methanotrophic cell culture (B)

4.2.4 Enrichment culture experiments in serum flasks

For the degradation experiments serum flasks of 118 mL volume were filled with 25 mL of bacterial suspension of either type I or type II enrichment cultures and sealed with 12 mm thick butyl rubber stoppers (Peter Oehmen GmbH, Essen, Germany) and aluminum crimp caps. For type I 5 mL, and for type II 10 mL of methane of 3.5 quality (Air Liquide, Düsseldorf, Germany) were injected with a 10-mL glass syringe (Poulten & Graf, Wertheim, Germany). Afterwards, the flasks were placed into an incubator set to 21°C (room temperature) or 30°C and shaken at 200 rpm to allow proper mixing of gas and liquid phase. Individual serum flasks were sacrificed at each sampling point for triplicate analysis by GC-IRMS after adding 1 mL of 35%-hydrochloric acid, in order to stop bacterial activity. Three independent runs of experiments for each cell type and temperature were performed unless stated otherwise.

4.3 Quantitative and stable isotope analysis

4.3.1 GC-IRMS

Gas concentrations and stable isotope composition of CH_4 and CO_2 were determined by means of GC-IRMS. The gas samples were analyzed with a GC Trace Ultra (Thermo Fisher Scientific, Bremen, Germany) using a 30-m Qbond column with an inner diameter of 0.32 mm and a film thickness of 10 µm (Restek GmbH, Bad Homburg, Germany). The helium carrier gas flow was 1.6 mL min^{-1} and the split ratio 100. Injection volumes varied between 0.05 mL and 0.5 mL

depending on the methane concentration in the sample. The GC was held at 30°C for 5 min. After separation by GC and combustion with Pt/Ni/Cu at 960°C via a GC-Combustion III Interface (Thermo Fisher Scientific, Bremen, Germany) the stable carbon isotope composition of the combustion product CO_2 was measured by a MAT 253 isotope ratio mass spectrometer (Thermo Fisher Scientific, Bremen, Germany). The reported delta values are based on the CO_2 reference gas calibrated relative to Vienna Pee Dee Belemnite (VPDB), except for the delta values of the batch reactor experiments (4.2.1) which were relative to the reference gas set to $\delta^{13}C = 0‰$. In general, the samples were measured at a minimum in triplicates.

4.3.2 Flow injection by LC-IRMS

The samples from the bacterial cell culture were analyzed by FIA with an LC-IsoLink coupled to a Delta V Advantage isotope mass spectrometer (both Thermo Fisher Scientific, Bremen, Germany). A loop of 20 µL was used for sample transfer by a six-port valve to the interface system. Phosphoric acid (85%) and sodium peroxodisulfate (both 99% purity, Fluka, Steinheim, Germany) were used to prepare the reagents for the interface. A total flow of 300 $\mu L min^{-1}$ was applied in the interface which consisted of 150 $\mu L min^{-1}$ of 1.5 M phosphoric acid and 150 $\mu L min^{-1}$ of an aqueous solution of sodium peroxodisulfate (200 $g L^{-1}$). The oxidation oven temperature was set to 99.9°C. The carrier gas flow of helium for the transfer of CO_2 was 2.3 $mL min^{-1}$.

4.4 Data acquisition, calculations, and statistics

The software Isodat 2.5 was used for data acquisition and processing. Microsoft Excel 2010 and Origin 2015G were used for tabular calculations, statistical testing, and construction of graphics.

Methods for the determination of the isotopic enrichment factor have been described in detail (Hayes, 2004; Mahieu et al., 2006; Scott et al., 2004). Based on equation (4.4.1), the isotopic enrichment factors of the microbial methane oxidation ε were obtained from linear regression of $\ln(R/R_0)$ against the natural logarithm of the remaining fraction of methane ($\ln(c/c_0)$). Also, as suggested by Elsner et al. (2005) the regression line was not forced through zero.

$$\ln\frac{R}{R_0} = \varepsilon \cdot \ln\frac{c}{c_0} \tag{4.4.1}$$

An equation for the determination of ε based on the concentration of the accumulated product $[CO_2]_i$ is given by the following in which $\delta^{13}C_{CO_2,i}$ equals the $\delta^{13}C$ value of carbon dioxide,

$\delta^{13}C_{CH_4,0}$ the initial isotopic signature of the reactant CH_4, $[CH_4]_0$ the initial concentration of CH_4, and *f* the fraction of methane (1-$[CO_2]_i/[CH_4]_0$).

$$\delta^{13}C_{CO_2,i} = \delta^{13}C_{CH_4,0} - 10^3 \varepsilon \frac{f \cdot \ln(f)}{1-f} \tag{4.4.2}$$

In certain cases, when non-methane derived carbon dioxide was present initially, the $\delta^{13}C$ values were corrected based on the following simplified isotopic mass balance.

$$n_{CO_2,\text{sample}} \cdot {}^{13}\delta_{CO_2,\text{sample}} = n_{CO_2,\text{measured}} \cdot {}^{13}\delta_{CO_2,\text{measured}} - n_{CO_2,0} \cdot {}^{13}\delta_{CO_2,0} \tag{4.4.3}$$

With $n_{CO_2,\text{sample}} = n_{CO_2,\text{measured}} - n_{CO_2,0}$ rearranging formula (4.4.3) yields the delta value of the sample.

$${}^{13}\delta_{CO_2,\text{sample}} = \frac{n_{CO_2,\text{measured}} \cdot {}^{13}\delta_{CO_2,\text{measured}} - n_{CO_2,0} \cdot {}^{13}\delta_{CO_2,0}}{n_{CO_2,\text{measured}} - n_{CO_2,0}} \tag{4.4.4}$$

For clarity and better comparison with the literature, the respective isotope enrichment factors (ε) were also recalculated into α_{ox} and then into the kinetic isotope effect (*KIE*) given as follows:

$$\alpha = \varepsilon + 1 \tag{4.4.4}$$

$$\alpha = 1/KIE \tag{4.4.5}$$

The kinetic rate constants were determined from the slope of the linear regression of $\ln(c/c_0)$ vs. *t*.

$$\ln\left(\frac{c}{c_0}\right) = -k \cdot t \tag{4.4.6}$$

The confidence intervals (*CI*) of the isotopic enrichment factors as well as kinetic rate constants were calculated and stated as described by the GUM (JCGM100:2008, 2008) as follows:

$$CI = \bar{x} \pm t_{99\%} \cdot \sigma / \sqrt{n} \tag{4.4.7}$$

x: Arithmetic mean value
$t_{99\%}$: Inverse t-value for 99% and n-1 degrees of freedom
σ: Experimental standard deviation
n: Number of observations

The statistical comparison in the given chapter focused on t-test and ANOVA.

The t-test compares mean values of sample data. Depending on the homogeneity of variance of the sample set which can be tested by F-test the t-test or a corrected version for dissimilar variances (Welch's t-test) can be applied. Also, both F- and t-test share the prerequisite that the sample data have to be normally distributed as can be investigated by several different approaches for example: By graphical means (e.g. a box and whiskers plot and a normal probability plot), by linear regression modelling (e.g. the Shapiro-Wilk test), and by investigation of kurtosis and skewness of the distribution of the sample data. In this chapter box and whiskers plots and the Shapiro-Wilk test were used for this purpose.

The Shapiro-Wilk test is a test conceptualized to test a complete sample for normality and was formerly introduced by Shapiro and Wilk (1965). It has a high power and is especially suitable for small sample sizes (Falk, 2014). The zero hypothesis H_0 is that the data are normally distributed. The test will only allow rejecting a sample set from normality but cannot prove a sample set to follow a normal distribution. Similar to a normal probability plot the sample data (x_i) are ordered by rank (y_i) and can be compared by graphical means. The Shapiro-Wilk test tests the sample data by an analysis of variance type procedure by comparing the sample data to a normal distribution based on a linear regression model. The goodness of fit can be evaluated by an F-type ratio (Shapiro and Wilk, 1965). In particular, the test score (W) corresponds to the squared slope of the probability plot regression line ($\hat{\sigma}^2$) multiplied by a constant (c) and divided by the total sum of squares (S^2) which is the squared slope of the normal probability plot.

$$W = c\frac{\hat{\sigma}^2}{S^2} \tag{4.4.8}$$

Ideally the test value (W) should be close to 1 as in case of normally distributed data both $\hat{\sigma}^2$ and S^2 should be equal. The closer W is to 1 the lower the probability that the data are not normally distributed (Shapiro and Wilk, 1965). In other terms, small values for W indicate non-normality (Falk, 2014).

4.5 Results and discussion

4.5.1 Degradation experiments batch reactors

The time dependent profiles of the concentrations and $\delta^{13}C$ values of CH_4 and CO_2 are depicted in Figure 4-3. In both cases, the concentration of methane decreases with time, and correspondingly the CO_2 concentration increases. In accordance with increasing methane consumption the isotopic fractionation increases also, which is visualized by the exponential profile of the delta values, becoming more and more positive with reaction time. In panel A II, the strong initial increase of the $\delta^{13}C$ values of CH_4 may be due to improper mixing within the reactor. This would lead to consumption of local methane without resupply. As a consequence, the isotopic fractionation appears to be a lot higher in the beginning. In case of carbon dioxide, the $\delta^{13}C$ values decrease in the beginning of the experiment up to 100 h. A possible explanation for this is the presence of atmospheric CO_2, which has a more positive delta value than the reactant. As soon as the concentration of produced carbon dioxide strongly exceeds the background values of atmospheric traces of CO_2 the delta values also become more positive at reaction times >100 h. The isotopic enrichment factors were determined from the slope of the regression line in Figure 4-5. They were ε (8 vol.-%) = -0.0263 and ε (20 vol.-%) = -0.0303.

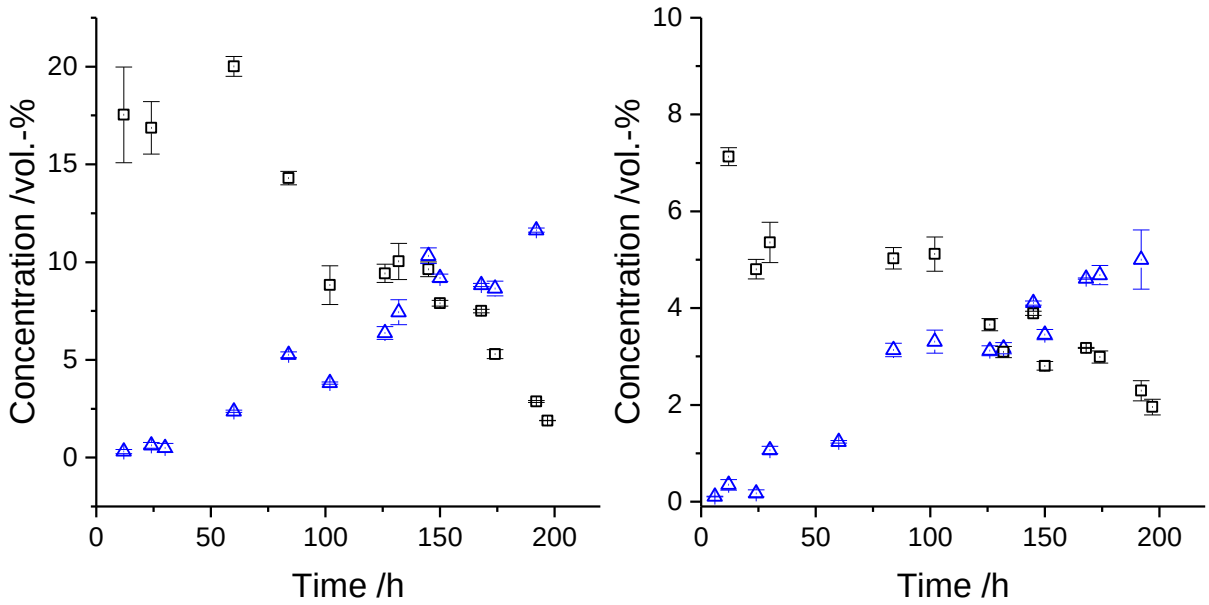

Figure 4-3 Concentration profiles of CH_4 and CO_2 in batch reactors
The change in concentration with time is shown for the two initial methane concentrations 20 vol.-% (left panel) and 8 vol.% (right panel). Black symbols are CH_4 and blue symbols are CO_2

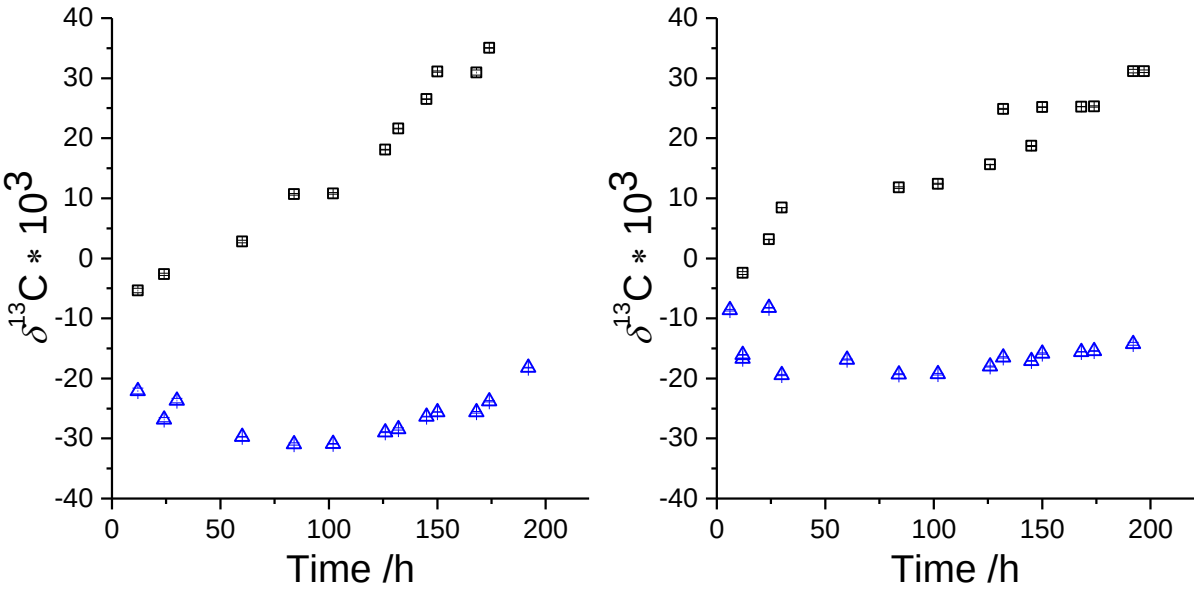

Figure 4-4 Profiles of the isotopic composition of CH_4 and CO_2 in batch reactors
The change in $\delta^{13}C$ values with time is shown for the two initial methane concentrations 20 vol.-% (left panel) and 8 vol.% (right panel). Black symbols are CH_4 and blue symbols are CO_2. Note the $\delta^{13}C$ values are relative to the CO_2 reference gas and not normalized against VPDB.

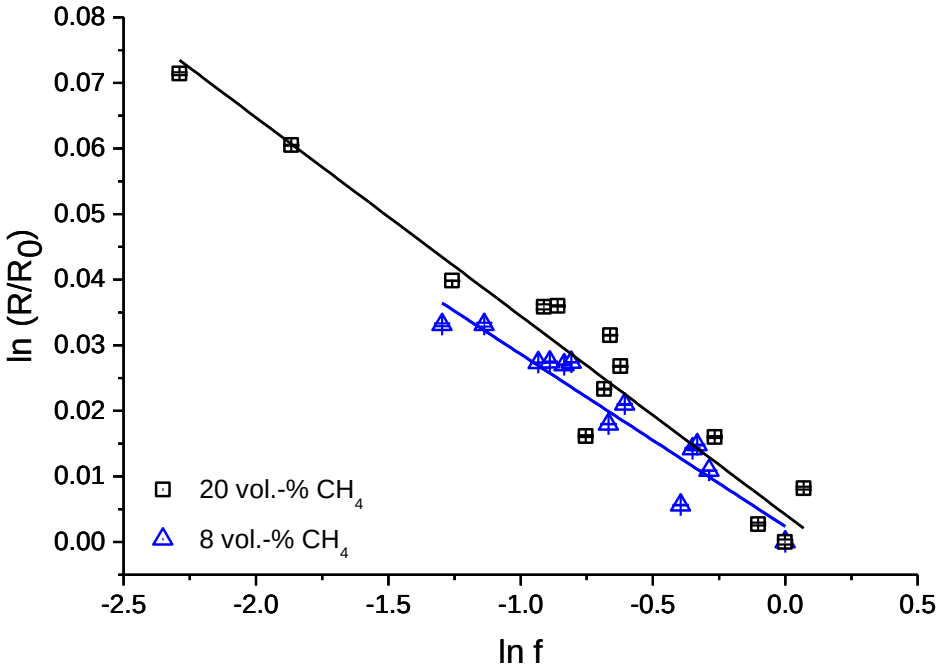

Figure 4-5 Determination of the isotopic enrichment factor from the batch reactor
The isotopic enrichment factors determined by linear regression for the two initial methane concentrations 8 vol.-% and 20 vol.-% were ε(8 vol.-%)= -0.0263 and ε(20 vol.-%)= -0.0303, respectively.

4.5.2 Centrifuge tube degradation experiments with topsoil

The development of the carbon isotopic fractionation of methane by methanotrophic degradation is depicted in Figure 4-6. It showed a characteristic behavior for a closed system Rayleigh distillation. In case of the accumulated product carbon dioxide the situation was different. In the beginning of the experiment, the offset between methane and carbon dioxide was not very high. This was due to the presence of carbon dioxide from air in the system. Towards the end of experiments, the δ^{13}C-values of carbon dioxide did not reach the expected initial value of methane. A possible cause was heterotrophic respiration - as the enrichment culture included co-cultured bacteria - and the assimilation of carbon dioxide by methanotrophs for anabolic purposes (see chapter 1.3 and Figure 1-5). A comparison of the isotopic enrichment factor assessed from the accumulated substrate CO_2 with the isotopic enrichment factor determined from the residual reactant CH_4 is therefore not feasible. However, based on methane the isotopic enrichment factors were determined from linear regression by equation (4.4.1). Figure 4-6 and Figure 4-7 show the results for the double logarithmic plots at the respective temperatures. The isotopic enrichment factors with their expanded uncertainties (calculated based on the GUM (JCGM100:2008)) with a coverage factor of $k = t_{0.99}$, and $\nu(22°C) = 13$ and $\nu(30°C) = 19$ degrees of freedom) were as follows: $\varepsilon_{22°C} = -0.0202 \pm 0.0037$ and $\varepsilon_{30°C} = -0.0231 \pm 0.0032$. Both values are well within the reported range in the literature (see Table 1-3).

In the literature concerning landfill studies, values for the isotopic fractionation are often reported as $\alpha = {}^{l}k / {}^{h}k$ and not as $\alpha = {}^{h}k / {}^{l}k$ (as in this thesis). The value $\alpha = {}^{l}k / {}^{h}k$ corresponds to the *KIE*, in case of CH_4. Consequently, for better comparison and to avoid confusion with definitions of α, the isotope enrichment factors of this study (ε_T) were converted into the respective kinetic isotopic effects $KIE_{22°C} = 1.0202 \pm 0.0013$ and $KIE_{30°C} = 1.0236 \pm 0.0012$ (for calculation see chapter 4.4).

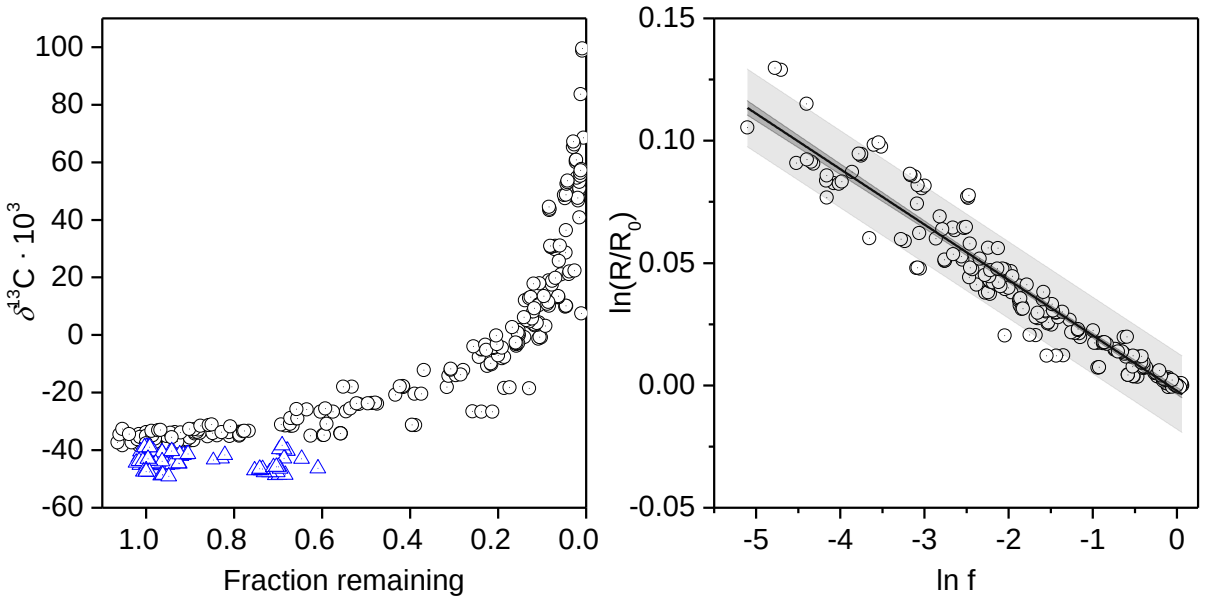

Figure 4-6 Rayleigh plot and double logarithmic plot for experiments at 22°C
The black (CH_4) and blue (CO_2) symbols are single measurements for individual experiments. On the right side the regression line is shown for the determination of the isotopic enrichment factor of the bacterial methane oxidation. The light gray area corresponds to the area of the prediction band and the dark gray area to the confidence band area. Regression line parameters: $R^2 = 0.94$; $s_y = 0.008$

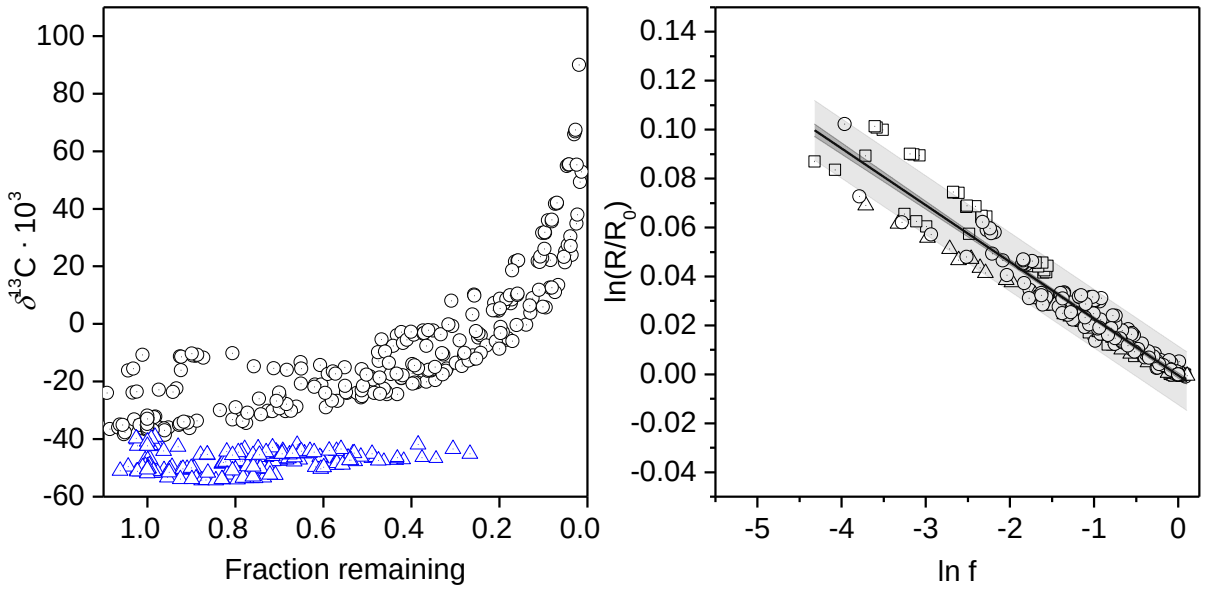

Figure 4-7: Rayleigh plot and double logarithmic plot for experiments at 30°C
The black (CH_4) and blue (CO_2) symbols are single measurements for individual experiments. On the right side the regression line is shown for the determination of the isotopic enrichment factor of the bacterial methane oxidation. The light gray area corresponds to the area of the prediction band and the dark gray area to the confidence band area. Regression line parameters: $R^2 = 0.94$; $s_y = 0.006$

Although the average values of the *KIE*s for the two temperatures are similar the individually determined values show a large span of approximately 17‰ (see Figure 4-8). When inspecting the data graphed as box and whiskers plot it becomes clear that for 22°C the box is split by the median nearly in the middle but with a slight shift to the upper end of the box. In case of 30°C, the shift of the median is more pronounced, and towards the lower end of the box. The shift shows a slight asymmetry of the distribution of the data points and indicates a possible deviation from a normal distribution. The box and whiskers plots of the two temperatures do not allow a good differentiation by visible means. Therefore, further statistical testing (by t-test) should investigate a possible difference of the *KIE*s in temperature.

As a prerequisite of investigating a possible difference of the *KIE*s for the two temperatures by a t-test the data has to follow a normal distribution. The Shapiro-Wilk test was applied to check whether a normal distribution had to be ruled out. The test results given in Table 4-1 do not reject the normal distribution of the data based on a confidence level of $1\text{-}\alpha = 99\%$. Thus it was assumed that both the F-test and t-test are applicable. As the F-test was not significant, the null hypothesis (H_0: both variances are equal) was not rejected. Therefore, the equal variance t-test was employed. The null hypothesis (H_0) was defined in such that both *KIE*s at 22°C and 30°C are equal (H_0: $\mu_{22°C} = \mu_{30°C}$, where $\mu_{22°C}$ and $\mu_{30°C}$ are the mean values of the *KIE* at 22°C and 30°C). Based on a significance level of $\alpha = 0.01$ the t-test was neither significant for H_1: $\mu_{22°C} \neq \mu_{30°C}$ nor for H_1: $\mu_{22°C} > \mu_{30°C}$ or H_1: $\mu_{22°C} < \mu_{30°C}$. Only for the values $\alpha > 0.095$ and $\alpha > 0.05$ would the test be significant for H_1: $\mu_{22°C} \neq \mu_{30°C}$ and H_1: $\mu_{22°C} < \mu_{30°C}$, respectively. Therefore, the *KIE*s of the two temperatures are rather invariant or at most $KIE_{30°C} > KIE_{22°C}$. The latter seems unrealistic because the isotopic fractionation decreases with increasing temperature, in general.

Table 4-1 Tests on normal distribution of the different isotopic fractionation factors
The individual values for KIE_T were tested for normality by the Shapiro-Wilk test with a significance level of $\alpha = 0.01$. *W* equals the test score.

KIE_T	Degrees of freedom	*W*	p-value
T = 22°C (this study)	**14**	**0.97**	**0.84**
T = 25°C (Chanton et al., 2008a)	**17**	**0.87**	**0.04**
T = 30°C (this study)	**20**	**0.91**	**0.06**

Table 4-2: F-test and equal variance two sample t-test on determined *KIE*s
The tests were performed for a significance level of α = 0.01; , degrees of freedom were n_1 = 14 (22°C), and , n_2 = 20 (30°C); $\nu = n_1+n_2-2$. Note, at this value for α neither test was significant.

	t-test			F-test		
H_0:	$\mu_{22°C} = \mu_{30°C}$			$\sigma^2_{22°C} = \sigma^2_{30°C}$		
H_1:	$\mu_{22°C} \neq \mu_{30°C}$	$\mu_{22°C} > \mu_{30°C}$	$\mu_{22°C} < \mu_{30°C}$	$\sigma^2_{22°C} \neq \sigma^2_{30°C}$	$\sigma^2_{22°C} > \sigma^2_{30°C}$	$\sigma^2_{22°C} < \sigma^2_{30°C}$
Test value	**1.72**	**1.72**	**-1.72**	**1.24**	**0.79**	**1.24**
Critical value	**2.74**	**2.45**	**2.45**	**3.70**	**3.24**	**3.68**
p-value	**0.10**	**0.05**	**0.95**	**0.68**	**0.34**	**0.66**

The t-test results also contradict the statements that the isotopic fractionation factors for the microbial methane oxidation are temperature dependent (Börjesson et al., 2001; Börjesson et al., 2007; Chanton and Liptay, 2000; Chanton et al., 2008a). However, the investigated temperature range of this study is smaller than that of the stated ones. For example, in the case of Börjesson et al. (2007) *KIE* was determined for six different landfill cover soils as well as a different and larger temperature range (3, 5, 10, and 20°C). The authors stated the regression lines of *KIE* versus temperature resulted in different slopes ranging from -0.000664°C^{-1} to -0.000098°C^{-1}. The respective correlation factors were r = 0.16 - 0.58. The standard deviations (estimated from supplemental information) were high with values up to $\sigma \approx$ 7.5‰ for individual temperatures. As stated by the authors ANOVA was not significant on the temperature and isotopic fractionation. Chanton and Liptay (2000) investigated the temperature dependence for mulch and clay soil (at 8, 12, 24, and 35°C) and with -0.000438°C^{-1} and -0.000433°C^{-1} determined similar slopes for both soils. In another study by Chanton et al. (2008a) the stated temperature dependence of *KIE* observed by Börjesson et al. (2007) was combined with data from other studies as well as data from their own studies. With an average value and its standard deviation of the mean of *KIE* = 1.022 ± 0.0015 at 25°C the temperature dependence for *KIE* for the range of 3-35°C was proposed as:

$$KIE_T = KIE_{25°C} - 0.00039C^{°-1}\left(T - 25°C\right) \tag{4.4.9}$$

The converted values are shown in the box and whiskers plot in Figure 4-8. After checking for normality and homogeneity of variances for each *KIE* by the Shapiro-Wilk test (Table 4-1) and F-test (Table 4-2) the respective values were compared by one and two sided t-tests with $KIE_{25°C}$ stated by Chanton et al. (2008a). Since the Shapiro-Wilk test on normality was significant for each

KIE and the F-test on variances was not, the equal variance t-test (Table 4-3) was performed. No statistical difference between the observed values was present at a significance level of 0.01.

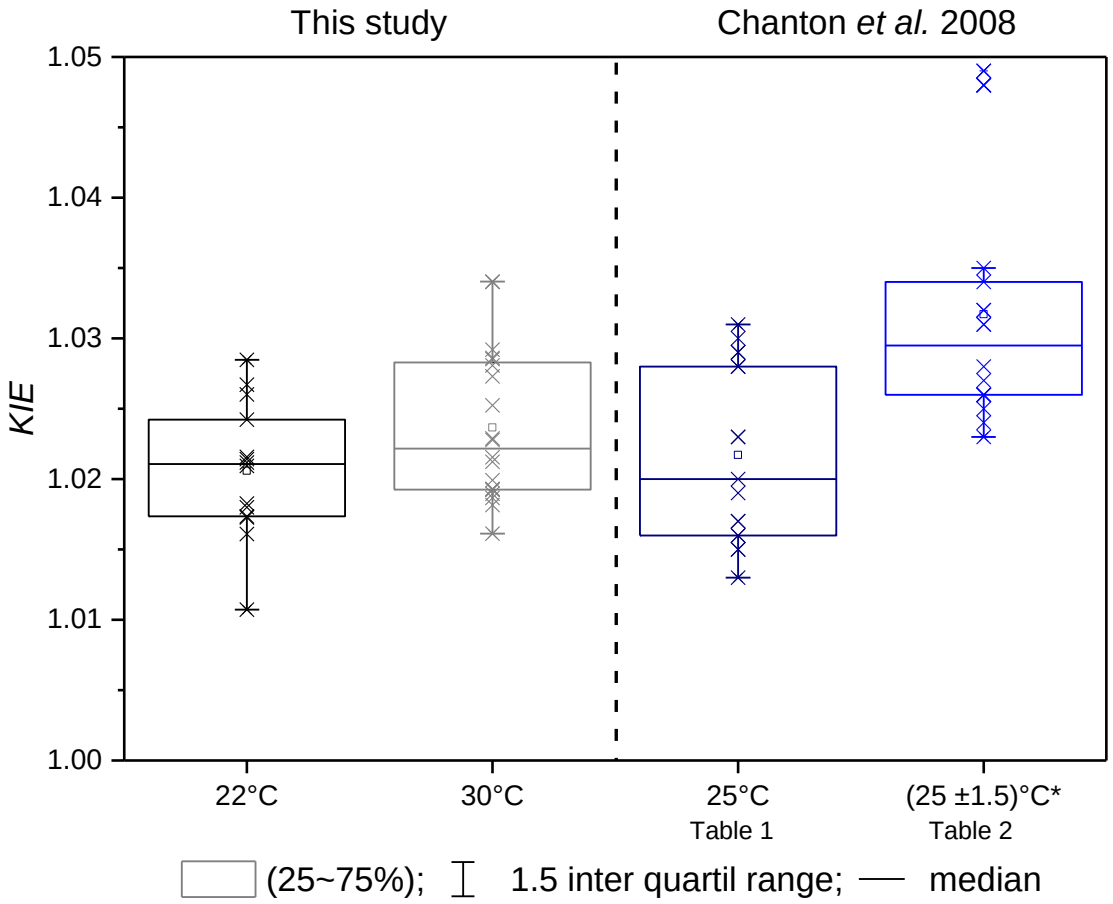

Figure 4-8 Box and Whiskers plot of the isotopic enrichment factors
The results of this study are shown on the left side for 22°C (n = 14) and 30°C (n = 20). The mean values ± their standard deviations of the mean were $KIE_{22°C}$ = 1.021 ± 0.0013 and $KIE_{30°C}$ = 1.024 ± 0.0012. On the right side Data was taken from tables 1 and 2 in (Chanton et al., 2008a). The mean values ± their standard deviations of the mean were $KIE_{25°C}$ = 1.022 ± 0.0015 (table 1), and $KIE_{(25±1.5)°C}$ = 1.032 ± 0.002 (table 2). In case of table 2 only the data for 25 ± 1.5°C were considered for comparison.
The crosses represent individual data points. Boxes cover the 25% quantile (quartile 1) through the 75% quantile (quartile 3). The horizontal line in the boxes is the 50% quantile border (median, quartile 2) and the small square inside is the mean of the data points. The whiskers are 1.5 times the inter quartile range (1.5·(quartile 3 - quartile 1)).

Table 4-3: Comparison of determined *KIE*s with the stated *KIE* in (Chanton et al., 2008a)
The experimentally determined values at 22°C and 30°C were compared with the stated one at 25°C by F-test and equal variance two sample t-test, all at a significance level of $\alpha = 0.01$; with: $n(KIE_{25°C}) = 17$ (Chanton et al., 2008a), $n_1(KIE_{22°C}) = 14$, $n_2(KIE_{30°C}) = 20$; degrees of freedom $\nu = n_1+n_2-2$

	t-test $KIE_{25°C}$ vs. $KIE_{22°C/30°C}$			F-test $KIE_{25°C}$ vs. $KIE_{22°C/30°C}$		
H_0	$\mu_{25°C} = \mu_T$			$\sigma^2_{25°C} = \sigma^2_T$		
H_1	$\mu_{25°C} \neq \mu_T$	$\mu_{25°C} > \mu_T$	$\mu_{25°C} < \mu_T$	$\sigma^2_{25°C} \neq \sigma^2_T$	$\sigma^2_{25°C} > \sigma^2_T$	$\sigma^2_{25°C} < \sigma^2_T$
Test value	**0.72/0.88**	**-0.72/0.88**	**0.72/-0.88**	**1.82/1.47**	**1.82/1.47**	**0.55/0.68**
Critical value	**2.76/2.72**	**2.46/2.44**	**2.46/2.44**	**4.41/3.54**	**3.78/3.12**	**3.50/3.28**
p-value	**0.48/0.39**	**0.76/0.19**	**0.24/0.81**	**0.14/0.21**	**0.86/0.79**	**0.14/0.21**

Correspondingly, when comparing the standard deviation of an isotopic fractionation factor at a specific temperature with a correction for a change in temperature by equation (4.4.9) it is of particular interest whether there is a statistical difference or not. As an example, one may consider the theoretical comparison of the stated $KIE = 1.022$ at 25°C with another *KIE* both with ten observations each and identical standard deviations each of $\sigma = 0.005$ (which is similar to the obtained values from this study as well as stated in the literature). For a two-sided t-test with a significance level of $\alpha = 0.01$, the temperature change from 25°C would have to be greater than 16.5°C to result in a statistically significant difference between both kinetic isotope effect *KIE*. In case of a one-sided test and $\alpha = 0.01$ the change would still have to be greater than 14.5°C.

Table 4-4 Two sample t-test on hypothetical *KIE*s
The hypothetically required temperature change from 25°C (41.5°C and 8.5°C) that results in a significant test value. Critical values are for a significance level of: $\alpha = 0.01$; with degrees of freedom $n_1=10$ (25°C) and $n_2=10$ (41.5°C/5.5°C); $\nu = n_1+n_2-2$

	t-test $KIE_{25°C}$ vs. $KIE_{8.5°C/41.5°C}$		
H_0:	$\mu_{25°C} = \mu_T$		
H_1:	$\mu_{25°C} \neq \mu_T$	$\mu_{25°C} > \mu_T$	$\mu_{25°C} < \mu_T$
Test	**2.88**	**2.88**	**-2.88**
Critical value	**2.88**	**2.55**	**2.55**
p-value	**0.010**	**0.005**	**0.005**

However, the usual operating temperatures of the methane oxidizing layer within the soil cover should fall within this range 25°C ± 14.5°C. For example, the oxidation rates of methane for biofilter materials were investigated by Gebert et al. (2003) and maximum activity was found for different enrichment cultures at 38°C for *Methylobacter sp.* and at 22°C for *Rhodococcus erythropolis* co-culture. Also, (Gehrke et al., 2013b) found maximum activity at ~35°C for an enrichment culture from tap water. Thus it is likely that a correction might not be relevant as the variance of *KIE* is probably greater than the resulting change from the respective temperature correction- at least from a statistical point of view. In addition, the thorough investigations of Chanton et al as exemplified in Figure 4-9 have been used to determine the temperature dependence of the *KIE* for a soil at two different depths, 10-20 cm and 20-30 cm. However, apart from excluding data at 43°C, the slopes were opposite in sign and thus will probably more or less cancel each other out at a landfill site amended with a thick layer of cover material.

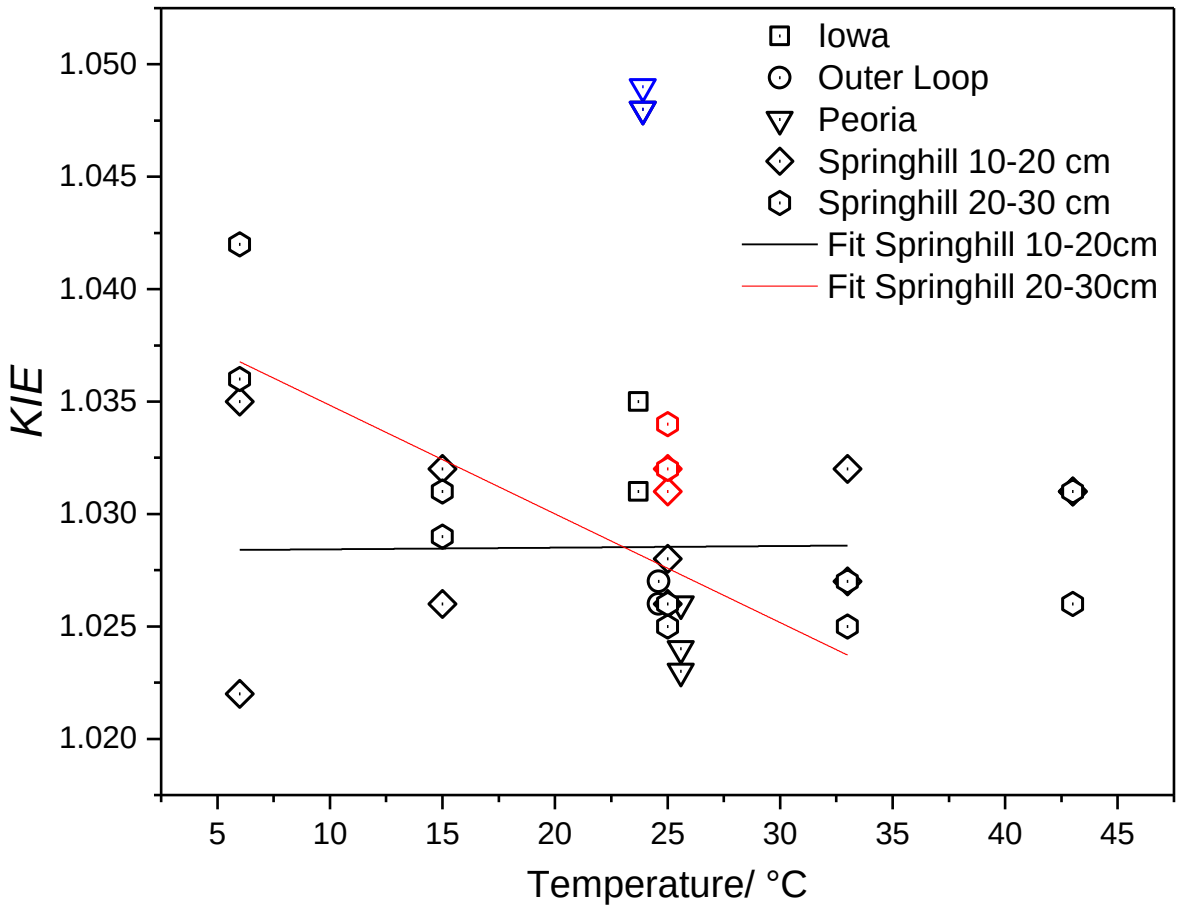

Figure 4-9 Isotopic fractionation factors taken from (Chanton et al., 2008a)
Depicted are the *KIE*s determined from different sites and soil depths. Black symbols represent results for soil samples preconditioned with CH_4 for at least 9 days. Blue symbols represent soil stored without CH_4 for 59 days prior to degradation experiments. Red data points represent values for degradation experiments in which the soil was preconditioned with CH_4 for one day. Linear regression was performed by the authors for Springhill at 10-20 cm and 20-30 cm. They excluded the red data points as well as the data points at 43°C for Springhill from liniear regression. Thus for Springhill the temperature dependence was determined in the range of 6-33°C. Note the different trends of the regression lines at 10-20 cm and 20-30 cm.

Apart from the temperature dependence the *KIE* has also been reported to depend on oxidation rate (Chanton et al., 2008a). Therefore, the enrichment factors for the microbial methane oxidation versus the kinetic rate constant were compared. They are depicted in Figure 4-10. The confidence intervals ($CI = \bar{x} \pm t_{99\%} \cdot \sigma/\sqrt{n}$) of the kinetic rate constants of the two temperatures 22°C and 30°C were $CI_{99\%}(k_{22°C}) = (2.1 \pm 1.1) \cdot 10^{-5} s^{-1}$, and $CI_{99\%}(k_{30°C}) = (8.6 \pm 4.5) \cdot 10^{-5} s^{-1}$. The kinetic rate constants show a high variability especially for 30°C. Also, no trend in enrichment factor versus the rate constant was observable. This is in agreement with observations by Börjesson et al. (2007) who did not observe correlation between α and methane consumption or soil moisture. In Feisthauer et al. (2011) it was argued that the observed *KIE*s of the bacterial methane oxidation for pure cultures supported the assumption that the isotopic enrichment factor is independent of cell density or activity and that it rather depends on Streitwieser semi

classical limits for kinetic isotope effects of C-H bond breakage. In fact, the observed average *KIE*s of this study ($KIE_{22°C}$ = 1.0206 and $KIE_{30°C}$ = 1.0236) are close to the theoretical value for a C-H bond breakage at 25°C of *KIE* = 1.021 (Aelion et al., 2010) and thus seem to support this statement.

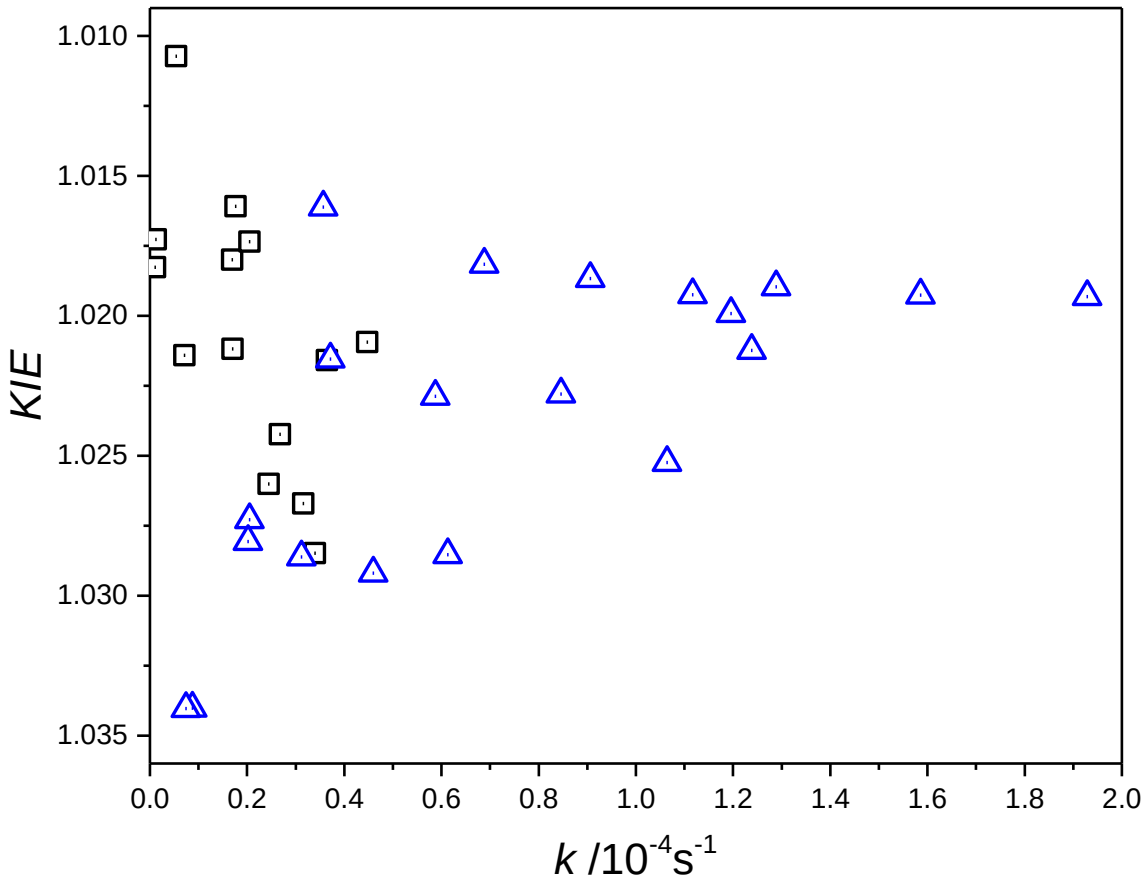

Figure 4-10: Enrichment factors for the microbial methane oxidation versus the kinetic rate constants
The black symbols are for the experiments at 22°C and the blue symbols for the ones at 30°C.

4.5.3 Centrifuge tube experiments with mixed methanotrophic cell culture

The results of the degradation study of the mixed methanotrophic cell culture are shown in (Figure 4-11). While the concentration of CH_4 decreased steadily with reaction time to roughly 50%, the concentration of CO_2 did indeed show a strong increase as would be expected when catabolic activity of the cell culture was dominant. In case of the cell culture, the result of the FIA indicated a continuous increase in biomass by the increase of the total carbon measured as signal intensity of CO_2 (Area m/z 44). However, this was also observed for the respiration control. As depicted in Figure 4-12 the $\delta^{13}C$ values of methane increased with decreasing

fraction. In contrast to the experimental results described in 4.5.2 the isotopic fractionation of methane in this experiment was not as pronounced. The experimental results returned less negative isotopic enrichment factors with a 99% confidence interval $CI_{99\%}(\varepsilon_{22°C})$ = -0.0136 ± 0.0044. In methanotrophs which have both types of MMO copper stress induces the expression of sMMO or when bacterial concentrations rise above 0.8 g dry weight L^{-1}(Stanley et al., 1983). In another study, Jahnke et al. (1999) discovered that the discrimination of ^{13}C-methane by the sMMO is lower than by the pMMO, in type I and II methanotrophs. Thus copper limitation in the cell suspension could be a probable cause for lower ^{13}C discrimination by the induction of sMMO.

The δ^{13}C values of carbon dioxide did not show the expected offset from the reactant methane, in the beginning of the experiment. With values around ~-40‰ at 20 h reaction time they started to decrease until 80 h and then increased slightly until the end of the experiment. An explanation for this might be the presence of traces of carbon dioxide from air as well as respiration derived carbon dioxide from the cell culture which had a significantly more positive value than methane. After 80 h the methane oxidation and subsequent carbon dioxide production seems to have outweighed the fractionation by respiration. Yet, as depicted in Figure 4-13 the δ^{13}C values decrease with decreasing fraction remaining. Given the fact that data for carbon dioxide covered only a very small range of fraction remaining, it was not expected to obtain a reasonable value for the isotopic enrichment factor based on (4.4.2). When regarding the mean and standard deviation of the isotopic fractionation between biomass and carbon dioxide $\Delta\left(\delta^{13}C_{\text{biomass}-CO_2}\right)$ = (11.2 ± 3.8)‰, the resulting value is comparable with $\Delta\left(\delta^{13}C_{\text{biomass}-CO_2}\right)$ = 15‰ for a mixed culture of methanotrophs obtained by Templeton et al. (2006). As with the change in signal intensity for CO_2 (measured as Area m/z 44), for the cell culture the trend of the isotopic signature of the respiration control was also very similar but with an average offset of: $\Delta\left(\delta^{13}C_{\text{biomass}-\text{respiration control}}\right)$ =(-6.1±1.7)‰.

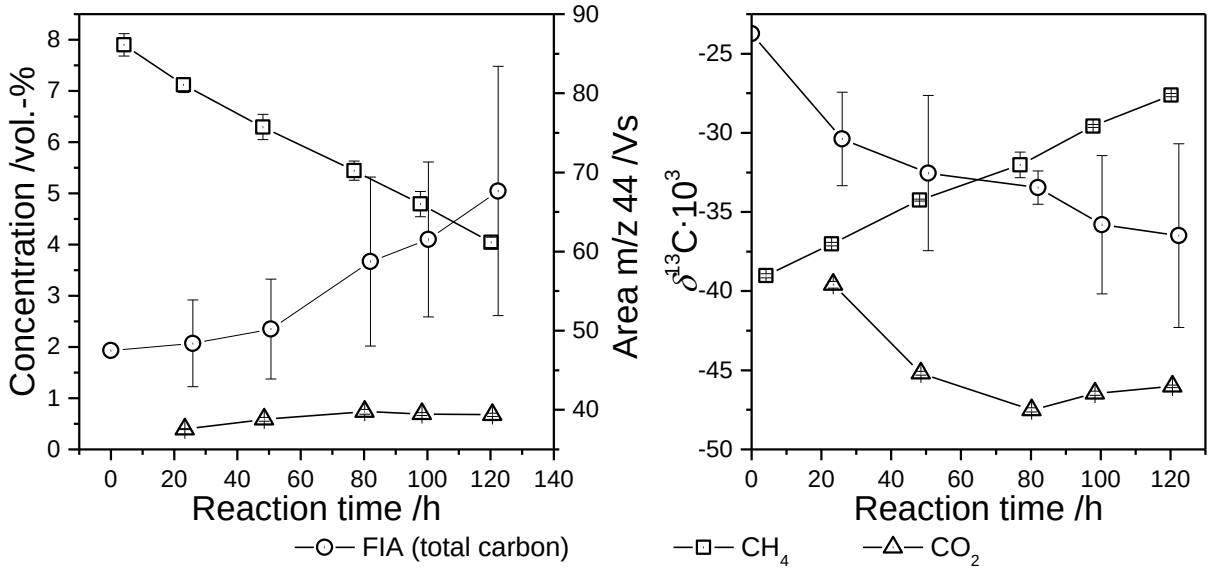

Figure 4-11 Amount and isotopic signature of cell culture, CH_4 and CO_2
On the left side the concentrations for CH_4 and CO_2 are depicted along with the area of m/z 44 which represents the total carbon in the liquid culture (TC) as obtained by FIA. On the right side the corresponding $\delta^{13}C$ values are shown.

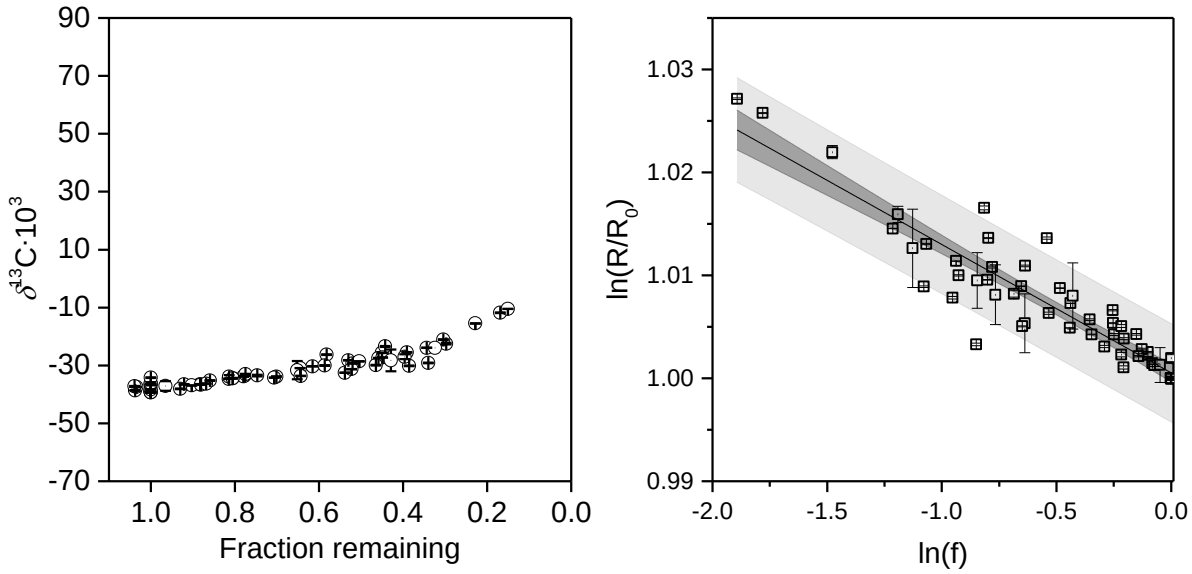

Figure 4-12 Rayleigh plot of CH_4 and double logarithmic plot in mixed cell culture
The left panel shows the isotopic fractionation of the residual methane with increasing consumption from left to right. On the right panel the average isotopic enrichment factor with its standard deviation $\varepsilon_{22°C}$ = -0.0136 ± 0.0036 was determined from linear regression.

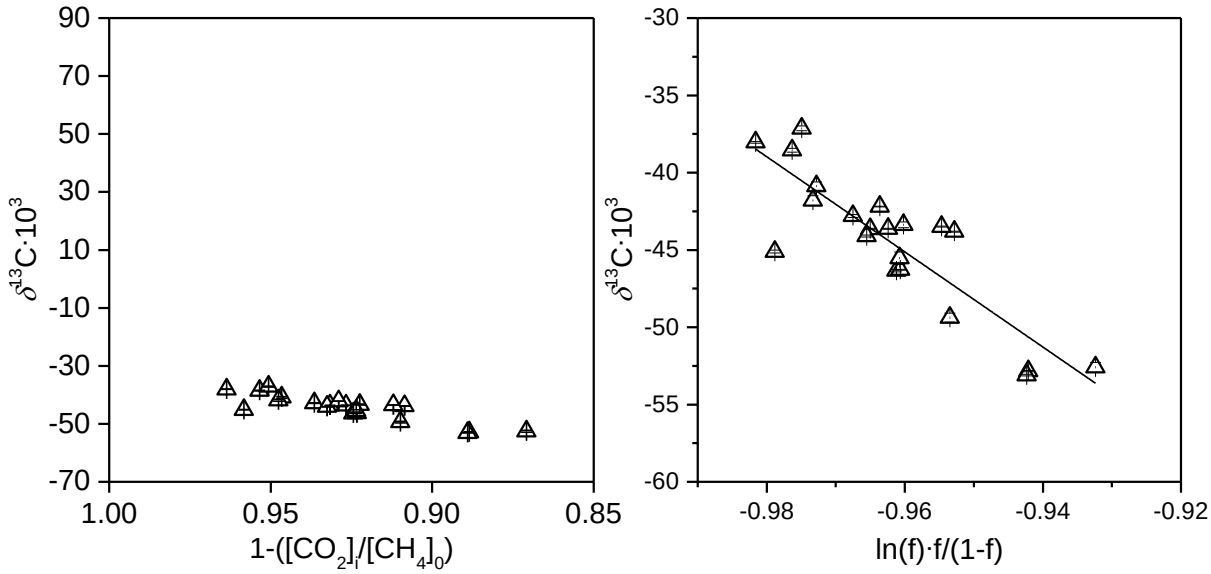

Figure 4-13 CO_2-derived enrichment factor
The left panel shows the isotopic signature of carbon dioxide along with the corresponding fraction of methane remaining ($1-([CO_2]_i/[CH_4]_0)$) in the gas phase of the mixed cell culture experiment at 22°C. The right panel shows the regression line for CO_2 based on (4.4.2).

4.5.4 Enrichment culture experiments in serum flasks

In this section the results of the degradation experiments with type I and type II methanotroph enrichment cultures in serum flasks will be investigated. In both cases, type I and type II, the $\delta^{13}C$ values of methane displayed a steady increase with a decrease in fraction of remaining CH_4 in the manner of a closed system Rayleigh distillation (black symbols in Figure 4-14). This confirms an isotopic fractionation of methane by bacterial oxidation since losses and changes in isotopic composition of methane in the controls were not observed and thus could be ruled out. The percent degradation of methane under type I conditions (~5 vol.-% CH_4) was generally higher than for type II (~10 vol.-% CH_4). For type I the percent degradation of methane was up to 99% (21°C) and 91% (30°C), and for type II up to 86% (21°C) and 83% (30°C), respectively. This led to large maximum isotopic fractionations between methane of the initial and final sampling points. The observed maximum values for methane went up to $\Delta(\delta^{13}C_0\text{-}\delta^{13}C_i) \approx$ 117‰ for type I and to $\Delta(\delta^{13}C_0\text{-}\ \delta^{13}C_i) \approx$ 41‰ for type II. Based on the isotopic signature of methane the isotopic enrichment factors $\varepsilon_T(CH_4)$ were determined from linear regression (Figure 4-15). Also, the isotopic signature of the accumulated carbon dioxide was used for the estimation of the isotopic enrichment factor (Figure 4-16).

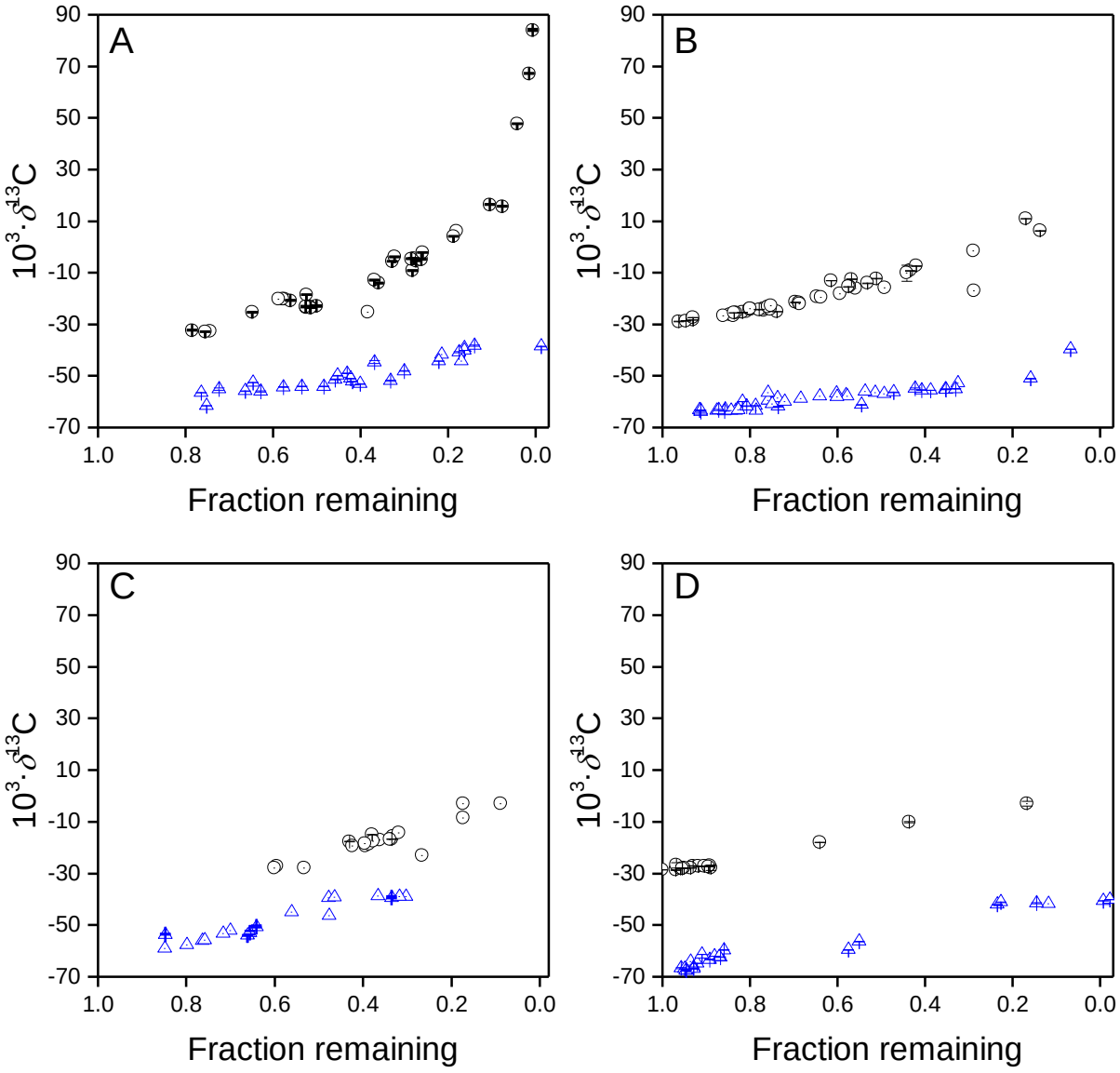

Figure 4-14 Rayleigh plot for CH_4 and CO_2 at 21°C and 30°C
The four panels A-D show the respective carbon isotopic fractionation of CH_4 (black circles) and CO_2 (blue triangles) by bacterial methane oxidation for type I methanotrophs at 21°C (A) and 30°C (C), and for type II methanotrophs at 21°C (B) and 30°C (D).

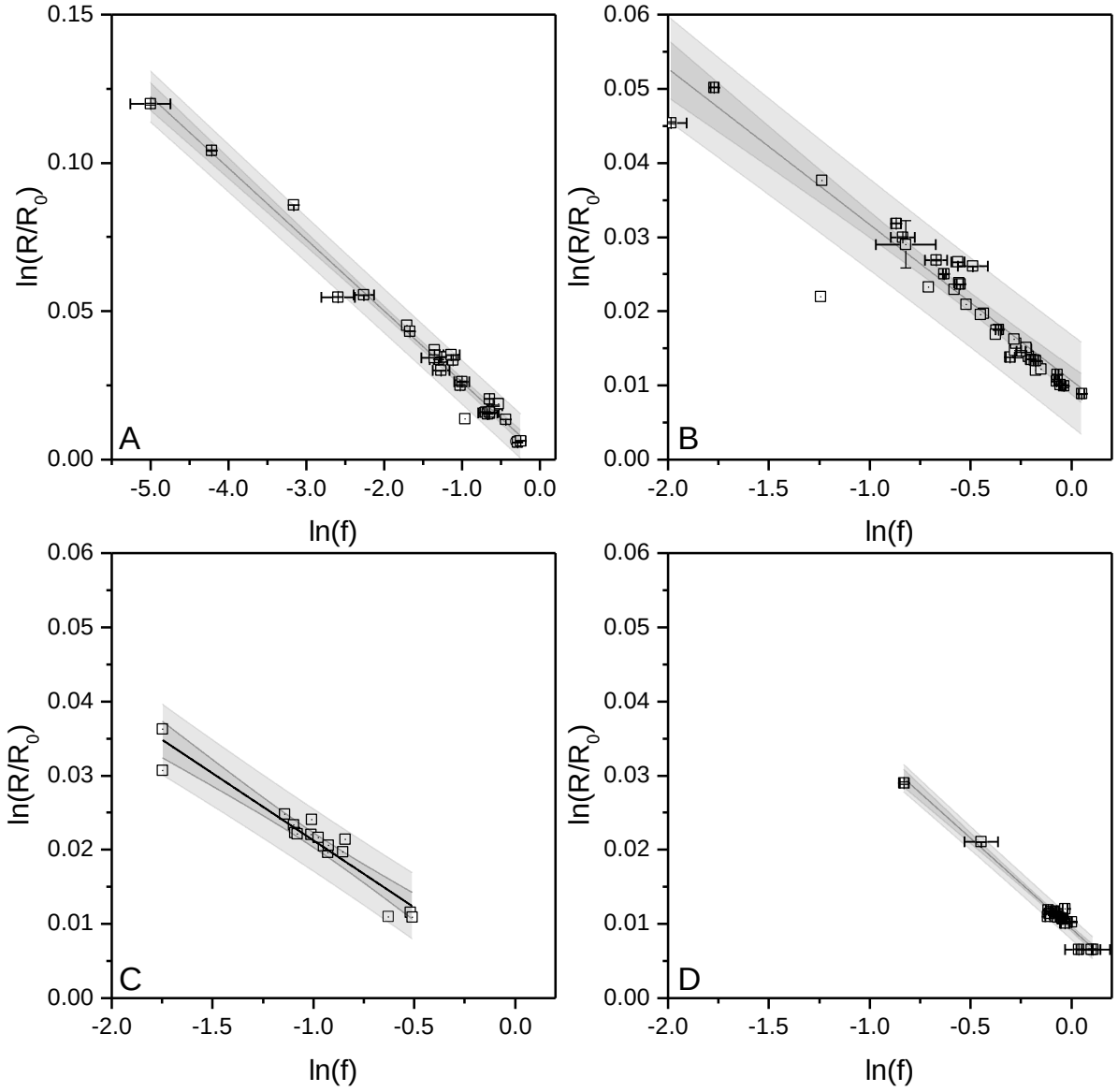

Figure 4-15 Isotope enrichment factors determined from methane for type I and II methanotrophs at 21°C and 30°C

The methane derived isotopic enrichment factors were determined from the slope of the regression line. Type I at 21°C (A) and 30°C (C), and type II at 21°C (B) and 30°C (D)

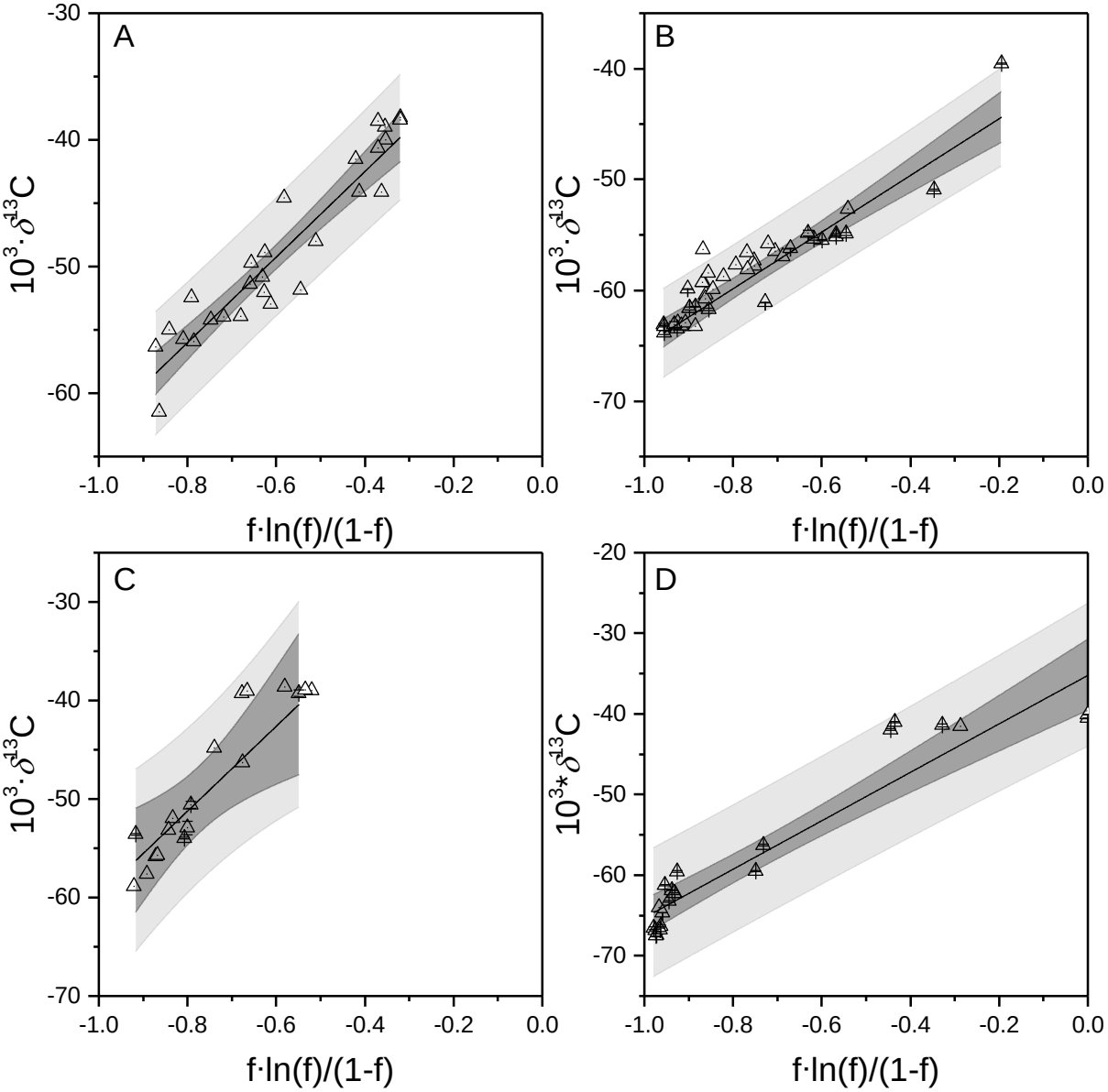

Figure 4-16 Isotope enrichment factors for bacterial methane oxidation determined from accumulated CO_2 for type I and II methanotrophs at 21°C and 30°C

The carbon dioxide derived isotopic enrichment factors were determined from the slope of the regression line. Type I at 21°C (A) and 30°C (C), and type II at 21°C (B) and 30°C (D)

The results of both approaches are summarized in Table 4-5. The values determined from methane are similar for each experimental condition and also comparable with the values obtained in chapter 4.5.2. In fact, no clear difference between the CH_4-derived isotopic enrichment factors and respective temperatures of incubation is observable for either type I or II conditions. Apparently, even between type I and type II conditions there is no difference. In contrast, the values obtained from carbon dioxide ($\varepsilon_T(CO_2)$) show a higher variation and are more negative than the corresponding $\varepsilon_T(CH_4)$. Yet, they are still within the reported range of isotopic enrichment factors (Table 1-3). Only for type II at 21°C, $\varepsilon_{21°C}(CO_2)$ = -0.0236 ± 0.0045 is well comparable with $\varepsilon_{21°C}(CH_4)$ = -0.0204 ± 0.0028. The general difference between $\varepsilon_T(CH_4)$ and $\varepsilon_T(CO_2)$ is probably due to processes involved in the conversion of methane into carbon dioxide. After conversion into methanol by MMO three further steps including the methanol dehydrogenase, formaldehyde dehydrogenase, and formate dehydrogenase are involved in the dissimilation process which finally leads to carbon dioxide. Consequently, if further discrimination of ^{13}C is involved in these steps, the isotopic signature of carbon dioxide is also altered. In this particular case, the dominating effect on the isotopic fractionation of CO_2 seems to have been the assimilation of methane by MMO.

Table 4-5 Summary of the isotopic enrichment factors for type I and II methanotroph conditions at different temperatures

Given are the average values ± standard deviations of triplicate experiments. The values with an asterisk represent results from single experiments.

Temperature	Type I		Type II	
	$\varepsilon_T(CH_4)$	$\varepsilon_T(CO_2)$	$\varepsilon_T(CH_4)$	$\varepsilon_T(CO_2)$
21°C	**-0.0242 ± 0.0007**	**-0.0352 ± 0.0026**	**-0.0204 ± 0.0028**	**-0.0236 ± 0.0045**
30°C	**-0.0202 ± 0.0030**	**-0.0431***	**-0.0232 ±0.0020**	**-0.0301***

For statistical comparison of the isotopic enrichment factors based on $\delta^{13}C_{CH_4}$ (ε (CH_4)) analysis of variance (ANOVA) was performed. The results are given in Table 4-6.

Table 4-6: ANOVA on the isotopic enrichment factors for type I and II for CH_4, and temperature

	Sum of squares	Mean of squares	F-test	p-value
Type I/II	$4.54 \cdot 10^{-7}$	$4.54 \cdot 10^{-7}$	**0.10**	**0.77**
22°C/30°C	$9.63 \cdot 10^{-7}$	$9.63 \cdot 10^{-7}$	**0.20**	**0.67**
Interaction: Type · Temperature	$3.13 \cdot 10^{-5}$	$3.13 \cdot 10^{-5}$	**6.61**	**0.04**
Model	$3.33 \cdot 10^{-5}$	$1.11 \cdot 10^{-5}$	**2.34**	**0.16**
Error	$3.32 \cdot 10^{-5}$	$4.74 \cdot 10^{-6}$	-	-
Total	$6.64 \cdot 10^{-5}$	-	-	-

Since the interaction between the two factors type of methanotrophs and incubation temperature was significant for a significance level α<0.04 (see also Figure 4-17), a possible influence of either factor on the isotopic enrichment factor could not be resolved. This is probably because the bacterial cultures of type I and II were only enrichment cultures and not pure culture. This may have influenced the overall isotopic enrichment factor caused by the individual strains as „temperature effects on isotopic discrimination are easily obscured by metabolic differences between individual methanotrophs and experimental variation between cultures of the same methanotroph." (Jahnke et al., 1999). Also, in a study by Feisthauer it was found that different methanotrophs have similar isotopic enrichment factors. However they ranged from -14.8 to -27.9‰ (Feisthauer et al., 2011).

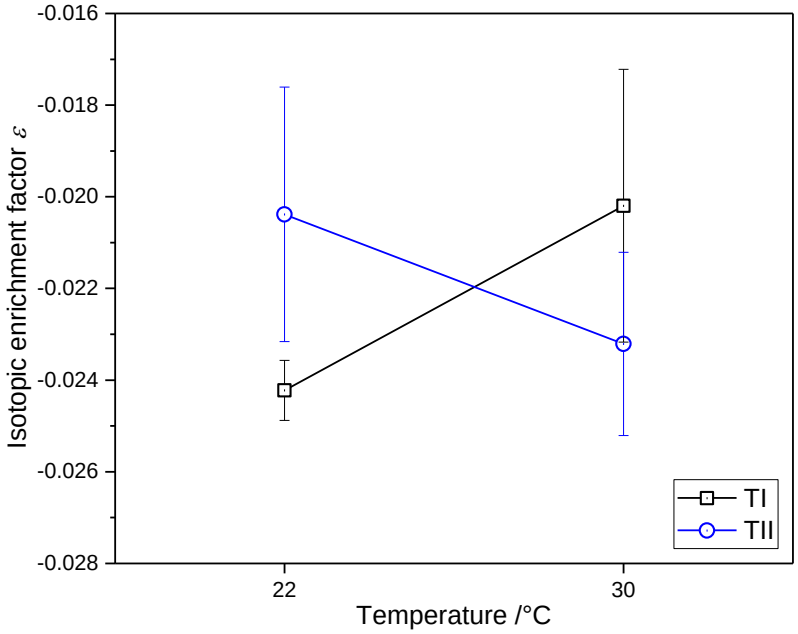

Figure 4-17 Comparison of isotopic enrichment factors for type and temperature
Indicated are the mean (symbols) and standard deviation (errror bars) of the isotopic enrichment factors for type of methanotroph and temperature.

4.6 Conclusion

Considering the reported different isotopic enrichment factors for different cover materials, landfill sites, and temperature ranges (Chanton et al., 2008a) the potential implications on field studies was investigated for a change in initial CH_4 concentration, temperature, and type of methanotroph. A difference of the isotopic enrichment factor for different initial CH_4 concentrations could not be resolved. Furthermore, the results of this study imply that the variability of the enrichment factors in terms of expanded uncertainty is higher for a specific temperature of interest than a value corrected for a change of temperature by proposed temperature dependencies. In addition, it was not possible to detect an oxidation rate dependence of the enrichment factor. Other factors such as cell density (Kampara et al., 2009; Templeton et al., 2006), bacterial strain, substrate limitations and type of expressed MMO (Jahnke et al., 1999) have been discussed to influence *KIE*s. However, with respect to type of methanotroph no statistical difference between type I and type II enrichment cultures was observed in this study. With an overall value of $\varepsilon \approx -0.021$ for all experiments, this supports the statement that the *KIE* of the bacterial methane oxidation is mainly due to C-H bond breakage as concluded from observations for degradation experiments with pure cultures under copper rich and copper free conditions by Feisthauer et al. (2011) in which the mean isotopic enrichment factor was $\varepsilon = -0.0218$. In terms of estimating the biodegradation of methane, the many factors influencing the isotopic enrichment factor of the bacterial methane oxidation will prevent a very precise determination (e.g. due to varying experimental conditions). If no further stable carbon isotopic data is available for a specific site one may consider a generic mean value and standard deviation of $\varepsilon = -0.021 \pm 0.005$. This will lead to estimates with a moderate measurement uncertainty in the range of ~10% of the biodegradation (see also chapter 5.6.4).

5 Characterizing the methane oxidation of a potential landfill cover material

5.1 Introduction

Methane emissions from landfills are mainly affected by physical characteristics of the landfill cover and the entire site landfill gas collection (Christophersen et al., 2001). For example, in a study on Swedish landfills with gas extraction systems the landfill gas recovery of the produced landfill gas was found to be highly variable with an average of 51% (Börjesson et al., 2009). Another study on field cells at three French landfill sites determined that the CH_4 gas recoveries were in the range of 41% to 94% of the theoretical CH_4 production and strongly depended on the presence and type of cover (Spokas et al., 2006). However, in case of several thousand old landfills in Germany and Europe active gas extraction systems have never been applied (Ritzkowski et al., 2006). This would result in the uncontrolled emissions of methane to the atmosphere. Even if an active gas extraction system is present the mitigation of the remaining emissions is still important. In general, possible solutions for the reduction of landfill gas emissions include the aeration of landfill waste (Ritzkowski et al., 2006), the utilization of biofilters, and the application of biocovers or soil covers as methane oxidation layer. Such systems are reviewed in (Huber-Humer et al., 2008). Several field and laboratory studies have investigated the performance of methane oxidation by different systems and materials such as biofilters (Powelson et al., 2006; Powelson et al., 2007), biocovers (Abichou et al., 2006; Cabral et al., 2009; Capanema and Cabral, 2012; Mei et al., 2015; Scheutz et al., 2014), intermediate covers (Abichou et al., 2006), and soil covers (Barlaz et al., 2004; Bogner et al., 1997; De Visscher et al., 1999). These systems are helpful in reducing methane emissions especially in the aftercare phase of a landfill and beyond when the utilization of the extracted landfill gas as energy source is no longer applicable due to its high CO_2/CH_4 ratio and consequently low energy density. Although a cover soil's methane oxidation performance requires monitoring its advantage is that it represents a passive system and does not need additional machinery like pumps or generators/gas flares.

However, the performance of a cover soil in terms of methane oxidation is susceptible to many factors such as temperature and others as summarized in (Scheutz et al., 2009). Another major challenge with these cover soils is to accurately determine how much methane they oxidize in order to control the cover soil's performance in terms of methane oxidation capacity and emission reduction in the field. As summarized by Chanton et al. (2009) different approaches exist for the estimation of methane oxidation. Methods for the estimation of the methane oxidation in landfill cover soils from stable isotope data have been described previously (Liptay et

al., 1998). By means of mass balancing and stable isotopes the biodegradation of methane by biofilters has been investigated for different cover materials (Cabral et al., 2009; Capanema and Cabral, 2012; Powelson et al., 2006; Powelson et al., 2007). In a study by Christophersen et al. (2001) the emissions of CO_2 and CH_4 from an old landfill and their lateral gas transport into adjacent soil were investigated by balancing the gas flux with the CO_2/CH_4 concentration ratios. Based on a similar methodology Gebert (2011) investigated the methane oxidation of laboratory columns filled either with mineral soil or two different types of compost. Another available technique is named gas push-pull test. It was formerly introduced by Urmann et al. (2005) and has been improved for the application in the field (Streese-Kleeberg et al., 2011) at different landfills and during different seasons.. While several investigations have been applied already, they most often compare only two techniques at a time, namely mass balance and an alternative one. A thorough approach comparing the calculated fraction of oxidized methane by mass balance, CO_2/CH_4 concentration ratios, and SIA to our knowledge has not been performed, so far.

The aim of this study was: (1) to investigate the oxidation potential of a reactor system during the simulation of three typical scenarios encountered in the aftercare phase of a landfill, and (2) to compare the biodegradation calculated by different techniques including mass balancing and stable isotope approaches by graphical and statistical methods.

5.2 Experimental setup

The reactor system was constructed of a stainless steel framework which was capped with Plexiglas facing on the front and the rear side. Its dimensions were 12 cm, 200 cm, 150 cm (length, width, height). Inside, a 15-cm layer of small circular plastic bodies (Figure 5-1) was placed at the bottom of the reactor plate which served as a gas distribution layer. It was covered with ~0.26 m^3 topsoil (water content: 9.7% w/w, organic dry substance: 2.2% w/w determined from 30 g soil by standard method DIN 12880, 2001). This methane oxidation layer had a height of 110 cm leaving a total headspace of ~25 cm. The reactor was supplied with humidified gases to avoid desiccation of the soil body. Methane and carbon dioxide of 3.5 quality (both Airliquide, Düsseldorf, Germany) were added at the bottom of the reactor by ten evenly distributed Rauclair-E PVC inlet tubings (Rehau AG&Co, Rehau, Germany). These inlets were amended with three-way stopcocks for gas regulation (Sarstedt AG und Co., Nümbrecht, Germany). At the top, air was added by seven inlets. The volume flows of the entering gases were regulated by mass flow controllers (Bürkert, Ingelfingen, Germany). Excess gas exiting the reactor by six exhaust lines was quantified by a mass flow monitor (Bürkert, Ingelfingen, Germany). The experimental setup is depicted in Figure 5-1.

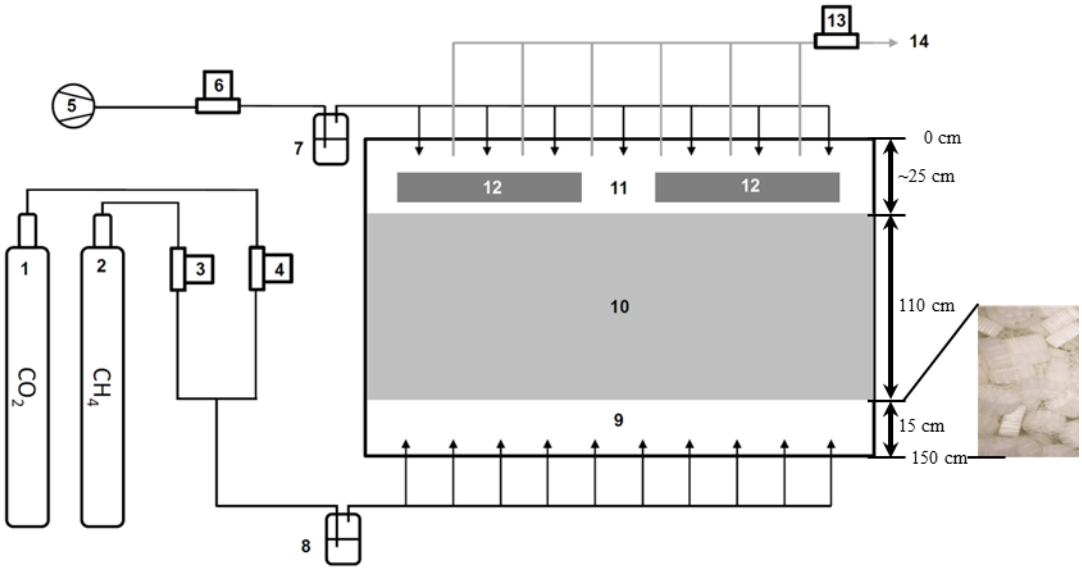

Figure 5-1: Reactor plate setup modified from Thom et al. (2016)
Scheme of the soil section:(1) carbon dioxide supply, (2) methane supply, (3) MFC for CH_4, (4) MFC for CO_2, (5) air compressor, (6) MFC for air, (7 + 8) humidifier, (9) gas distribution layer composed of platic bodies (shown on the right); (10) soil body, (11) atmospheric gas phase, (12) heat exchanger, (13) MFM for air, (14) off-gas.

Three different scenarios were investigated. These included the normal state with regular gas flow ("normal"), an increase in local CH_4 gas load ("hotspot"), and the cooling of the atmospheric gas phase ("cooling"). The parameters of the different scenarios are given in Table 1. The "normal" state should simulate a standard situation for a methane oxidation layer of a landfill in its aftercare period with relatively low gas loads of methane and carbon dioxide. In case of the hotspot, a local increase in gas load as can be observed on landfills, e.g., due to vegetation (soil penetration by roots) or settling of the deposited waste material (degradation of high organic waste) leading to preferential flow should be simulated. To that end, the outer three gas inlets at the bottom of both sides of the plate were shut while leaving the remaining four in the middle open. Thus the entering gas flow was focused in the center of the plate. The "cooling" should simulate a seasonally affected decrease in temperature. For this purpose, two heat exchangers cooling the incoming airstream were installed in the headspace. A glycerin water mixture served as cooling agent circulating in the system.

Table 5-1: Summary of the actions at the reactor plate and adjustments of the gas flow

Day of experiment	Action	CH_4 / CO_2 / air / $mLmin^{-1}$
1	Start of reactor	14/7/114
18	Reduction of air supply	14/7/68
27	Start of hotspot scenario	14/7/68
43	End of hotspot scenario	14/7/68
59	Turnoff CO_2-supply	14/0/114
66	Shutdown / installation heat exchanger	-/-/-
82	Restart of reactor	14/0/114
85	Start of air condition	14/0/114
87	Increase of CH_4-supply	21/0/114
92	Cooling of reactor headspace	21/0/114
107	End of Cooling experiment	21/0/114

5.3 Sampling

The reactor was sampled from the back where the top edge of the reactor corresponded to 0 cm and the bottom edge to 150 cm. The distances of the reported sampling ports represent the vertical distance (depth) below the top edge. The headspace was sampled at two sampling ports in the headspace at 6.5 cm depth. The gas inlet at 148.5 cm was monitored, too. At each sampling point a luer stainless steel cannula (B Braun AG, Melsungen, Germany) was inserted into the center of the reactor plate and adapted with a three-way stopcock (Sarstedt AG und Co., Nümbrecht, Germany). The reactor plate was sampled with single use 10-mL plastic syringes (Omnifix by B Braun AG, Melsungen, Germany) amended with luer three-way stopcocks. In order to avoid dead volume and CO_2 contamination from the air, 5 mL of gas sample was withdrawn from the reactor plate and discarded via the stopcock to the surrounding air. Afterwards, the reactor gas was mixed by pulling and pushing the syringe plunger for two times before the 10 mL were taken and the stopcock was closed. The 10-mL samples were measured directly afterwards within the same day of sampling.

Figure 5-2 Back side of the reactor with sampling port
The sampling ports for the headspace (three way stop cock with amended with a canule reaching into the reactor body) are shown for the back side of the reactor; In the picture on the right an example is given of how the 10-mL syringe was connected to a sampling port.

5.4 Quantitative and stable isotope analysis

Gas concentrations and stable isotope composition of CH_4 and CO_2 were determined by means of GC-IRMS. Depending on the concentrations of the analytes the injection volumes and split flow had to be adjusted to ensure linearity of the ion source of the mass spectrometer and the corresponding isotope data. Three calibrations were performed to cover the range 0.05 to 80 vol-% and the method detection limits were obtained as described by Jochmann et al. (2006), and limits of detection and quantification by DIN 32 645. Calibration gas mixtures were prepared in multilayer foil gas sampling bags composed of a 5-layer barrier of: (1) 60-gauge nylon (outer layer), (2) metalized aluminum, (3) polyethylene - 0.0003", (4) aluminum foil - 0.002", and (5) polyethylene (inner layer) (Restek, Bad Homburg, Germany) using gas tight syringes of 1, 2, 5, 10, and 100 mL volume (Hamilton, Bonaduz, Switzerland, and Vici Precision Sampling, Baton Rouge, USA). Methane of 4.5 and carbon dioxide of 3.5 were diluted in helium of 5.0 quality (all Airliquide, Düsseldorf, Germany). Table 5-2 summarizes the calibration parameters and Figure 5-3 shows the regression lines as well as the stable isotope compositions of the gases. The confidence interval of the $\delta^{13}C$ value of the methane used for calibration was $CI = (-38.45 \pm 0.10)‰$ (with $CI = \bar{x} \pm t_{99\%} \cdot \sigma/\sqrt{n}$; with $\sigma = 0.28‰$, and $n = 57$). It was normalized to an isotopic standard (Methane #1, CH_4, CAS # 74-82-8, with a 99% confidence interval for the $\delta^{13}C$ value of $CI = (-38.25 \pm 0.05)‰$ ($t_{99\%} \cdot \sigma/\sqrt{n}$; with $\sigma = 0.03‰$, and $n = 6$)).

Table 5-2: Calibration parameters for CO_2 and CH_4
a: Slope of regression line; b: y-intercept of regression line; LOD: Limit of detection (in vol.-%) determined by DIN 32 645; LOQ: Limit of quantification (in vol.-%) determined by DIN 32 645 with a coverage factor k = 5; MDL: Method detection limit (in vol.-%); DF: Degrees of freedom; s_y: Residual standard deviation; Vx_0: Coefficient of variation

Analyte	Range /vol.%	a	b	$R^2_{corrected}$	LOD	LOQ	MDL	DF	s_y	Vx_0 /%
CH_4	0.05-2	30.73	-0.54	0.999	0.02	0.14	0.05	20	0.45	1.87
	1-16	2.60	-0.80	0.994	0.63	2.74	1	17	0.75	3.66
	10-80	0.47	-0.28	0.996	4.79	10.03	10	17	0.50	2.69
CO_2	0.1-2	30.58	-0.61	0.998	0.02	0.21	0.1	20	0.69	2.85
	1-16	2.57	-0.73	0.993	0.68	2.93	3	17	0.79	3.93
	10-80	0.45	0.03	0.995	5.72	11.63	20	17	0.57	3.16

Prior to the first sample analysis, a total volume of 0.5 mL of sample was withdrawn twice with a gas tight syringe (pressure-lok A-2, Vici Precision Sampling, Baton Rouge, USA) and discarded to remove residual air in the three-way stopcock attached to the sample syringe. Gas samples were analyzed with a GC Trace Ultra (Thermo Fisher Scientific, Bremen, Germany) using a 30-m Qbond column with an inner diameter of 0.32 mm and a film thickness of 10 µm (Restek GmbH, Bad Homburg, Germany). The helium carrier gas flow was 1.6 mL min^{-1}. The split flow was either 10 or 160 mL min^{-1}. Injection volumes were 0.05, 0.25, and 0.5 mL. The oven temperature was held constant at 30°C for 5 min. Following the separation by GC and combustion with Pt/Ni/Cu at 960°C via a GC-Combustion III Interface (Thermo Fisher Scientific, Bremen, Germany) the stable carbon isotope composition of the combustion product CO_2 was measured by a MAT 253 isotope ratio mass spectrometer (Thermo Fisher Scientific, Bremen, Germany). The reported delta values are based on the CO_2 reference gas calibrated relative to Vienna Pee Dee Belemnite (VPDB). The samples were measured at a minimum in triplicates.

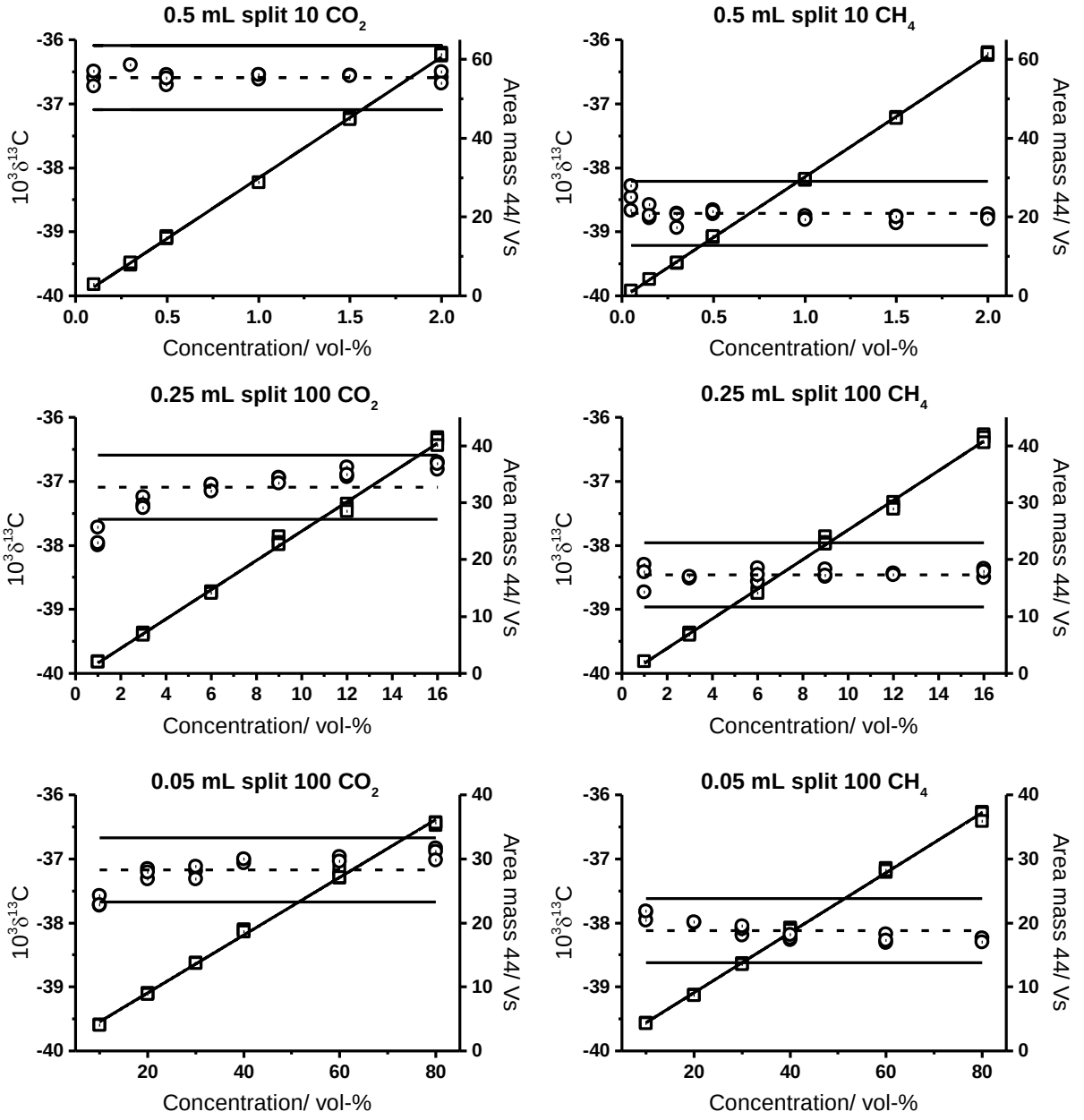

Figure 5-3: Calibration for different gas concentrations

The different calibration ranges are depicted for carbon dioxide and methane. Headings include the injection volume and split is the split flow in mLs^{-1}. The symbols represent single measurements; squares correspond to areas and circles to delta values. Each calibration point was measured in triplicates at minimum. The horizontal dashed lines correspond to the mean $\delta^{13}C$ values of CO_2 and CH_4 while the lines below and above are the 0.5‰ intervals covering the total analytical error.

5.5 Data acquisition

The software Isodat 2.5 was used for data acquisition and processing. Microsoft Excel 2010 and Origin 2015G were used for tabular calculations, statistical testing, and construction of graphics.

5.6 Calculations

In the literature, the fraction of oxidized methane is often termed differently (e.g., efficiency, relative biodegradation, biodegradation, fraction oxidized, etc.). In this work, either biodegradation or fraction of oxidized methane was used and both terms were treated identical.

In order to estimate the fraction of oxidized methane by the reactor system, the following three different methods were compared and evaluated: 1. Mass balancing, 2. Stable carbon isotope analysis, and 3. Stoichiometry based on CO_2/CH_4 ratio. For reasons of brevity, the fraction of oxidized methane was designated as f_{ox}^{*}, where the suffix "ox" stands for oxidized methane and the asterisk in the exponent symbolizes the abbreviation of the respective method that was applied for the calculation of the fraction of oxidized methane. The list below and Figure 5-4 summarize the different methods with their respective abbreviations.

1. **Mass balancing by quantitative measures (see 5.6.1)**
    a. Based on exiting gas measured by mass flow monitor: MFM
    b. Based on sum of gas flow of mass flow controllers: MFC
2. **Stable carbon isotope analysis of CH_4 (see 5.6.2)**
    c. Closed system
        i. Simplified Rayleigh equation: CSI
        ii. Correction for tortuous flow: CSIC
    d. Open system
        i. Simplified open system: OSI
        ii. Correction for diffusion: OSIC
3. **Stoichiometric considerations based on CO_2/CH_4 ratio (see 5.6.3)**
    e. No assimilation of CO_2: RATIO
    f. Corrected for assimilation of CO_2: RATIOC

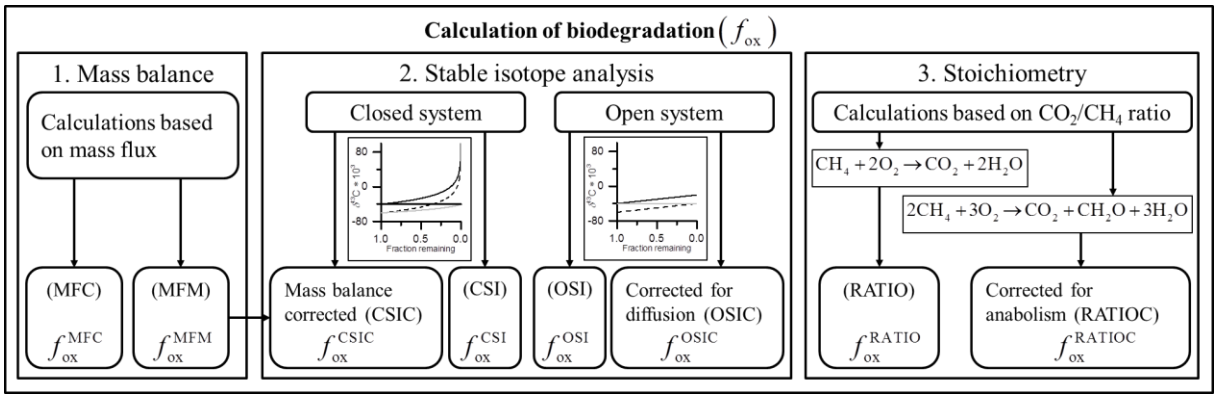

Figure 5-4 Schematic overview of the calculation of biodegradation of CH_4
The three major approaches mass balance, stable isotope analysis, and stoichiometry were utilized for the calculation of the biodegradation of methane.

5.6.1 Calculations based on mass balancing

In case of mass balancing, the calculations included the measured volume concentration of methane at the inlet and in the headspace as well as the total gas flow of methane, carbon dioxide, and air. Also, the gas exiting the reactor was monitored. This permitted the comparison of the biodegradation based on the sum of the net fluxes of the gases (MFM) and based on the total "exhaust gas" flux (MFC).

Equation (5.6.1) and (5.6.2) express the fraction of oxidized methane by mass balancing (f_{ox}^{MFM} and f_{ox}^{MFC}). It is proportional to the ratio of methane outflow (J_{out}) divided by the methane influx (J_{in}). The methane fluxes are the products of the respective volume concentrations of gas ($c_{CH_4,0}$ or $c_{CH_4,hs}$) and the volume gas flows ($\dot{V}_0$ or $\dot{V}_{hs}$). The entering gas flow $\dot{V}_0$ equals the sum of the gas flows of methane and carbon dioxide from the gas supply. The exiting gas flow $\dot{V}_{hs}$ (5.6.3) can be calculated from the sum of the net gas flows entering the system controlled by the mass flow controllers ($\dot{V}_{MFC}$) or directly from the exiting gas flow measured by the mass flow monitor ($\dot{V}_{MFM}$). The corresponding biodegradations were termed f_{ox}^{MFC} and f_{ox}^{MFM}.

$$f_{ox}^{MFM} = 1 - \frac{J_{out}}{J_{in}} = \frac{c_{CH_4,0} \cdot \dot{V}_0 - c_{CH_4,hs} \cdot \dot{V}_{MFM}}{c_{CH_4,0} \cdot \dot{V}_0} \quad (5.6.1)$$

$$f_{ox}^{MFC} = 1 - \frac{J_{out}}{J_{in}} = \frac{c_{CH_4,0} \cdot \dot{V}_0 - c_{CH_4,hs} \cdot \sum \dot{V}_{MFC}}{c_{CH_4,0} \cdot \dot{V}_0} \quad (5.6.2)$$

J_{out}: Volume flow exiting the reactor
J_{in}: Volume flow entering the reactor
$c_{CH_4,0}$: Gas concentration of methane at gas inlet
$c_{CH_4,hs}$: Gas concentration of methane at headspace of reactor
$\dot{V}_0$: Total volume flow of methane and carbon dioxide at gas inlet (e.g. Ls^{-1})
$\dot{V}_{hs}$: Total volume flow of gas at gas outlet/headspace of reactor (e.g. Ls^{-1})

$$\dot{V}_{hs} = \dot{V}_{MFM} = \sum \dot{V}_{MFC} = \dot{V}_{CO_2} + \dot{V}_{CH_4} + \dot{V}_{air} \quad (5.6.3)$$

$\dot{V}_{MFM}$: Total volume flow of gas exiting the reactor measured by MFM (e.g. Ls^{-1})
$\sum \dot{V}_{MFCs}$: Sum of volume flow of CH_4, CO_2, and air at exiting reactor (e.g. Ls^{-1})

5.6.2 Calculations based on stable carbon isotope analysis of CH_4

In case of the stable carbon isotope data obtained for CH_4, the calculations of the biodegradation were based on a closed system (CSI) or an open system (OSI). The calculation of the fraction of oxidized methane for a closed system (f_{ox}^{CSI}) is given by equation (5.6.4). It is based on the Rayleigh distillation equation. Next to the enrichment factor (ε) the stable carbon isotopic signature of the initial reactant and the residual reactant have to be known. In the reactor system, this corresponds to the δ^{13}C-value of the methane entering the reactor ($\delta_{CH_4,0}$) and exiting the reactor at its headspace ($\delta_{CH_4,m}$). For the calculations in this study the enrichment factor ε = -0.0202 ± 0.0046 was used that had been determined in previous experiments (see chapter 4). This is well in accordance with an applied generic value of -0.02 (Capanema and Cabral, 2012; Rachor et al., 2011).

$$f_{ox}^{CSI} = 1 - \left(\frac{\delta_{CH_4,m} + 1}{\delta_{CH_4,0} + 1} \right)^{\frac{1}{\varepsilon}} \quad (5.6.4)$$

For low estimates of biodegradation based on the closed system calculations by equation (5.6.4) Powelson et al. (2007) suggested a correction for the biodegradation, which will be abbreviated as CSIC. The corrected fraction of oxidized methane (f_{ox}^{CSIC}) is given in equation (5.6.5). The term "1-*P*" was described as "tortuous flow fraction that slowly seeps through small pores, resulting in complete oxidation" (Powelson et al., 2007) and is defined in equation (5.6.6).

$$f_{ox}^{CSIC} = 1 - P + P \cdot f_{ox}^{CSI} \quad (5.6.5)$$

$$P = \frac{1 - f_{ox}^{MFM}}{1 - f_{ox}^{CSI}} \tag{5.6.6}$$

When regarding an open system of isotopic fractionation, the biodegradation can be expressed by the following equation.

$$f_{ox}^{OSIE} = \frac{\left(\delta_{CH_4,m} - \delta_{CH_4,0}\right)}{\delta_{CH_4,m} - \varepsilon - \delta_{CH_4,m} \cdot \alpha} \tag{5.6.7}$$

f_{ox}^{OSIE}: Fraction of oxidized methane
$\delta_{CH_4,0}$: δ^{13}C-value of methane at gas inlet (reactant)
$\delta_{CH_4,m}$: δ^{13}C-value of methane at headspace of reactor (unutilized reactant)
ε: Isotopic enrichment factor of the bacterial methane oxidation (BMO)
α: Isotopic fractionation factor of the BMO

Corrections for the open system calculations have been suggested due to lower estimates of biodegradation in comparison to mass balance methods. These include corrections for the isotopic fractionation by diffusion (OSIC). If mainly advective transport is present, no correction for isotopic fractionation by diffusion is required. This has been assumed in several studies (Cabral et al., 2009; Liptay et al., 1998; Widory et al., 2012). However, when gas collection systems at landfill sites are present this may require a correction for the isotopic fractionation by diffusion as these systems increase the inward flow leading to a negative pressure gradient and thus also affect diffusive transport (Chanton et al., 2009). Estimates for the kinetic isotope effect (KIE_{diff}) associated with diffusion ($KIE_{diff}=1/\alpha_{diff}$) have been determined experimentally for different cover soils (Gebert et al., 2013), glass beads (De Visscher, 2004), peaty tundra soils (Preuss et al., 2013), and a cover material in this thesis (see chapter 3). The suggested corrections range from $KIE_{diff} = 1$ ($\alpha_{diff} = 1$, where $\alpha_{diff} = 1/KIE_{diff}$) to the theoretical value for the diffusion of methane in air with $KIE_{diff} = 1.0195$ ($\alpha_{diff} = 0.9809$). A fairly exact expression for the open system calculation corrected for diffusion is given in the following.

$$f_{ox}^{OSIEC} = \frac{\left(\delta_{CH_4,m} - \delta_{CH_4,0}\right)}{\delta_{CH_4,m} - \left(\alpha - \alpha_{diff}\right) - \delta_{CH_4,m}\left(\left(\alpha - \alpha_{diff}\right) + 1\right)} \tag{5.6.8}$$

f_{ox}^{OSIEC}: Fraction of oxidized methane with correction for diffusion
α: Isotopic fractionation factor of the BMO ($\alpha = 1/KIE$)
α_{diff}: Isotopic fractionation factor of CH_4 by diffusion ($\alpha_{diff} = 1/KIE_{diff}$)

If the isotopic fractionation factor $\alpha_{ox} \approx 1$ both (5.6.7) and (5.6.8) can be simplified further to (5.6.9) and (5.6.10).

$$f_{ox}^{OSI} = \frac{\delta_{CH_4,0} - \delta_{CH_4,m}}{\varepsilon} \quad (5.6.9)$$

f_{ox}^{OSI}: Fraction of oxidized methane (simplified)

$$f_{ox}^{OSIC} = \frac{\delta_{CH_4,0} - \delta_{CH_4,m}}{\varepsilon - \varepsilon_{diff}} \quad (5.6.10)$$

f_{ox}^{OSIC}: Fraction of oxidized methane (simplified) with correction for diffusion

As the calculations by the exact and the simplified equations did not result in significant differences, the reported calculations of the fractions of oxidized methane for an open system were limited to f_{ox}^{OSI} (equation (5.6.9)) and f_{ox}^{OSIC} (equation (5.6.10)).

5.6.3 Calculations based on stoichiometry

The approach by stoichiometry of the chemical reaction of the bacterial methane oxidation was similar to a previously described method by Gebert (2011). If methanotrophs live primarily catabolic the chemical reaction of the bacterial methane oxidation in principle yields carbon dioxide and water.

$$CH_{4(g)} + 2O_{2(g)} \rightarrow CO_{2(g)} + 2H_2O_{(l)} \quad (5.6.11)$$

Since methanotrophs also utilize CH_4 as carbon source the balance between catabolism and anabolism may have a significant influence on the estimated biodegradation. In case of respiration and carbon assimilation may be applied as suggested by De Visscher and Van Cleemput (2003). This is very close to the approximate 48% of carbon assimilation in methanotrophs after subtraction of background soil respiration (Scheutz and Kjeldsen, 2004).

$$CH_{4(g)} + 1.5O_{2(g)} \rightarrow 0.5CO_{2(g)} + 0.5CH_2O_{(s)} + 1.5H_2O_{(l)} \quad (5.6.12)$$

If certain assumptions and simplifications are made the biodegradation of CH_4 can be estimated from the CO_2/CH_4 concentration ratio as described by (Gebert, 2011). These include that (1) the non-methane derived respiration (e.g., from soil microorganisms or plant root respiration) is negligible compared to methane oxidation and (2) no loss of CO_2 occurs in the soil body by sorption/dissolution in water (e.g., as HCO_3^-) or due to high CO_2 assimilation caused by carbon substrate limitation. The stoichiometric balance of the gas fluxes is given in equation (5.6.13). The initial methane flux (J_{in}) is composed of the volume concentration ($c_{CH_4,0}$) and the volume

flow ($\dot{V}_0$). As a result of the chemical reaction the sum of the gas concentrations of carbon dioxide and methane $\left(c_{CO_2,m} + c_{CH_4,m}\right)$ are multiplied by the volume flow at the sampling site ($\dot{V}_m$). Next, the fraction of oxidized methane $\left(f_{ox}^{RATIO}\right)$ can be calculated by equation (5.6.14).

$$c_{CH_4,0} \cdot \dot{V}_0 = \left(c_{CO_2,m} + c_{CH_4,m}\right) \cdot \dot{V}_m \tag{5.6.13}$$

$$f_{ox}^{RATIO} = 1 - \left(\frac{c_{CO_2,m}}{c_{CH_4,m}} + 1\right)^{-1} \tag{5.6.14}$$

$c_{CH_4,0}$: Gas concentration of methane at gas inlet
$c_{CH_4,m}$: Gas concentration of methane at sampling site
$c_{CO_2,0}$: Gas concentration of carbon dioxide at gas inlet
$c_{CO_2,m}$: Gas concentration of carbon dioxide at sampling site
$\dot{V}_0$: Total volume flow of gas at gas inlet
$\dot{V}_m$: Total volume flow of gas at sampling site

In cases where carbon dioxide was added to the reactor system (normal and hotspot) the entering carbon dioxide had to be considered in the calculations as described below (5.6.15). In this case the stoichiometric balance is altered as follows:

$$c_{CH_4,0} \cdot \dot{V}_0 = \left(c_{CO_2,ox} + c_{CH_4,m}\right) \cdot \dot{V}_m \tag{5.6.15}$$

$c_{CO_2,ox}$: Gas concentration of carbon dioxide at sampling site resulting from BMO

Here, the initial methane flux ($c_{CH_4,0} \cdot \dot{V}_0$) is considered to be the sum of the carbon dioxide concentration from BMO and the measured methane concentration ($c_{CO_2,ox} + c_{CH_4,m}$) multiplied with $\dot{V}_m$. Furthermore, the initial carbon dioxide flux ($c_{CO_2,0} \cdot \dot{V}_0$) is the volume flow at the sampling site ($\dot{V}_m$) multiplied by the difference of the measured carbon dioxide at the respective sampling site and the carbon dioxide that results from BMO ($c_{CO_2,m} - c_{CO_2,ox}$).

$$c_{CO_2,0} \cdot \dot{V}_0 = \left(c_{CO_2,m} - c_{CO_2,ox}\right) \cdot \dot{V}_m \tag{5.6.16}$$

Based on the mass balances from equations (5.6.15) and (5.6.16) the carbon dioxide that results from BMO is calculated by the following equation.

$$c_{CO_2,ox} = \left(c_{CO_2,m} - \frac{c_{CO_2,0}}{c_{CH_4,0}} \cdot c_{CH_4,m} \right) \left(1 + \frac{c_{CO_2,0}}{c_{CH_4,0}} \right)^{-1} \quad (5.6.17)$$

Inserting (5.6.17) in (5.6.18) allows calculating the fraction of oxidized methane.

$$f_{ox}^{RATIO} = 1 - \left(\frac{c_{CO_2,ox}}{c_{CH_4,m}} + 1 \right)^{-1} \quad (5.6.18)$$

5.6.4 Calculation of errors and uncertainties

Unless stated otherwise, the uncertainties of the different measurements are reported as combined standard uncertainty $u_c^2(y)$.

$$u_c^2(y) = \sum_{i=1}^{N} \left[c_i u(x_i) \right]^2 \quad (5.6.19)$$

The combined standard uncertainty is the sum of the product of the sensitivity coefficient c_i and standard uncertainty $u_c^2(y)$ of each individual input variable x_i. The input quantities were regarded to be uncorrelated. Thus the calculations are based on a first-order Taylor series approximation and each respective sensitivity coefficient corresponds to the first partial derivative $\partial f/\partial x_i$. The complete calculation for the partial derivatives for each method and input variable is given in the Appendices (see A4 pages 148 and following).

$$\Delta c_i = \frac{\partial f}{\partial x_i} \quad (5.6.20)$$

In general, the standard uncertainty $u(x_i)$ itself was based on a Type A standard uncertainty which is equal to the experimental standard deviation of the mean $s(\bar{x})$ (JCGM100:2008, 2008).

$$u^2(x_i) = s^2(\bar{x}) \quad (5.6.21)$$

$$s^2(\bar{x}) = \frac{s^2(x_i)}{n} \quad (5.6.22)$$

$$s(x_i) = \frac{1}{n-1} \sum_{i=1}^{N} (x_i - \bar{x})^2 \quad (5.6.23)$$

In case of the input variables CH_4- and CO_2-concentration which were determined from calibration the standard uncertainty of the concentration $u(c_i)$ was estimated by the standard error of prediction $s_{\hat{x}}$. The standard error of prediction is an absolute measure of precision of a calibration (Funk et al., 2005).

$$u(c_i) = s_{\hat{x}} \tag{5.6.24}$$

$$s_{\hat{x}} = s_{x_0}\sqrt{\frac{1}{N_s} + \frac{1}{N_c} + \frac{\hat{\bar{y}} - \bar{y}}{b^2 \cdot Q_{xx}}} \tag{5.6.25}$$

$$s_{x_0} = \frac{s_y}{b} \tag{5.6.26}$$

$u(c_i)$: Standard uncertainty of concentration of either CO_2- or CH_4-concentration estimated from standard error of prediction $s_{\hat{x}}$

s_{x_0}: Process standard deviation

N_s: Number of sample measurements

N_c: Number of calibration standards

$\bar{y}$: Average signal (Vs) from calibration

$\hat{\bar{y}}$: Average signal (Vs) from N_s measurements of sample

b: Slope of regression line

s_y: Residual standard deviation

Q_{xx}: Sum of squares $\left(\sum(x_i - \bar{x})^2\right)$

x_i: Individual concentration value from calibration

$\bar{x}$: Average concentration determined from calibration

5.7 Results and discussion

5.7.1 Comparison of biodegradation in hotspot, normal, and cooling scenario

The estimation of the biodegradation by the reactor system is an important procedure in order to evaluate the performance of a material as a potential methane oxidation layer. For this purpose, the fraction of CH_4 oxidized by the soil body was investigated during the three different scenarios described above. The results calculated by the different equations as described in chapter 5.5 are depicted in Figure 5-5.

The hotspot event was investigated during the days 28 to 42. Up to day 35 the methane concentration was below the LOD in the headspace of the reactor. Therefore, the minimum

biodegradation was approximated from the LOQ and the respective volume flows. The curves of the two mass balance approaches MFM & MFC in Figure 5-5 A and B show a similar behavior. In the beginning, the biodegradation of methane is steady until day 30 and then drops to as low as $f_{ox}^{MFM} = 0.76$ at day 37. Although the curve of the mass balance approach MFC shares this drop in oxidation the calculated biodegradations differ by $f_{ox}^{MFC} - f_{ox}^{MFM} = 0.1$. Still, this difference is within the range of the combined measurement uncertainty of each. From there on the biodegradation finally recovers within the 14th day of the simulation at day 42. The response to the local increase in methane load during the hotspot event shows that the methanotrophic community in the soil requires a certain time for adaptation but is able to restore the previous state of nearly complete oxidation.

During the normal state (days 44 - 86) the BMO remains fairly unchanged and above 99% (f_{ox}^{MFM}) and 98% (f_{ox}^{MFC}) except for the drop in oxidation at day 84. This is likely due to the installation of the heat-exchangers for the cooling state because the reactor had to be opened and the gas supply was switched off throughout days 66 to 82. As a consequence, the methanotrophic bacteria had to recover from substrate limitation. The cooling event took place throughout experiment days 87 to 106 under the parameters given in Table 5-1.

In the cooling state the values for (f_{ox}^{MFM}) at days 88 and 91 had to be excluded due to reading errors of the exiting gas flow by the mass flow monitor at days 88 and 91 (6.6 and 2.81 mLmin^{-1}) which resulted in an overestimation of methane oxidation. Apart from these, the biodegradation was affected towards lower efficiencies, on average. A temperature profile for the cooling event is given in Figure 5-6. Clearly, the headspace and topsoil are cooled down by the heat exchangers but apparently did not affect the BMO. All in all, mass balancing with either of the volume flows seems applicable.

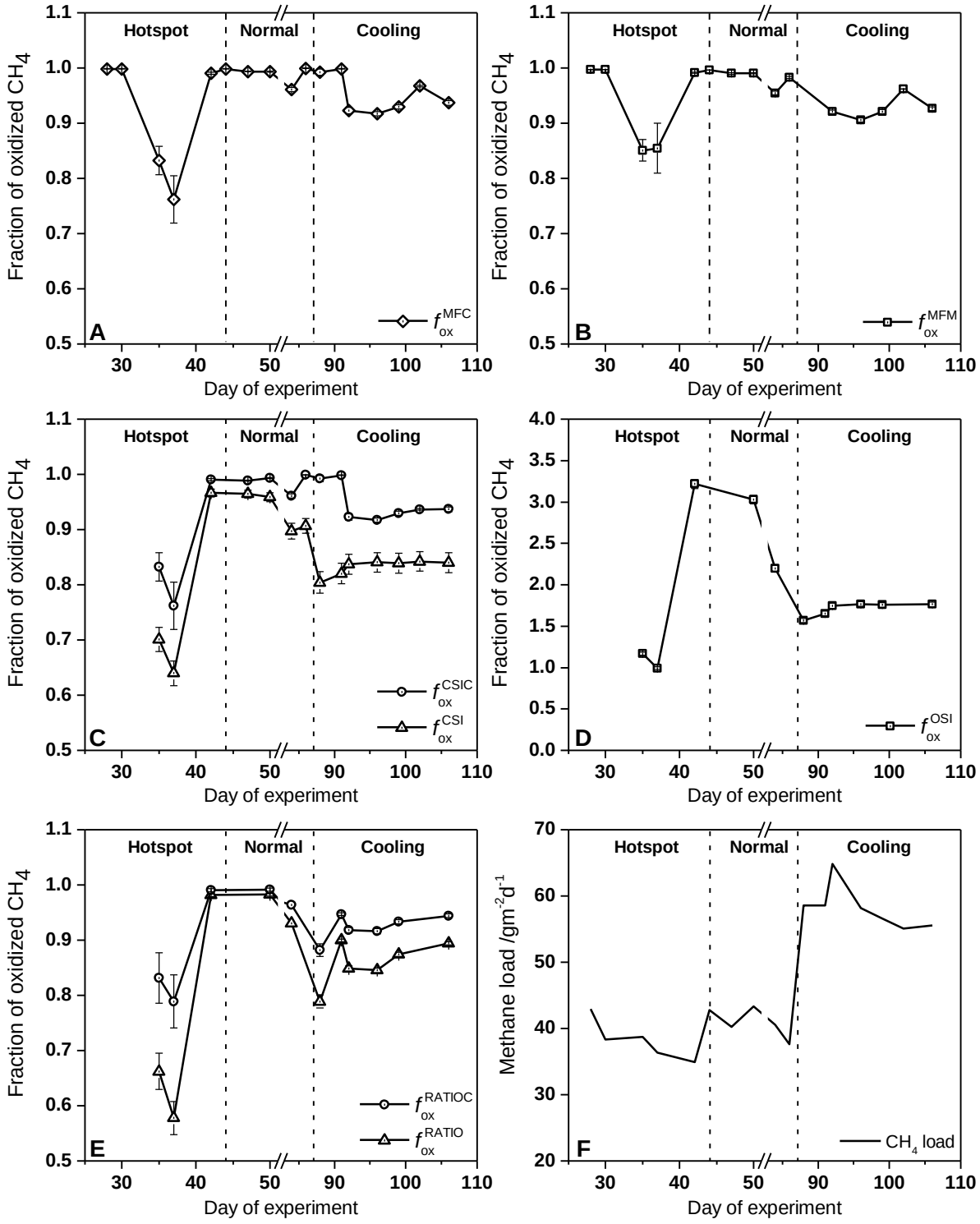

Figure 5-5 Comparison of calculated bacterial methane oxidation

Depicted are the fractions of oxidized methane throughout the experiment and the different conditions. The biodegradation was calculated by mass balance (A: f_{ox}^{MFC} and B: f_{ox}^{MFM}), (C) closed system stable isotope approach (f_{ox}^{CSI} and f_{ox}^{CSIC}), (D) open system stable isotope approach (f_{ox}^{OSI}), and (E) by CO_2/CH_4-ratio (f_{ox}^{RATIO} and f_{ox}^{RATIOC}). The corresponding methane load of the reactor is shown as well (F). Symbols represent average values of both sampling profiles and error bars are the corresponding combined uncertainties of the measurement estimted from error propagation.

The progression of the biodegradation calculated by the closed system stable isotope approach (f_{ox}^{CSI}) is illustrated in Figure 5-5 C. It correlates with the mass balance approach (panel A) but returns lower estimates for the biodegradation during all three states. Powelson et al. (2006) investigated the fraction of oxidized methane in water-spreading and compost biofilters and observed that biodegradation calculated by stable isotopes was almost always smaller than the mass balance approach. As a possible solution for the mismatch they suggested a correction for the biodegradation based on a binary closed-system model which included partitioning of the entering methane and complete oxidation of gas parcels (Powelson et al., 2007). Although the corrections by Powelson and colleagues were made for completely different biofilter systems and with significantly greater gas loads of 250 and 500 $gm^{-2}d^{-1}$ a correction by such a binary closed-system model certainly adjusts the values determined in this work (see f_{ox}^{CSIC} in Figure 5-5 C).

The open system stable isotope approach also shares the trends with the other methods during hotspot, normal state, and cooling (Figure 5-5 D). Yet, the predicted biodegradation is always above 1 but for day 37 ($f_{ox}^{OSI} = 0.99$). It even rises up to $f_{ox}^{OSI} = 3.4$ at day 42. In a laboratory column study De Visscher (2004) found that α_{diff} negatively correlated with CH_4 flux in the range of 20 – 36.5 $molm^{-2}d^{-1}$. In this study, the flux ranged between 2.2 – 3.7 $molm^{-2}d^{-1}$. At these lower fluxes, α_{diff} should show an even stronger impact on the isotopic fractionation of CH_4. However, when considering α_{diff} = 1.0195 this would even increase the estimated biodegradation to values ranging from 180% to 600%! Therefore, with the given values for α_{ox} and α_{diff} it may be concluded that the open system calculations are not suitable to assess the BMO in this particular setup.

As depicted in Figure 5-5 E the determined curve for f_{ox}^{RATIO} shows a response that apparently is in between f_{ox}^{MFM} and f_{ox}^{CSI}. The only exception is the drop during the hotspot event at days 35 and 37 where it is smaller than f_{ox}^{CSI}. Also, while f_{ox}^{CSI} remains fairly steady towards the end of the cooling simulation throughout days 92 to 106 f_{ox}^{RATIO} shows a slight increase. When considering carbon assimilation by both catabolic and anabolic activity (with respect to (5.6.12)) the obtained values increase especially for the hotspot simulation and are closer to the mass balance.

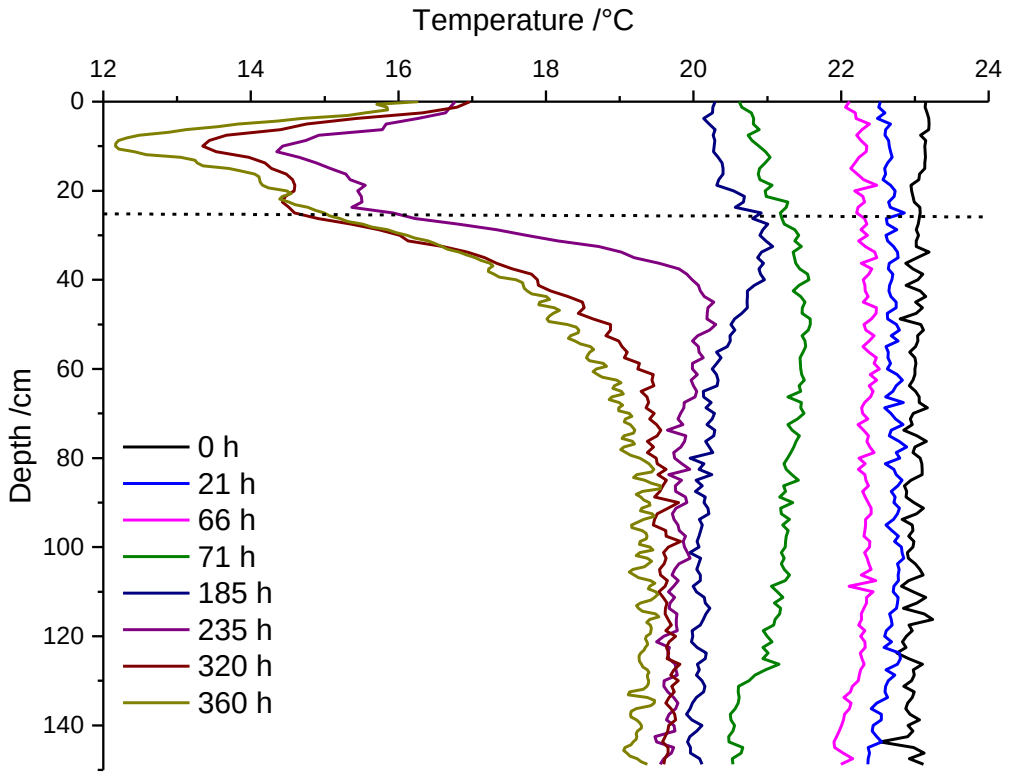

Figure 5-6 Development of the temperature profile of the reactor plate during the cooling event
The temperature was monitored over a period of 320 h. The lines correspond to the average temperatures of the reactor plate's surface. The broken line at 25 cm represents the soil-gas boundary of the reactor.

Summarizing, the efficiencies calculated by the different methods share a trend during the three simulations. This also includes the drop in oxidation during the hotspot. Still, the calculated biodegradations during the hotspot are different and follow the order:

$$f_{ox}^{MFC} > f_{ox}^{MFM} > f_{ox}^{RATIO} > f_{ox}^{CSI}.$$

The maximum difference was up to $f_{ox}^{MFC} - f_{ox}^{RATIO} = 0.28$. This already indicates the different outcome of the estimated BMO depending on which method has been applied.

5.7.2 Correlation of the calculated biodegradation between the different methods

Regarding the similar trends of the methods but different results for the biodegradation a set of techniques for comparison shall be discussed in the following. Figure 5-7 illustrates how the biodegradation of methane was compared between the different methods.

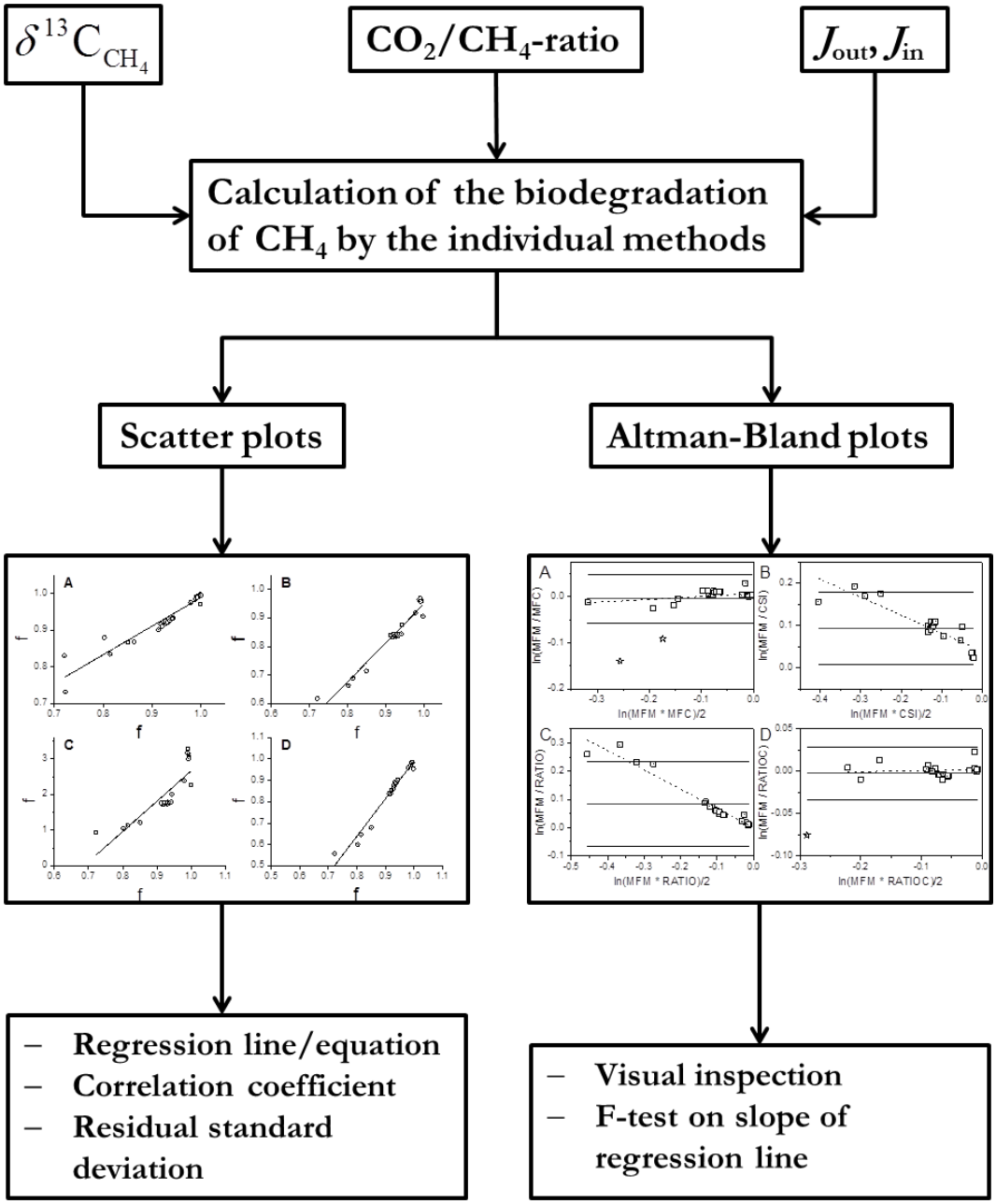

Figure 5-7 Flow chart of the graphical comparison of the different methods
The flow chart exemplarily shows how the data of from SIA, CO_2/CH_4-ratio, and mass balance were compared by different graphical approaches.

A very common one is the direct comparison of two methods by plotting one method on the *y*-axis and the other method on the *x*-axis. This approach is similar to calibration means and thus the "true" value (in terms of relative methane oxidation from mass balance (f_{ox}^{MFM}) may be predicted from a linear regression model. The results of this are shown in Figure 5-8. By plotting the methods' calculated biodegradation vs. f_{ox}^{MFM} the best fit was obtained in the order $f_{ox}^{RATIO} > f_{ox}^{CSI} > f_{ox}^{MFC} > f_{ox}^{OSI}$ (exclusive of the corrected values) which will be compared in this order in the following.

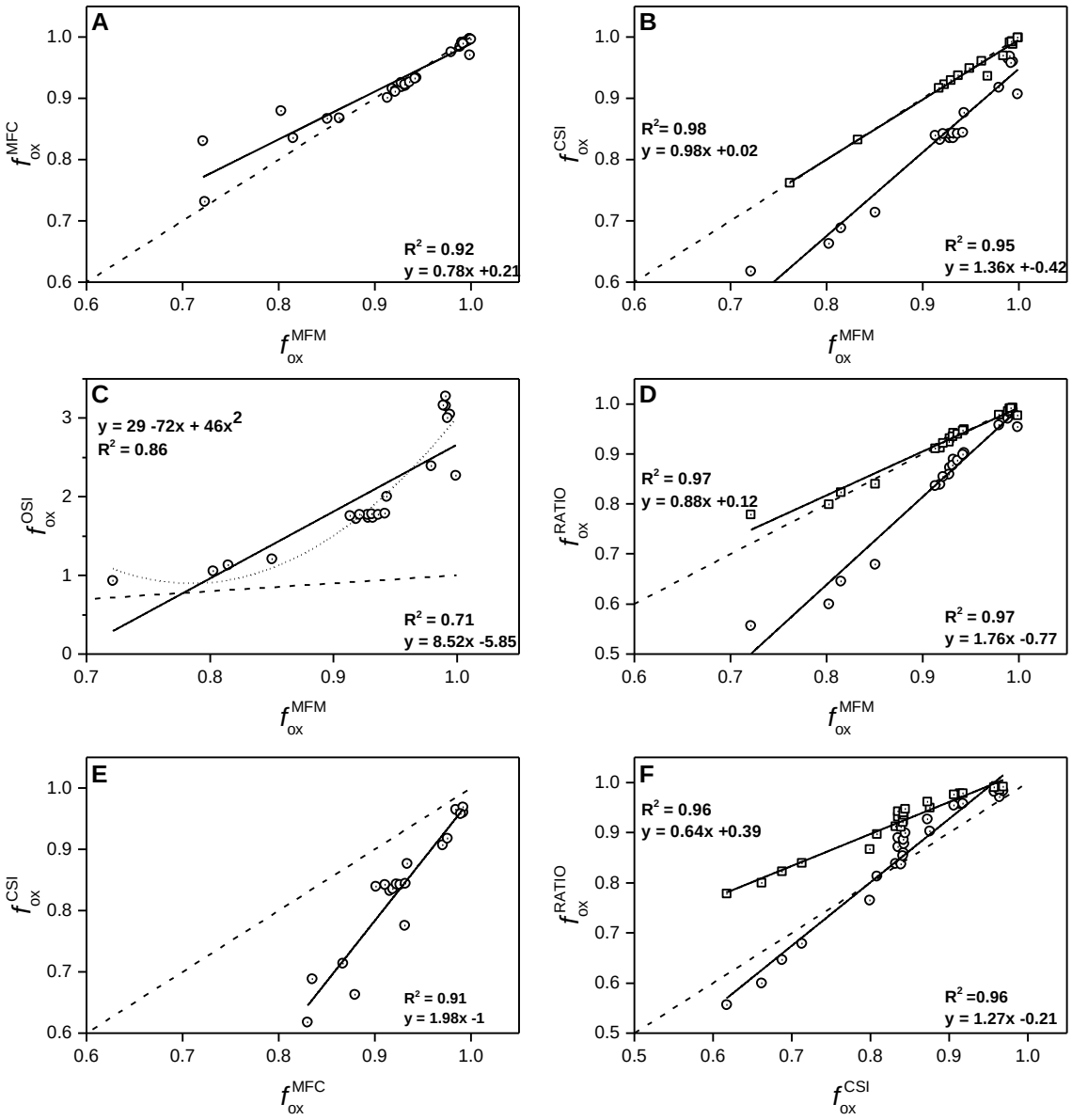

Figure 5-8: Scatter plot comparison of calculated biodegradation
Depicted are scatter plots of the differently calculated fractions of oxidized methane versus the mass balance method (A-D) and versus the closed system stable isotope approach (E & F). The regression line (solid) and reference line (broken) are given next to the formula and correlation coefficients. The symbols represent the averages of each sampling day. Squares correspond to the corrected y-values (e.g. f_{ox}^{CSIC} and f_{ox}^{RATIOC}). The dotted line in panel C corresponds to the second order polynomial fit.

A good correlation between the two methods f_{ox}^{RATIO} and f_{ox}^{MFM} was found in this work with $R^2 = 0.97$ and $s_y = 0.023$ (see Figure 5-8 D). Yet, in this case the CO_2/CH_4-ratio method rather underestimates the oxidation of methane within the reactor system ($y = 1.76x - 0.77$) which could be due to increased carbon assimilation by the methanotrophs or loss of CO_2 by dissolution into pore water. When treating the scatter plot like a calibration, one may estimate the critical value x_c for f_{ox}^{MFM} from twice the limit of detection (LOD). In case of f_{ox}^{RATIO} vs. f_{ox}^{MFM} the critical value was $x_c = 2 \cdot \mathrm{LOD} = 0.14$. The high value is partially due to the observed low range of relative

methane oxidation. However, the minimum observed relative methane oxidation in this experiment was $f_{ox}^{MFM} = 0.72$. It therefore must be emphasized that the comparison by the given linear regression is only applicable for limits of this investigated range. Previously, Gebert (2011) investigated the biodegradation of methane in laboratory columns filled either with mineral soil or two different types of compost amended soil and gravel mixtures. They found a good linear correlation for the comparison of methane oxidation by CO_2/CH_4-ratio versus the mass balance with correlation coefficients of up to $R^2 = 0.97$ (Gebert, 2011) for the mineral soil. In case of the compost filled columns the CO_2/CH_4-ratio method overestimated the methane oxidation. The authors discussed the deviations from the ideal $f_{ox}^{RATIO} = f_{ox}^{MFM}$ to have different causes including increased carbon assimilation during proliferation of methanotrophs and increased respiration during stress. They applied a correction for soil respiration which led to adequate estimations. Correspondingly, a correction of the values for carbon assimilation based on equation (5.6.12) was applied which returns higher estimates for the methane oxidation. This resulted in both an intercept and a slope closer to the reference line with $y = 0.88x + 0.12$. Although $R^2 = 0.97$ and $x_c = 0.14$ remain unchanged, the value for the residual standard deviation improved ($s_y = 0.011$). On the one side, this improvement of the fit has the disadvantage of slightly overestimating the relative methane oxidation because f_{ox}^{MFM} is always smaller than f_{ox}^{RATIO}. On the other side, the values calculated from the regression line are within the range of the method's error of the experimental results. For example, the lowest observed fraction of oxidized methane by CO_2/CH_4-ratio method was $f_{ox}^{RATIO} = 0.78$. Then the calculated 99% confidence interval from the regression line is equal to $\hat{x} \pm t_{99\%} \cdot s_{\hat{x}} = 0.76 \pm 0.04$ compared to the "true" value from the mass balance $f_{ox}^{MFM} = 0.72$. Consequently, when the circumstances influencing CO_2 are known a correction can improve values to be better comparable with the mass balance method.

The correlation of the closed system stable isotope approach and the mass balance (panel B) is comparable with the one for f_{ox}^{RATIO} vs. f_{ox}^{MFM} as the fit returns similar results with $R^2 = 0.95$ and $s_y = 0.024$. Likewise, the regression line with $y = 1.36x - 0.42$ is below the reference line and thus f_{ox}^{CSI} also underestimates the methane oxidation. The critical value for f_{ox}^{CSI} was higher with $x_c = 0.18$. Of course, when correcting the values (f_{ox}^{CSIC}) the correlation is very high as they are adjusted to f_{ox}^{MFM}.

The comparison of f_{ox}^{MFC} versus f_{ox}^{MFM} is shown in panel A. Except for two points ($P_1 = 0.72; 0.83$ and $P_2 = 0.80; 0.88$) which correspond to values during the hotspot simulation at

day 37 the data points are close to the reference line, as would be expected from the theoretical mass balance of the respective gas flows. The regression line was $y = 0.78x + 0.21$ with a residual standard deviation of $s_y = 0.019$. Excluding the two data points leads to the equation $y = 0.94x + 0.056$ with $R^2 = 0.98$ and $s_y = 0.008$.

With respect to the comparison of an open system stable isotope approach (f_{ox}^{OSIC}, based on equation (5.6.10) with $\alpha_{diff} = 1$) and mass balance Widory et al. (2012) found a good correlation of $R^2 = 0.91$. In contrast Capanema and Cabral (2012) found a lower correlation with $R^2 = 0.56$. Here in this work, the corresponding correlation was in between both with $R^2 = 0.72$. Still, when looking at the equation of the regression line ($y = 8.52x - 5.85$) and the high residual standard deviation ($s_y = 0.393$) it is evident that the two methods return completely different values for the fraction of oxidized methane. Using a second order polynomial fit improved the model as the comparison of the residual standard deviations of linear and polynomial fit by F-test was significant ($p<0.0002$). However, when comparing both the closed and open system approach it appears that the former is preferable in this study as f_{ox}^{OSI} does not return realistic values for the biodegradation.

Additionally, the method CSI was compared with RATIO and RATIOC as shown in Figure 5-8 in panel F. The correlation between f_{ox}^{RATIO} and f_{ox}^{CSI} with $R^2 = 0.96$ and $s_y = 0.025$ is similar to the respective comparisons with f_{ox}^{MFM} in panels B and D with a regression line of $y = 1.26x - 0.20$ and the critical value $x_c = 0.21$. In case of f_{ox}^{RATIOC} vs. f_{ox}^{MFM} the regression line is very different with $y = 0.63x + 0.40$. The residual standard deviation is improved ($s_y = 0.012$) and the critical value is similar with $x_c = 0.20$.

Finally, the fraction of oxidized methane determined by mass balance (f_{ox}^{MFM}) may be estimated from f_{ox}^{RATIO} and f_{ox}^{CSI} by multiple linear regression of f_{ox}^{MFM} versus f_{ox}^{RATIO} and f_{ox}^{CSI}. It returned the following equation:

$$f_{ox}^{MFM} = 0.468 + 0.153 f_{ox}^{CSI} + 0.385 f_{ox}^{RATIO} \quad (5.6.27)$$

Further parameters are given in Table 5-3. With a fairly good correlation of $R^2_{corrected} = 0.98$ the methane oxidation can also be estimated from both parameters.

Table 5-3 Multiple linear regression parameters for f_{ox}^{MFM} versus f_{ox}^{RATIO} and f_{ox}^{CSI}

Parameter	Value	Standard error
b_0	**0.468**	**0.021**
b_1(f_{ox}^{CSI})	**0.153**	**0.090**
b_2(f_{ox}^{RATIO})	**0.385**	**0.072**

The scatter plots have shown the correlation between the different methods and in some cases the methods appear to return very similar results for the fraction of oxidized methane. Thus the determined correlations will allow a better comparison of present and future studies using either of the investigated techniques.

However, when an apparent interchangeability of two methods is to be investigated instead of a correlation it is more appropriate to use a graphical method suggested by Altman and Bland (Altman and Bland, 1983). With this method it can be checked whether there is any relative bias. In the following selected methods are compared by Altman-Bland plots (Figure 5-9). In order to check for a trend regression lines were constructed and the significance of the slope was tested by F-tests.

In Figure 5-9 except for panels A and D all slopes of the regression lines were significantly different from zero. In the former case the data point/s for day 37 (hotspot) were excluded. Only in this case are the slopes not significantly different from zero (for A: $p = 0.01$; for D: $p = 0.71$). Panels B and C reveal the bias towards larger differences between the methods such as observed during the hotspot event between the mass balance methods and the stable isotope and CO_2/CH_4-ratio approach, respectively. The slopes of the regression lines were significantly different from zero (for panel B: $p = 2.6 \cdot 10^{-8}$; for panel C: $p = 9.5 \cdot 10^{-14}$). The comparison of the closed system stable isotope approach and the CO_2/CH_4-ratio approach in panels E ($p = 1.4 \cdot 10^{-7}$) and F ($p = 6.5 \cdot 10^{-13}$) also show a trend towards larger differences. All in all, the mass balance method MFC and the corrected CO_2/CH_4-ratio approach seem to be interchangeable with the mass balance method MFM when excluding data from the hotspot. However, the little data available for low fractions of methane oxidation was only available from the hotspot event. Also, because the local increase in methane oxidation was not distributed evenly along the width of the reactor plate this might have affected the trends that are observed both in the scatter plots and the Altman-Bland plots differently than an evenly spread, increased methane load. Thus it is prudent to expect no interchangeability between the methods and rather expect different results.

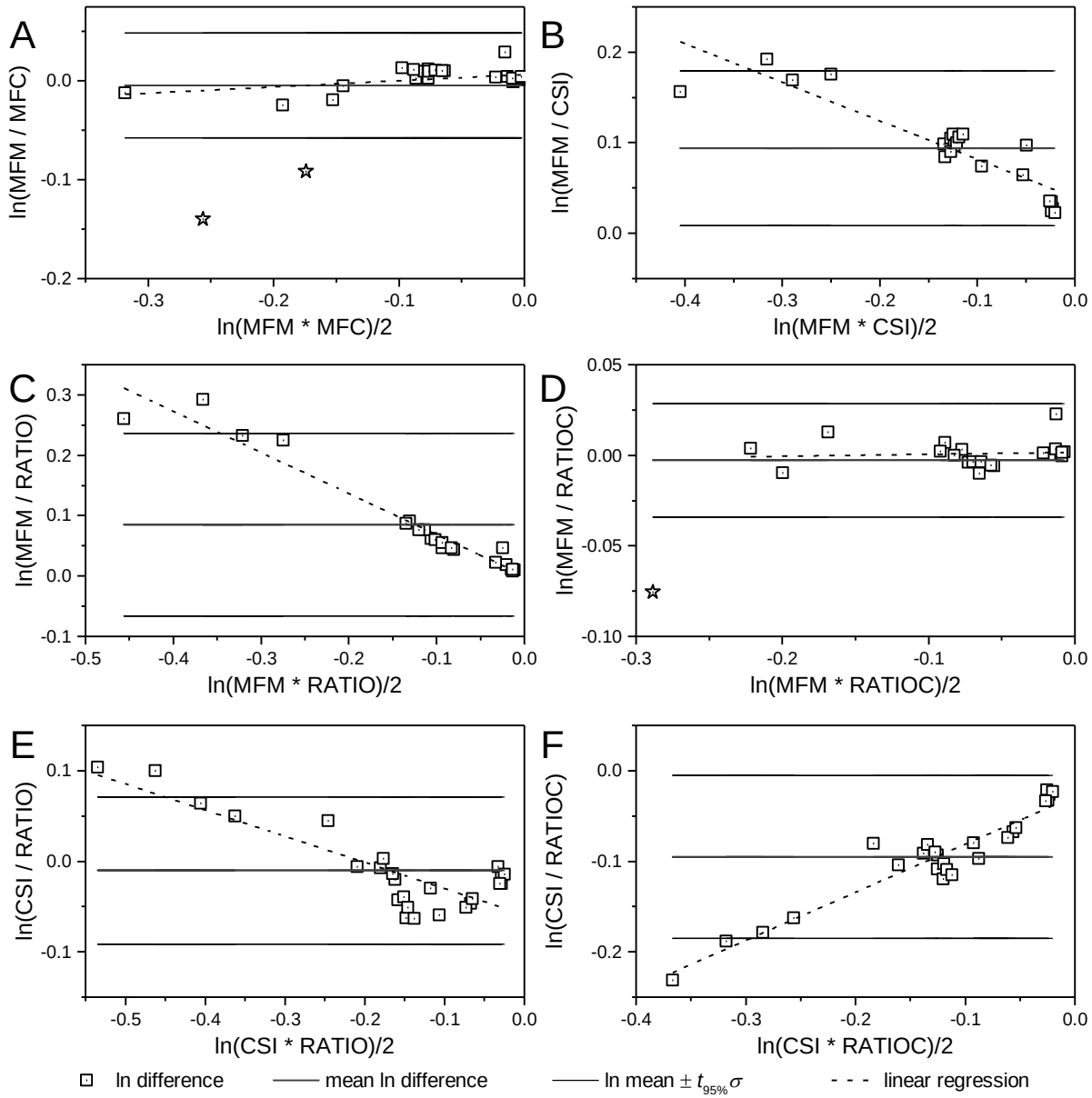

Figure 5-9 Altman-Bland plot

Depicted are the transformed Altman-Bland plots comparing the differences of methods versus their mean vaules. Note, in plots A and D the data points symbolized by stars were excluded from linear regresssion. By excluding these from regression the slopes were not significantly different from zero (with $p > 0.01$ (for A) and $p = 0.71$ (for B)).

5.7.3 Statistical comparison of the biodegradation determined by different methods

Since the scatter plots showed good correlation in certain cases and the Altman-Bland plots revealed relative bias in panels B, C, E, and F in Figure 5-9 additional statistical testing was necessary to further clarify whether the methods differed from one another or not. For this purpose, the procedure was as depicted below:

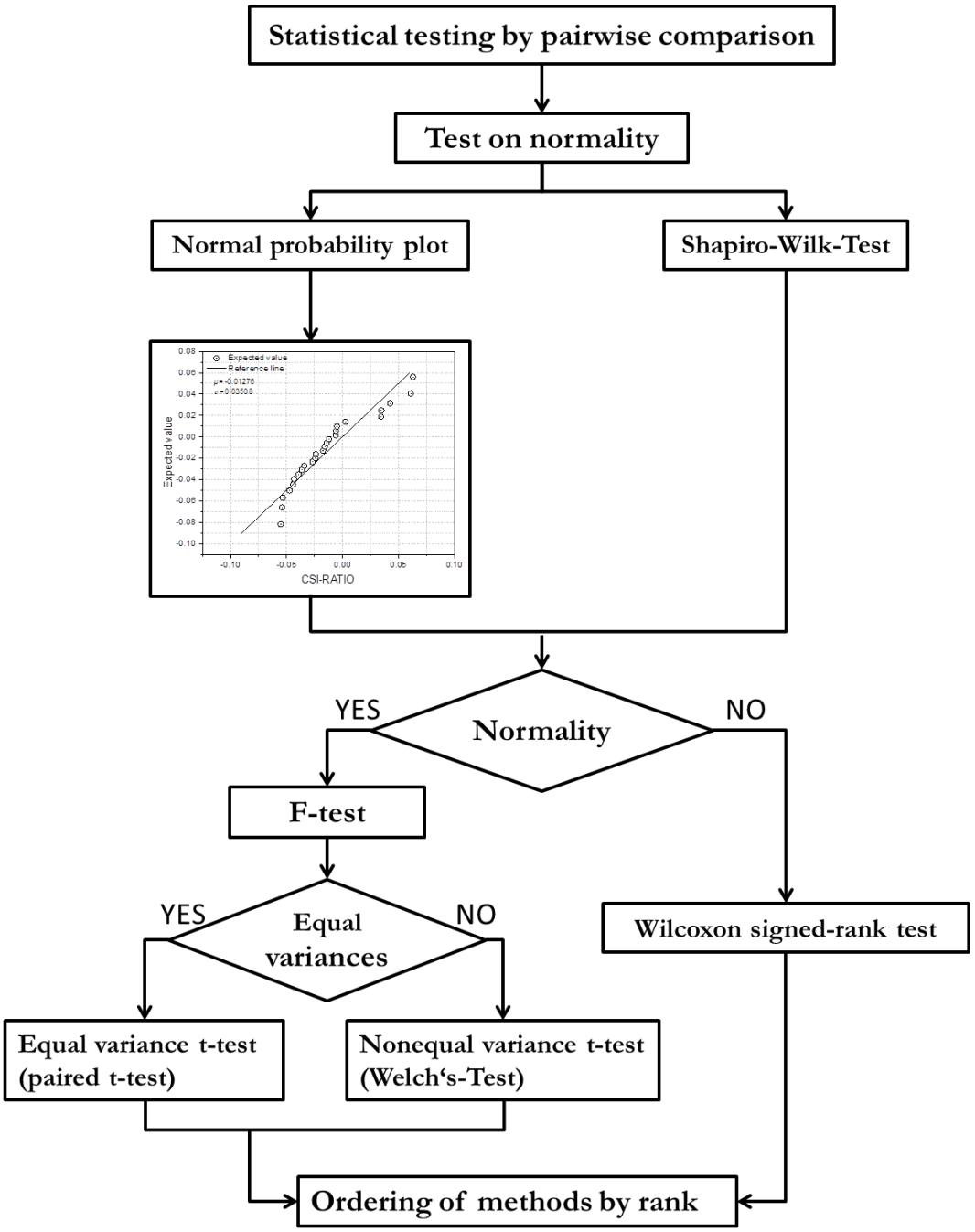

Figure 5-10 Flow chart showing the procedure for the comparison of biodegradation
The differently calculated biodegradation of methane was compared further by statistical means. Two prerequisites for statistical testing were normality of the sample data and the homogeneity of variance.

It was decided to perform paired t-tests for comparison. Prior to the test, the data were checked by QQ-plots and by the Shapiro-Wilk-test if the differences of fractions between two methods are normally distributed and by F-test on homogeneity of variances. The QQ-plots are shown in Figure 5-11. In case of the difference between the mass balance methods in panel A (MFM-MFC) the data does not show a good correlation with the reference line. The large deviation at the lower end is again due to the data from the hotspot event at day 37. In contrast, when comparing the data points with the reference line in panel B the difference MFM-CSI seems to

follow a normal distribution. Panels C and D correspond to the comparison of the mass balance MFM with the CO_2/CH_4-ratio approach (RATIO) and its correction for anabolism (RATIOC). In both cases it is not obvious whether the data is normally distributed or not. Additionally, in panel D a single data point clearly drops off from the reference line. This is also a value for the hotspot at day 37. In contrast, panels E and F seem to show a good correlation because the data points show the least deviation from the reference line compared to panels A-D. They represent the comparison of the closed system stable isotope and CO_2/CH_4-ratio approach (CSI-RATIO and CSI-RATIOC). As already indicated from the scatter plots as well as the observations from the Altman-Bland plots, the hotspot seems to cause problems when comparing the mass balance methods MFC or MFM with either CSI or RATIO. In contrast, the agreement between the methods CSI and RATIO/RATIOC seems better also during the hotspot event.

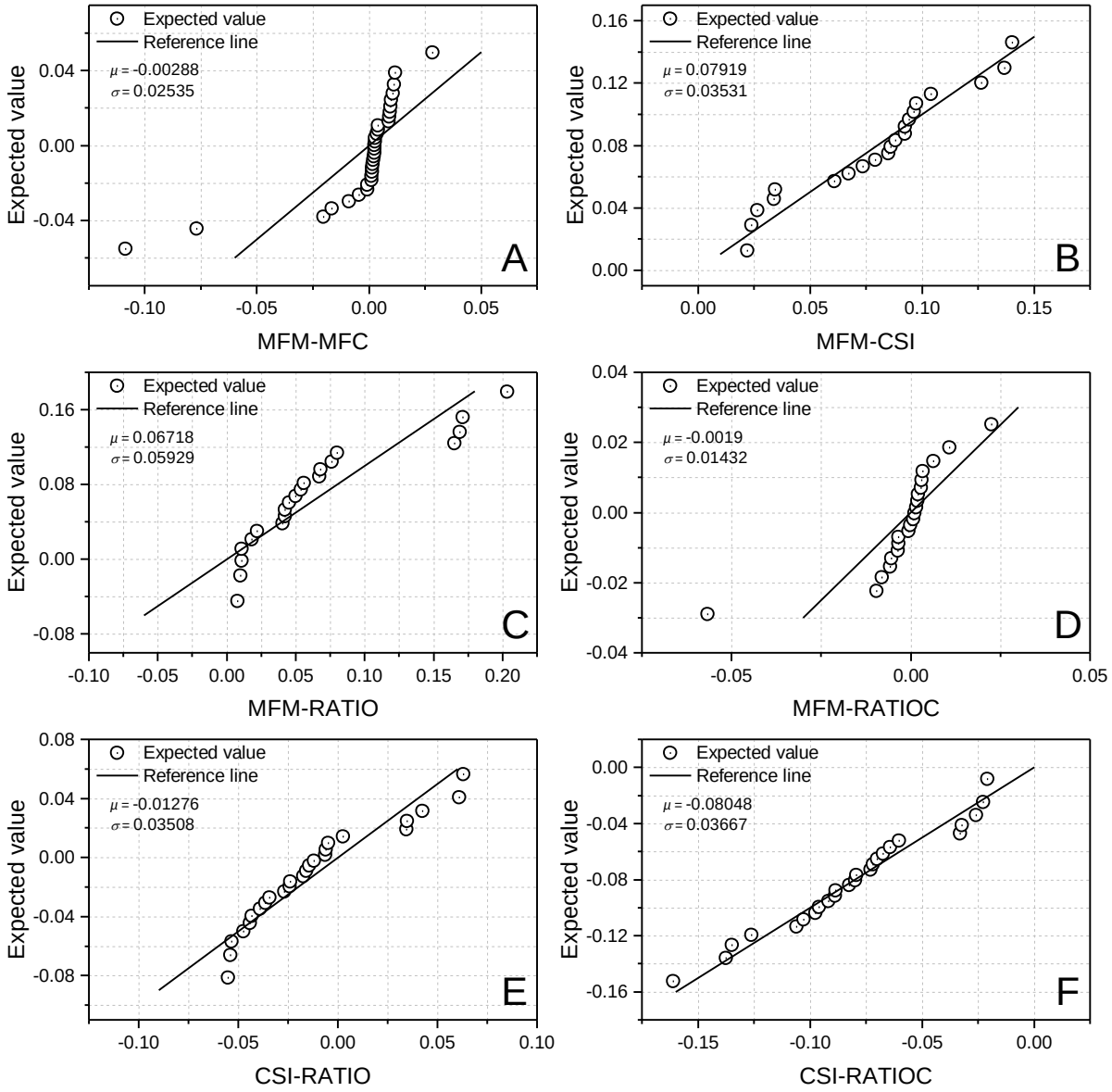

Figure 5-11: QQ-plots on the differences of methods
Given are the QQ-plots determined for the differences between each method as indicated by the label of the *x*-axes. The solid line represents the reference line. The slopes and *y*-intercepts are indicated by μ and σ, respectively.

The results of the Shapiro-Wilk test are given in Table 5-4. At a confidence level of 99% the comparison of the MFM-MFC, MFM-RATIO, and MFM-RATIOC are not significant with respect to normal distribution. The highest p-value was calculated for CSI-RATIOC which is in agreement with the respective scatter plot in Figure 5-8 F and the QQ-plot in Figure 5-11 F.

Table 5-4 Test on normality of differences and on homogeneity of variances of fractions of oxidized methane
Degrees of freedom (df) include the values for the two sampling sides of the reactor plate.

Difference of fractions oxidized	df	Shapiro-Wilk (p-value)	F-test (p-value)
MFM - MFC	**32**	**$1.4 \cdot 10^{-8}$**	**0.26**
MFM - CSI	**21**	**0.16**	**0.08**
MFM - RATIO	**21**	**$1.3 \cdot 10^{-3}$**	**$2.4 \cdot 10^{-3}$**
MFM – RATIOC	**21**	**$1.4 \cdot 10^{-5}$**	**0.66**
CSI – RATIO	**25**	**$1.5 \cdot 10^{-2}$**	**0.22**
CSI - RATIOC	**25**	**0.47**	**0.04**

Following the Shapiro-Wilk-test the differences of methods that were normally distributed were investigated for the three alternative hypotheses by paired t-tests (given in Table 5-5): (1) The methods differ (H_1: $\mu_d \neq 0$), and one of the methods returns (2) smaller (H_1: $\mu_d > 0$) or (3) larger (H_1: $\mu_d < 0$) values for the calculated relative methane oxidation. The differences that were not normally distributed were investigated by the Wilcoxon-sign-rank test (see Table 5-6).

Table 5-5 Paired t-tests of different methods for relative methane oxidation
d refers to the arithmetic mean of differences of A minus B, t is the test result, SD_d is the standard deviation of differences ($\sigma_{(A-B)}$), and n_d the number of pairs

T-test A-B	H_0: $\mu_d = 0$	H_1: $\mu_d \neq 0$	H_1: $\mu_d > 0$	H_1: $\mu_d < 0$	t	d	SD_d	n_d
A = f_{ox}^{CSI} **B =** f_{ox}^{MFM}	**p-value**	**$2.00 \cdot 10^{-9}$**	**1.00**	**$1.00 \cdot 10^{-10}$**	**-10.3**	**-0.079**	**0.035**	**21**
A = f_{ox}^{CSI} **B =** f_{ox}^{RATIO}	**p-value**	**0.081**	**0.959**	**0.041**	**-1.82**	**-0.013**	**0.035**	**25**
A = f_{ox}^{CSI} **B =** f_{ox}^{RATIOC}	**p-value**	**$7.76 \cdot 10^{-11}$**	**1.00**	**$3.88 \cdot 10^{-11}$**	**-11.0**	**-0.080**	**0.037**	**25**

According to the t-test statistics and based on a significance level of $\alpha = 0.01$, the results are significant for H_1: $\mu_d \neq 0$ and H_1: $\mu_d > 0$ for the comparison of CSI-MFM and CSI-RATIOC but not for CSI-RATIO. In case of the Wilcoxon-sign-rank test, only the comparison of f_{ox}^{MFM} - f_{ox}^{RATIO} is significant, in particular for H_1: f_{ox}^{MFM} - $f_{ox}^{RATIO} \neq 0$ and H_1: f_{ox}^{MFM} - $f_{ox}^{RATIO} > 0$. When comparing the results of the paired t-test and the Wilcoxon-sign-rank test one may order the methods in terms of calculated relative methane oxidation after the Bonferroni correction (Falk, 2014) for the significance level (with $\alpha_{corrected} = \alpha/n$; with n = number of pairwise comparisons). In this case the order is as follows: $f_{ox}^{RATIOC} = f_{ox}^{MFM} = f_{ox}^{MFC} > f_{ox}^{RATIO} = f_{ox}^{CSI}$.

As a result, the estimation of the biodegradation calculated from either stable isotope data for a closed system (CSI) or from the CO_2/CH_4-ratio (RATIO) is not identical with the respective mass balance method (MFM) and can be regarded to result in lower estimates. For CSI this is in accordance with the literature where the stable isotope method returns lower estimates than a mass balance (Chanton et al., 2008b; Powelson et al., 2007).

Table 5-6 Wilcoxon-sign-rank test of different methods for relative methane oxidation
W is the test score, Z is the score, and N the number of observations

A-B	H_0: $\mu_d = 0$	H_1: A ≠ B	H_1: A > B	H_1: A < B	*W*	Z	N
A = f_{ox}^{MFM} B = f_{ox}^{MFC}	p-value	0.05	0.03	0.97	367	1.92	32
A = f_{ox}^{MFM} B = f_{ox}^{RATIO}	p-value	9.5×10^{-7}	$4.8 \cdot 10^{-7}$	1	231	4.00	21
A = f_{ox}^{MFM} B = f_{ox}^{RATIOC}	p-value	0.81	0.61	0.41	108	-0.24	21
A = f_{ox}^{MFC} B = f_{ox}^{RATIOC}	p-value	0.45	0.78	0.23	93	-0.76	21

5.7.4 Average biodegradation and criteria for the release from aftercare

The calculated average biodegradation of each of the four methods is summarized in Table 5-7. Based on the mass balance the biodegradation of methane was always above 92% which emphasizes the cover soil's capability of oxidizing moderate gas loads in the investigated range of 35 - 65 $gm^{-2}d^{-1}$. This is in the range of CH_4 gas fluxes (~85 $gm^{-2}d^{-1}$) typical for older landfills or landfills with gas extraction systems (Scheutz et al., 2009). In case of the calculations by stable isotopes and CO_2/CH_4-ratio, the efficiencies were always lower, especially during the hotspot and cooling. Still, the minimum methane oxidation rate would correspond to 1.7 - 3.4 $Lm^{-2}h^{-1}$ based on the stable isotope approach, 1.6 - 3.0 $Lm^{-2}h^{-1}$ based on CO_2/CH_4-ratio, and to 2.0 - 3.8 $Lm^{-2}h^{-1}$ based on mass balance, all of which are within reported methane oxidation capacities for cover materials (Rachor et al., 2011; Scheutz et al., 2009).

Table 5-7: Average calculated biodegradation: for normal, hotspot, and cooling simulation

Summarized are the average methane loads with their standard deviations, and the fractions of oxidized methane of the different approaches by mass balance (MFM, MFC), CO2/CH4-ratio (RATIO), and closed system stable isotopes (CSI) along with their expanded uncertainties (calculated based on the GUM (JCGM100:2008)) with a coverage factor of k = $t_{95\%}$(df) with (df) = degrees of freedom.

Method	Hotspot	df	Normal	df	Cooling	df
CH_4 load /$gm^{-2}d^{-1}$	**38.2 ± 3.0**		**41.0 ± 2.3**		**57.4 ± 4.4**	
f_{ox}^{MFM}	**0.92 ± 0.04**	**9**	**0.99 ± 0.01**	**9**	**0.95 ± 0.01**	**13**
f_{ox}^{MFC}	**0.94 ± 0.03**	**9**	**0.98 ± 0.02**	**9**	**0.92 ± 0.01**	**13**
f_{ox}^{CSI}	**0.77 ± 0.08**	**5**	**0.92 ± 0.02**	**7**	**0.83 ± 0.01**	**12**
f_{ox}^{RATIO}	**0.74 ± 0.1**	**5**	**0.95 ± 0.01**	**7**	**0.86 ± 0.01**	**12**

With respect to the criteria for the release of old landfills from aftercare, Stegmann (2005) suggested a maximum CH_4 emission of 0.5 - 1.0 $Lm^{-2}h^{-1}$ or a maximum landfill gas (LFG) extraction of 50 - 70 m^3h^{-1} based on a 1 - 2 ha landfill for a gas composition of 50% CH_4 and 50% CO_2. This is equivalent to a methane load to the cover soil of 1.75 - 3.5 $Lm^{-2}h^{-1}$, considering the extracted methane relates to 100% of the total produced methane within the anaerobic zone. Regarding the results of this study (see Table 5-8), the maximum CH_4 load (2.2 - 4.1 $Lm^{-2}h^{-1}$) as well as the maximum surface emissions (0.0 - 0.7 $Lm^{-2}h^{-1}$) were thus comparable with the conditions suggested by Stegmann (2005). Finally, based on the soil volume of ~0.26m^3 (110 cm soil thickness) the maximum methane oxidation rate was in the range of 5.1 - 9.7 $gm^{-3}h^{-1}$. Similarly, in a study by Felske (2003) a reactor filled with a recultivation soil with a comparable soil thickness of 105 cm and a soil volume of ~0.21m^3 was able to oxidize CH_4 loads of 5.7 $Lm^{-3}h^{-1}$.

Table 5-8 Average surface emissions of methane for the different scenarios

Given are the maximum loads and surface emissions calculated based on Table 5 7.

Gas flow /$Lm^{-2}h^{-1}$	Hotspot	Normal	Cooling
Maximum average CH_4 load	**2.7**	**2.7**	**4.1**
Maximum emission by MFM	**0.2**	**0.0**	**0.2**
Maximum emission by MFC	**0.2**	**0.1**	**0.3**
Maximum emission by CSI	**0.6**	**0.2**	**0.7**
Maximum emission by RATIO	**0.7**	**0.1**	**0.6**

With respect to the methane emission, the oxidation ratio of the fraction of oxidized methane from closed system stable isotope calculations divided by the fraction of oxidized methane for mass balance ($f_{ox}^{CSI} / f_{ox}^{MFM}$) was reported to depend on the inflow of methane (Powelson et al., 2007) with ($f_{ox}^{CSI} / f_{ox}^{MFM} = 1 - 0.640e^{-0.00317 \cdot J_{out}}$) and also the oxidation rate was reported to depend on methane input (Powelson et al., 2006) with $J_{ox} = 4.24 J_{in}^{0.687}$ and $R^2 = 0.855$ for a compost biofilter; and $J_{ox} = 0.623 J_{in}$ and $R^2 = 0.944$ for a water-spreading biofilter. In this study, these observations were not confirmed. However, the respective gas flows of this study did not cover the same range as in the studies referred to. As can be seen in Figure 5-12 no trend is observable for the plot of the oxidation ratio ($f_{ox}^{CSI} / f_{ox}^{MFM}$) versus the methane outflow (J_{out}). Regarding the linear regression in Figure 5-12 with $J_{ox} = 0.997 J_{in}$ and $R^2 = 0.999$ the methane oxidation rate (J_{ox}) was directly proportional to the methane gas load (J_{in}). Nearly no deviation from the ideal y = x is present which is to some part due to the high oxidation of methane that was not strongly decreased during the hotspot and cooling simulation.

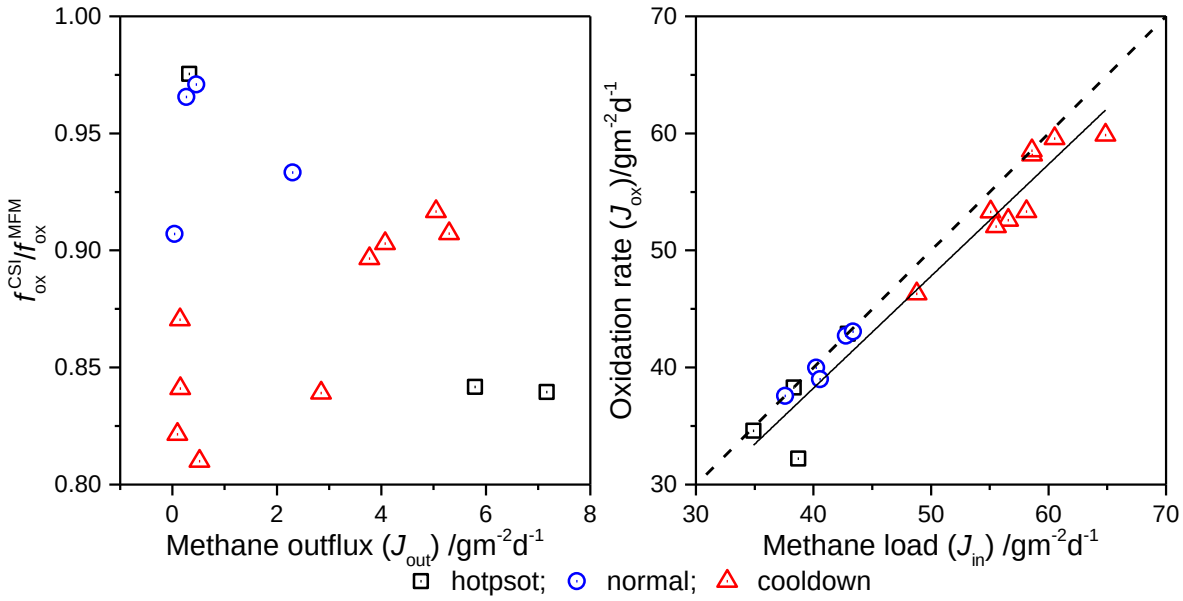

Figure 5-12 Oxidation ratio $f_{ox}^{CSI} / f_{ox}^{MFM}$ versus outflux and oxidation rate versus gas load

In the left panel the oxidation ratios versus the methane outflux (J_{out}) for the different investigated scenarios are shown. The right panel shows reference line $J_{ox} = J_{in}$ (broken line), the linear regression (solid line) performed on the data points for all three scenarios hotspot, normal, and cooling. The regression parameters were: $J_{ox} = 0.997 J_{in}$; $R^2 = 0.999$.

5.7.5 Implications of measurement uncertainties of the different methods

When comparing the mass balancing methods with the stable isotope methods the error in the estimation of the fraction of oxidized methane based on stable isotopes is a very important aspect. This problem has been addressed previously in studies applying stable isotope analysis. However, the actual resulting error in the fraction of oxidized methane based on the error of the enrichment factor has not been dealt with thoroughly. For example in (Capanema and Cabral, 2012) a value of $KIE = 1.0235 \pm 0.0047$ was taken from (Cabral et al., 2010) to calculate the oxidation efficiencies. It was stated that the standard deviation was $\Delta KIE \approx 0.5\%$ and "that a mere 0.5% change in KIE value resulted in an important dispersion in oxidation efficiencies" (Capanema and Cabral, 2012). Yet, the actual parameter that is determined from degradation studies is:

$$\varepsilon = \frac{1}{KIE} - 1.$$

This "mere" change of $\Delta KIE = 0.0047$ thus more adequately corresponds to the change of:

$$\Delta\varepsilon = \frac{1}{\Delta KIE + 1} - 1 \approx 19.5\%.$$

Nevertheless, the problem of over- or underestimating the fraction oxidized is pointed out well in in (Capanema and Cabral, 2012). Another problem is the choice of which system is present, a closed or an open one. This strongly affects both the estimated biodegradation as well as corresponding error. Interestingly, while choosing an open system returns higher estimates - which is "good" when higher estimates are wanted (e.g., landfill operator)- it is much more affected by the error of the isotopic enrichment factor. The closed system in return will give lower estimates of the fraction of oxidized methane but with a lower error. For the purpose of visualization, the following graphs may be regarded (Figure 5-13). An average value for $\varepsilon = -0.02$ with a standard deviation of $\Delta\varepsilon = 0.0005$ was chosen. These values are very similar to the values determined in chapter 3 but also in comparison with results from the literature (see Chanton et al. (2008a)). In Figure 5-13 both calculations show similar errors up to a fraction of oxidized methane of 0.3. The maximum error of the fraction of oxidized methane for a closed system is <0.11 at a value of ~0.6. This is up to 2.5 times lower than the maximum error for the open system. Essentially, the error on the fraction of oxidized methane is dominated by the error of the enrichment factor.

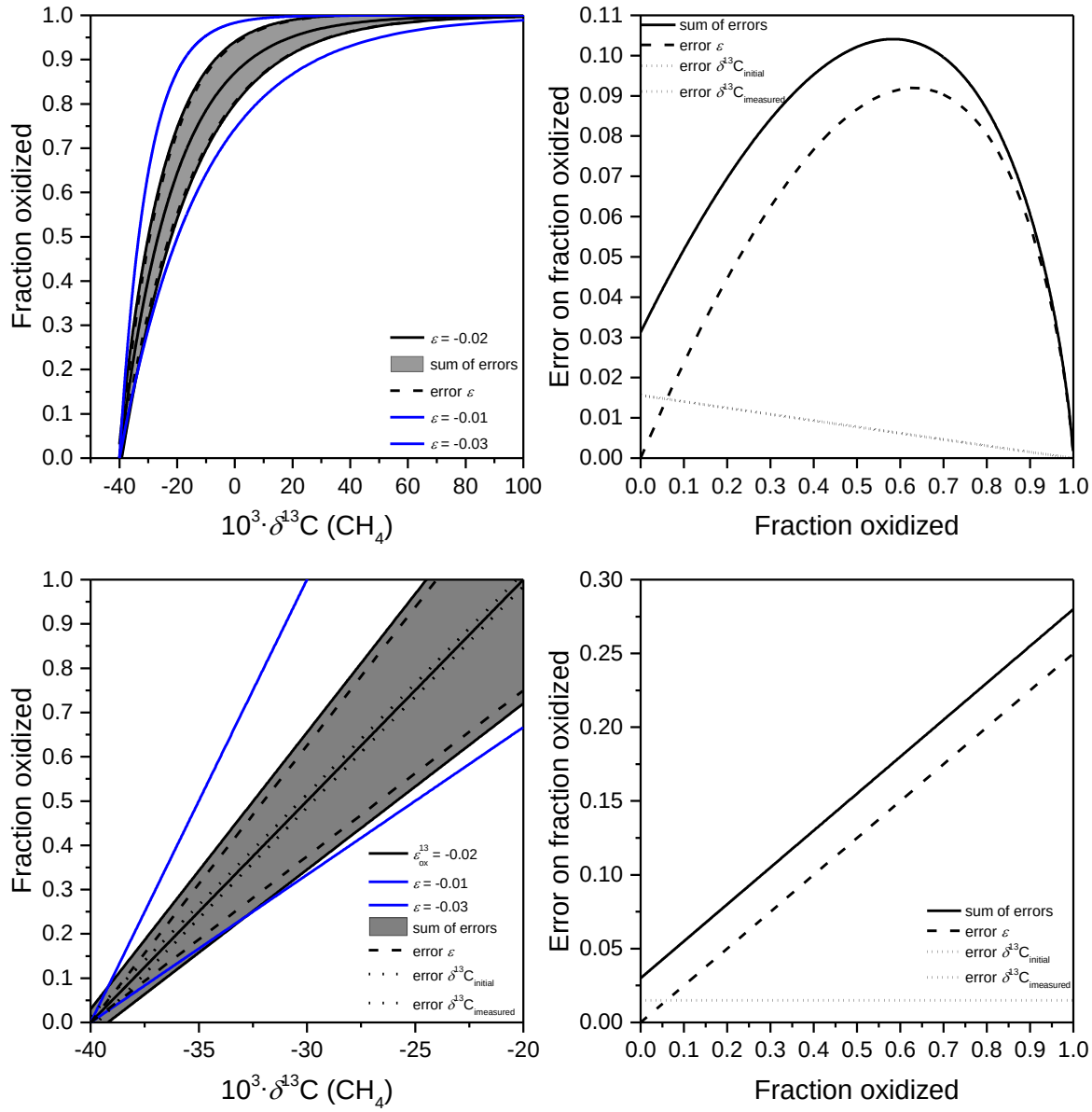

Figure 5-13 Comparison of fraction oxidized and the effect of errors for stable isotopes
At the top: Comparison of closed system (CSI). On the left side the fraction of oxidized methane (black line) versus its stable carbon isotopic signature is shown. The initial value of methane is $\delta^{13}C_0$ = -40‰. The gray area around the fraction remaining corresponds to the sum of errors ($\Delta\delta^{13}C$ = 0.3‰., and $\Delta\varepsilon$ = 5‰) The blue lines correspond to the profile for an enrichment factor of = -10‰ and -30‰, respectively. On the right side it is clearly visible that the major input of error on the fraction oxidized is the error in enrichment factor.
At the bottom: Comparison of open system (OSI). The blue lines correspond to the profile for an enrichment factor of ε = -10‰ and -30‰, respectively. On the right side it is clearly visible that the major input of error on the fraction oxidized is the error in enrichment factor. It increases linearly and is even larger than for a closed system.

In case of the RATIO method the error on the fraction oxidized can be regarded as almost even over the entire range with a slight decrease towards higher fractions of oxidized methane. The step in the right panel in Figure 5-14 is due to the different coefficients of variation for the three calibration ranges.

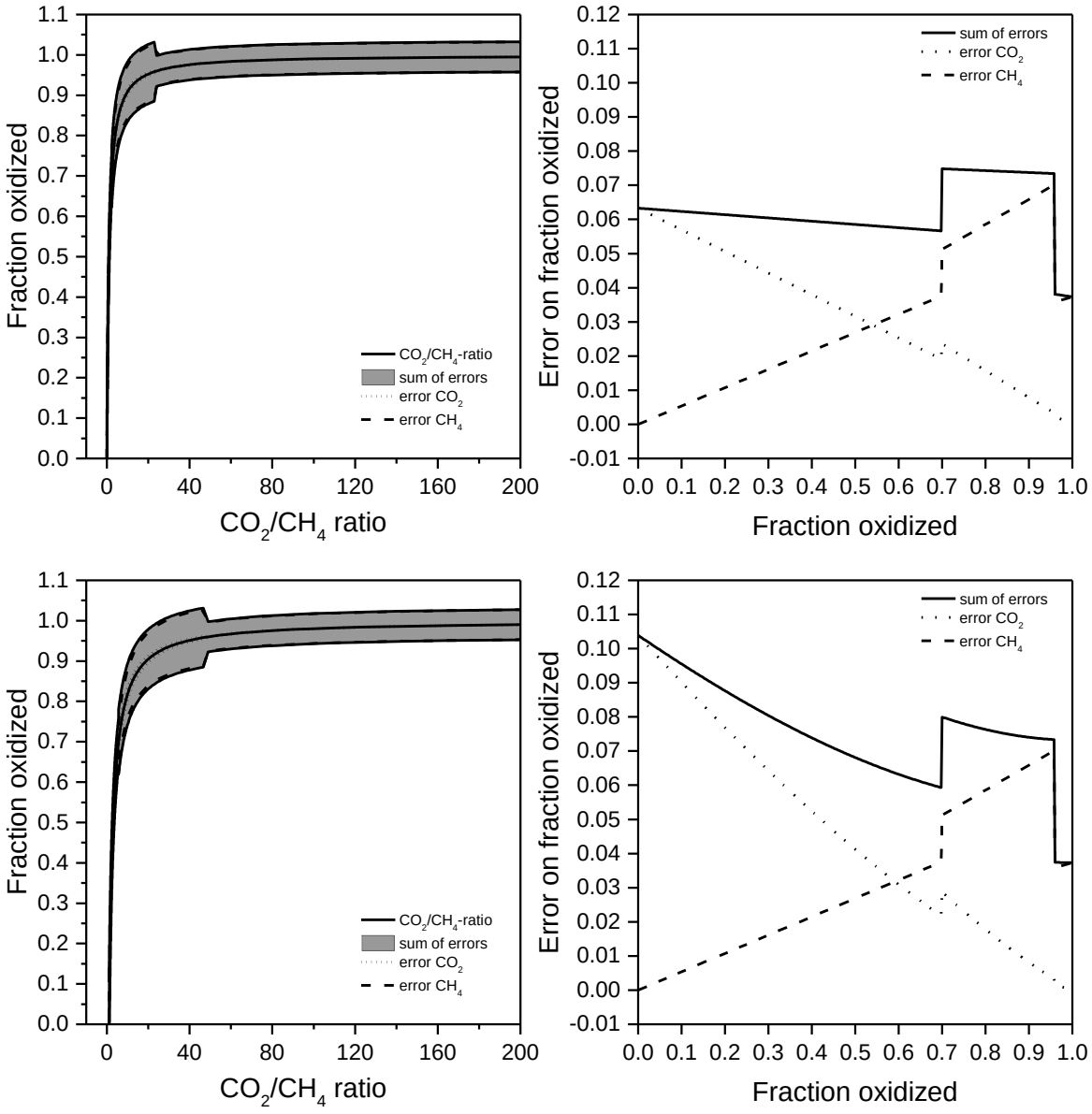

Figure 5-14 Comparison of fraction oxidized vs. CO2/CH4 ratio and the effect of errors
The fraction of oxidized methane vs. the CO_2/CH_4-ratio (based on the RATIO method) without an initial CO_2 concentration (top) and with 50 vol.-% initial CO_2 concentration (bottom). The initial CH_4 concentration was 50 vol.-%. Note the steps in errors is due to three different calibration ranges with three different coefficients of variation (see Table 5-2).

Also, important inputs of uncertainty are soil and plant root respiration, and differential solubility in water (Chanton et al., 2009), which were not considered in the calculations here. It would increase the error on the fraction oxidized and result in higher estimates. Clearly, the mass balance method has the lowest error of all methods (Figure 5-15). In the field, the estimation of the mass fluxes is very difficult, however.

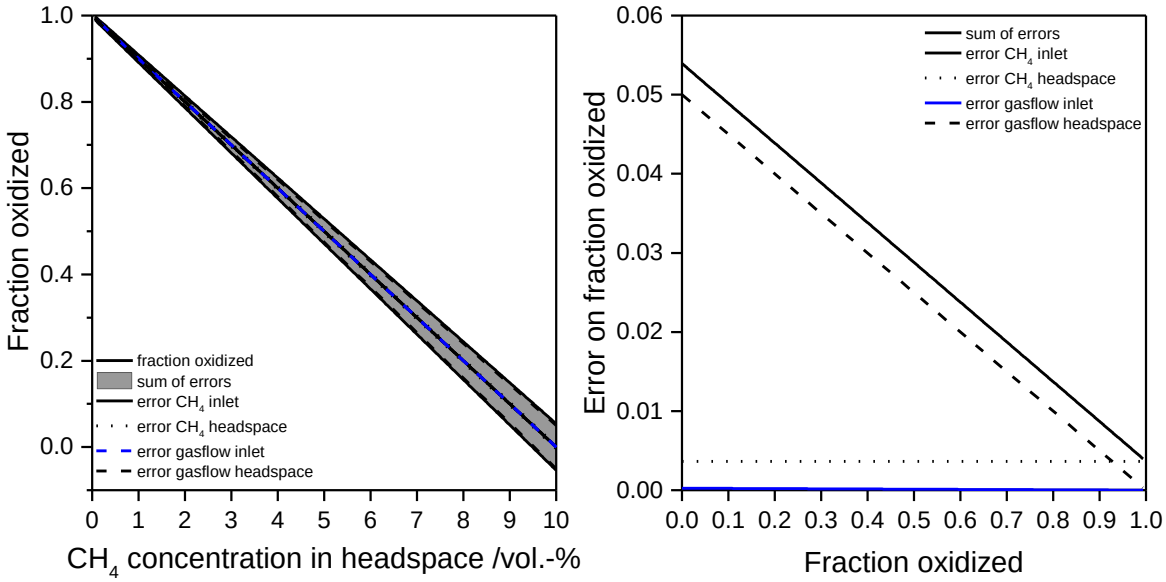

Figure 5-15 Comparison of mass balance method of fraction oxidized vs. CH4 concentration and the effect of errors on the fraction oxidized

The errors were estimated based on the following input parameters: CH_4 concentration at inlet 50 vol.-%; inlet gas flow: 20 $mLmin^{-1}$; headspace gas flow: 100 $mLmin^{-1}$; error on inlet gas flow: 1 $mLmin^{-1}$; error on headspace gas flow: 5 $mLmin^{-1}$; error on CH_4 concnetration at inlet: 2.69 vol.-% and headspace 3.66 vol.-% (see Table 5-2).

5.8 Conclusion

In summary, the three scenarios hotspot, normal state, and cooling were investigated, with respect to the relative methane oxidation by three independent methods. Within the hotspot simulation, the methane oxidation was significantly reduced by the locally increased gas load. During the normal scenario, the biodegradation was between 92% and 99% (depending on the method of calculation) and thus the cover soil was capable of reducing the methane load down to a level of emission at which old landfills have been suggested to be released from aftercare. In the cooling scenario, the temperature of the soil was decreased by heat exchangers, but the drop in methane biodegradation was rather due to the increase in total gas load than due to the decrease in temperature. Overall, the soil body was well capable of oxidizing the methane load to a considerable extent which -given the same conditions on a landfill- would indeed fulfill the requirements for releasing a landfill from aftercare. Also, greater gas loads would probably be oxidized to a high extent as well since the oxidation rate correlated with the methane load nearly 1:1 (J_{in} = 0.997 J_{ox}) and no decline was observed. With respect to the calculated response to the three scenarios in terms of biodegradation of methane, the different methods showed similar trends. A direct comparison of the methods by scatter plots revealed a good correlation from linear regression. In particular, the CO_2/CH_4-ratio approach and the closed system stable isotope approach as well as the comparison of the CO_2/CH_4-ratio approach corrected for anabolism and mass balance showed a good fit. However, an apparent interchangeability could not be proven as relative bias was found by Altman-Bland plots. In addition, paired t-tests and Wilcoxon-sign-rank tests on the pairs of different methods allowed a rough classification with respect to the degree of calculated relative methane oxidation. The mass balance methods return higher estimates compared to CSI and RATIO method. A correction for anabolism in case of RATIOC returned the highest estimates, however. This emphasizes, that the correction for anabolism represents a fitting parameter and if known allows substituting the RATIOC method for the mass balance method in the field.

Based on these results the following question may arise: Which method is suitable or applicable and what considerations have to be made in field studies? On the one hand, a mass balance approach similar to MFM and MFC is very precise. For biofilters or reactor systems this approach has been applied in different studies (Capanema and Cabral, 2012; De Visscher, 2004; Gebert, 2011; Powelson et al., 2006; Powelson et al., 2007) and is easily achieved by monitoring the respective gas flows directly and by quantification of the CH_4 gas concentrations. On the other hand, it requires the knowledge of the volume flow of methane entering (J_{in}) and exiting (J_{out}) the system. While in the field the emitting gas flow is usually determined by static flux

chambers (as for example (Christophersen et al., 2001; Rachor et al., 2013)) the flux from the anaerobic zone has to be estimated e.g. from the stoichiometry of the chemical reaction of methane oxidation (Christophersen et al., 2001; Gebert, 2011). The CO_2/CH_4-ratio method is a mass balance method based on the chemical reaction of methane oxidation. Its advantage is that the respective volume flows cancel out (considering CO_2 and CH_4 traverse within the same gas parcel) and thus only the respective concentrations are necessary to estimate the fraction of oxidized methane. Since it is more or less independent of volume flow the methane oxidation by soil depth can be determined, too. It also is a simple methodology and does not require expensive equipment. Jet, relevant processes such as increased soil respiration, dissolution of CO_2 into soil water, and changes between anabolism and catabolism or type of methanotrophs have a significant influence on the estimated methane oxidation. Still, for mineral soils this method is very suitable as CO_2 production from soil respiration becomes negligible at methane oxidation rates higher than 3.6 $\mu g g^{-1}_{dry\text{-}weight} h^{-1}$(Gebert, 2011). For the estimation of biodegradation of methane by stable isotope analysis both the stable isotopic composition of the reactant and the residual reactant need to be measured. This corresponds to the methane entering and exiting the system in biofilters or reactor systems, and to methane from the anaerobic zone and above the active zone or from the soil surface in the field. In addition, the isotopic fractionation factor for the microbial methane oxidation (α) and the isotopic fractionation factor for diffusion of methane (α_{diff}) have to be known. Also, choosing between the open and closed system method is not always straightforward. While both the open system (Chanton et al., 1999; Liptay et al., 1998) and the closed system have been considered (Chanton et al., 2008b; Powelson et al., 2006) it is not always obvious which approach is suitable or even the correct one in the field. It has been stated that "the closed-system assumption that a sample of gas moves through soil without mixing with other CH_4 may not be realistic" (Chanton et al., 2009). In fact, a combination of both systems may also be possible ((Fry, 2008) pp 212 – 214). In addition to choosing either method the existing gas flow conditions may require a correction for α_{diff}. When advective transport dominates the gas flow α_{diff} is regarded to be negligible ($\alpha_{diff} = 1$) but requires consideration in case of diffusive transport. For the latter the proper value for α_{diff} has to be determined or estimated individually at each landfill site as different values have been reported ((Börjesson et al., 2007; Chanton et al., 2008a; Gebert et al., 2013) and were stated to depend on gas permeability of cover material and soil type, as well as atmospheric air pressure and landfill gas capture (De Visscher and Van Cleemput, 2003). In some studies the $\delta^{13}C$ values for methane in the gas phase/atmosphere are often more negative than in the soil body near the surface (see (Cabral et al., 2009; Chanton et al., 2008b; De Visscher, 2004)). The experimental data of this work also supported this observation in some cases. Thus a more conservative estimation of the

biodegradation will result from samples collected from the gas phase. For the determination of the biodegradation at landfill sites it has been suggested to use the estimates near the soil surface as an indication of maximum yield and the values obtained from the gas phase as the conservative turnover (Chanton et al., 2008b). Concluding for field measurements, both CSI and RATIO show different advantages and disadvantages. However, if the circumstances on site are known either method or even a combination of CSI and RATIO can be chosen carefully to get the best estimate of the microbial methane oxidation.

6 Localizing the active zone of bacterial methane oxidation in a simulated landfill cover system

6.1 Introduction

The biodegradation of methane in the experimental soil cover was investigated for the three different conditions as described in the previous chapter. At landfill sites in Germany, a soil cover's thickness has to be at least 1 m as regulated by the "Deponieverordnung" (Deponieverordnung, 2013). However, the required thickness of the methane oxidation layer is influenced by many factors which are reviewed in (Huber-Humer et al., 2008; Scheutz et al., 2009). Among these are the spatial and temporal variations of the soil's physical and chemical properties which have a strong impact on soil gas transport and the methanotrophic activity (Scheutz et al., 2009). These include factors such as soil temperature, moisture, and gas composition. At an old landfill in northern Germany, the influence of soil temperature, soil moisture, and barometric pressure on the soil gas composition was investigated (Gebert et al., 2011b; Rachor et al., 2013). When gas transport of methane was mainly diffusive the soil gas composition showed a seasonal variability which was mainly controlled by soil temperature (Gebert et al., 2011b; Rachor et al., 2013). For so called hotspots with increased advective gas flow (e.g., due to fissures in soil) the barometric pressure had the strongest influence on the soil gas composition (Gebert et al., 2011b; Rachor et al., 2013). Under dry conditions methane emissions from hotspots were found to be independent from soil moisture but instead increased with decreasing soil temperature (Rachor et al., 2013). In contrast, when soil moisture strongly reduced the gas permeability, the methane emissions decreased with an increase in soil moisture content (Rachor et al., 2013).

Consequently, and in order for a cover layer to effectively reduce methane emissions, it is important to understand and forecast its response to different environmental conditions. This requires the characterization of the active zone of methane oxidation. Finding the active zone and identifying its dimensions within biofilters or cover layers, so as to predict alterations or shifts by changing conditions may be achieved by monitoring temperature and soil gas profiles (e.g., "intersection" of oxygen and methane concentrations, from CO_2/CH_4-ratio, and stable isotope analysis). Furthermore, the bacterial communities within the soil cover can be identified by different strategies such as fluorescence in situ hybridization (FISH)(Gehrke et al., 2013a) and Stable isotope probing (SIP)(Cebron et al., 2007; Crossman et al., 2004; Maxfield et al., 2012), as well as from 16srRNA genes (McDonald et al., 2008). For example, the influence of advective and diffusive soil gas transport on the active zone has been investigated with respect to the soil

bacterial community (Gebert and Perner, 2015). At sites with the highest surface methane concentrations (hotspots) the bacterial diversity was reduced and a purple discoloration at the soil surface was associated with methanotrophic community (type II *Burkholderiales*, *Rhodospirillales* and *Bradyrhizobiaceae*). With respect to highest methane oxidation soil samples are usually taken at different depths and then measured in individual batch experiments in the lab, for example see (Bogner et al., 2003; De Visscher et al., 1999).

A thermodynamically consistent model that considers conversion, diffusion and advection processes as well as the energy production and temperature has been introduced by (Thom et al., 2016). It was validated in terms of heat generation based on a new experimental setup which used the thermal imaging technique.

The aim of this chapter was to localize the site of the active zone by stable isotopes and CO_2/CH_4-ratios, and to examine whether the identified site correlates with an increase in temperature which results from bacterial methane oxidation.

6.2 Experimental setup

The same reactor system as described in chapter 5.2 was used. Thermographic imaging was performed daily using a testo 875-1i thermographic camera (Testo SE & Co. KGaA, Lenzkirch, Germany). In order to reduce the possibility of thermographic artefacts formed by light scattering and reflection the front was finished with a black varnish (Figure 6-1).

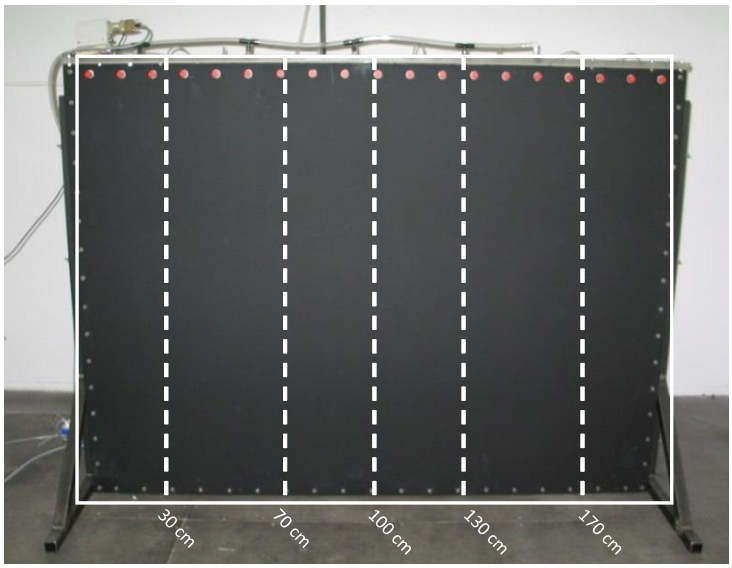

Figure 6-1: Image of the front facing of the reactor plate
The front facing of the reactor plate was painted with black varnish to minimize reflections. The broken lines represent individual sampling profiles.

6.3 Sampling

The reactor was sampled from the back at two vertical lines at 70 cm (left) and at 130 cm (right) with eight sampling points each. For the left profile these were at 6.5, 23.5, 40.5, 58, 75.5, 93, 111, and 129 cm, and for the right at 6.5, 23.5, 40.5, 59.5, 77.5, 95, 113, and 132 cm. The sampling profiles at 30, 100, and 170 cm were used for experiments described in section 6.6.3. Each of these had five sampling ports at 40.5, 60, 77.5, 95, and 146 cm depth. The gas inlet at 148.5 cm was monitored, too. At each sampling point a luer stainless steel cannula (B Braun AG, Melsungen, Germany) was inserted into the center of the reactor plate and adapted with a three-way stopcock (Sarstedt AG und Co., Nümbrecht, Germany). The reactor plate was sampled with single use 10-mL plastic syringes (Omnifix by B Braun AG, Melsungen, Germany) amended with luer three-way stopcocks. In order to avoid dead volume and CO_2 contamination from the air 5 mL of gas sample was withdrawn from the reactor plate and discarded via the stopcock to the surrounding air. Afterwards, the reactor gas was mixed by pulling and pushing the syringe plunger for two times before 10 mL were taken and the stopcock was closed. The 10-mL samples were analyzed directly afterwards within the same day of sampling.

6.4 Quantitative and stable isotope analysis

The quantitative and stable isotope analysis was performed with the same calibration data as described in section 5.4.

6.5 Data acquisition and calculations

The data acquisition was based on the software Isodat 2.5. Microsoft Excel 2010 and Origin 2015G were used for tabular calculations, statistical testing, and construction of graphics. Calculations were based on the CO_2/CH_4-ratio method (RATIO) and on the closed system stable isotope approach (CSI) as described in section 5.5. In addition, the partial difference quotients $\left(\Delta f_{ox} / \Delta x\right)$ were calculated by equation (6.5.1). The partial difference quotient is the difference of the calculated fraction oxidized (f_{ox}) by either method (CSI or RATIO) of the respective higher sampling point $f_{ox,i}$ and the next lower one $f_{ox,j}$ divided by the difference (Δx) of the corresponding sampling depths x_i and x_j. The dimension of the partial difference quotient is cm^{-1} and its vertical position in the reactor is the mean of the two sampling depth x_i and x_j.

$$\frac{\Delta f_{ox}}{\Delta x} = \frac{f_{ox,i} - f_{ox,j}}{x_i - x_j} \qquad (6.5.1)$$

6.6 Results and discussion

6.6.1 Concentration and stable carbon isotope profiles of CH_4 and CO_2

The three scenarios normal state, hotspot, and cooling that were investigated in chapter 5 for the biodegradation of CH_4 were inspected further with respect to the site specific biodegradation of CH_4 within the reactor body (see section 5.2 for further details).

Figure 6-2 illustrates the normal state with its average concentration profiles of methane and carbon dioxide for both sampling sites as well as their stable isotopic composition. The concentration of methane drops nearly exponentially from the gas inlet at the bottom to the headspace at the top. In the headspace, the concentration of methane falls down to an average of 0.2 ± 0.2 vol -%. In several cases of GC-IRMS analysis CH_4 was below the limit of detection (LOD = 0.028 vol-%). This was particularly the case for samples taken at 59 cm and 40.5 cm depth. Yet, at the soil-gas boundary (sampling point at 23.5 cm depth) and moreover in the headspace (6.5 cm depth) CH_4 was detected. In case of CO_2, the drop in concentration is less pronounced and it ceases at about 6 vol-% in the headspace of the reactor. In contrast to CH_4 CO_2 was generally measurable at each sampling point. With an average of $\Delta^{13}C_{out\text{-}in}$ = 54‰ the fractionation between the inlet and headspace is higher than maximum fractionation as for example reported in (Chanton et al., 2008b)($\Delta^{13}C$ = 13.6‰) and for biofilters given in (Powelson et al., 2007)($\Delta^{13}C$ = 5.8‰ and $\Delta^{13}C$ = 10.6‰). In comparison, the $\delta^{13}C$ values for CO_2 remain fairly constant along the profile with an average of $\delta^{13}C$ = -36.0 ± 3.5‰. Isotopic fractionation of CO_2 either due to bacterial methane oxidation soil respiration or diffusion could not be identified.

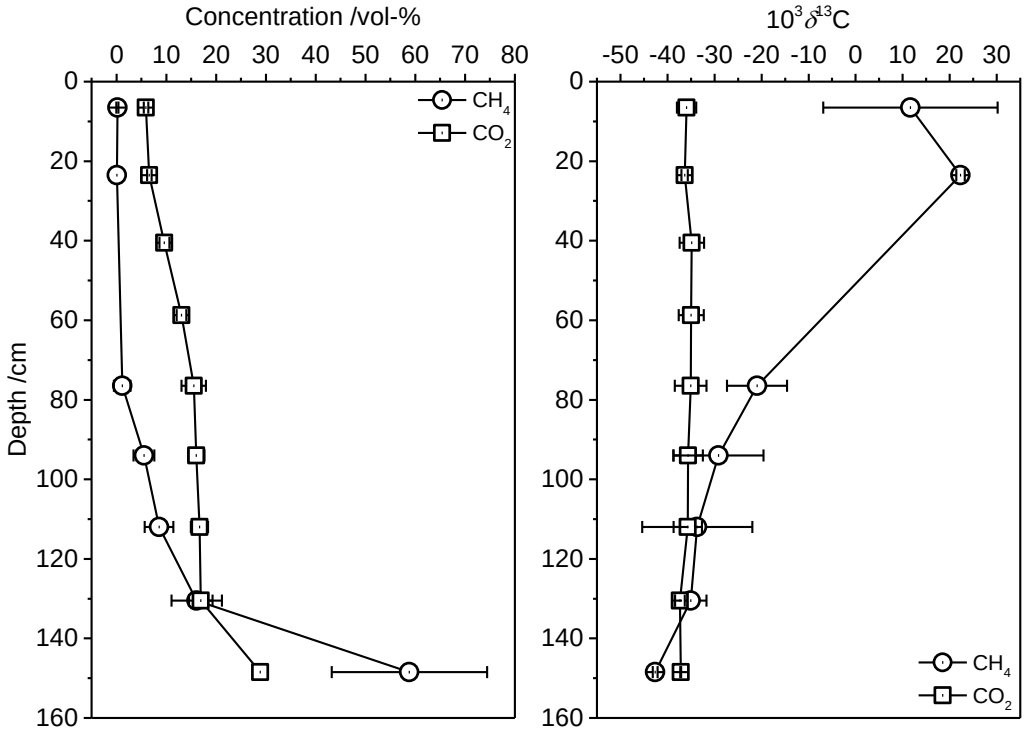

Figure 6-2: Profile of the concentration and stable isotope composition of methane and carbon dioxide (normal)
The normal state with its profile of the concentration (left) and stable carbon isotope composition (right) of methane and carbon dioxide. The symbols are the average values from triplicate measurements of both sampling lines throughout experiment day 44-86 and error bars represent the combined standard deviations.

The hotspot event is shown in Figure 6-3. While the concentration and stable carbon isotope profiles of CO_2 are very similar to the "normal" state the situation for CH_4 is completely different. For one part, the drop in concentration of CH_4 towards the soil surface shows a higher variability. For another, it also remains at a higher value in the headspace than in the normal state (with 1.4 ± 1.7 vol-%). Looking at the stable carbon isotope profile for methane it becomes evident that the $\delta^{13}C$ values stray more- especially in the headspace and the soil/gas boundary. Also, with $\Delta^{13}C_{out\text{-}in} = 38‰$ the average isotopic fractionation of methane from the top to the bottom is less than in the normal state. Both concentration and isotopic fractionation indicate a reduction of the methane oxidation compared to the normal state. The observed large variability of concentration and delta values requires a closer look at their dynamics as will be discussed later.

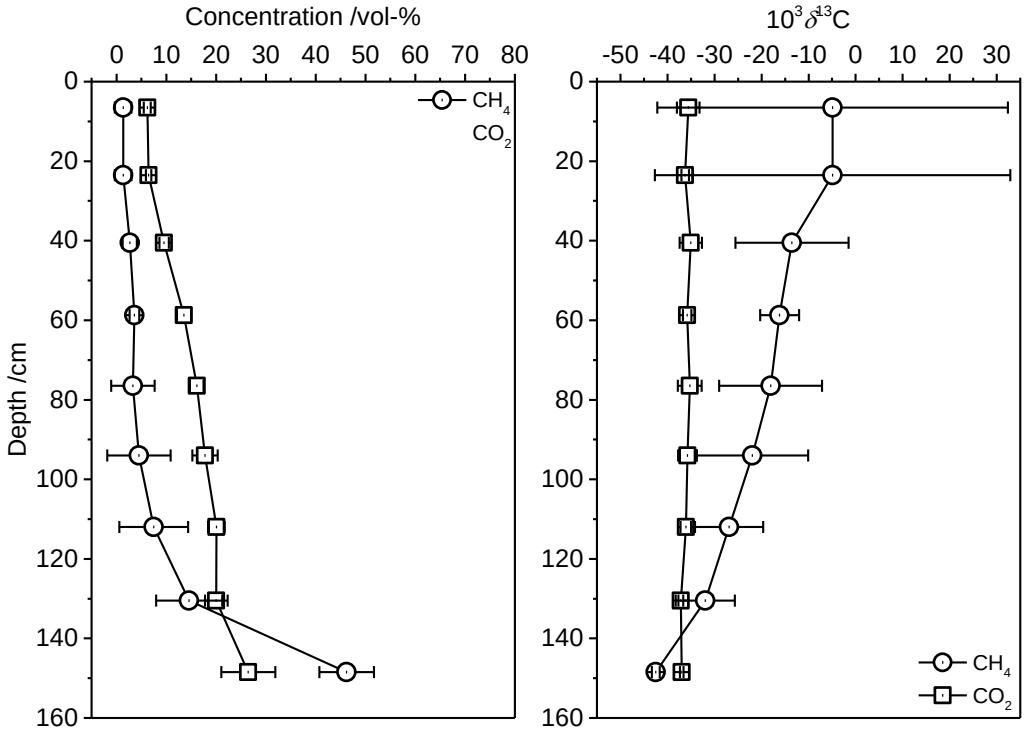

Figure 6-3: Profile of concentration and stable isotope composition of methane and carbon dioxide (hotspot)

Shown is the hotspot event with its profile of the concentration (left) and stable carbon isotope composition (right) of methane and carbon dioxide. The symbols are the average values of both sampling lines throughout experiment day 28-42 and error bars represent the combined standard deviations. Note the large standard deviations for the delta values for methane especially at the top are due to the day-to-day variations.

In the case of cooling scenario, the concentration profile of CH_4 shows less variability than the hotspot state (see Figure 6-4). The concentration in the headspace is in between the normal and the hotspot state. In contrast to the former situations where the $\delta^{13}C$ values for CH_4 became more and more positive from the bottom to the top, the profile in the cooling state shows an unexpected trend. This is particularly the case in the range from 130 cm to 59 cm. Here, the delta value first decreases by roughly 9‰ from 130 cm to 112 cm and then steadily increases again to reach about the same value as it was at 130 cm. From there on the delta value increases once more to sampling depth 40.5 cm and finally shows a decrease in the headspace, similar to the observation in the normal state. Interestingly, in the cooling scenario the variability of the $\delta^{13}C$ values of the CH_4 exiting the system is smallest for all three states, i.e., normal, hotspot and cooling. This indicates that the biodegradation of methane remained fairly constant also within the soil body. All in all, the presence of bacterial methane oxidation is apparent as shown by both the decrease in concentration as well as the stable carbon isotopic fractionation of methane.

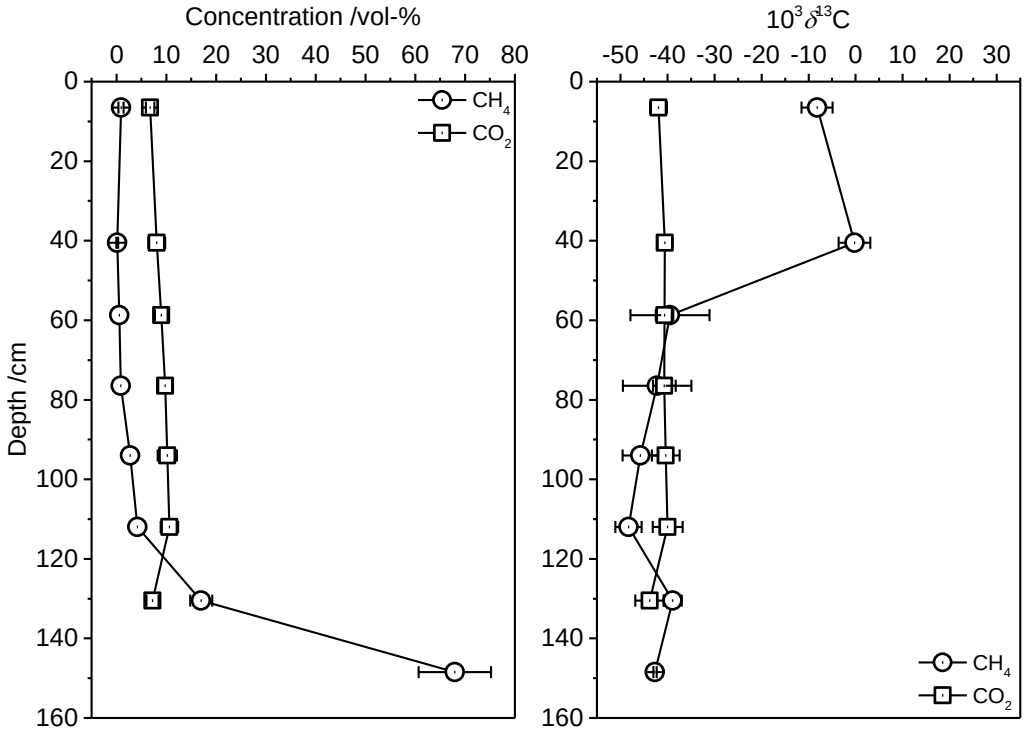

Figure 6-4: Profile of the concentration and stable isotope composition of methane and carbon dioxide (cooling)
Cooling event with its profile of the concentration (left) and stable carbon isotope composition (right) of methane and carbon dioxide. The symbols are the average values of both sampling lines throughout experiment day 88-106 and error bars represent the combined standard deviations. Note the fractionation of methane towards more negative values at 112 cm.

The observation in this work of $\delta^{13}C$ values of methane often being more negative right above the soil's surface than in the topmost soil layer has also been reported in the literature (Chanton et al., 2008b; De Visscher, 2004; Gebert et al., 2013). Three different possible causes for this phenomenon have been proposed: Diffusive fractionation, bypass mixing, and differential flow path oxidation (Chanton et al., 2008b). All three causes cannot be ruled out in this experiment. On the one hand, when regarding the low gas loads, diffusion plays an important role across the gas stream and especially near the walls (Kraume, 2012). On the other hand, also a high degree of gaps near the wall would result in higher gas permeability leading to bypass mixing (see (Kraume, 2012)). This could be caused by inhomogeneous compaction of the soil body. Since the reactor plate has a larger surface area compared to cylindrical reactors these processes have greater impact and thus may strongly affect isotopic fractionation. In order to at least reduce the degree of gaps near the walls, the surface roughness of the inner walls of the reactor plate was increased by coating them with a thin layer of gypsum.

The overall concentrations and stable isotope compositions for carbon dioxide and methane are summarized in Table 6-1.

Table 6-1: Concentration and $\delta^{13}C$ values of CH_4 and CO_2 at reactor inlet and headspace
Values are the respective arithmetic mean ± standard deviation

Parameter	Hotspot	Normal	Cooling
CH_4-out/ vol-%	**1.4 ± 1.7**	**0.2 ± 0.2**	**0.9 ± 0.5**
CH_4-in/ vol-%	**45.1 ± 5.1**	**57.0 ± 10.2**	**67.8 ± 7.3**
CO_2-out/ vol-%	**6.0 ± 1.7**	**5.9 ± 1.1**	**6.6 ± 1.9**
CO_2-in/ vol-%	**25.8 ± 1.6**	**29.2 ± 1.8**	**-**
$10^3 \cdot \delta^{13}C_{CH_4\text{-out}}$	**-4.9 ± 37.3**	**11.6 ± 18.5**	**-8.2 ± 3.3**
$10^3 \cdot \delta^{13}C_{CH_4\text{-in}}$	**-42.5 ± 0.8**	**-42.6 ± 0.6**	**-42.7 ± 0.4**
$10^3 \cdot \delta^{13}C_{CO_2\text{-out}}$	**-35.4 ± 2.7**	**-36.0 ± 1.9**	**-42.0 ± 1.8**
$10^3 \cdot \delta^{13}C_{CO_2\text{-in}}$	**-36.9 ± 0.4**	**-37.2 ± 0.1**	**-**
$10^3 \cdot \Delta^{13}C_{CH_4\text{- out - in}}$	**37.6**	**54**	**34.5**
$10^3 \cdot \Delta^{13}C_{CO_2\text{- out - in}}$	**1.5**	**1.2**	**-**

6.6.2 Vertical profiles of the biodegradation of methane in the soil cover

The two methods for the calculation of f_{ox}^{CSI} and f_{ox}^{RATIO} at the surface of the reactor have shown to be very similar as visualized by a scatter plot in Figure 5-8 F. Since they are not directly reliant on gas flow the biodegradation depending on the sampling depth in the reactor may be inspected. This is shown in Figure 6-5 for the hotspot-simulation. By following the profiles for f_{ox}^{CSI} (Figure 6-5 A and B) day by day the varying response to the locally increased gas load can be observed. In detail the oxidation by depth shifts to lower efficiencies at days 35 and 37 and then seems to recover near the top at day 42. Both sides of the reactor show similar responses at the headspace and soil surface (6.5 cm and 23.5 cm) but the profiles are somewhat different in the soil body. On the right side the variation by sampling day is higher than on the left side. Interestingly, f_{ox}^{CSI} shows a negative trend at days 35 and 37 by bending towards lower values at 40.5 cm on the left side and at 77.5 cm on the right side. In case of f_{ox}^{RATIO} (Figure 6-5 C and D) the profiles of the different sampling days are comparable with the corresponding ones for f_{ox}^{CSI} by showing similar shifts in methane oxidation throughout the simulation. As in the case of f_{ox}^{CSI} a negative trend of f_{ox}^{RATIO} is also present at ~77.5 cm depth on the right side of the reactor. The differences between right and left sampling side as well as the negative trends at days 35 and 37 may indicate the problems concerning differential flow paths/oxidation, sampling, and diffusion within the reactor as discussed above. Consequently, these could also lead to an uneven distribution of active methanotrophs within the soil body due to changes in the optimum

O_2/CH_4 mixing ratio. In return this would explain different amounts of methane oxidation at specific sites within the reactor. Overall, the development of the BMO by reactor depth is shown quite well by both methods.

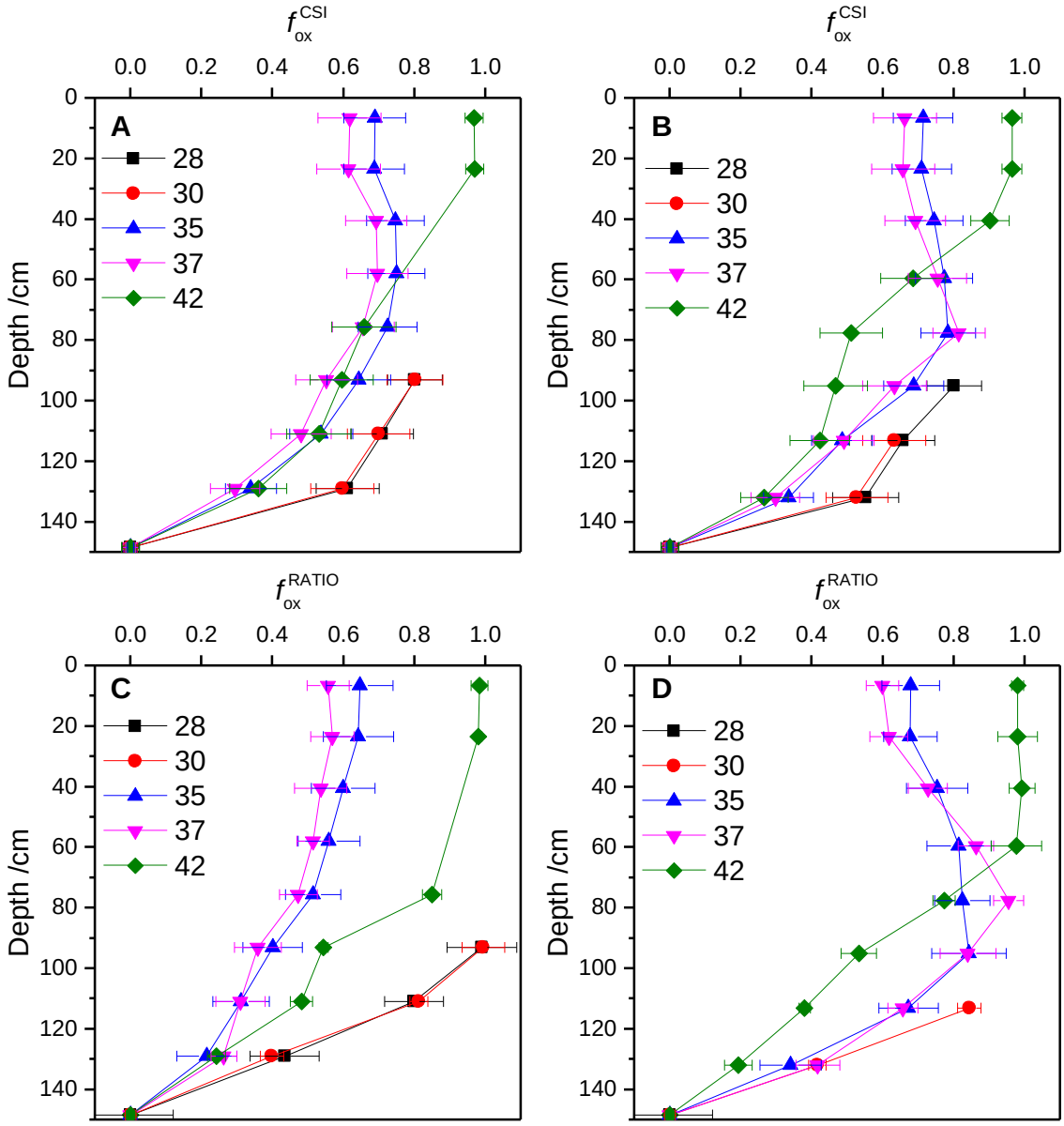

Figure 6-5: Biodegradation by sampling depth (hotspot)
The hotspot scenario was investigated for the experiment days 28-42. For both left (A and C) and right (B and D) side of the reactor vertical profiles were sampled and measured by GC-IRMS. The biodegradation for each left and right vertical sampling profile was calculated by the CSI (A and B) and RATIO (C and D) method. Symbols with lines are average values of triplicate measurements and error bars represent combined measurement uncertainty.The colors indicate the sampling day.

A comparison of the fractions of oxidized methane by soil depth for the normal state is given in Figure 6-6. Although f_{ox}^{CSI} is similar in the headspace throughout the normal state its progress from bottom to top differs significantly between right and left side. Moreover, f_{ox}^{CSI} for the two

sampling points at 95 and 113 cm is shifted towards lower values which results in differences of up to $\Delta(f_{ox}^{CSI}(\text{left}) - f_{ox}^{CSI}(\text{right})) = 0.25$. In contrast, the profiles of methane oxidation on the right and left side determined by the CO_2/CH_4-ratio show less fluctuation.

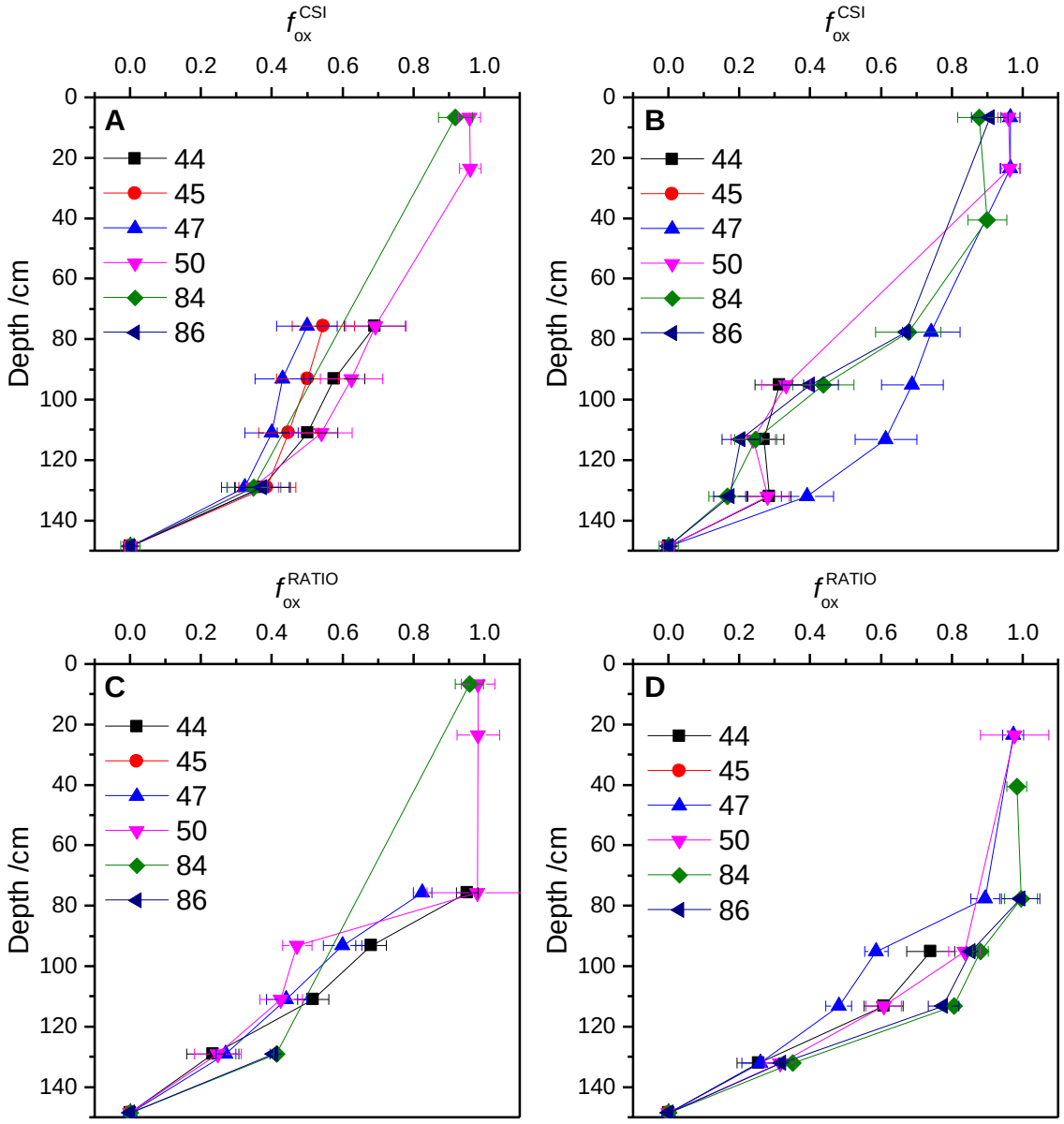

Figure 6-6: Biodegradation by sampling depth (normal)
The normal scenario was investigated for the experiment days 44-86. For both left (A and C) and right (B and D) side of the reactor vertical profiles were sampled and measured by GC-IRMS. The biodegradation for each left and right vertical sampling profile was calculated by the CSI (A and B) and RATIO (C and D) method. The symbols with lines are average values of triplicate measurements and error bars represent combined measurement uncertainty. The colors indicate the sampling day.

The Cooling simulation is depicted in Figure 6-7. At the left side of the reactor, values for the calculation of the efficiencies were only available from the three sampling points at 129 cm, 40.5 cm, and 6.5 cm (Figure 6-7 A and C). In contrast, the biodegradation was assessable from

most of the sampling points on the right side. These additional data points reveal that the stable isotope approach returns negative efficiencies between 77.5 cm and 113 cm depth (all points left of the broken line in Figure 6-7 B). This was due to problems with leaking sampling ports possibly causing isotopic fractionation by effusion. In case of the CO_2/CH_4-ratio method the situation on the left side of the reactor is comparable to the stable isotope approach while the right side is not. The right side shows a fairly exponential increase in oxidation towards the top and no negative biodegradation.

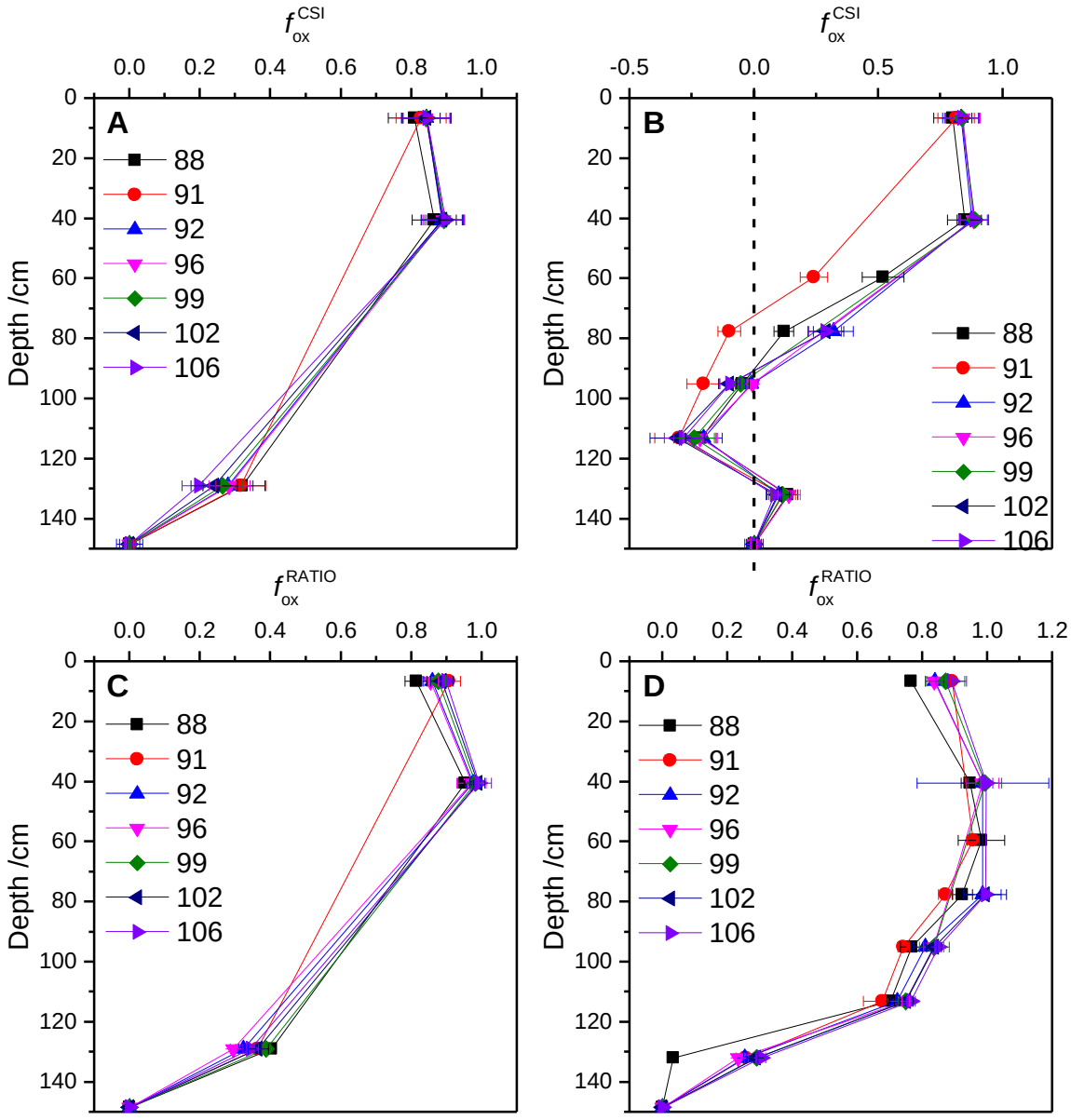

Figure 6-7: Biodegradation by sampling depth (Cooling)
The cooling scenario was investigated for the experiment days 88-106. For both left (A and C) and right (B and D) side of the reactor vertical profiles were sampled and measured by GC-IRMS. The biodegradation for each left and right vertical sampling profile was calculated by the CSI (A and B) and RATIO (C and D) method. The symbols with lines are average values of triplicate measurements and error bars represent combined measurement uncertainty. The colors indicate the sampling day.

Overall, the methane was largely consumed at depths > 60 cm which corresponds to a soil depth of ~45 cm and deeper. This is more or less in agreement with observations in the literature. For example, by combining soil gas composition from soil columns with kinetic data from flask incubations De Visscher et al. (1999) determined the methane oxidation which was mainly in the top 30 cm of the cover soil. In another study, soil from a landfill was sampled at different depth and the maximum methane oxidation rate determined from batch experiments was between 40 and 50 cm (Bogner et al., 2003). However, the O_2 penetration is often the limiting factor of CH_4 oxidation and the greatest oxidation potential in simulated landfill soil covers is where CH_4 and O_2 concentration profiles overlap (Scheutz et al., 2009). Thus the observation in this study that the biodegradation mainly takes place at ~45 cm depth might be due to a deep oxygen penetration that results from a high air flow at the top and a relatively low methane load at the bottom of the reactor.

In biocovers the active zone of methane oxidation is often near the gas-soil boundary (Czepiel et al., 1996; Scheutz and Kjeldsen, 2004). However, the BMO strongly depends on aeration/optimal gas mixing of methane and oxygen which again depends on soil gas permeability (e.g. air-filled pore space). For example, in a laboratory column study by (Rachor et al., 2011) the isotopic fractionation by depth depended on the methane load. While for low gas loads (25 $gm^{-2}d^{-1}$) the fractionation was highest in the lower part of the reactor (between inlet gas at 100 cm and 75 cm depth), it was highest in the upper part (between ~15 and 35 cm) for higher gas loads (80 $gm^{-2}d^{-1}$). Thus inhomogeneous soil compaction during the experiment and also the increased gas load during the "hotspot" could have been reasons for the findings above. As already mentioned for the isotopic fractionation above, this is also supported by a study by Rachor et al. (2011) in which the oxidation efficiency was highest between 75 and 95 cm (near the gas inlet at 100 cm) for 25 $gm^{-2}d^{-1}$ CH_4 and highest between 5 and 15 cm for 80 $gm^{-2}d^{-1}$ CH_4.

In general, the active layer of BMO is associated with a high turnover of CH_4. This corresponds to a drop of O_2 and CH_4 concentration, an increase of CO_2, and a local increase of temperature. In case of the hotspot simulation the profiles show a high variability regarding the calculated efficiencies which indicates a potential shift of the active layer of methanotrophs. An inspection of the difference quotients, in particular the partial differences of fractions of methane oxidized and sampling depths could allow locating methanotrophic activity by soil depth and monitoring its progress within the soil cover. The difference quotient corresponds to the fraction of methane that is oxidized between two sampling points (f_{ox}^{*} /cm). Thus the BMO between two sampling ports is higher, the higher the corresponding difference quotient is.

A comparison of the difference quotients of the two methods by stable isotopes (CSI) and CO_2/CH_4-ratio (RATIO) is shown in Figure 6-8 for the hotspot scenario. For the calculations by CSI the highest values (global maxima) strongly decrease after day 30 on both sides of the reactor but remain in the lower part of the reactor (~140 cm depth) near the actual methane inlet. Consequently, most of the methane had been already consumed within the gas distribution layer at the bottom. This observation was supported by the discovery of methanotrophs on the growth bodies as shown by purple biofilm formation and the detection by fluorescence in situ hybridization (FISH) on 16srRNA (personal communication Gehrke (2015)). Yet, the presence of local maxima in the profile of the hotspot scenario may represent an additional active layer as these at least represent a local increase in methane consumption. They are indicated by vertical broken lines and numbers 3, 4, and 5 in Figure 6-8 (panel A and B). The numbers are in the order of the respective sampling days (i.e., number 3 equals sampling day 30, number 4 equals sampling day 35, etc.). This apparent active layer moves up to a depth of 50 cm on both sides of the reactor at day 42.

In the case of the partial difference quotient for the RATIO method, the global maximum is between the first and second sampling spot (between 120 and 140 cm) and thus is comparable to the global maximum for the partial difference quotient of the CSI-method. On the left side of the reactor (panel C in Figure 6-8), local maxima are mainly present at ~84 cm depth. On the right side of the reactor (panel D in Figure 6-8), local maxima are present only for sampling day 35 at ~64 cm and for sampling day 42 at ~84 cm. Still, both methods suggest an additional active methanotrophic zone which either adjusts to or is altered due to the increased local gas load during the hotspot scenario.

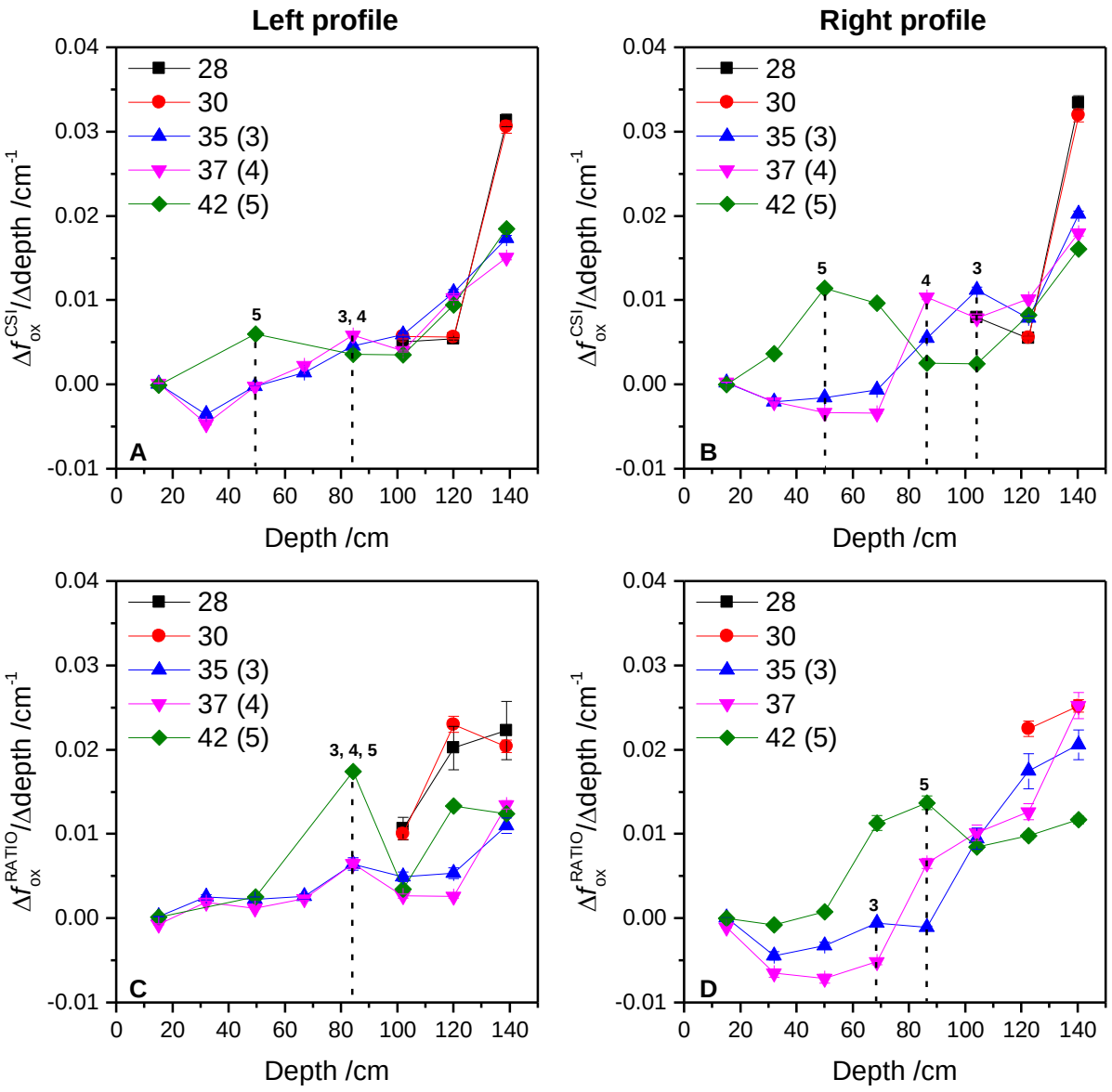

Figure 6-8: Partial differences of fraction oxidized by sampling depth (hotspot)
Based on the biodegradation during the hotspot scenario (Figure 6-5) the partial diffference-quotients were calculated for left (A and C) and right (B and D) side of the vertical profiles of the reactor. This was done for the CSI (A and B) and RATIO (C and D) method. The symbols with lines are average values of triplicate measurements and error bars represent combined measurement uncertainty. The colors indicate the corresponding sampling day. The highest activity was usually ~140 cm depth in the gas distribution layer. Above the gas distribution layer a second active horizon of methane oxidation was suspected based on the second maxima. These second maxima are indicated by the broken lines which are numbered in the order of the respective sampling days.

In case of the normal state, the partial difference quotients calculated by stable isotopes (CSI) and CO_2/CH_4-ratio (RATIO) are plotted against the reactor depth in Figure 6-9. Based on stable isotopes additional activity was apparent between ~50 cm and ~90 cm on the left side of the reactor. Yet, there were less data points available for the upper part of the reactor because in most cases no methane was detected above 80 cm depth.

On the right side however, the highest activity is in the lower part of the reactor in the beginning (sampling days 44 to 50). But it moves up to ~84 cm at days 84 and 86 so that the highest methane consumption is more in the middle of the reactor than at the bottom. From this one may infer the active layer is not an even horizon but rather a dynamic zone with an inclination towards the top of the reactor from the left to the right side.

The profiles of the partial difference quotients based on the RATIO method in Figure 6-9 panel C and D are different from the profiles of the CSI method. Yet, additional activity may be present between ~80 cm and ~90 cm as indicated by the vertical broken lines.

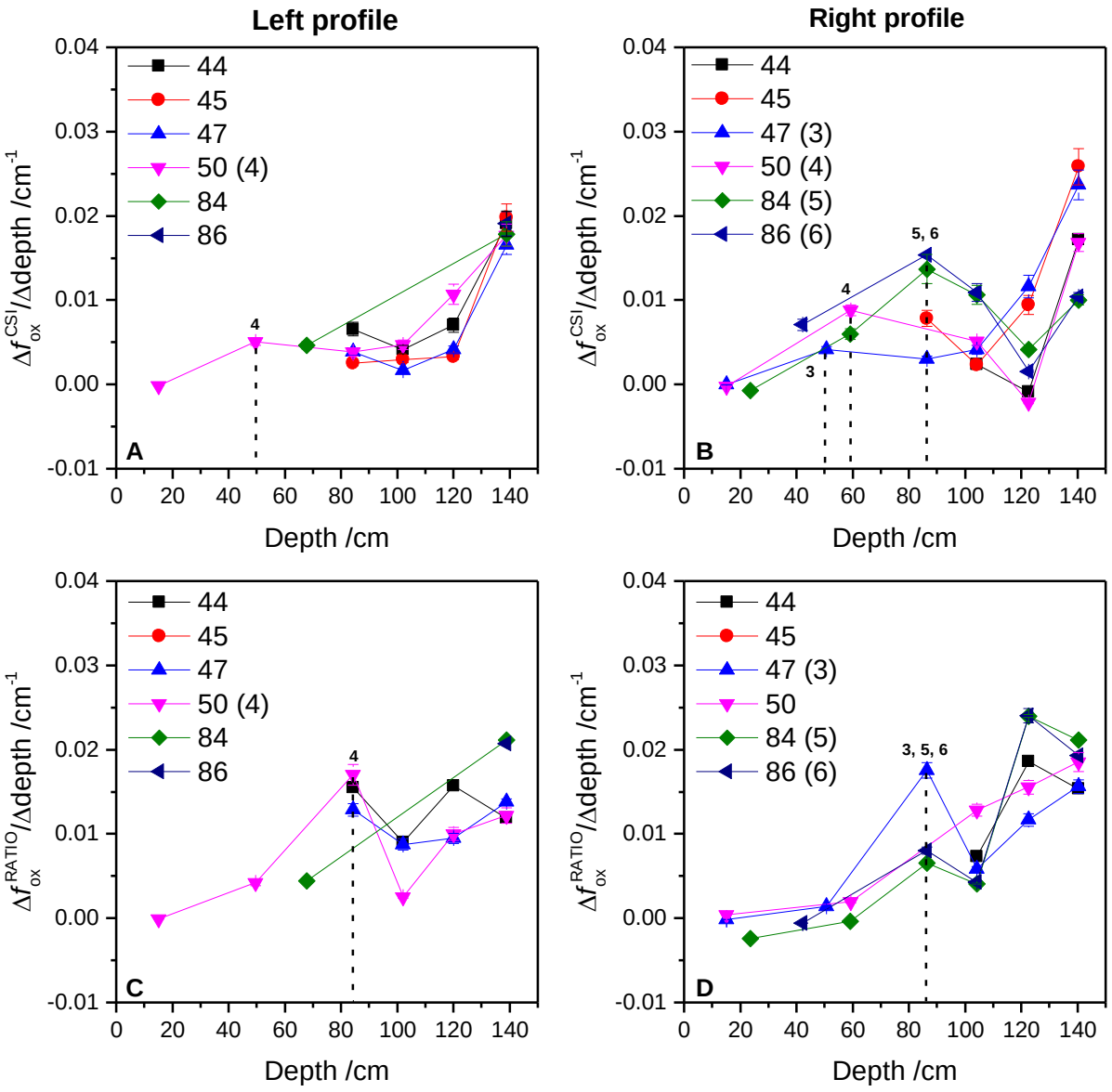

Figure 6-9 Partial differences of fraction oxidized by sampling depth (normal)
Based on the biodegradation during the normal scenario (Figure 6-6) the partial diffference-quotients were calculated for each left (A and C) and right (B and D) side. This was done for the CSI (A and B) and RATIO (C and D) method. The symbols with lines are average values of triplicate measurements and error bars represent combined measurement uncertainty. The colors indicate the corresponding sampling day. The highest activity was usually ~140 cm depth in the gas distribution layer. Above the gas distribution laye a second active horizon of methane oxidation was suspected based on further maxima - usually the second maxima. These second maxima are indicated by the broken lines which are numbered in the order of the respective sampling days (e.g. sampling day 44 corresponds to the number 1).

In the cooling scenario the BMO apparently decreases steadily towards the surface on the left side of the reactor for both approaches based on CSI and RATIO (Figure 6-10 panels A and C). This seems to correlate with the reduction of soil temperature which would explain decreasing methanotrophic activity towards the upper part of the reactor because the temperature decreases towards the soil surface above 80 cm depth (see Figure 5-6). At the right side of the reactor the situation is completely different. The partial differences based on CSI return negative values at 120 cm. A calculated negative biodegradation based on CSI can only result from ^{13}C depletion of the methane in the system compared to the source (methane at the reactor feeding from below coming from the gas cylinder). Effusion of methane out of the reactor would result in the negative values due to isotopic fractionation and thus the negative values indicate that a leak at the sampling site seems to have been the cause. The contrary situation is present for the partial differences based on RATIO where the highest methane consumption seems to occur at 120 cm. This could be due to a loss of CH_4 which would artificially increase the CO_2/CH_4 ratio and also increase the calculated fraction of oxidized methane. Nevertheless, when considering the results at the sampling site at 120 cm incorrect the highest values of partial difference quotients are in the range of ~70 cm to ~90 cm reactor depth for the CSI approach and at ~84 cm for the RATIO approach.

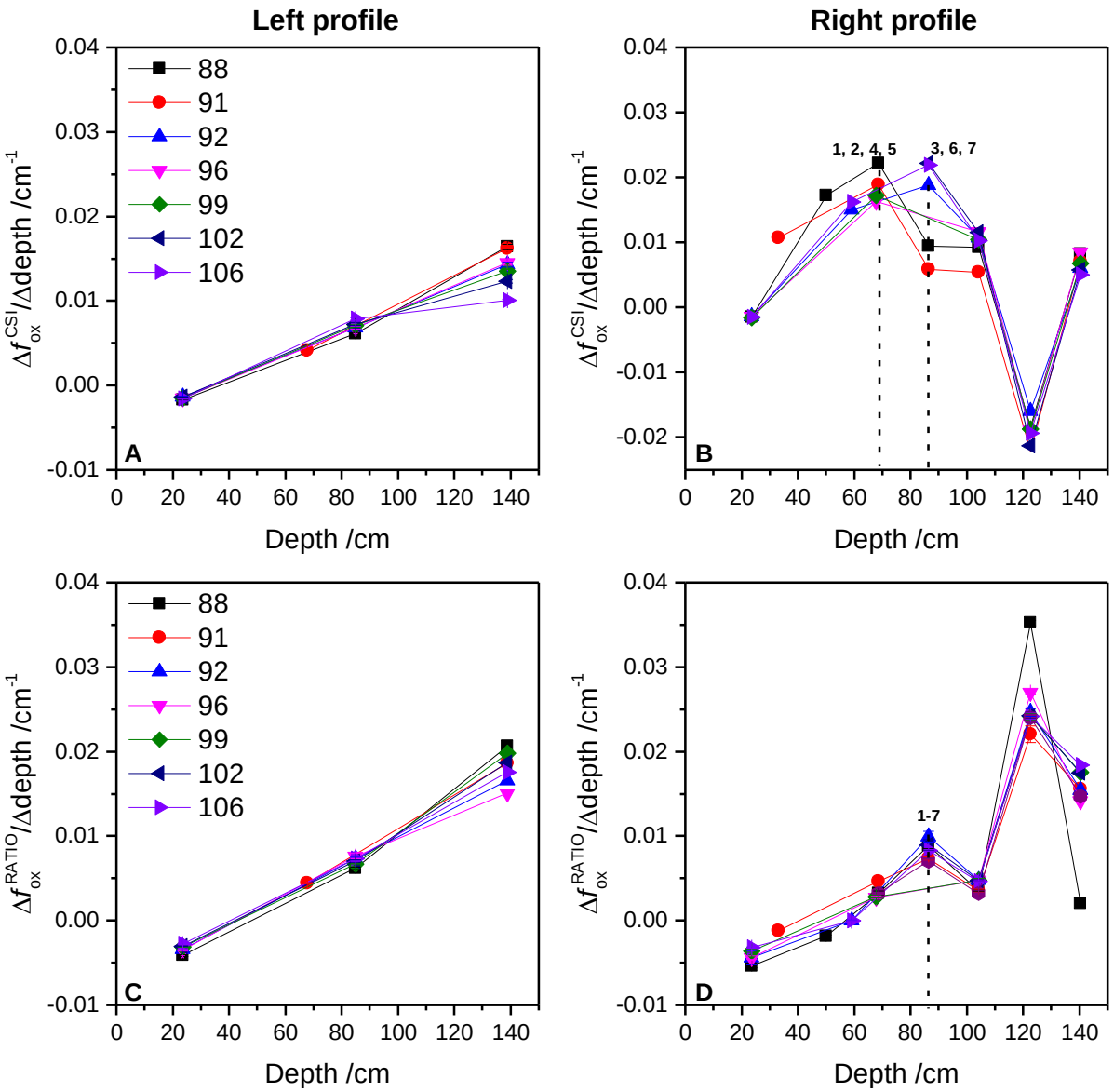

Figure 6-10 Partial differences of fraction oxidized by sampling depth (cooling)
Based on the biodegradation during the cooling scenario (Figure 6-7) the partial diffference-quotients were calculated for each left (A and C) and right (B and D) side of the reactor. This was done for the CSI (A and B) and RATIO (C and D) method. The symbols with lines are average values of triplicate measurements and error bars represent combined measurement uncertainty. The colors indicate the corresponding sampling day. Unlike the hotspot and normal scenario there is no clear additional maximum on the left side (A and C) for either method CSI and RATIO. On the left side the second maxima are indicated by the broken lines.
.

6.6.3 Comparing the site-specific methane oxidation with thermographic imaging

Based on the assumption that temperature correlates with the BMO the spatial resolution of the site-specific methane oxidation was improved by three additional sampling profiles (see section 6.2). Also, as most of the methanotrophic activity was observed within the gas distribution layer composed of plastic growth bodies it was decided to replace them by a layer of sand to see whether this would affect the methane oxidation at the bottom of the reactor or not. The modified reactor was monitored for the normal scenario.

A 2D contour plot of the reactor plate's temperature profile for the normal state (with sand in the gas distribution layer) is depicted in Figure 6-11. The temperature profile shows a warm zone (red area) around the center of the reactor plate. It clearly indicates an active zone which is not evenly horizontal but expresses a slight incline from the left to the right side of the reactor. This is perhaps due to uneven soil gas transportation inflicting a shift of the optimal gas mixing conditions for the active zone. In addition, the second maxima from the partial differences calculated with the CSI and RATIO methods are included as symbols in the plot. It must be noted that the symbols with an asterisk at 30 cm width represent the first maxima as no further methane was detected above this depth. Still, the second maxima edge around the warmest zone (red area) and thus show quite well the correlation of methanotrophic activity and the increase of temperature. Their general offset might be due to the fact that no further methane could be detected above these sampling points. At 100 cm width a low sampling resolution is the reason for the shift of the second maximum further down the reactor plate because there was a difference of 50 cm between the topmost sampling point (95cm) and the next lower one (145 cm). Consequently, the partial difference quotient moves more downward to the mean depth of these two sampling points and also exhibits a large y-error. For clarity, the maximum temperature and their respective depths at each sampling profile are included together with the corresponding second maxima obtained from the partial differences for CSI and RATIO (Table 6-2).

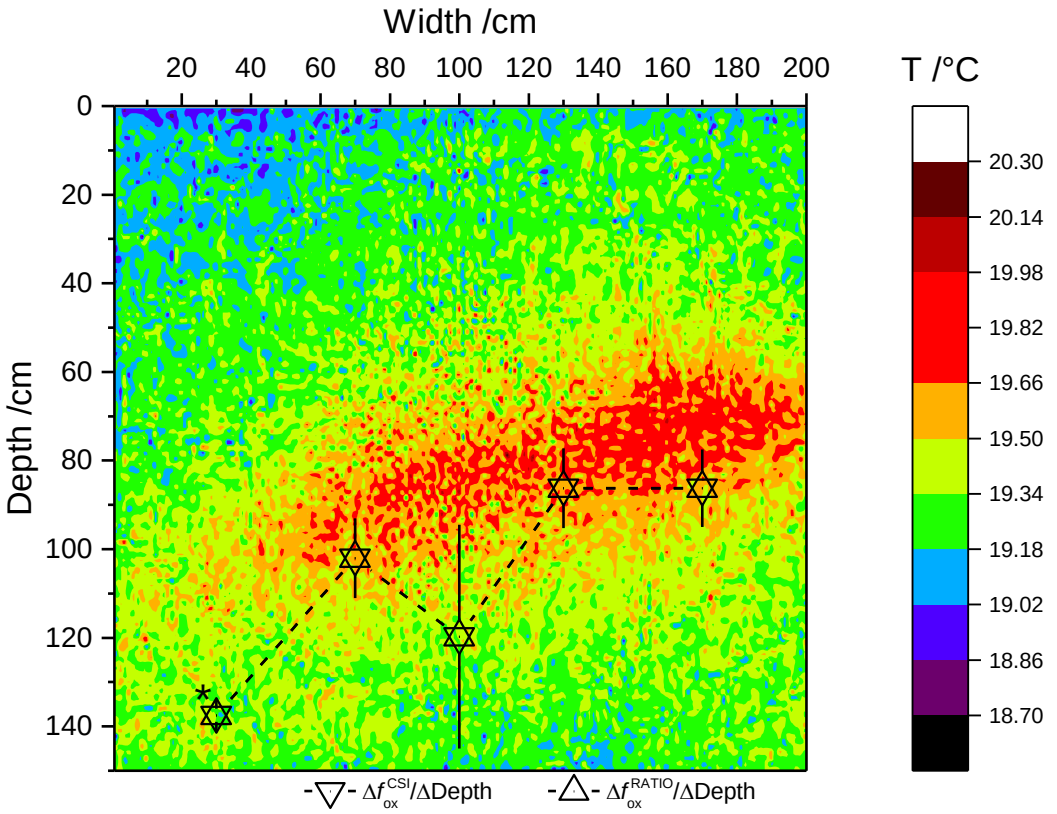

Figure 6-11 Thermographic image of the reactor plate (normal)
The contour plot of the temperature along the surface of the reactor plate indicates high methanotrophic activity (red zone). Symbols are 2nd maxima obtained from partial differences of fractions oxidized and reactor depth by either RATIO or CSI. Error bars represent half the distance (Δdepth/ cm) between each two subsequent sampling points considered for the calculation of the partial differences of the 2nd maxima. Note the symbols with an asterisk at 30 cm width represent the 1st maxima as no further methane was detected above this depth.

Table 6-2: Maximum temperatures and their location in the reactor plate
Numbers in brackets at 30 cm width are the first maxima as no other methane was detected above this depth.

Width /cm	30	70	100	130	170
Maximum temperature /°C	19.7	19.8	20.2	20.0	19.9
Depth at maximum temperature /cm	108	93	87	78	72
Depth of 2nd maximum for CSI /cm	(147)	102	120	86	86
Depth of 2nd maximum for RATIO /cm	(147)	102	120	86	86

When looking in detail at the site-specific fractions of oxidized methane along with their corresponding temperature profiles as illustrated for CSI and for RATIO in Figure 6-13 both seem to show a similar response with reactor depth. In particular, the general trend of showing an increase in methane oxidation from left to right (0 to 200 cm width) and from the bottom

towards the center of the reactor plate (150 - 75 cm depth) is present for both methods. The trend also correlates with the change of the temperature profile which shows a shift from the left to the right side of the reactor with respect to the depth of the maximum temperature. Yet, the absolute values for f_{ox}^{CSI} and f_{ox}^{RATIO} differ. A possible reason could have been an increase in soil respiration causing an increase in CO_2/CH_4 ratio and subsequently greater fractions of oxidized methane.

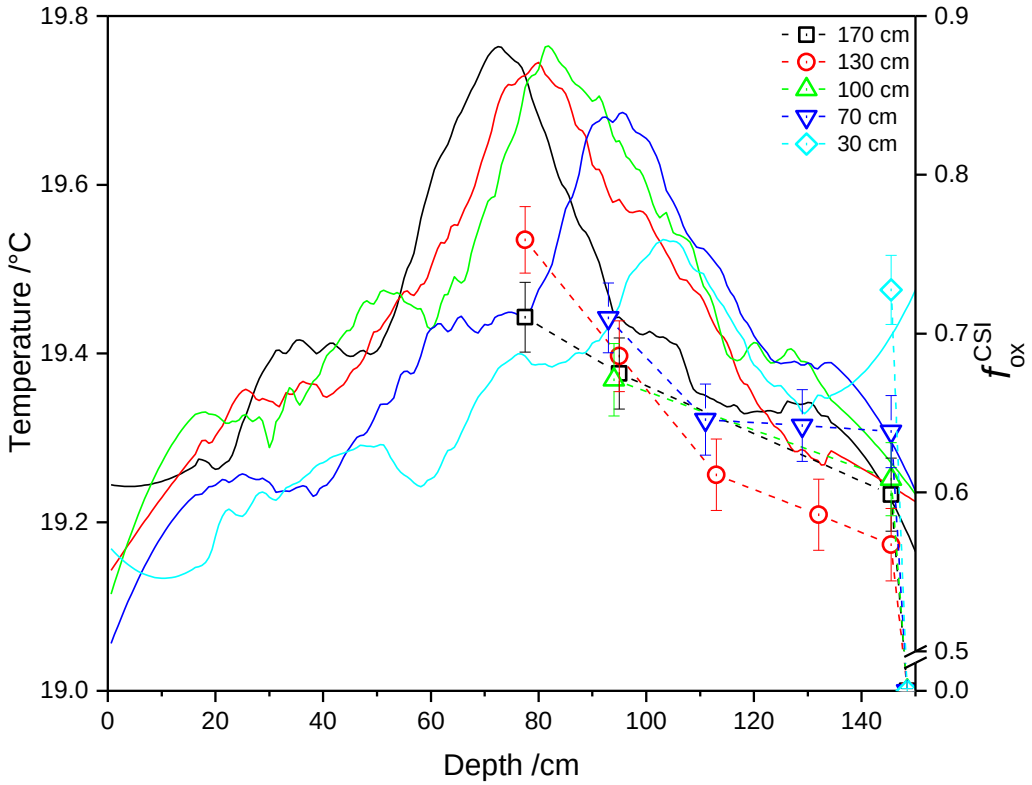

Figure 6-12 Profiles of temperature and biodegradation (f_{ox}^{CSI}) versus reactor depth (normal)
The colored lines show the temperature for the respective sampling profile at different widths. The symbols with broken lines correspond to the fraction of oxidized methane calculated by the closed system stable isotope approach (CSI). Error bars are the combined measurement uncertainty.

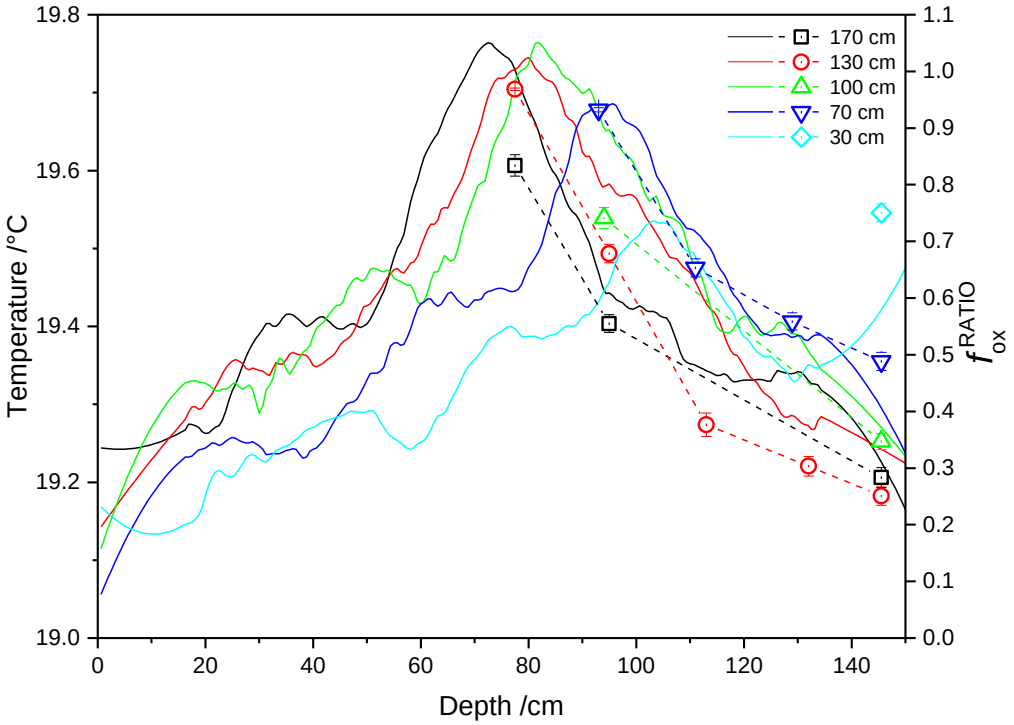

Figure 6-13 Profiles of temperature and biodegradation (f_{ox}^{RATIO}) versus reactor depth (normal)

The colored lines show the temperature for the respective sampling profile at different widths. The symbols with broken lines correspond to the fraction of oxidized methane calculated by the CO_2/CH_4-ratio method (RATIO). Error bars are the combined measurement uncertainty.

6.7 Conclusion

In summary, the main activity of methane oxidation was found in the lower part of the reactor. However, additional methane oxidation in the upper part of the reactor was indicated by the partial differences of the fraction of oxidized methane and soil depth by either the closed system stable isotope or CO_2/CH_4-ratio method. The active zone of methane oxidation was identified to be a dynamic system which reacts to changes in environmental conditions, especially during the hotspot event. Sampling the reactor at two sites revealed this dynamic behavior both within the vertical and lateral profile of the soil body because in some cases the results between the left and right sampling site were very different. This could have been due to an uneven soil gas transport within the reactor as it is difficult to achieve a completely homogenous soil layer as well as corresponding gas flow conditions. Nevertheless, the general trend between the CSI and RATIO method agreed well with respect to the local maxima of methane oxidation. An increase of the number of sampling sites in order to expand the spatial resolution of the methane oxidation gave further insight into the dynamics of the bacterial methane oxidation. The thermographic imaging has shown to be very powerful in locating methane oxidizing activity as maximum temperatures and the fraction of oxidized methane by depth correlated quite well. Furthermore, the thermographic imaging revealed a slightly uneven distribution of the active zone within the reactor which was supported by the results from calculations based on stable isotope analysis and CO_2/CH_4-ratio. Thus thermal imaging represents an easy tool for monitoring changes in methanotrophic activity within the investigated reactor system. In addition, this technique may be very promising for studies on the effects of environmental changes (e.g. desiccation, atmospheric pressure gradients, and increased soil gas permeability due to settling events or plant root penetration, etc.) on the bacterial methane oxidation as potential shifts in methanotrophic activity can be monitored in real time. Finally, the correlation between temperature and methane oxidation supports the method's applicability of modelling a soil cover's response to environmental effects from thermographic imaging as investigated in (Thom et al., 2016).

7 General conclusions and outlook

The knowledge of isotopic enrichment factors is important for the estimation of biodegradation by stable isotope analysis. However, the determination in case of methane oxidation may not be straightforward as multiple factors such as temperature (Börjesson et al., 2007; Chanton et al., 2008a), cell density (Kampara et al., 2009; Templeton et al., 2006), type of methane monooxygenase (Feisthauer et al., 2011; Jahnke et al., 1999), and substrate availability (Jahnke et al., 1999; Nihous, 2008; Nihous, 2010) seem to influence the measured isotopic fractionation of the residual substrate and thus also alter the precision of the determined enrichment factor. In case of temperature, corrections have been suggested for isotopic fractionation. However, no significant influence of temperature, type of methanotrophic enrichment culture, or oxidation rate on the isotopic enrichment factor was observable in this study. In addition, a comparison with own results from chapter 4 and literature values revealed that relative standard deviations of the isotopic enrichment factor at a given temperature are usually high (up to 20% for ε), especially when regarding different environments/landfill cover types. Correcting a value for a change in temperature as suggested by Chanton et al. (2008a) will result in an isotopic enrichment factor that is within the range of the standard uncertainty of an uncorrected value, in general. As a consequence, a correction over a broad range of temperature (~10-40°C), which covers the main operational temperatures of methane oxidation, will not result in a statistically significant difference. Albeit the literature data may show a trend of the isotopic enrichment factor with temperature, it remains questionable how much such a correction will improve the precision of the estimated biodegradation from stable isotopes. The results of this thesis support the assumption of Feisthauer et al. (2011) that the *KIE* of methane oxidation is mainly due to C-H bond breakage.

Furthermore, many studies have solely investigated the change in the isotopic signature of either the reactant (CH_4) or product (e.g., CO_2 and biomass). In this thesis, the analysis of the stable carbon isotopic composition of the bacterial cell suspension by LC-IRMS was applied in addition to the analysis of CH_4 and CO_2 by GC-IRMS. For future studies, the validation of the LC-IRMS technique (e.g., comparison with bulk analysis of biomass by an elemental analyzer isotope ratio mass spectrometer) represents one important step in being able to balance degradation experiments such as were performed in this thesis. An approach of balancing a system of methane oxidation has been performed in a recent study by Vavilin et al. (2016). A kinetic model of aerobic enzymatic methane oxidation was created for non-linear dynamics of stable carbon and hydrogen isotope signatures. The model considered the influence of formaldehyde at the crucial metabolic branching point of carbon assimilation as well as the resulting formic acid,

carbon dioxide, and resulting biomass. The model was fed with ^{2}H and ^{13}C data for CH_4 and partially with ^{13}C data for CO_2 from (Feisthauer et al., 2011) in which degradation studies with pure methanotrophic cultures were performed. Likewise to the combined approach in this thesis, a more thorough investigation that assesses both ^{13}C isotopic signatures of the reactant CH_4 as well as the stable carbon isotopic signature of the products in degradation experiments could be used to further validate the respective model by Vavilin et al..

During the three investigated scenarios in chapter 5, the topsoil was capable of reducing the methane load down to a level of emission at which old landfills have been suggested to be released from aftercare. The direct comparison of different methods for the determination of the biodegradation by scatter plots revealed a good correlation from linear regression. In particular, the CO_2/CH_4-ratio approach and the closed system stable isotope approach as well as the comparison of the CO_2/CH_4-ratio approach corrected for anabolism and mass balance showed a good fit. The calculated biodegradation followed the order: $f_{ox}^{RATIOC} = f_{ox}^{MFM} = f_{ox}^{MFC} > f_{ox}^{RATIO} = f_{ox}^{CSI}$. A central point in applying SIA for the estimation of the biodegradation of methane in landfill studies is the actual system of reaction that is present. In general, there are two equations for the calculation of the biodegradation when using the isotopic enrichment factor. One is equation (1.4.27) which holds true for an irreversible reaction in a closed system (as well as a reversible reaction in an open system). The other is equation (1.4.28) which describes an irreversible reaction in an open system at steady state (and a reversible reaction in a closed system, as well as a reversible reaction in an open system at steady state). The reactor setup in chapter 5 apparently represents an open system at steady state where the reaction is irreversible. With the continuous supply of reactant and the continuous removal of the product, the system should be described by equation (1.4.28). However, the biodegradation of methane in chapter 5 was better described by equation (1.4.27) in comparison to mass balancing as the open system approach always overestimated the biodegradation of methane. Also, a correction of the isotopic fractionation by diffusion was not applicable as this would have led to even higher values. The apparent closed system behavior may be compared to contaminant plumes in groundwater studies. Groundwater systems represent open systems, also. The change of concentration and isotopic signature of contaminants in such systems is due to transport and degradation which was also the case for CH_4 in the investigated reactor system in this thesis. In groundwater system studies the equations describing the Rayleigh distillation behavior (e.g., equations (1.4.24) and (1.4.25)) are often applied to determine ε. Also the biodegradation is often calculated based on equation (1.4.27) or corresponding simplifications. However, the stable isotope approach results in lower estimates in comparison with reactive transport models considering diffusion and

dispersive transport (Breukelen and Prommer, 2008). Regarding the stable isotope fractionation by methane oxidation and diffusion Mahieu et al. (2008) and coworkers have developed a model for the estimation of the biodegradation of methane. In future studies, the data of this thesis could be applied in such a model and might give further insight on what kind of system approach (open or closed) might be the more appropriate one.

A major aspect of concern at old landfills is the emission of CH_4 from hotspots which can rise up to 9.2-9.7 Lh^{-1} (Gebert et al., 2011b; Rachor et al., 2013). In chapter 6 the response of the given reactor setup to a local increase in methane load was investigated with regard to the biodegradation. In detail, the vertical position of the active zone of biodegradation of methane in the reactor's soil body was variable during the simulation of the hotspot scenario. It required about one week for adaptation in terms of restoring the initial fraction of oxidized methane. In future studies, the response to more severe hotspot events such as the formation of fissures (e.g. desiccation, atmospheric pressure gradients, and increased soil gas permeability due to settling events or plant root penetration, etc.) could be investigated also in terms of possible remediation techniques (e.g. for intermediate covers the placement of individualized compost cells over high emission zones has been proposed (Abichou et al., 2006)). This could be performed together with the newly implemented technique of thermographic imaging. It clearly was able to resolve the dynamics of methanotrophic activity as was proven from stable isotope analysis and CO_2/CH_4 ratio by the partial differences of the fraction of oxidized methane and soil depth. Thus thermographic imaging, SIA, and the CO_2/CH_4 ratio approach represent powerful techniques to monitor changes in methanotrophic activity in real time within the investigated reactor system. Finally, the correlation between temperature and methane oxidation supports the method's applicability of modelling a soil cover's response to environmental effects from thermographic imaging as investigated in (Thom et al., 2016).

8 References

Abichou, T., Chanton, J., Powelson, D., Fleiger, J., Escoriaza, S., Lei, Y., Stern, J., 2006. Methane flux and oxidation at two types of intermediate landfill covers. Waste Manag 26, 1305-1312.

Aelion, C.M., Höhener, P., Hunkeler, D., Aravena, R., 2010. Environmental Isotopes in Biodegradation and Bioremediation. CRC Press, Boca Raton, FL 33487-2742.

Altman, D.G., Bland, J.M., 1983. Measurement in Medicine: The Analysis of Method Comparison Studies. The Statistician 32, 307.

Ballantyne, A.P., Alden, C.B., Miller, J.B., Tans, P.P., White, J.W., 2012. Increase in observed net carbon dioxide uptake by land and oceans during the past 50 years. Nature 488, 70-72.

Barker, J.F., Fritz, P., 1981. Carbon isotope fractionation during microbial methane oxidation. Nature 293, 289-291.

Barlaz, M.A., Green, R.B., Chanton, J.P., Goldsmith, C.D., Hater, G.R., 2004. Evaluation of a biologically active cover for mitigation of landfill gas emissions. Environ Sci Technol 38, 4891-4899.

Bastviken, D., Ejlertsson, J., Tranvik, L., 2002. Measurement of Methane Oxidation in Lakes: A Comparison of Methods. Environmental Science & Technology 36, 3354-3361.

Bender, M., 1992. Mikrobieller Abbau von Methan und anderen Spurengasen in Böden und Sedimenten, Faculty of Biology. University of Konstanz, Hartung Gorre Verlag, , pp. 1–133.

Boeckx, P., Cleemput, O.v., Villaralvo, I., 1996. Methane emission from a landfill and the methane oxidising capacity of its covering soil. Soil Biology and Biochemistry 28, 1397-1405.

Bogner, J., Chanton, J., Blake, D., Morcet, M., Kjeldsen, P., 2003. Comparative Oxidation and Net Emissions of Methane and Selected Non-Methane Organic Compounds in Landfill Cover Soils. Environmental Science & Technology 37, 5150-5158.

Bogner, J., Pipatti, R., Hashimoto, S., Diaz, C., Mareckova, K., Diaz, L., Kjeldsen, P., Monni, S., Faaij, A., Gao, Q., Zhang, T., Ahmed, M.A., Sutamihardja, R.T., Gregory, R., Intergovernmental Panel on Climate Change Working, G., III, 2008. Mitigation of global greenhouse gas emissions from waste: conclusions and strategies from the Intergovernmental Panel on Climate Change (IPCC) Fourth Assessment Report. Working Group III (Mitigation). Waste Manag Res 26, 11-32.

Bogner, J.E., Spokas, K.A., Burton, E.A., 1997. Kinetics of Methane Oxidation in a Landfill Cover Soil: Temporal Variations, a Whole-Landfill Oxidation Experiment, and Modeling of Net CH4Emissions. Environmental Science & Technology 31, 2504-2514.

Boley, C., 2012. Handbuch Geotechnik - Grundlagen - Anwendung - Praxiserfahrung. Vieweg+Teubner Verlag | Springer Fachmedien Wiesbaden GmbH, Wiesbaden.

Börjesson, G., Chanton, J., Svensson, B.H., 2001. Methane oxidation in two Swedish landfill covers measured with carbon-13 to carbon-12 isotope ratios. J Environ Qual 30, 369-376.

Börjesson, G., Samuelsson, J., Chanton, J., 2007. Methane oxidation in Swedish landfills quantified with the stable carbon isotope technique in combination with an optical method for emitted methane. Environ Sci Technol 41, 6684-6690.

Börjesson, G., Samuelsson, J., Chanton, J., Adolfsson, R., Galle, B.O., Svensson, B.H., 2009. A national landfill methane budget for Sweden based on field measurements, and an evaluation of IPCC models. Tellus B 61, 424-435.

Börjesson, G., Sundh, I., Svensson, B., 2004. Microbial oxidation of CH_4 at different temperatures in landfill cover soils. FEMS Microbiol Ecol 48, 305-312.

Bouchard, D., Cornaton, F., Hohener, P., Hunkeler, D., 2011. Analytical modelling of stable isotope fractionation of volatile organic compounds in the unsaturated zone. J Contam Hydrol 119, 44-54.

Bouchard, D., Hunkeler, D., Gaganis, P., Aravena, R., Höhener, P., Broholm, M.M., Kjeldsen, P., 2008. Carbon Isotope Fractionation during Diffusion and Biodegradation of Petroleum Hydrocarbons in the Unsaturated Zone: Field Experiment at Værløse Airbase, Denmark, and Modeling. Environmental Science & Technology 42, 596-601.

Bousquet, P., Ciais, P., Miller, J.B., Dlugokencky, E.J., Hauglustaine, D.A., Prigent, C., Van der Werf, G.R., Peylin, P., Brunke, E.G., Carouge, C., Langenfelds, R.L., Lathiere, J., Papa, F., Ramonet, M., Schmidt, M., Steele, L.P., Tyler, S.C., White, J., 2006. Contribution of anthropogenic and natural sources to atmospheric methane variability. Nature 443, 439-443.

Bowman, J., 2006. The Methanotrophs — The Families Methylococcaceae and Methylocystaceae. 266-289.

Brand, W.A., Assonov, S.S., Coplen, T.B., 2010. Correction for the ^{17}O interference in $\delta^{13}C$ measurements when analyzing CO_2 with stable isotope mass spectrometry (IUPAC Technical Report). Pure Appl. Chem. 82, 1719-1733.

Breukelen, B.M.V., Prommer, H., 2008. Beyond the Rayleigh Equation: Reactive Transport Modeling of Isotope Fractionation Effects to Improve Quantification of Biodegradation. Environmental Science & Technology 42, 2457-2463.

Cabral, A.R., Capanema, M.A., Gebert, J., Moreira, J.F., Jugnia, L.B., 2009. Quantifying Microbial Methane Oxidation Efficiencies in Two Experimental Landfill Biocovers Using Stable Isotopes. Water, Air, & Soil Pollution 209, 157-172.

Cabral, A.R., Moreira, J.F.V., Jugnia, L.B., 2010. Biocover Performance of Landfill Methane Oxidation: Experimental Results. Journal of Environmental Engineering 136, 785-793.

Cadieux, S.B., White, J.R., Sauer, P.E., Peng, Y., Goldman, A.E., Pratt, L.M., 2016. Large fractionations of C and H isotopes related to methane oxidation in Arctic lakes. Geochimica et Cosmochimica Acta 187, 141-155.

Capanema, M.A., Cabral, A.R., 2012. Evaluating Methane Oxidation Efficiencies in Experimental Landfill Biocovers by Mass Balance and Carbon Stable Isotopes. Water, Air, & Soil Pollution 223, 5623-5635.

Cebron, A., Bodrossy, L., Chen, Y., Singer, A.C., Thompson, I.P., Prosser, J.I., Murrell, J.C., 2007. Identity of active methanotrophs in landfill cover soil as revealed by DNA-stable isotope probing. FEMS Microbiol Ecol 62, 12-23.

Cerling, T.E., Solomon, D.K., Quade, J., Bowman, J.R., 1991. On the isotopic composition of carbon in soil carbon dioxide. Geochimica et Cosmochimica Acta 55, 3403-3405.

Chanton, J., Abichou, T., Langford, C., Hater, G., Green, R., Goldsmith, D., Swan, N., 2011. Landfill methane oxidation across climate types in the U.S. Environ Sci Technol 45, 313-319.

Chanton, J., Liptay, K., 2000. Seasonal variation in methane oxidation in a landfill cover soil as determined by an in situ stable isotope technique. Global Biogeochemical Cycles 14, 51-60.

Chanton, J.P., Powelson, D.K., Abichou, T., Fields, D., Green, R., 2008a. Effect of temperature and oxidation rate on carbon-isotope fractionation during methane oxidation by landfill cover materials. Environ Sci Technol 42, 7818-7823.

Chanton, J.P., Powelson, D.K., Abichou, T., Hater, G., 2008b. Improved Field Methods to Quantify Methane Oxidation in Landfill Cover Materials Using Stable Carbon Isotopes. Environmental Science & Technology 42, 665-670.

Chanton, J.P., Powelson, D.K., Green, R.B., 2009. Methane oxidation in landfill cover soils, is a 10% default value reasonable? J Environ Qual 38, 654-663.

Chanton, J.P., Rutkowski, C.M., Mosher, B., 1999. Quantifying Methane Oxidation from Landfills Using Stable Isotope Analysis of Downwind Plumes. Environmental Science & Technology 33, 3755-3760.

Christophersen, M., Kjeldsen, P., Holst, H., Chanton, J., 2001. Lateral gas transport in soil adjacent to an old landfill: factors governing emissions and methane oxidation. Waste Management & Research 19, 595-612.

Ciais, P., Sabine, C., Bala, G., Bopp, L., Brovkin, V., Canadell, J., Chhabra, A., DeFries, R., Galloway, J., Heimann, M., Jones, C., Le Quéré, C., Myneni, R.B., Piao, S., Thornton, P., 2013. Carbon and Other Biogeochemical Cycles, in: Stocker, T.F., D. Qin, G.-K. Plattner, M. Tignor, S.K. Allen, J. Boschung, A. Nauels, Y. Xia, V. Bex and P.M. Midgley (Ed.), *Climate Change 2013: The Physical Science Basis. Contribution of Working Group I to the Fifth Assessment Report of the Intergovernmental Panel on Climate Change*. Cambridge University Press, Cambridge, UK and New York, NY, USA.

Coleman, D.D., Risatti, J.B., Schoell, M., 1981. Fractionation of carbon and hydrogen isotopes by methane-oxidizing bacteria. Geochimica et Cosmochimica Acta 45, 1033-1037.

Conrad, R., 2009. The global methane cycle: recent advances in understanding the microbial processes involved. Environ Microbiol Rep 1, 285-292.

Coplen, T.B., 2011. Guidelines and recommended terms for expression of stable-isotope-ratio and gas-ratio measurement results. Rapid Communications in Mass Spectrometry 25, 2538-2560.

Crossman, Z.M., Abraham, F., Evershed, R.P., 2004. Stable isotope pulse-chasing and compound specific stable carbon isotope analysis of phospholipid fatty acids to assess methane oxidizing bacterial populations in landfill cover soils. Environ Sci Technol 38, 1359-1367.

Czepiel, P.M., Mosher, B., Crill, P.M., Harriss, R.C., 1996. Quantifying the effect of oxidation on landfill methane emissions. Journal of Geophysical Research: Atmospheres 101, 16721-16729.

Dalsøren, S.B., Myhre, C.L., Myhre, G., Gomez-Pelaez, A.J., Søvde, O.A., Isaksen, I.S.A., Weiss, R.F., Harth, C.M., 2016. Atmospheric methane evolution the last 40 years. Atmospheric Chemistry and Physics 16, 3099-3126.

De Visscher, A., 2004. Isotope fractionation effects by diffusion and methane oxidation in landfill cover soils. Journal of Geophysical Research 109.

De Visscher, A., Thomas, D., Boeckx, P., Van Cleemput, O., 1999. Methane Oxidation in Simulated Landfill Cover Soil Environments. Environmental Science & Technology 33, 1854-1859.

De Visscher, A., Van Cleemput, O., 2003. Simulation model for gas diffusion and methane oxidation in landfill cover soils. Waste Manag 23, 581-591.

Deponieverordnung, 2013. Verordnung über Deponien und Langzeitlager - Deponieverordnung – DepV, BGBl. I S. 973, 1017 Bundesrepublik Deutschland.

Dlugokencky, E., 2016. www.esrl.noaa.gov/gmd/ccgg/trends_ch4/ and www.esrl.noaa.gov/gmd/ccgg/trends_co2/ (accessed on August 24th 2016). NOAA/ESRL

Dlugokencky, E.J., Nisbet, E.G., Fisher, R., Lowry, D., 2011. Global atmospheric methane: budget, changes and dangers. Philos Trans A Math Phys Eng Sci 369, 2058-2072.

Elsner, M., Zwank, L., Hunkeler, D., Schwarzenbach, R.P., 2005. A new concept linking observable stable isotope fractionation to transformation pathways of organic pollutants. Environ Sci Technol 39, 6896-6916.

Etheridge, D.M., Steele, L.P., Francey, R.J., Langenfelds, R.L., 1998. Atmospheric methane between 1000 A.D. and present: Evidence of anthropogenic emissions and climatic variability. Journal of Geophysical Research: Atmospheres 103, 15979-15993.

Falk, M., 2014. Schätzen in Normalverteilungsmodellen. Springer-Verlag Berlin Heidelberg.

Feisthauer, S., Vogt, C., Modrzynski, J., Szlenkier, M., Krüger, M., Siegert, M., Richnow, H.-H., 2011. Different types of methane monooxygenases produce similar carbon and hydrogen isotope fractionation patterns during methane oxidation. Geochimica et Cosmochimica Acta 75, 1173-1184.

Felske, 2003. Minimierung von Restgasemissionen aus Siedlungsabfalldeponien durch Methanoxidation in Deponieabdeck. Universität Duisburg-Essen, Aachen : Shaker, p. 155.

Foster-Wittig, T.A., Thoma, E.D., Green, R.B., Hater, G.R., Swan, N.D., Chanton, J.P., 2015. Development of a mobile tracer correlation method for assessment of air emissions from landfills and other area sources. Atmospheric Environment 102, 323-330.

Fry, B., 2008. Stable Isotope Ecology. Springer Science+Business Media, LLC, New York.

Funk, W., Dammann, V., Donnevert, G., 2005. Qualitatssicherung in der Analytischen Chemie - Anwendungen in der Umwelt-, Lebensmittel- und Werkstoffanalytik, Biotechnologie und Medizintechnik. WILEY-VCH Verlag GmbH & Co. KGaA, Weinheim, Germany.

Gebert, J., 2011. Can soil gas profiles be used to assess microbial CH_4 oxidation in landfill covers? waste Management 31, 987-994.

Gebert, J., Groengroeft, A., Miehlich, G., 2003. Kinetics of microbial landfill methane oxidation in biofilters. Waste Management 23, 609-619.

Gebert, J., Groengroeft, A., Pfeiffer, E.-M., 2011a. Relevance of soil physical properties for the microbial oxidation of methane in landfill covers. Soil Biology and Biochemistry 43, 1759-1767.

Gebert, J., Perner, M., 2015. Impact of preferential methane flow through soil on microbial community composition. European Journal of Soil Biology 69, 8-16.

Gebert, J., Rachor, I., Grongroft, A., Pfeiffer, E.M., 2011b. Temporal variability of soil gas composition in landfill covers. Waste Manag 31, 935-945.

Gebert, J., Streese-Kleeberg, J., Pfeiffer, E.-M., 2013. Limitations to the quantification of methane oxidation using stable isotopes, Forte Village, S. Margherita di Pula (CA), Italy.

Gehrke, T., 2015. Department Urban Water- and Waste Management, University of Duisburg-Essen, Universitätsstr. 15, 45141 Essen, Germany.

Gehrke, T., Möller, J., Denecke, M., 2013a. Use of quantitative fluorescence in situ hybridisation (FISH) to determine the methane oxidation capacity in landfill covers. CISA, Forte Village, S. Margherita di Pula (CA), Italy.

Gehrke, T., Möller, J., Denecke, M., 2015. Methanoxidation in der Deponieoberfläche, in: Kranert, M. (Ed.), Zeitgemäße Deponietechnik. DIV - Deutscher Industrieverlag GmbH, Stuttgart, Germany.

Gehrke, T., Möller, J., Denecke, M., Widmann, R., 2013b. Mikro- und molekularbiologische Methoden zur quantitativen und qualitativen Erfassung von Einflussgrößen der biologischen Methanoxidation, 3. Wissenschaftskongress Abfall- und Ressourcenwirtschaft, Stuttgart, Germany.

Gruyters, M., 2013. Incineration Slag as a Key Element within a Methane Oxidation Layer on a Closed Landfill -Assessment of Suitability: A Case Study -, Fachbereich Ingenieurwesen, Abteilung Bauwissenschaften. Duisburg-Essen, Shaker Verlag Aachen.

Hanson, R.S., Hanson, T.E., 1996. Methanotrophic bacteria. Microbiol Rev 60, 439-471.

Haubrichs, R., 2007. Entwicklung eines verteilt-geregelt belüfteten Filtersystems zur biologischen Behandlung von methanhaltigen Deponieschwachgasen, Fachbereich Bauwissenschaften Fachgebiet Siedlungswasser- und Abfallwirtschaft. Duisburg-Essen, Shaker Verlag Aachen.

Hayes, J.M., 2004. An Introduction to Isotopic Calculations, in: Institution, W.H.O. (Ed.), Woods Hole, MA 02543, USA.

Heyer, K.-U., Hupe, K., Stegmann, R., 2006. Kriterien für die Beendigung der Nachsorge - Resultate eines UFOPLAN-Vorhabens in: Abfallwirtschaft, I.I.f. (Ed.). Deponietechnik, Hamburg, pp. 60 - 67

Huber-Humer, M., Gebert, J., Hilger, H., 2008. Biotic systems to mitigate landfill methane emissions. Waste Manag Res 26, 33-46.

Hunkeler, D., Chollet, N., Pittet, X., Aravena, R., Cherry, J.A., Parker, B.L., 2004. Effect of source variability and transport processes on carbon isotope ratios of TCE and PCE in two sandy aquifers. J Contam Hydrol 74, 265-282.

Jahnke, L.L., Summons, R.E., Hope, J.M., Des Marais, D.J., 1999. Carbon isotopic fractionation in lipids from methanotrophic bacteria II: the effects of physiology and environmental parameters on the biosynthesis and isotopic signatures of biomarkers. Geochimica et Cosmochimica Acta 63, 79-93.

JCGM100:2008, 2008. Evaluation of measurement data — Guide to the expression of uncertainty in measurement in: Metrology, J.C.f.G.i. (Ed.), 1 ed. BIPM, www.bipm.org.

Jochmann, M., Schmidt, T.C., 2012. Compound-specific Isotope Analysis. The Royal Society of Chemistry, Thomas Graham House, Science Park, Milton Road, CambridgeCB4 0WF, UK.

Jochmann, M.A., Blessing, M., Haderlein, S.B., Schmidt, T.C., 2006. A new approach to determine method detection limits for compound-specific isotope analysis of volatile organic compounds. Rapid Commun Mass Spectrom 20, 3639-3648.

Kampara, M., Thullner, M., Harms, H., Wick, L.Y., 2009. Impact of cell density on microbially induced stable isotope fractionation. Appl Microbiol Biotechnol 81, 977-985.

King, S.L., Quay, P.D., Lansdown, J.M., 1989. The13C/12C kinetic isotope effect for soil oxidation of methane at ambient atmospheric concentrations. Journal of Geophysical Research 94, 18273.

Kinnaman, F.S., Valentine, D.L., Tyler, S.C., 2007. Carbon and hydrogen isotope fractionation associated with the aerobic microbial oxidation of methane, ethane, propane and butane. Geochimica et Cosmochimica Acta 71, 271-283.

Kranert, M., 2010. Einführung in die Abfallwirtschaft. Vieweg+Teubner Verlag Springer, Fachmedien Wiesbaden GmbH Wiesbaden.

Kraume, M., 2012. Transportvorgänge in der Verfahrenstechnik - Grundlagen und apparative Umsetzungen. Springer-Verlag, Berlin.

LANUV, 2012. Deponien in NRW 2012. Landesamt für Natur- Umwelt- und Verbraucherschutz Nordrhein-Westfalen.

Lelieveld, J., 2006. Climate change: a nasty surprise in the greenhouse. Nature 443, 405-406.

Lieberman, R.L., Rosenzweig, A.C., 2004. Biological methane oxidation: regulation, biochemistry, and active site structure of particulate methane monooxygenase. Crit Rev Biochem Mol Biol 39, 147-164.

Liptay, K., Chanton, J., Czepiel, P., Mosher, B., 1998. Use of stable isotopes to determine methane oxidation in landfill cover soils. Journal of Geophysical Research: Atmospheres 103, 8243-8250.

Mahieu, K., De Visscher, A., Vanrolleghem, P.A., Van Cleemput, O., 2008. Modelling of stable isotope fractionation by methane oxidation and diffusion in landfill cover soils. Waste Manag 28, 1535-1542.

Mahieu, K., Visscher, A.D., Vanrolleghem, P.A., Cleemput, O.V., 2006. Carbon and hydrogen isotope fractionation by microbial methane oxidation: improved determination. Waste Manag 26, 389-398.

Maxfield, P.J., Dildar, N., Hornibrook, E.R., Stott, A.W., Evershed, R.P., 2012. Stable isotope switching (SIS): a new stable isotope probing (SIP) approach to determine carbon flow in the soil food web and dynamics in organic matter pools. Rapid Commun Mass Spectrom 26, 997-1004.

Maxfield, P.J., Evershed, R.P., Hornibrook, E.R.C., 2008. Physical and Biological Controls on the In Situ Kinetic Isotope Effect Associated with Oxidation of Atmospheric CH4in Mineral Soils. Environmental Science & Technology 42, 7824-7830.

McDonald, I.R., Bodrossy, L., Chen, Y., Murrell, J.C., 2008. Molecular ecology techniques for the study of aerobic methanotrophs. Appl Environ Microbiol 74, 1305-1315.

Mei, C., Yazdani, R., Han, B., Mostafid, M.E., Chanton, J., VanderGheynst, J., Imhoff, P., 2015. Performance of green waste biocovers for enhancing methane oxidation. Waste Manag 39, 205-215.

Mohammadzadeh, H., Clark, I., Marschner, M., St-Jean, G., 2005. Compound Specific Isotopic Analysis (CSIA) of landfill leachate DOC components. Chemical Geology 218, 3-13.

Monster, J., Samuelsson, J., Kjeldsen, P., Scheutz, C., 2015. Quantification of methane emissions from 15 Danish landfills using the mobile tracer dispersion method. Waste Manag 35, 177-186.

Myhre, G., D. Shindell, F.-M. Bréon, W. Collins, J. Fuglestvedt, J. Huang, D. Koch, J.-F. Lamarque, D. Lee, B. Mendoza,, T. Nakajima, A.R., G. Stephens, T. Takemura and H. Zhang,, 2013. Anthropogenic and Natural Radiative Forcing. Cambridge University Press, Cambridge, United Kingdom and New York, NY, USA.

Nihous, G.C., 2008. A quantitative interpretation of recent experimental results on stable carbon isotope fractionation by aerobic CH_4-oxidizing bacteria. Geochimica et Cosmochimica Acta 72, 4469-4475.

Nihous, G.C., 2010. Notes on the temperature dependence of carbon isotope fractionation by aerobic CH_4-oxidising bacteria. Isotopes Environ Health Stud 46, 133-140.

Nitzsche, H.M., Czegka, W., Hanisch, C., Zerling, L., Junge, F.W., 2009. The potential for releasing methane from artificial lakes in Central Germany--a 13C study. Isotopes Environ Health Stud 45, 231-246.

Park, J.R., Moon, S., Ahn, Y.M., Kim, J.Y., Nam, K., 2005. Determination of environmental factors influencing methane oxidation in a sandy landfill cover soil. Environ Technol 26, 93-102.

Pasteris, G., Werner, D., Kaufmann, K., Höhener, P., 2002. Vapor Phase Transport and Biodegradation of Volatile Fuel Compounds in the Unsaturated Zone: A Large Scale Lysimeter Experiment. Environmental Science & Technology 36, 30-39.

Petersen, J.M., Dubilier, N., 2009. Methanotrophic symbioses in marine invertebrates. Environ Microbiol Rep 1, 319-335.

Powelson, D.K., Chanton, J., Abichou, T., Morales, J., 2006. Methane oxidation in water-spreading and compost biofilters. Waste Manag Res 24, 528-536.

Powelson, D.K., Chanton, J.P., Abichou, T., 2007. Methane Oxidation in Biofilters Measured by Mass-Balance and Stable Isotope Methods. Environmental Science & Technology 41, 620-625.

Preuss, I., Knoblauch, C., Gebert, J., Pfeiffer, E.M., 2013. Improved quantification of microbial CH4 oxidation efficiency in arctic wetland soils using carbon isotope fractionation. Biogeosciences 10, 2539-2552.

Rachor, I., Gebert, J., Grongroft, A., Pfeiffer, E.M., 2011. Assessment of the methane oxidation capacity of compacted soils intended for use as landfill cover materials. Waste Manag 31, 833-842.

Rachor, I.M., Gebert, J., Gröngröft, A., Pfeiffer, E.M., 2013. Variability of methane emissions from an old landfill over different time-scales. European Journal of Soil Science 64, 16-26.

Raghoebarsing, A.A., Smolders, A.J., Schmid, M.C., Rijpstra, W.I., Wolters-Arts, M., Derksen, J., Jetten, M.S., Schouten, S., Sinninghe Damste, J.S., Lamers, L.P., Roelofs, J.G., Op den Camp, H.J., Strous, M., 2005. Methanotrophic symbionts provide carbon for photosynthesis in peat bogs. Nature 436, 1153-1156.

Rasmussen, R.A., Khalil, M.A.K., 1981. Atmospheric methane (CH4): Trends and seasonal cycles. Journal of Geophysical Research 86, 9826.

Rettenberger, G., 1996. Erkenntnisse aus dem Deponierückbau bezüglich Langzeitverhalten der Deponiegasentwicklung – Empfehlungen für die Entgasung älterer Deponien, in: Rettenberger, G. (Ed.), Deponiegas 1995 - Nutzung und Erfassung, Trierer Berichte zur Abfallwirtschaft. Economica Verlag.

Rettenberger, G., Stegmann, R., 1996. Landfilling of Waste: Biogas. E & FN Spoon, London.

Ritzkowski, M., Heyer, K.U., Stegmann, R., 2006. Fundamental processes and implications during in situ aeration of old landfills. Waste Manag 26, 356-372.

Roth, J., 2015. Entsorgung- und Verwertungskonzeption von Schwachgas der Deponie Eichelbuck. In: Kranert, M.: Zeitgemäße Deponietechnik 2015. *Aktuelle Aspekte des Deponiebetriebs-Behandlung von Schwachgas und Sickerwasser, Belüftung, Nachsorge*, Stuttgart.

Santrock, J., Studley, S.A., Hayes, J.M., 1985. Isotopic analyses based on the mass spectra of carbon dioxide. Analytical Chemistry 57, 1444-1448.

Scheutz, C., Kjeldsen, P., 2004. Environmental Factors Influencing Attenuation of Methane and Hydrochlorofluorocarbons in Landfill Cover Soils. Journal of Environment Quality 33, 72.

Scheutz, C., Kjeldsen, P., Bogner, J.E., De Visscher, A., Gebert, J., Hilger, H.A., Huber-Humer, M., Spokas, K., 2009. Microbial methane oxidation processes and technologies for mitigation of landfill gas emissions. Waste Manag Res 27, 409-455.

Scheutz, C., Pedersen, R.B., Petersen, P.H., Jorgensen, J.H., Ucendo, I.M., Monster, J.G., Samuelsson, J., Kjeldsen, P., 2014. Mitigation of methane emission from an old unlined landfill in Klintholm, Denmark using a passive biocover system. Waste Manag 34, 1179-1190.

Schmaljohann, R., Flugel, H.J., 1987. Methane-oxidizing bacteria in pogonophora. Sarsia 72, 91-99.

Scott, K.M., Lu, X., Cavanaugh, C.M., Liu, J.S., 2004. Optimal methods for estimating kinetic isotope effects from different forms of the Rayleigh distillation equation. Geochimica et Cosmochimica Acta 68, 433-442.

Semrau, J.D., DiSpirito, A.A., Yoon, S., 2010. Methanotrophs and copper. FEMS Microbiol Rev 34, 496-531.

Shapiro, S.S., Wilk, M.B., 1965. An Analysis of Variance Test for Normality (Complete Samples). Biometrika 52, 591-611.

Sharp, Z., 2007. Principles of Stable Isotope Geochemistry, 1st ed. ed. Pearson Education, Inc., Upper Saddle River, NJ, 07458, US.

Snover, A.K., Quay, P.D., 2000. Hydrogen and carbon kinetic isotope effects during soil uptake of atmospheric methane. Global Biogeochemical Cycles 14, 25-39.

Spokas, K., Bogner, J., Chanton, J.P., Morcet, M., Aran, C., Graff, C., Golvan, Y.M., Hebe, I., 2006. Methane mass balance at three landfill sites: what is the efficiency of capture by gas collection systems? Waste Manag 26, 516-525.

Stanley, S.H., Prior, S.D., Leak, D.J., Dalton, H., 1983. Copper stress underlies the fundamental change in intracellular location of methane mono-oxygenase in methane-oxidizing organisms: Studies in batch and continuous cultures. Biotechnology Letters 5, 487-492.

Stegmann, R., 2005. Landfill aftercare - scope for actions, duration, costs and quantitative criteria for the completion. Proceedings Sardinia 2005, Tenth International Waste Management and Landfill Symposium S. Margherita di Pula, Cagliari, Italy; 3 - 7 October 2005.

Streese-Kleeberg, J., Rachor, I., Gebert, J., Stegmann, R., 2011. Use of gas push-pull tests for the measurement of methane oxidation in different landfill cover soils. Waste Manag 31, 995-1001.

Templeton, A.S., Chu, K.H., Alvarez-Cohen, L., Conrad, M.E., 2006. Variable carbon isotope fractionation expressed by aerobic CH_4-oxidizing bacteria. Geochimica Et Cosmochimica Acta 70, 1739-1752.

Thom, A., Ricken, T., Widmann, R., Denecke, M., Gehrke, T., Bluhm, J., Schulte, M., 2016. A multi-constituent strongly coupled monolithic FE-model for bacterial methane oxidation in landfill cover layers with validation by thermal imaging. In prep.

Tyler, S.C., Crill, P.M., Brailsford, G.W., 1994. Fractionation of methane during oxidation in a temperate forested soil. Geochimica et Cosmochimica Acta 58, 1625-1633.

Urmann, K., Gonzalez-Gil, G., Schroth, M.H., Hofer, M., Zeyer, J., 2005. New field method: Gas push-pull test for the in-situ quantification of microbial activities in the vadose zone. Environmental Science & Technology 39, 304-310.

Van De Steene, J., Hohener, P., 2009. Tracer test for the measurement of gas diffusion and non-aqueous phase liquid (NAPL) saturation in soil. Chemosphere 74, 224-231.

Vavilin, V.A., Rytov, S.V., Shim, N., Vogt, C., 2016. Non-linear dynamics of stable carbon and hydrogen isotope signatures based on a biological kinetic model of aerobic enzymatic methane oxidation. Isotopes Environ Health Stud 52, 185-202.

Wahlen, M., 1993. The Global Methane Cycle. Annual Review of Earth and Planetary Sciences 21, 407-426.

Widory, D., Proust, E., Bellenfant, G., Bour, O., 2012. Assessing methane oxidation under landfill covers and its contribution to the above atmospheric CO_2 levels: the added value of the isotope $\delta^{13}C$ and $\delta^{18}O$ CO_2; $\delta^{13}C$ and δD CH_4 approach. Waste Manag 32, 1685-1692.

Wimmer, B., Hrad, M., Huber-Humer, M., Watzinger, A., Wyhlidal, S., Reichenauer, T.G., 2013. Stable isotope signatures for characterising the biological stability of landfilled municipal solid waste. Waste Manag 33, 2083-2090.

Yang, Y., Belghazi, M., Lagadec, A., Miller, D.J., Hawthorne, S.B., 1998. Elution of organic solutes from different polarity sorbents using subcritical water. Journal of Chromatography A 810, 149-159.

Zyakun, A.M., Muravyev, A.I., Baskunov, B.P., Laurinavichius, K.S., Zakharchenko, V.N., Peshenko, V.P., Lykov, I.N., Shestakova, G.A., 2010. Estimation of microbial methane generation and oxidation rates in the municipal solid waste landfill of Kaluga city, Russia. Isotopes Environ Health Stud 46, 78-90.

Appendices

A1. Chapter 1

In the following the thorough combination of equations (1.4.36), (1.4.37), and (1.4.38) is given.

$$\begin{aligned} {}^{46}R &= {}^{18}R + 2^{13}R\,{}^{18}R^{\alpha}K + \left({}^{18}R^{\alpha}K\right)^2 \\ \Leftrightarrow {}^{46}R &= 2^{18}R + 2^{13}R\,{}^{18}R^{\alpha}K + {}^{18}R^{2\alpha}K^2 \\ \Leftrightarrow {}^{13}R &= \frac{{}^{46}R - 2^{18}R - {}^{18}R^{2\alpha}K^2}{2^{18}R^{\alpha}K} \end{aligned} \tag{7.1.1}$$

$$\begin{aligned} {}^{45}R &= {}^{13}R + 2^{17}R \\ \Leftrightarrow {}^{13}R &= {}^{45}R - 2^{18}R^{\alpha}K \end{aligned} \tag{7.1.2}$$

Combining (7.1.1) and (7.1.2) gives:

$$\begin{aligned} {}^{45}R - 2^{18}R^{\alpha}K &= \frac{{}^{46}R - 2^{18}R - {}^{18}R^{2\alpha}K^2}{2^{18}R^{\alpha}K} \\ \Leftrightarrow 2^{18}R^{\alpha}K\,{}^{45}R - 4^{18}R^{2\alpha}K^2 &= {}^{46}R - {}^{18}R - {}^{18}R^{2\alpha}K^2 \\ \Leftrightarrow 2^{18}R^{\alpha}K\,{}^{45}R - 3^{18}R^{2\alpha}K^2 + 2^{18}R - {}^{46}R &= 0 \end{aligned} \tag{7.1.3}$$

A2. Chapter 3

Table 0-1 Diffusion coefficients of methane determined by GC-IRMS

The diffusion coefficients determined based on the model described by De Visscher (2004) at the respective sampling heights are listed. Values were determined from single measurement.

22.5°C			30°C		
z /cm	D_m /10^{-2}cm^{2}s^{-1}	$R^2_{corrected}$	z /cm	D_m /10^{-2}cm^{2}s^{-1}	$R^2_{corrected}$
0	5.93	0.76	0	7.33	0.90
0	5.55	0.87	0	-	-
0	4.92	0.93	0	-	-
9	6.25	0.49	5	6.32	0.92
9	5.11	0.73	5	8.89	0.94
9	6.00	0.63	5	7.51	0.88
14	6.75	0.92	9	9.18	0.87
14	6.53	0.92	9	8.55	0.97
14	7.78	0.96	9	9.16	0.97

A3. Chapter 4

Table 0-2 Isotopic enrichment factors of mixed methanotrophs in topsoil at 22°C
Given are the enrichment factors ε and kinetic rate constants ${}^{h}k$ along with the correlation coefficients R^2 for each individual centrifuge tube experiment and for CH_4 and CO_2.

CH_4				**CO_2**	
ε	R^2	$10^{-6} \cdot {}^{h}k$ /s^{-1}	R^2	ε	R^2
-0.0220	0.99	5.50	0.96	-	-
-0.0109	0.93	5.33	0.97	-	-
-0.0175	0.96	1.12	0.94	-	-
-0.0168	0.93	1.22	0.91	-0.0284	0.67
-0.0176	0.99	15.19	0.91	-	-
-0.0157	0.97	18.35	0.89	-	-
-0.0168	0.98	21.57	0.89	-	-
-0.0256	0.97	24.78	0.91	-	-
-0.0264	0.96	33.57	0.90	-0.0097	0.63
-0.0214	0.97	38.03	0.79	-0.0078	1.00
-0.0205	0.99	45.21	0.94	-0.0143	0.51
-0.0206	0.96	16.45	0.94	-	-
-0.0277	0.99	34.03	0.98	-	-
-0.0237	0.99	27.39	0.95	-	-

Table 0-3 Isotopic enrichment factors of mixed methanotrophs in topsoil at 30°C
Given are the enrichment factors ε and kinetic rate constants ${}^{h}k$ along with the correlation coefficients R^2 for each individual centrifuge tube experiment and for CH_4 and CO_2.

CH_4				CO_2	
ε	R^2	$10^{-6} \cdot {}^{h}k$ /s^{-1}	R^2	ε	R^2
-0.0247	0.98	46.18	0.98	-	-
-0.0274	0.93	16.99	0.95	-	-
-0.0152	0.95	41.21	0.96	-	-
-0.0198	0.98	43.27	0.98	-	-
-0.0204	0.98	174.76	0.93	-	-
-0.0246	0.99	121.05	0.99	-0.0099	0.90
-0.0183	0.99	130.75	0.97	-0.0163	0.97
-0.0239	0.97	14.95	0.96	-	-
-0.0185	1.00	157.60	0.94	-	-
-0.0186	0.99	98.98	0.94	-	-
-0.0191	1.00	191.38	0.92	-	-
-0.0228	0.99	87.28	0.98	-0.0162	0.64
-0.0179	0.99	69.61	0.99	-	-
-0.0195	1.00	125.66	0.95	-0.0218	0.92
-0.0278	0.99	18.96	0.76	-	-
-0.0344	0.99	7.99	0.90	-	-
-0.0368	0.96	5.68	0.77	-	-
-0.0188	1.00	255.51	0.97	-0.0169	0.92
-0.0321	0.98	56.56	0.95	-	-
-0.0248	0.99	57.34	0.84	-	-

Table 0-4 Isotopic enrichment factors of type I/II conditions at different temperatures
Given are the enrichment factors $\varepsilon_{22°C}$ and kinetic rate constants ${}^{h}k$ along with the corrected correlation coefficients $R^2_{corrected}$ for each individual centrifuge tube system.

ε	$R^2_{corrected}$	$10^{-6} \cdot {}^{h}k$ /s^{-1}	$R^2_{corrected}$
-0.0122	1.00	1.90	0.98
-0.0082	0.93	1.77	0.96
-0.0146	0.98	3.30	0.99
-0.0102	0.98	2.71	0.96
-0.0162	1.00	1.28	1.00
-0.0129	0.98	1.36	0.99
-0.0198	0.95	1.24	0.91
-0.0146	0.79	0.60	0.89

A4. Chapter 5

1. Calculations based on stable isotope approach

In the following the calculation of the measurement errors of the respective methods are given for the stable isotope approach.

Parameters:

$\delta_{CH_4,0}$: Gas concentration of methane at gas inlet
$\delta_{CH_4,m}$: Gas concentration of methane at sampling site
$\delta_{CO_2,0}$: Gas concentration of carbon dioxide at gas inlet
$\delta_{CO_2,m}$: Gas concentration of carbon dioxide at sampling site
$\delta_{CO_2,ox}$: Gas concentration of carbon dioxide at sampling site resulting from the BMO
ε: Enrichment factor of the BMO
ε_{diff}: Enrichment factor of diffusion

Maximum error for the **closed system approach** calculated based on partial derivatives:

1. $$f_{ox}^{CSI} = f\left(\delta_{CH_4,0}, \delta_{CH_4,m}, \varepsilon_{ox}\right) = 1 - \left(\frac{\delta_{CH_4,m}+1}{\delta_{CH_4,0}+1}\right)^{\frac{1}{\varepsilon}}$$

$$\Delta f_{ox}^{CSI} = \left|\frac{\partial f_{ox}^{CSI}}{\partial \varepsilon}\right| \Delta\varepsilon_{ox} + \left|\frac{\partial\left(f_{ox}^{CSI}\right)}{\partial\left(\delta_{CH_4,m}\right)}\right| \Delta\delta_{CH_4,m} + \left|\frac{\partial\left(f_{ox}^{CSI}\right)}{\partial\left(\delta_{CH_4,0}\right)}\right| \Delta\delta_{CH_4,0}$$

With individual errors:

$$\left|\frac{\partial f_{ox}^{CSI}}{\partial \varepsilon}\right| \Delta\varepsilon = \left|-(\varepsilon)^{-2} \cdot \left(\frac{\delta_{CH_4,m}+1}{\delta_{CH_4,0}+1}\right)^{\frac{1}{\varepsilon}} \cdot \ln\left(\frac{\delta_{CH_4,m}+1}{\delta_{CH_4,0}+1}\right)\right| \Delta\varepsilon$$

$$\left|\frac{\partial f_{ox}^{CSI}}{\partial \delta_{CH_4,m}}\right| \Delta\delta_{CH_4,0} = \left|\frac{1}{\varepsilon(\delta_{CH_4,0}+1)}\left(\frac{\delta_{CH_4,m}+1}{\delta_{CH_4,0}+1}\right)^{\frac{1}{\varepsilon}-1}\right| \Delta\delta_{CH_4,m}$$

$$\left|\frac{\partial f_{ox}^{CSI}}{\partial \delta_{CH_4,0}}\right| \Delta\delta_{CH_4,0} = \left|-\frac{\delta_{CH_4,m}+1}{\varepsilon\left(\delta_{CH_4,0}+1\right)^2}\left(\frac{\delta_{CH_4,m}+1}{\delta_{CH_4,0}+1}\right)^{\frac{1}{\varepsilon}-1}\right| \Delta\delta_{CH_4,0}$$

Derivation of $\frac{\partial f_{ox}^{CSI}}{\partial \varepsilon_{ox}}$:

Based on real exponential function: $f\left(a^x\right)=e^{x\cdot ln(a)}$ the derivative is: $f'\left(a^x\right)=a^x\cdot\ ln\left(a\right)$.

In this case the respective function can be described as: $f\left(a^{x^{-1}}\right)=e^{x^{-1}\cdot\ln(a)}$. Its derivative $f'(a^{x^{-1}})=-x^{-2}\cdot a^{x^{-1}}\cdot\ln(a)$ can be calculated based on the chain rule as:

The outer function:

$$f\left(u\right)\ =\ e^u\rightarrow\left(e^u\right)'=\ e^u$$

and inner function:

$$f\left(v\right)=x^{-1}\cdot\ln\left(a\right)\ \rightarrow v'=-x^{-2}\cdot\ln\left(a\right)$$

combining yields:

$$f'(a^{x^{-1}})=a^{x^{-1}}\cdot\ln(a)\ \cdot\left(\text{-}x^{-2}\right)$$

Derivation of $\frac{\partial\left(f_{ox}^{CSI}\right)}{\partial\left(\delta_{CH_4,m}\right)}$ and $\frac{\partial\left(f_{ox}^{CSI}\right)}{\partial\left(\delta_{CH_4,0}\right)}$

Using the chain rule for outer and inner function as well as the quotient rule for the derivative of the inner function:

Substitution:

$$u=u\left(\varepsilon\right)=\varepsilon$$

Thus the outer function is:

$$f_{ox}^{CSI}\ =\ f\left(u\right)=\left(\frac{\delta_{CH_4,m}+1}{\delta_{CH_4,0}+1}\right)^{\frac{1}{u}}\Rightarrow\frac{\partial f_{ox}^{CSI}}{\partial u}=\frac{1}{u}\left(\frac{\delta_{CH_4,m}+1}{\delta_{CH_4,0}+1}\right)^{\frac{1}{u}-1}$$

Inner function:

$$u = u\left(\delta_{CH_4,m}\right) \Rightarrow \frac{\partial f_{ox}^{CSI}}{\partial u} = \frac{\partial f_{ox}^{CSI}}{\partial \delta_{CH_4,m}} = \frac{1\cdot\left(\delta_{CH_4,0}+1\right)-\left(\delta_{CH_4,m}+1\right)\cdot 0}{\left(\delta_{CH_4,0}+1\right)^2} = \left(\frac{\delta_{CH_4,0}+1}{\left(\delta_{CH_4,0}+1\right)^2}\right) = \frac{1}{\delta_{CH_4,0}+1}$$

Inner function:

$$u = u\left(\delta_{CH_4,0}\right) = \left(\frac{\delta_{CH_4,m}+1}{\delta_{CH_4,0}+1}\right) \Rightarrow \frac{\partial f_{ox}^{CSI}}{\partial \delta_{CH_4,0}} = \frac{\partial f_{ox}^{CSI}}{\partial u} = \left(\frac{0\cdot\left(\delta_{CH_4,0}+1\right)-\left(\delta_{CH_4,m}+1\right)\cdot 1}{\left(\delta_{CH_4,0}+1\right)^2}\right) = \left(-\frac{\delta_{CH_4,m}+1}{\left(\delta_{CH_4,0}+1\right)^2}\right)$$

Reinserting the inner function into the respective outer function results in the equations shown above for the errors.

For the open system different corrections can be considered as follows:

1. $f_{ox}^{OSI} = \dfrac{\delta_{CH_4,0} - \delta_{CH_4,m}}{\varepsilon}$

2. $f_{ox}^{OSIC} = \dfrac{\delta_{CH_4,0} - \delta_{CH_4,m}}{\varepsilon - \varepsilon_{trans}}$

Maximum error based on the **open system** subdivided for the two approaches given above:

1. $f_{ox}^{OSI} = f\left(\delta_{CH_4,m}, \delta_{CH_4,0}, \varepsilon\right)$

$$\Delta f_{ox}^{OSI} = \left|\frac{\partial f_{ox}^{OSI}}{\partial \varepsilon}\right| \Delta\varepsilon + \left|\frac{\partial f_{ox}^{OSI}}{\partial\left(\delta_{CH_4,m}\right)}\right| \Delta\delta_{CH_4,m} + \left|\frac{\partial f_{ox}^{OSI}}{\partial\left(\delta_{CH_4,0}\right)}\right| \Delta\delta_{CH_4,0}$$

$$\left|\frac{\partial f_{ox}^{OSI}}{\partial \varepsilon}\right| \Delta\varepsilon = \left|\frac{0\cdot(\varepsilon)-\left(\delta_{CH_4,0}-\delta_{CH_4,m}\right)\cdot 1}{(\varepsilon)^2}\right| \cdot \Delta\varepsilon = \left|-\frac{\delta_{CH_4,0}-\delta_{CH_4,m}}{\varepsilon^2}\right| \cdot \Delta\varepsilon$$

$$\left|\frac{\partial f_{ox}^{OSI}}{\partial \delta_{CH_4,m}}\right| \Delta\delta_{CH_4,m} = \left|\frac{(1-0)\cdot\varepsilon-\left(\delta_{CH_4,0}-\delta_{CH_4,m}\right)\cdot 0}{(\varepsilon)^2}\right| \cdot \Delta\delta_{CH_4,m} = \left|\frac{1}{\varepsilon}\right| \cdot \Delta\delta_{CH_4,m}$$

$$\left|\frac{\partial f_{ox\text{-}OSI}}{\partial \delta_{CH_4,0}}\right| \Delta\delta_{CH_4,0} = \left|\frac{(0-1)\cdot\varepsilon-\left(\delta_{CH_4,0}-\delta_{CH_4,m}\right)\cdot 0}{(\varepsilon)^2}\right| \cdot \Delta\delta_{CH_4,m} = \left|-\frac{1}{\varepsilon}\right| \cdot \Delta\delta_{CH_4,m}$$

2. $f_{ox}^{OSIC} = f(\delta_{CH_4,m}, \delta_{CH_4,0}, \varepsilon, \varepsilon_{diff})$

$$\Delta f_{ox}^{OSIC} = \left|\frac{\partial f_{ox}^{OSIC}}{\partial \varepsilon}\right| \Delta\varepsilon + \left|\frac{\partial f_{ox}^{OSIC}}{\partial \varepsilon_{diff}}\right| \Delta\varepsilon_{diff} + \left|\frac{\partial f_{ox}^{OSIC}}{\partial\left(\delta_{CH_4,m}\right)}\right| \Delta\delta_{CH_4,m} + \left|\frac{\partial f_{ox}^{OSIC}}{\partial\left(\delta_{CH_4,0}\right)}\right| \Delta\delta_{CH_4,0}$$

$$\left|\frac{\partial f_{ox}^{OSIC}}{\partial \varepsilon}\right| \Delta\varepsilon = \left|\frac{0\cdot\left(\varepsilon-\varepsilon_{diff}\right)-\left(\delta_{CH_4,0}-\delta_{CH_4,m}\right)\cdot 1}{\left(\varepsilon-\varepsilon_{diff}\right)^2}\right| \cdot \Delta\varepsilon = \left|-\frac{\delta_{CH_4,0}-\delta_{CH_4,m}}{\left(\varepsilon-\varepsilon_{diff}\right)^2}\right| \cdot \Delta\varepsilon$$

$$\left|\frac{\partial f_{ox}^{OSIC}}{\partial \varepsilon_{diff}}\right| \Delta\varepsilon_{diff} = \left|\frac{0\cdot\left(\varepsilon-\varepsilon_{diff}\right)+\left(\delta_{CH_4,0}-\delta_{CH_4,m}\right)\cdot 1}{\left(\varepsilon-\varepsilon_{diff}\right)^2}\right| \cdot \Delta\varepsilon_{diff} = \left|\frac{\delta_{CH_4,0}-\delta_{CH_4,m}}{\left(\varepsilon-\varepsilon_{diff}\right)^2}\right| \cdot \Delta\varepsilon_{diff}$$

$$\left|\frac{\partial f_{ox}^{OSIC}}{\partial \delta_{CH_4,m}}\right| \Delta\delta_{CH_4,m} = \left|\frac{(1-0)\cdot\left(\varepsilon-\varepsilon_{diff}\right)-\left(\delta_{CH_4,0}-\delta_{CH_4,m}\right)\cdot 0}{\left(\varepsilon-\varepsilon_{diff}\right)^2}\right| \cdot \Delta\delta_{CH_4,m} = \left|\frac{1}{\varepsilon-\varepsilon_{diff}}\right| \cdot \Delta\delta_{CH_4,m}$$

$$\left|\frac{\partial f_{ox}^{OSIC}}{\partial \delta_{CH_4,0}}\right| \Delta\delta_{CH_4,0} = \left|\frac{(0-1)\cdot\left(\varepsilon-\varepsilon_{diff}\right)-\left(\delta_{CH_4,0}-\delta_{CH_4,m}\right)\cdot 0}{\left(\varepsilon-\varepsilon_{diff}\right)^2}\right| \cdot \Delta\delta_{CH_4,0} = \left|-\frac{1}{\varepsilon-\varepsilon_{diff}}\right| \cdot \Delta\delta_{CH_4,0}$$

2. Based on mass balance

Parameters:

$c_{CH_4,0}$: Gas concentration of methane at gas inlet

$c_{CH_4,hs}$: Gas concentration of methane in reactor headspace

$\dot{V}_0$: Total volume flow of gas at gas inlet (e.g. Ls^{-1})

$\dot{V}_{hs}$: Total volume flow of gas at gas outlet/headspace of reactor (e.g. Ls^{-1})

$$f_{ox}^{MFC/MFM} = 1 - \frac{J_{out}}{J_{in}} = \frac{c_{CH_4,0}\cdot\dot{V}_0 - c_{CH_4,hs}\cdot\dot{V}_{hs}}{c_{CH_4,0}\cdot\dot{V}_0}$$

$\dot{V}_{hs}$ was either taken from the MFM directly or calculated from the sum of the MFC (gas inlets).

$$\dot{V}_{hs} = \dot{V}_{MFM} \text{ or } \dot{V}_{hs} = \sum\dot{V}_{MFCs} = \dot{V}_{CO_2} + \dot{V}_{CH_4} + \dot{V}_{air\text{-}in}$$

Error of gas flow:

$$\Delta\dot{V}_{hs} = \Delta\dot{V}_{MFM} \text{ or } \Delta\dot{V}_{hs} = \sqrt{\sum\Delta\dot{V}_{MFCs}^{\,2}} = \sqrt{\Delta\dot{V}_{CO_2}^{\,2} + \Delta\dot{V}_{CH_4}^{\,2} + \Delta\dot{V}_{air\text{-}in}^{\,2}}$$

$\Delta\dot{V}_{CO_2}, \Delta\dot{V}_{CH_4}, \Delta\dot{V}_{air\text{-}in}$: Standard deviation of the gas flow of the respective MFC calculated from data of the corresponding sampling day from 8:00 a.m. to 12:00 a.m.

Error of concentration:

$$\Delta(c) = u(c) = s_{\hat{x}}$$

$$s_{\hat{x}} = s_{x0}\sqrt{\frac{1}{N_s} + \frac{1}{N_c} + \frac{\hat{\bar{y}} - \bar{y}}{b^2 \cdot Q_{xx}}}$$

With $s_{x_0} = \frac{s_y}{b}$

$u(c_i)$: Standard uncertainty of concentration of either CO_2- or CH_4-concentration estimated from standard error of prediction $s_{\hat{x}}$

N_s: Number of sample measurements

N_c: Number of calibration standards

$\bar{y}$: Average signal (Vs) from calibration

$\hat{\bar{y}}$: Average signal (Vs) from N_s measurements of sample

b: Slope of regression line

s_y: Residual standard deviation

Q_{xx}: Sum of squares $\left(\sum(x_i - \bar{x})^2\right)$

x_i: Individual concentration value from calibration

$\bar{x}$: Average concentration from calibration

Error propagation by partial differentiation:

$$f_{ox}^{MFC/MFM} = f\left(c_{CH_4,0}, \dot{V}_0, c_{CH_4,hs}, \dot{V}_{hs}\right) = \frac{c_{CH_4,0} \cdot \dot{V}_0 - c_{CH_4,hs} \cdot \dot{V}_{hs}}{c_{CH_4,0} \cdot \dot{V}_0}$$

$$\Rightarrow \Delta f_{ox}^{MFC/MFM} = \left|\frac{\partial f_{ox}^{MFC/MFM}}{\partial c_{CH_4,0}}\right| \Delta c_{CH_4,0} + \left|\frac{\partial f_{ox}^{MFC/MFM}}{\partial c_{CH_4,hs}}\right| \Delta c_{CH_4,hs} + \left|\frac{\partial f_{ox}^{MFC/MFM}}{\partial \dot{V}_0}\right| \Delta\dot{V}_0 + \left|\frac{\partial f_{ox}^{MFC/MFM}}{\partial \dot{V}_{hs}}\right| \Delta\dot{V}_{hs}$$

$$\left|\frac{\partial f_{ox}^{MFC/MFM}}{\partial c_{CH_4,0}}\right| \Delta c_{CH_4,0} = \left|\frac{\dot{V}_0 \cdot c_{CH_4,0} \cdot \dot{V}_0 - \left(c_{CH_4,0} \cdot \dot{V}_0 - c_{CH_4,hs} \cdot \dot{V}_{hs}\right) \cdot \dot{V}_0}{\left(c_{CH_4,0} \cdot \dot{V}_0\right)^2}\right| \Delta c_{CH_4,0}$$

$$\Leftrightarrow \left|\frac{c_{CH_4,hs} \cdot \dot{V}_{hs} \cdot \dot{V}_0}{\left(c_{CH_4,0} \cdot \dot{V}_0\right)^2}\right| \Delta c_{CH_4,0} = \left|\frac{c_{CH_4,hs} \cdot \dot{V}_{hs}}{c_{CH_4,0}^{\ 2} \cdot \dot{V}_0}\right| \Delta c_{CH_4,0}$$

$$\left|\frac{\partial f_{ox}^{\mathrm{MFC/MFM}}}{\partial c_{\mathrm{CH_4,hs}}}\right|\Delta c_{\mathrm{CH_4,hs}} = \left|\frac{\dot{V}_{\mathrm{hs}}\cdot\left(c_{\mathrm{CH_4,0}}\cdot\dot{V}_0\right)-\left(c_{\mathrm{CH_4,0}}\cdot\dot{V}_0-c_{\mathrm{CH_4,hs}}\cdot\dot{V}_{\mathrm{hs}}\right)\cdot 0}{\left(c_{\mathrm{CH_4,0}}\cdot\dot{V}_0\right)^2}\right|\Delta c_{\mathrm{CH_4,hs}}$$

$$= \left|\frac{\dot{V}_{\mathrm{hs}}\cdot c_{\mathrm{CH_4,0}}\cdot\dot{V}_0}{\left(c_{\mathrm{CH_4,0}}\cdot\dot{V}_0\right)^2}=\frac{\dot{V}_{\mathrm{hs}}}{c_{\mathrm{CH_4,0}}\cdot\dot{V}_0}\right|\Delta c_{\mathrm{CH_4,hs}}$$

$$\left|\frac{\partial f_{ox}^{\mathrm{MFC/MFM}}}{\partial \dot{V}_0}\right|\Delta\dot{V}_0 = \left|\frac{c_{\mathrm{CH_4,0}}\cdot c_{\mathrm{CH_4,0}}\cdot\dot{V}_0-\left(c_{\mathrm{CH_4,0}}\cdot\dot{V}_0-c_{\mathrm{CH_4,hs}}\cdot\dot{V}_{\mathrm{hs}}\right)\cdot c_{\mathrm{CH_4,0}}}{\left(c_{\mathrm{CH_4,0}}\cdot\dot{V}_0\right)^2}\right|\Delta\dot{V}_0 = \left|\frac{c_{\mathrm{CH_4,hs}}\cdot\dot{V}_{\mathrm{hs}}}{c_{\mathrm{CH_4,0}}\cdot\dot{V}_0^{\,2}}\right|\Delta\dot{V}_0$$

$$\left|\frac{\partial f_{ox}^{\mathrm{MFC/MFM}}}{\partial \dot{V}_{\mathrm{hs}}}\right|\Delta\dot{V}_{\mathrm{hs}} = \left|\frac{-c_{\mathrm{CH_4,hs}}\cdot c_{\mathrm{CH_4,0}}\cdot\dot{V}_0-\left(c_{\mathrm{CH_4,0}}\cdot\dot{V}_0-c_{\mathrm{CH_4,hs}}\cdot\dot{V}_{\mathrm{hs}}\right)\cdot 0}{\left(c_{\mathrm{CH_4,0}}\cdot\dot{V}_0\right)^2}\right|\Delta\dot{V}_{\mathrm{hs}} = \left|-\frac{c_{\mathrm{CH_4,hs}}}{c_{\mathrm{CH_4,0}}\cdot\dot{V}_0}\right|\Delta\dot{V}_{\mathrm{hs}}$$

3. Based on corrections by Powelson

$$f_{ox}^{CSIC} = f\left(P, f_{ox}^{CSI}\right)$$

$$f_{ox}^{CSIC} = 1-P+P\cdot f_{ox}^{CSIC}$$

$$\Delta f_{ox}^{CSIC} = 1\cdot\Delta f_{\mathrm{ox}}^{\mathrm{MFM}} + \left|\frac{-2 f_{\mathrm{ox}}^{\mathrm{CSI}}}{\left(1-f_{\mathrm{ox}}^{\mathrm{CSI}}\right)^2}\right|\Delta f_{\mathrm{ox}}^{\mathrm{CSI}}$$

$$f_{\mathrm{ox}}^{\mathrm{CSIC}} = 1\cdot\Delta f_{\mathrm{ox}}^{\mathrm{MFM}} + \left|\frac{-2 f_{\mathrm{ox}}^{\mathrm{CSI}}}{\left(1-f_{\mathrm{ox}}^{\mathrm{CSI}}\right)^2}\right|\Delta f_{\mathrm{ox}}^{\mathrm{CSI}}$$

$$P = f\left(f_{\mathrm{ox}}^{\mathrm{MFM}}, f_{\mathrm{ox}}^{\mathrm{CSI}}\right)$$

$$P = \frac{1-f_{\mathrm{ox}}^{\mathrm{MFM}}}{1-f_{\mathrm{ox}}^{\mathrm{CSI}}}$$

$$\Leftrightarrow f_{\mathrm{ox}}^{\mathrm{CSIC}} = 1+\left(f_{\mathrm{ox}}^{\mathrm{CSI}}-1\right)\frac{1-f_{\mathrm{ox}}^{\mathrm{MFM}}}{1-f_{\mathrm{ox}}^{\mathrm{CSI}}}$$

$$\left|\frac{\partial f_{ox}^{CSIC}}{\partial f_{ox}^{CSI}}\right| = \left|\frac{\left(1-f_{ox}^{MFM}-0+0\right)\left(1-f_{ox}^{CSI}\right)-\left(f_{ox}^{CSI}-f_{ox}^{CSI}\cdot f_{ox}^{MFM}-1+f_{ox}^{MFM}\right)\cdot(-1)}{\left(1-f_{ox}^{CSI}\right)^2}\right|$$

$$\Leftrightarrow \left|\frac{1-f_{ox}^{CSI}-f_{ox}^{MFM}+\left(f_{ox}^{CSI}\cdot f_{ox}^{MFM}\right)+f_{ox}^{CSI}-\left(f_{ox}^{CSI}\cdot f_{ox}^{MFM}\right)-1+f_{ox}^{MFM}}{\left(1-f_{ox}^{CSI}\right)^2}\right|$$

$$\Leftrightarrow \left|\frac{0}{\left(1-f_{ox}^{CSI}\right)^2}\right| = 0$$

$$\left|\frac{\partial f_{ox}^{CSIC}}{\partial f_{ox}^{MFM}}\right| = \left|\frac{\left(0-f_{ox}^{CSI}-0+1\right)\left(1-f_{ox}^{CSI}\right)-(...)\cdot 0}{\left(1-f_{ox}^{CSI}\right)^2}\right| = 1$$

4. Based on CO_2/CH_4 ratio

Estimation of biodegradation based on CO_2/CH_4 ratio

Assumption 1:

$CH_{4\,(g)} + 2O_{2\,(g)} \rightarrow CO_{2\,(g)} + 2H_2O_{(l)}$; each converted mol of CH_4 results in one mol CO_2 (see also (Gebert, 2011))

Assumption 2:

If only CH_4 is added to the reactor from below then the resulting CO_2 comes from the reaction in assumption 1.

Parameter:

$c_{CH_4,0}$: Gas concentration of methane at gas inlet
$c_{CH_4,m}$: Gas concentration of methane at sampling site
$c_{CO_2,0}$: Gas concentration of carbon dioxide at gas inlet
$c_{CO_2,m}$: Gas concentration of carbon dioxide at sampling site
$c_{CO_2,ox}$: Gas concentration of carbon dioxide at sampling site resulting from BMO
$\dot{V}_0$: Total volume flow of gas at gas inlet (e.g. Ls^{-1})
$\dot{V}_m$: Total volume flow of gas at sampling site

Mass balance:

$$\dot{n}_{CO_2,ox} = \dot{n}_{CO_2,m}$$

$$\dot{n}_{CH_4,0} = \dot{n}_{CO_2,m} + \dot{n}_{CH_4,m}$$

$$c_{CH_4,0} \cdot \dot{V}_0 = \left(c_{CO_2,m} + c_{CH_4,m}\right) \cdot \dot{V}_m$$

$$f_{ox}^{MFC/MFM} = 1 - \frac{J_{out}}{J_{in}} = \frac{c_{CH_4,0} \cdot \dot{V}_0 - c_{CH_4,m} \cdot \dot{V}_m}{c_{CH_4,0} \cdot \dot{V}_0} = 1 - \frac{c_{CH_4,m} \cdot \dot{V}_m}{c_{CH_4,0} \cdot \dot{V}_0}$$

Unknown: $\dot{V}_m$

Wanted: f_{ox}^{RATIO}

Solution:

$$c_{CH_4,0} \cdot \dot{V}_0 = \left(c_{CO_2,m} + c_{CH_4,m}\right) \cdot \dot{V}_m \;\big|:\left(c_{CH_4,m} \cdot \dot{V}_m\right)$$

$$\Leftrightarrow \frac{c_{CH_4,0}}{c_{CH_4,m}} \cdot \frac{\dot{V}_0}{\dot{V}_m} = \frac{c_{CO_2,m}}{c_{CH_4,m}} + 1 \;\big|\, x^{-1}$$

$$\Leftrightarrow \frac{c_{CH_4,m}}{c_{CH_4,0}} \cdot \frac{\dot{V}_m}{\dot{V}_0} = \frac{1}{\frac{c_{CO_2,m}}{c_{CH_4,m}} + 1} \;\big|+1$$

$$\Leftrightarrow 1 - \frac{c_{CH_4,m}}{c_{CH_4,0}} \cdot \frac{\dot{V}_m}{\dot{V}_0} = 1 - \frac{1}{\frac{c_{CO_2,m}}{c_{CH_4,m}} + 1} = 1 - \left(\frac{c_{CO_2,m}}{c_{CH_4,m}} + 1\right)^{-1} = \underline{f_{ox}^{RATIO}}$$

Error calculation:

No CO_2 in synthetic landfill gas at feeding of reactor:

$$f_{ox}^{RATIO} = f\left(c_{CO_2,m}, c_{CH_4,m}\right)$$

Partial derivatives based on chain rule:

$$\Rightarrow \Delta f_{ox}^{RATIO} = \left|\frac{\partial f_{ox}^{RATIO}}{\partial c_{CO_2,m}}\right| \Delta c_{CO_2,m} + \left|\frac{\partial f_{ox}^{RATIO}}{\partial c_{CH_4,m}}\right| \Delta c_{CH_4,m}$$

$$\Leftrightarrow \Delta f_{ox}^{RATIO} = \left|-\left(\frac{c_{CO_2,m}}{c_{CH_4,m}} + 1\right)^{-2} \frac{1}{c_{CH_4,m}}\right| \cdot \Delta c_{CO_2,m} + \left|\left(\frac{c_{CO_2,m}}{c_{CH_4,m}} + 1\right)^{-2} \frac{c_{CO_2,m}}{c_{CH_4,m}^{\,2}}\right| \Delta c_{CH_4,m}$$

$$\frac{\partial f_{ox}^{RATIO}}{\partial c_{CO_2,m}} = -\left(\frac{c_{CO_2,m}}{c_{CH_4,m}} + 1\right)^{-2} \cdot \frac{1 \cdot c_{CH_4,m} - c_{CO_2,m} \cdot 0}{c_{CH_4,m}^{\ 2}} = \underline{-\left(\frac{c_{CO_2,m}}{c_{CH_4,m}} + 1\right)^{-2} \cdot \frac{1}{c_{CH_4,m}}}$$

$$\frac{\partial f_{ox}^{RATIO}}{\partial c_{CH_4,m}} = -\left(\frac{c_{CO_2,m}}{c_{CH_4,m}} + 1\right)^{-2} \cdot \frac{0 \cdot c_{CH_4,m} - c_{CO_2,m} \cdot 1}{c_{CH_4,m}^{\ 2}} = \underline{\left(\frac{c_{CO_2,m}}{c_{CH_4,m}} + 1\right)^{-2} \cdot \frac{c_{CO_2,m}}{c_{CH_4,m}^{\ 2}}}$$

Problem 2: CO_2 in synthetic landfill gas

CO_2 addition has to be considered in calculations.

Assumption 1:

$CH_{4\,(g)} + 2O_{2\,(g)} \rightarrow CO_{2\,(g)} + 2H_2O_{(l)}$; each converted mol of CH_4 results one mol CO_2 (see also (Gebert, 2011))

Assumption 2:

The volume flows of CH_4 and CO_2 are identical at each respective sampling point.

Assumption 3:

Substitution allows elimination of unknown volume flow.

Parameter:

$c_{CO_2,ox}$: Subsequent CO_2 that results from oxidation of CH_4
$c_{CO_2,m}$: CO_2 measured at sampling point
$c_{CH_4,0}$: CH_4 at reactor inlet
$c_{CH_4,m}$: CH_4 measured at sampling point

Mass balance:

$$\dot{n}_{CO_2,0} = \dot{n}_{CO_2,m} - \dot{n}_{CO_2,ox}$$

$$\dot{n}_{CH_4,0} = \dot{n}_{CH_4,m} + \dot{n}_{CO_2,ox}$$

With respect to the mass balance: $c_{CO_2} \cdot V_{CO_2} = n_{CO_2}$ & $V_{CO_2,m} = V_{CO_2,ox}$ *n* may be substituted by c; and correspondingly for n_{CH_4}.

Thus:

$$c_{CH_4,0} \cdot \dot{V}_0 = \left(c_{CO_2,ox} + c_{CH_4,m} \right) \cdot \dot{V}_m$$

$$c_{CO_2,0} \cdot \dot{V}_0 = \left(c_{CO_2,m} - c_{CO_2,ox} \right) \cdot \dot{V}_m$$

WANTED: Biodegradation

$$f_{ox}^{RATIO} = 1 - \left(\frac{c_{CO_2,ox}}{c_{CH_4,m}} + 1 \right)^{-1} = 1 - \frac{c_{CH_4,m}}{c_{CH_4,0}} \cdot \frac{\dot{V}_m}{\dot{V}_0}$$

Solution:

$$\dot{V}_m \left(c_{CH_4,m} + c_{CO_2,ox} \right) = \dot{V}_0 \cdot c_{CH_4,0} \; \left| : \left(\dot{V}_m \cdot c_{CH_4,m} \right) \right.$$

$$\Leftrightarrow \frac{c_{CO_2,ox}}{c_{CH_4,m}} + 1 = \frac{c_{CH_4,0}}{c_{CH_4,m}} \cdot \frac{\dot{V}_0}{\dot{V}_m} \; \left| x^{-1} \right| \cdot (-1)$$

$$\Leftrightarrow -\left(\frac{c_{CO_2,ox}}{c_{CH_4,m}} + 1 \right)^{-1} = -\frac{c_{CH_4,m}}{c_{CH_4,0}} \cdot \frac{\dot{V}_m}{\dot{V}_0} \; \left| + \frac{c_{CH_4,0}}{c_{CH_4,0}} \frac{\dot{V}_0}{\dot{V}_0} \right.$$

$$\Leftrightarrow 1 - \left(\frac{c_{CO_2,ox}}{c_{CH_4,m}} + 1 \right)^{-1} = 1 - \frac{c_{CH_4,m}}{c_{CH_4,0}} \cdot \frac{\dot{V}_m}{\dot{V}_0} = \underline{\underline{f_{ox}^{RATIO}}}$$

Finding the substitution for $c_{CO_2,ox}$:

Based on the mass balance:

$$c_{CO_2,0} \cdot \dot{V}_0 = \left(c_{CO_2,m} - c_{CO_2,ox} \right) \cdot \dot{V}_m$$

and

$$c_{CH_4,0} \cdot \dot{V}_0 = \left(c_{CO_2,ox} + c_{CH_4,m} \right) \cdot \dot{V}_m$$

Combining both equations gives:

$$\frac{c_{CO_2,0}}{c_{CH_4,0}} \cdot \frac{\dot{V}_0}{\dot{V}_0} = \frac{c_{CO_2,m} - c_{CO_2,ox}}{c_{CH_4,m} + c_{CO_2,ox}} \cdot \frac{\dot{V}_m}{\dot{V}_m}$$

By the following rearrangements one obtains an expression for $c_{CO_2,ox}$:

$$\Leftrightarrow \frac{c_{CO_2,0}}{c_{CH_4,0}} = \frac{c_{CO_2,m} - c_{CO_2,ox}}{c_{CH_4,m} + c_{CO_2,ox}} \Bigg| \cdot \left(c_{CH_4,m} + c_{CO_2,ox}\right)$$

$$\Leftrightarrow \frac{c_{CO_2,0}}{c_{CH_4,0}}\left(c_{CH_4,m} + c_{CO_2,ox}\right) = c_{CO_2,m} - c_{CO_2,ox} \Big| + c_{CO_2,ox} \Big| - \frac{c_{CO_2,0}}{c_{CH_4,0}} c_{CH_4,m}$$

$$\Leftrightarrow \left(1 + \frac{c_{CO_2,0}}{c_{CH_4,0}}\right) \cdot c_{CO_2,ox} = c_{CO_2,m} - \frac{c_{CO_2,0}}{c_{CH_4,0}} \cdot c_{CH_4,m} \Big| : \left(1 + \frac{c_{CO_2,0}}{c_{CH_4,0}}\right)$$

$$\Leftrightarrow c_{CO_2,ox} = \frac{c_{CO_2,m} - \frac{c_{CO_2,0}}{c_{CH_4,0}} c_{CH_4,m}}{\left(1 + \frac{c_{CO_2,0}}{c_{CH_4,0}}\right)}$$

Inserting $c_{CO_2,ox}$ into the equation for the biodegradation (f_{ox}^{RATIO}) above will allow calculating the respective value.

Error calculation for problem 1:

$$f_{ox}^{RATIO} = f\left(c_{CO_2,m}, c_{CH_4,m}\right)$$

$$\Rightarrow \Delta f_{ox}^{RATIO} = \left|\frac{\partial f_{ox}^{RATIO}}{\partial c_{CO_2,ox}}\right| \Delta c_{CO_2,ox} + \left|\frac{\partial f_{ox}^{RATIO}}{\partial c_{CH_4,m}}\right| \Delta c_{CH_4,m}$$

$$\Leftrightarrow \Delta f_{ox}^{RATIO} = \left| -\left(\frac{c_{CO_2,ox}}{c_{CH_4,m}} + 1\right)^{-2} \left(\frac{1}{c_{CH_4,m}}\right) \right| \cdot \Delta c_{CO_2,ox} + \left| \left(\frac{c_{CO_2,ox}}{c_{CH_4,m}} + 1\right)^{-2} \frac{c_{CO_2,ox}}{c_{CH_4,m}^{\ 2}} \right| \cdot \Delta c_{CH_4,m}$$

$$\frac{\partial f_{ox}^{RATIO}}{\partial c_{CH_4,m}} = -\left(\frac{c_{CO_2,ox}}{c_{CH_4,m}} + 1\right)^{-2} \cdot \frac{0 \cdot c_{CH_4,m} - c_{CO_2,ox} \cdot 1}{c_{CH_4,m}^{\ 2}} = \left(\frac{c_{CO_2,ox}}{c_{CH_4,m}} + 1\right)^{-2} \cdot \frac{c_{CO_2,ox}}{c_{CH_4,m}^{\ 2}}$$

$$\frac{\partial f_{ox}^{RATIO}}{\partial c_{CO_2,ox}} = -1 \cdot \left(\frac{c_{CO_2,ox}}{c_{CH_4,m}} + 1\right)^{-2} \cdot \left(\frac{1 \cdot c_{CH_4,m} - c_{CO_2,ox} \cdot 0}{c_{CH_4,m}^{\ 2}}\right) = -\left(\frac{c_{CO_2,ox}}{c_{CH_4,m}} + 1\right)^{-2} \left(\frac{1}{c_{CH_4,m}}\right)$$

Error calculation for problem 2:

$$f\left(c_{CO_2,ox}\right) = f\left(c_{CO_2,m}, c_{CO_2,0}, c_{CH_4,m}, c_{CH_4,0}\right)$$

$$\Rightarrow \Delta f\left(c_{CO_2,ox}\right)=\left|\frac{\partial f\left(c_{CO_2,ox}\right)}{\partial c_{CO_2,m}}\right|\Delta c_{CO_2,m}+\left|\frac{\partial f\left(c_{CO_2,ox}\right)}{\partial c_{CO_2,0}}\right|\Delta c_{CO_2,0}$$
$$+\left|\frac{\partial f\left(c_{CO_2,ox}\right)}{\partial c_{CH_4,0}}\right|\Delta c_{CH_4,0}+\left|\frac{\partial f\left(c_{CO_2,ox}\right)}{\partial c_{CH_4,m}}\right|\Delta c_{CH_4,m}$$

$$\frac{\partial f\left(c_{CO_2,ox}\right)}{\partial c_{CO_2,m}}=\frac{(1-0)\left(1+\frac{c_{CO_2,0}}{c_{CH_4,0}}\right)-\left(c_{CO_2,m}-\frac{c_{CO_2,0}}{c_{CH_4,0}}\cdot c_{CH_4,m}\right)\cdot 0}{\left(1+\frac{c_{CO_2,0}}{c_{CH_4,0}}\right)^2}=\frac{\left(1+\frac{c_{CO_2,0}}{c_{CH_4,0}}\right)}{\left(1+\frac{c_{CO_2,0}}{c_{CH_4,0}}\right)^2}=\underline{\left(1+\frac{c_{CO_2,0}}{c_{CH_4,0}}\right)^{-1}}$$

$$\frac{\partial f\left(c_{CO_2,ox}\right)}{\partial c_{CO_2,0}}=\frac{\left(0-\frac{1}{c_{CH_4,0}}\cdot c_{CH_4,m}\right)\cdot\left(1+\frac{c_{CO_2,0}}{c_{CH_4,0}}\right)-\left(c_{CO_2,m}-\frac{c_{CO_2,0}}{c_{CH_4,0}}\cdot c_{CH_4,m}\right)\cdot\frac{1}{c_{CH_4,0}}}{\left(1+\frac{c_{CO_2,0}}{c_{CH_4,0}}\right)^2}$$

$$\Leftrightarrow\frac{-\frac{c_{CH_4,m}}{c_{CH_4,0}}\cdot\left(1+\frac{c_{CO_2,0}}{c_{CH_4,0}}\right)-\left(c_{CO_2,m}-\frac{c_{CO_2,0}}{c_{CH_4,0}}\cdot c_{CH_4,m}\right)\cdot\frac{1}{c_{CH_4,0}}}{\left(1+\frac{c_{CO_2,0}}{c_{CH_4,0}}\right)^2}$$

$$\Leftrightarrow\frac{-\frac{c_{CH_4,m}}{c_{CH_4,0}}-\frac{c_{CH_4,m}\cdot c_{CO_2,0}}{{c_{CH_4,0}}^2}-\frac{c_{CO_2,m}}{c_{CH_4,0}}+\frac{c_{CO_2,0}\cdot c_{CH_4,m}}{{c_{CH_4,0}}^2}}{\left(1+\frac{c_{CO_2,0}}{c_{CH_4,0}}\right)^2}=\underline{-\frac{c_{CH_4,m}+c_{CO_2,m}}{c_{CH_4,0}\left(1+\frac{c_{CO_2,0}}{c_{CH_4,0}}\right)^2}}$$

$$\frac{\partial f\left(c_{CO_2,ox}\right)}{\partial c_{CH_4,0}} = \frac{\left(0+\frac{c_{CO_2,0}\cdot c_{CH_4,m}}{{c_{CH_4,0}}^2}\right)\left(1+\frac{c_{CO_2,0}}{c_{CH_4,0}}\right)-\left(c_{CO_2,m}-\frac{c_{CO_2,0}}{c_{CH_4,0}}\cdot c_{CH_4,m}\right)\left(-\frac{c_{CO_2,0}}{{c_{CH_4,0}}^2}\right)}{\left(1+\frac{c_{CO_2,0}}{c_{CH_4,0}}\right)^2}$$

$$\Leftrightarrow \frac{\frac{c_{CO_2,0}\cdot c_{CH_4,m}}{{c_{CH_4,0}}^2}+\frac{{c_{CO_2,0}}^2\cdot c_{CH_4,m}}{{c_{CH_4,0}}^3}+\frac{c_{CO_2,m}\cdot c_{CO_2,0}}{{c_{CH_4,0}}^2}+\frac{{c_{CO_2,0}}^2\cdot c_{CH_4,m}}{{c_{CH_4,0}}^3}}{\left(1+\frac{c_{CO_2,0}}{c_{CH_4,0}}\right)^2}$$

$$\Leftrightarrow \frac{\frac{c_{CO_2,0}\cdot c_{CH_4,m}}{{c_{CH_4,0}}^2}+\frac{{c_{CO_2,0}}^2\cdot c_{CH_4,m}}{{c_{CH_4,0}}^3}+\frac{c_{CO_2,m}\cdot c_{CO_2,0}}{{c_{CH_4,0}}^2}+\frac{{c_{CO_2,0}}^2\cdot c_{CH_4,m}}{{c_{CH_4,0}}^3}}{\left(1+\frac{c_{CO_2,0}}{c_{CH_4,0}}\right)^2}$$

$$\Leftrightarrow \frac{\frac{c_{CO_2,0}\cdot c_{CH_4,m}}{{c_{CH_4,0}}^2}+\frac{c_{CO_2,m}\cdot c_{CO_2,0}}{{c_{CH_4,0}}^2}}{\left(1+\frac{c_{CO_2,0}}{c_{CH_4,0}}\right)^2} = \frac{c_{CO_2,0}\left(c_{CH_4,m}+c_{CO_2,m}\right)}{{c_{CH_4,0}}^2\left(1+\frac{c_{CO_2,0}}{c_{CH_4,0}}\right)^2}$$

$$\frac{\partial f\left(c_{CO_2,ox}\right)}{\partial c_{CH_4,m}} = \frac{\left(0-\frac{c_{CO_2,0}}{c_{CH_4,0}}\cdot 1\right)\left(1+\frac{c_{CO_2,0}}{c_{CH_4,0}}\right)-\left(c_{CO_2,m}-\frac{c_{CO_2,0}}{c_{CH_4,0}}\cdot c_{CH_4,m}\right)(0+0)}{\left(1+\frac{c_{CO_2,0}}{c_{CH_4,0}}\right)^2}$$

$$\Leftrightarrow \frac{-\frac{c_{CO_2,0}}{c_{CH_4,0}}+\left(\frac{c_{CO_2,0}}{c_{CH_4,0}}\right)^2}{\left(1+\frac{c_{CO_2,0}}{c_{CH_4,0}}\right)^2} = -\frac{\left(\frac{c_{CO_2,0}}{c_{CH_4,0}}+\left(\frac{c_{CO_2,0}}{c_{CH_4,0}}\right)^2\right)}{\left(1+\frac{c_{CO_2,0}}{c_{CH_4,0}}\right)^2}$$

A5. Chapter 6

Calculation of the maximum turnover by the difference quotient of the corresponding functions for f_{ox}:

$$\Delta y_{ij} = y_j - y_i$$

$$\Delta x_{ij} = x_j - x_i$$

y_{ij}: Corresponding turnover of f_{ox}

x_{ij}: Corresponding sampling depth

Error propagation

$$\left|\Delta\left(\Delta y_{ij}\right)\right| = \left|\Delta y_j\right| + \left|\Delta y_i\right|$$

Δy_i: Error of the corresponding function f_{ox} at the given sampling depth

The error of sampling depth is neglected.

$$\left|\Delta\left(\Delta x_{ij}\right)\right| = \left|\Delta x_j\right| + \left|\Delta x_i\right|$$

Thus:

$$\left|\Delta\left(\frac{\Delta y_{ij}}{\Delta x_{ij}}\right)\right| = \left|\Delta\left(\Delta y_{ij}\right)\right|$$

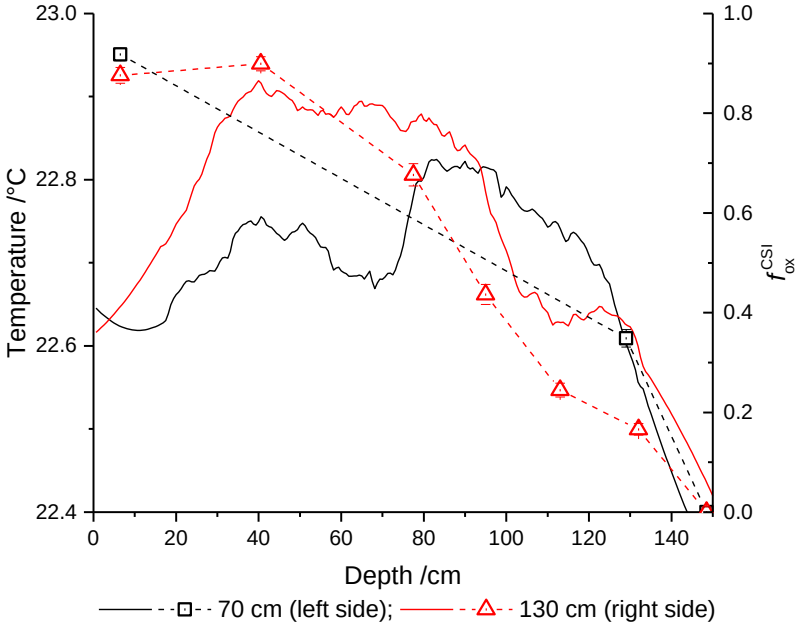

Figure 0-1 Temperature and f_{ox}^{CSI} versus reactor depth at day 84 (normal state 150511)

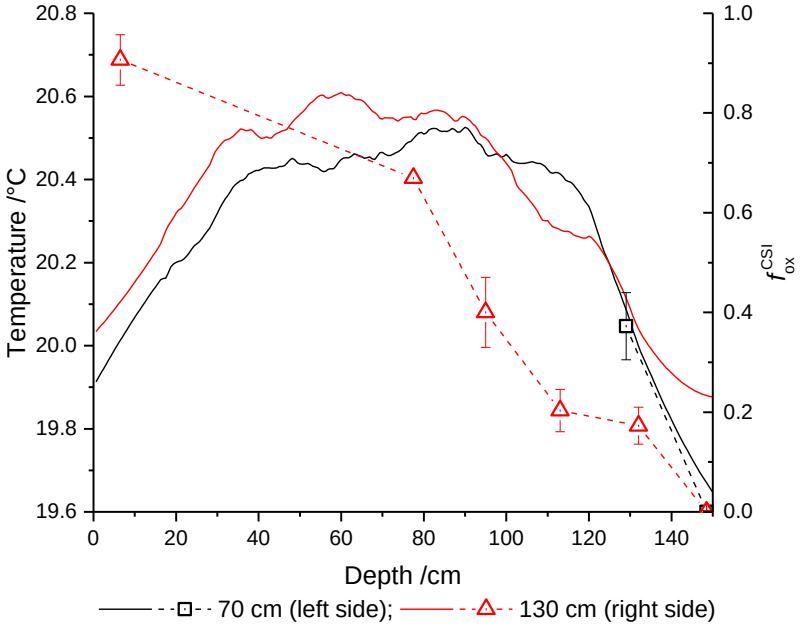

Figure 0-2 Temperature and f_{ox}^{CSI} versus reactor depth at day 86 (normal state 150513)

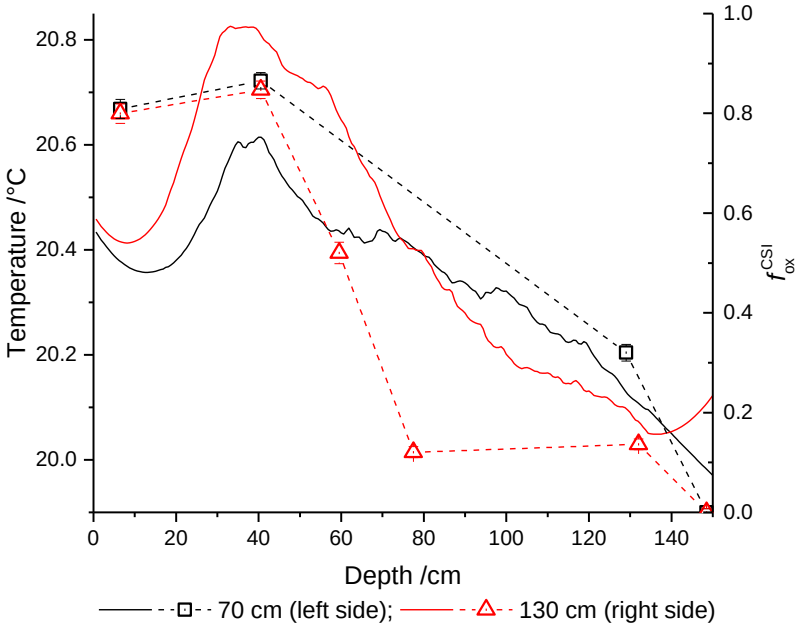

Figure 0-3 Temperature and f_{ox}^{CSI} versus reactor depth at day 88 (cooling scenario 150515)

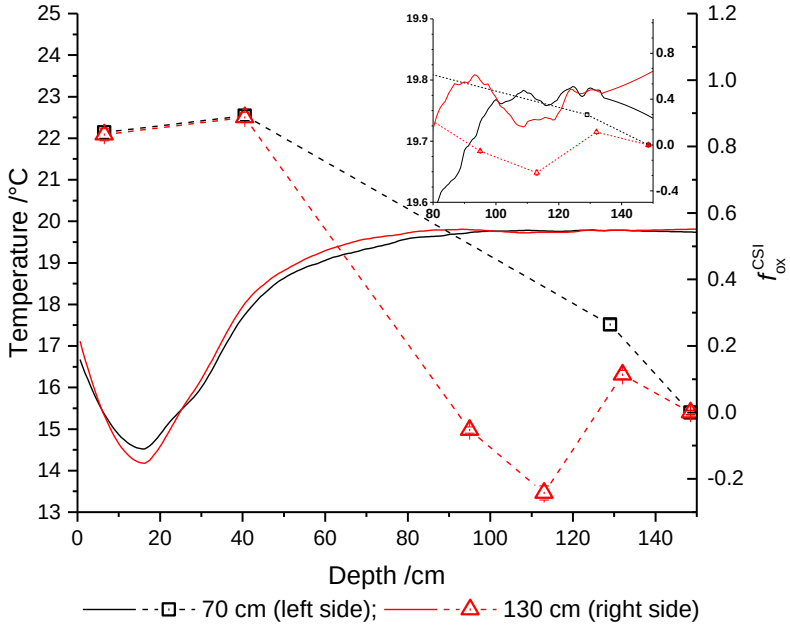

Figure 0-4 Temperature and f_{ox}^{CSI} versus reactor depth at day 99 (cooling scenario 150526)

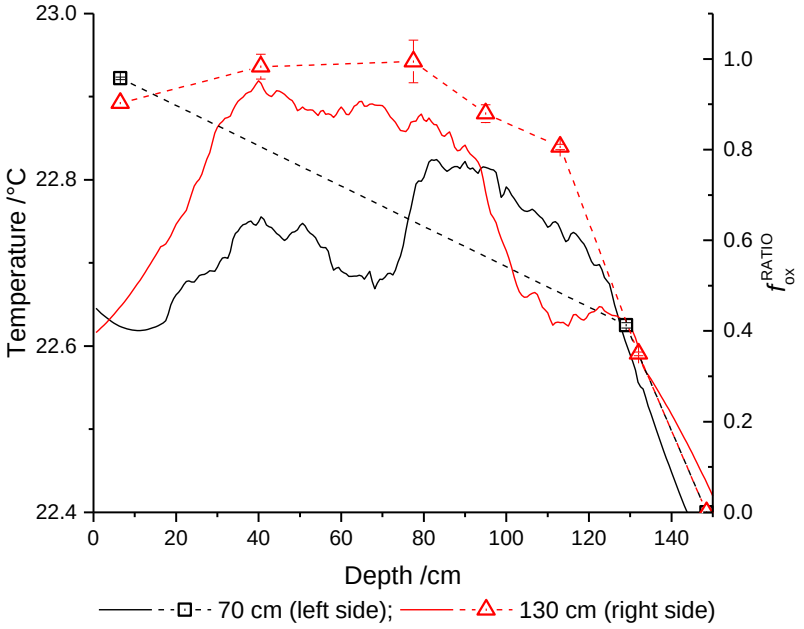

Figure 0-5 Temperature and f_{ox}^{RATIO} versus reactor depth at day 84 (normal state 150511)

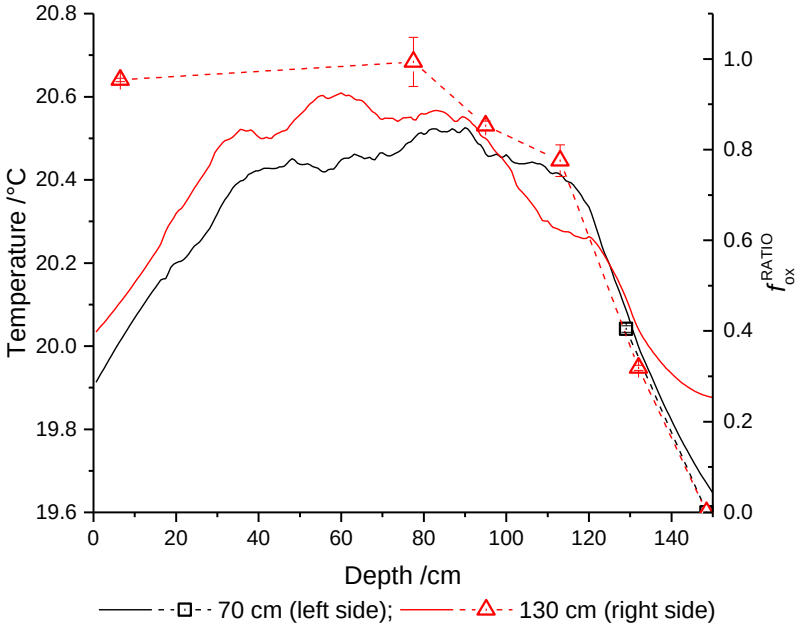

Figure 0-6 Temperature and f_{ox}^{RATIO} versus reactor depth at day 86 (normal state 150513)

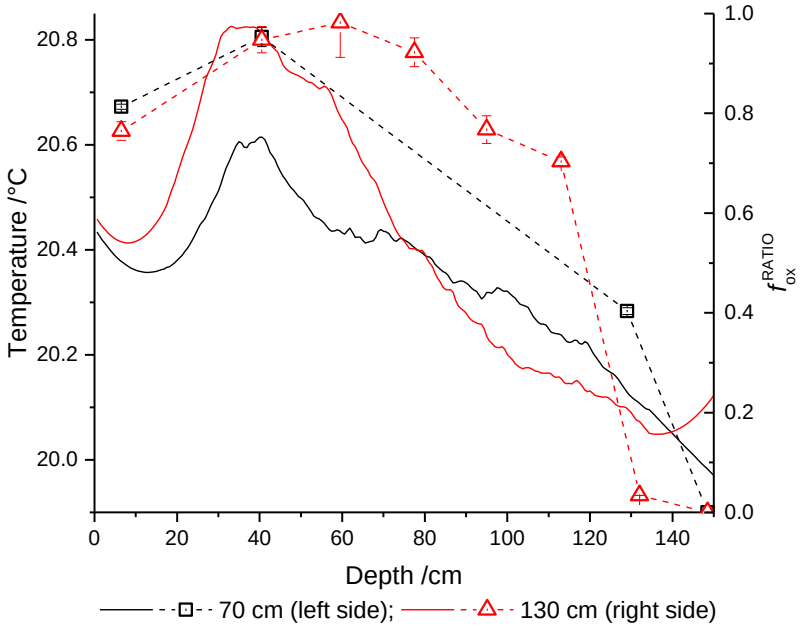

Figure 0-7 Temperature and f_{ox}^{RATIO} versus reactor depth at day 88 (cooling scenario 150515)

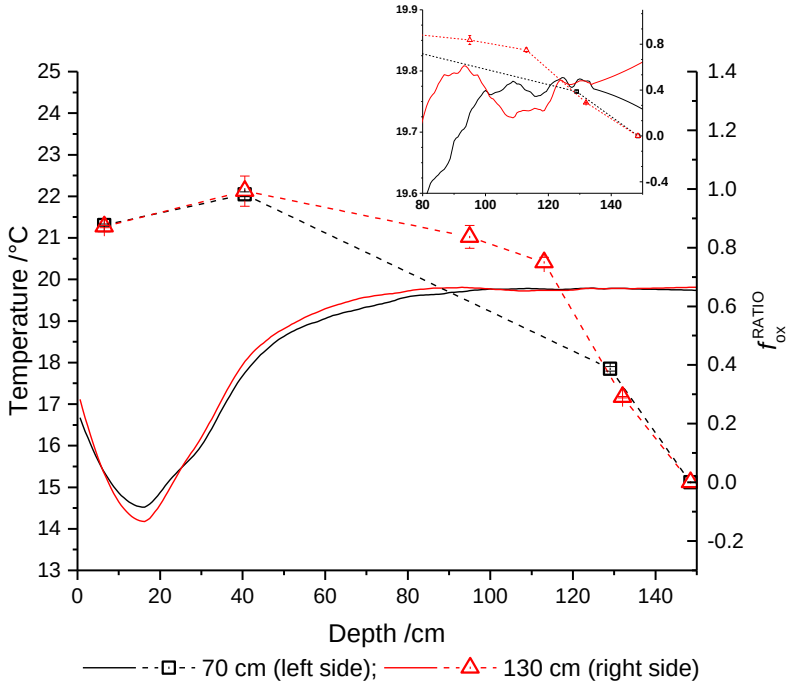

Figure 0-8 Temperature and f_{ox}^{RATIO} versus reactor depth at day 99 (cooling scenario 150526)

List of Figures

List of Tables

List of Abbreviations

α	Isotopic fractionation factor
α_{diff}	Isotopic fractionation factor of diffusion
BMO	Bacterial Methane Oxidation
CSI	Closed system stable isotope approach
ε	Isotopic enrichment factor
ε_{diff}	Isotopic enrichment factor of diffusion
EIE	Equilibrium isotope effect
f_{ox}^{CSI}	Biodegradation calculated by closed system stable isotope approach
f_{ox}^{MFC}	Biodegradation calculated by mass balance approach using volume flow obtained from mass flow controllers
f_{ox}^{MFM}	Biodegradation calculated by mass balance approach using volume flow obtained from mass flow controllers and mass flow monitor
f_{ox}^{OSI}	Biodegradation calculated by open system stable isotope approach
FIA	Flow injection analysis
GC	Gas chromatography
HPLC	High performance liquid chromatography
IRMS	Isotope ratio mass spectrometer
KIE	Kinetic isotope effect
KIE_{diff}	Kinetic isotope effect of diffusion
MDL	Method detection limit
MFC	Mass flow controller
MFM	Mass flow monitor
MMO	Methane monooxygenase
OSI	Open system stable isotope approach
pMMO	Particulate methane monooxygenase
SIA	Stable isotope analysis
sMMO	Soluble methane monooxygenase
VPDB	Vienna Pee Dee Belemnite

Publikationsliste

Poster und Vorträge

Vorträge:

- St. Margherita di Pula, It, Sardiniasymposium, Oktober 2015
  M. S. Schulte, M. A. Jochmann, T. C. Schmidt, T. Gehrke, M. Denecke:
  "Horizontal Profiling of Microbial Methane Oxidation in a Reactor System by Stable Isotope Analysis"

- Essen, Umweltseminar, Mai 2012
  M. S. Schulte, M. A. Jochmann, T. C. Schmidt:
  "GC-IRMS: Application of an automated preconcentration unit for low level landfill gases CO2 and CH4"

Poster:

- Braunschweig, ASI, Oktober 2013
  M. S. Schulte, M. A. Jochmann, T. C. Schmidt, T. Gehrke, M. Denecke:
  "Comparison of the carbon isotope fractionation by microbial methane oxidation between batch reactor and cell culture experiments"

- Essen, Anakon, Januar 2013
  M. S. Schulte, A. Kremser, M. A. Jochmann, T. C. Schmidt:
  "Development of an Automated Preconcentration Unit for Stable Isotope Analysis of Low Level Concentrations of Methane and Carbon Dioxide by GC-IRMS"

- Leipzig, JESIUM, September 2012
  M. S. Schulte, M. A. Jochmann, T. C. Schmidt, T. Gehrke, M. Denecke:
  "Carbon Isotope Fractionation of Methane Oxidation by Methanotrophs at Different Conditions in a Batch Reactor System"

Lebenslauf

Der Lebenslauf ist in der Online-Version aus Gründen des Datenschutzes nicht enthalten.

Erklärung

Hiermit versichere ich, dass ich die vorliegende Arbeit mit dem Titel

„Characterization of the microbial methane oxidation for landfill studies by stable isotope analysis"

selbst verfasst und keine außer den angegebenen Hilfsmitteln und Quellen benutzt habe, und dass die Arbeit in dieser oder ähnlicher Form noch bei keiner anderen Universität eingereicht wurde.

Essen, im November 2016

Sven Marcel Schulte

Danksagung

Ein großer Dank gilt Professor Torsten C. Schmidt für die Betreuung und der damit einhergehenden langjährigen und professionellen Betreuung sowie der Begutachtung der vorliegenden Arbeit.

Für die Übernahme des Zweitgutachtens und für die anregungsvollen und interdisziplinären Diskussionen spreche ich Herrn Professor Martin Denecke meinen Dank aus.

Bei Herrn Dr. Maik A. Jochmann möchte ich mich für die moralische und fachliche Unterstützung bei der Analytik stabiler Isotope bedanken.

Für die intensiven und hilfreichen Diskussionen, sowie das tatkräftige Mitwirken im Labor, danke ich insbesondere Kamil Michalski, Jens-Benjamin Wolbert und Daniel Köster. Im genaueren danke ich Jens-Benjamin Wolbert für die für Kapitel 4 gegebene Unterstützung bei experimentellen Vorbereitungen und Analysen am LC-IRMS.

Meinem ehemaligen Projektpartner Tobias Gehrke gilt mein ausdrücklicher Dank für die praktischen Ratschläge und das Mitwirken bei Problemstellungen rund um die experimentellen Herausforderungen zur Untersuchungen der mikrobiellen Methanoxidation, und für die zur Verfügung gestellten Materialien und Bakterienkulturen für Kapitel 3 und 4.

Für sein besonderes Engagement während seiner Tätigkeit als Bachelorstudent, welches erheblich zu Kapitel 5 und 6 beigetragen hat, danke ich Tomasz Michal Heluszka.

Bei meiner Familie bedanke ich mich von ganzem Herzen für ihre langjährige Unterstützung.

Julia danke ich für ihr Vertrauen in mich und ihre fortwährende Unterstützung und Geduld, die mir die Kraft gaben diese Arbeit zu verfassen und zu vollenden.